Multidentate Thioether-Based Ligands Controlling the Stability and Size of Gold Nanoparticles

Inauguraldissertation

zur

Erlangung der Würde eines Doktors der Philosophie

vorgelegt der

Philosophisch-Naturwissenschaftlichen Fakultät

der Universität Basel

von

Mario Lehmann

aus Belp (BE), Schweiz

Bern, 2017

Genehmigt von der Philosophisch-Naturwissenschaftlichen Fakultät
auf Antrag von

Prof. Dr. Marcel Mayor und Prof. Dr. Christof Sparr

Basel, den 23. Mai 2017

Prof. Dr. Martin Spiess
Dekan der Philosophisch-
Naturwissenschaftlichen Fakultät

"Es ist nicht alles Gold, was glänzt.
Aber es glänzt auch nicht alles, was Gold ist."
Christian Friedrich Hebbel

Acknowledgments

I want to thank my supervisor Prof. Dr. Marcel Mayor for the opportunity to work on this fascinating topic, your support throughout my studies and the freedom in my research. I enjoyed our conversations, and I feel honored for having worked with you.

I would like to thank Prof. Dr. Christof Sparr for kindly accepting to be the co-referee for this thesis and Prof. Dr. Catherine Housecroft for chairing the exam.

A special thank goes to Annika Büttner and Cedric Wobill for measuring TGA measurements whenever I needed them. I am grateful to Dr. Markus Dürrenberger and his team for letting me measure TEM images on their delicate devices and being there whenever I had troubles. I greatly thank PD Dr. Daniel Häussinger and Thomas Müntener for the NMR experiments and analysis. I also thank Dr. Heinz Nadig for ESI analyses and Sylvie Mittelheisser for elemental analyses.

I am also grateful to the technical staff of the Department of Chemistry for helping me to solve upcoming technical issues. I am thankful to Brigitte Howald, Beatrice Erismann and Maria Mambelli and Brigitte Howald, as well as Markus Hauri and Roy Lips for their support.

I would like to thank the former and present golden boys and girls Dr. Ulrike Fluch, Dr. Jens Hermes, Dr. Fabian Sander and Henrik Peters for the nice team spirit and the interesting discussions not only about gold nanoparticles.

Especially my gratefulness goes to my lab mates Viktor and Thomas and non-lab mates Loïc, Michal, Rajesh and Alfredo for their great company and support over the last few years.

I like to thank Dr. Almudena Gallego Gonzalez, Thomas Brandl, Dr. Loïc Le Pleux, and Prof. Dr. Michal Juríček for proofreading my thesis.

Also, I would like to thank all the current and former members of the Mayor group, including the awesome people from Karlsruhe for the exchange of knowledge and great hospitality.

I would like to acknowledge all the students for the contribution during their Wahlpraktikum.

For their support and for being there for me in good and in bad times, I would like to deeply thank my family.

Steffi, I can't describe how thankful I am for your love and support during the last eight years. Merci.

Table of Content

1 Introduction

1.1 Gold Nanoparticles: Historical Background

Gold has been fascinated mankind for several millennia due to its shiny appearance and its chemical inertness, both attributes desirable for the crafting of decorative objects and jewelry. While the extraction of gold is believed to start in the 5th millennium BC, the most ancient use of "soluble" gold (colloidal gold) is estimated around the 5th century BC by alchemists in Egypt.[1] These nanosized colloidal particles with their brilliant colors where used as colorants to stain glass and ceramics, and these applications are still in use nowadays.[2] A famous example is the dichroic Lycurgus cup from the 4th century AD, which appears ruby red in transmitted light and green in reflected light due to the presence of colloidal gold.[3,4] In the Middle Ages, sols of gold nanoparticles had also the reputation of having curative powers for various diseases.[5]

The route towards the scientific engagement with gold nanoparticles (AuNPs) accompanied with the birth of nanotechnology as we know it today, dates back to the 19th century (Figure 1). In 1857, Faraday described in his seminal work the interaction between 'diffused' gold and light.[6] Ever since his discovery of ruby red solutions with their optical properties by reduction of a tetrachloroaurate solution ($HAuCl_4$) by phosphorus in carbon disulfide, more interesting attributes are to be found in this noble metal.[7] The term 'colloid' was introduced shortly after by Graham in 1961.[8] Note that this term is earlier used for all forms of colloidal solution while nowadays it is replaced - depending on the size, shape and uniformity - by 'nanoparticle' (NP), 'nanocrystal' or 'cluster' (NC).[9] Within this work, the term 'nanoparticle', will be used for gold particles with a sizes larger than 1 nm that are not uniform in size. Gold 'cluster' on the other hand exhibits atomically precise stoichiometry with uniform structures and are usually smaller than 1 nm ('nanocrystal' when crystal structure was obtained), even when the boundary is not clearly assignable in some cases.[10] While Faraday first attributed the bright colors to colloidal gold, Mie explained almost 50 years later the origin of the phenomenon by solving Maxwell's electromagnetic equation for the interaction of light with spherical particles in 1908.[11] Almost at the time, Zsigmondy merged his technology with Faraday's discovery and introduced the procedure called "seed mediated method", which is still used nowadays for the synthesis of various-sized NPs.[12,13] He further contribute to the field of nanotechnology by his pioneering inventions of an ultrafiltration device as well as an ultramicroscope which for the first time enables the characterization of the shape and size of NPs.[14,15] A few years later Svedberg introduced an ultracentrifuge and showed that the motion of colloids depended on their shape and size.[16–18] The theoretical understanding of the unique

properties of AuNPs (*vide infra*) with the scope for future applications leads to the first modern milestone from the second half of the 20th century. Turkevich and coworkers developed in 1951 a synthetic *bottom up* method for creating AuNPs by addition of trisodium citrate dihydrate under vigorous stirring to hydrogen tetrachloroaurate in boiling water. In this case, the citrate acts as both reducing as well as stabilization agent. After a few minutes, the wine-red colloidal suspension is obtained with AuNPs of about 20 nm in size.[19] This method was further refined two decades later by Frens by changing the gold-to-citrate ratio to control particle size.[20] This so-called Turkevich-Frens method has been widely employed to prepare dilute solutions of moderately stable AuNPs with diameter from 15-150 nm, however particles larger than 20 nm were always polydispersed (Figure 2). Nowadays, this approach is mostly used if a loose ligand shell is desired for example for further ligand exchange.[21]

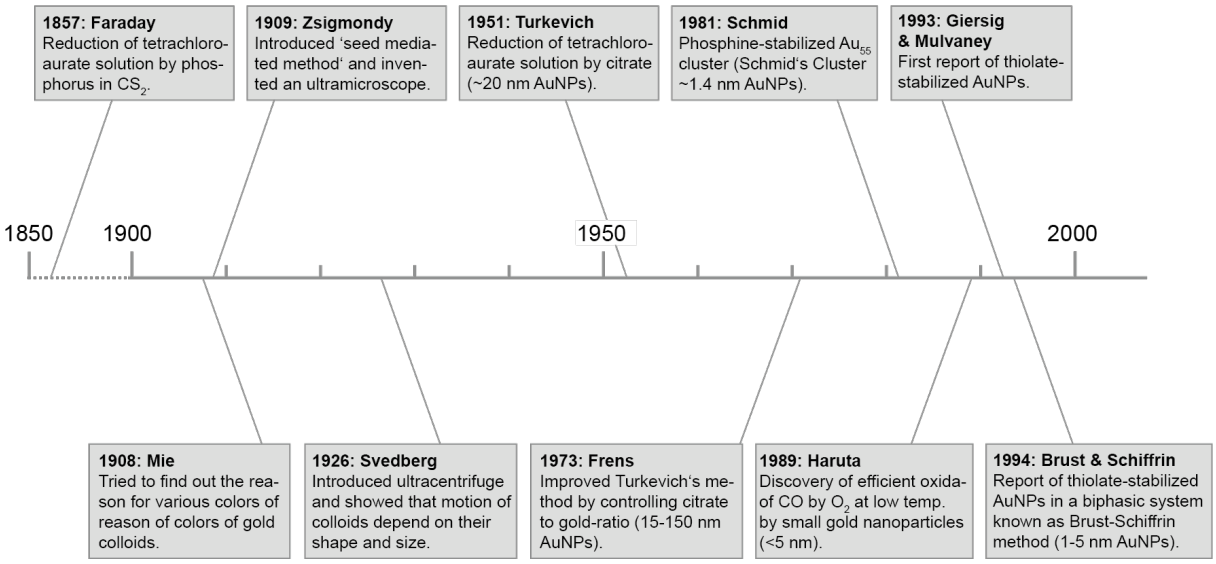

Figure 1: Modern milestones in nanotechnology in the past 150 years.

A decade later in 1981, Schmid published his work about phosphine-stabilized cluster, nowadays known as 'Schmid Au_{55}-cluster' $[Au_{55}(PPh_3)_{12}Cl_6]$. Despite the delicate synthesis, they remained unique for a long time due to their narrow dispersity (1.4 ± 0.4 nm) for the study of a quantum-dot nanomaterial, despite its delicate synthesis.[22,23] Another major milestone in the last century for nanotechnology, was pioneered in the late 80ies by Haruta and coworkers.[24] They found that AuNPs - mostly - supported on metal-oxides were highly active catalysts, under high dispersion, for various transformations (*e.g.* CO and H_2 oxidation) at very low temperatures. Catalysis with AuNPs is now an expanding area, and a large number of new catalytic systems for various reactions are now being explored.[25–28] The very first publication of thiolate-stabilized AuNPs was reported by Giersig and Mulvaney in 1993, showing the possibilities of using alkylthiols of various chain

length to stabilize them.[29] One year later, Brust and Schiffrin came up in their seminal work with a biphasic reduction protocol (Figure 2). This two-phase protocol was the first method that enables the preparation of thiolate-stabilized AuNPs *via in situ* synthesis, with tetraoctylammonium bromide (TOAB) as the phase transfer reagent (transferring the gold-salt from the water to toluene as the organic phase) and sodium borohydride ($NaBH_4$) as mild reducing agent. This method had a tremendous impact in the field due to the facile synthesis in ambient conditions which yields relatively high thermal and air stable AuNPs. This methodology produces low dispersity AuNPs ranging from 1 to 5 nm depending on the selected reaction conditions such as the gold-to-thiol ratio, reduction rate, and reaction temperature.[30–32] Due to this breakthrough, this method had attracted great attention in the scientific community with exponentially growing amounts of annually reported publications. Finally, in the past two decades, the two-step seed-growth mediated technique gained more attention due to its advanced size and shape control of AuNPs larger than 70 nm (Figure 2).[13] Compared with the in situ syntheses, the seed-growth method enlarges the particles step by step, enabling an easier control over the size and shape (rods, cubes, triangles, hexapods, ribbons, hollow cages, branches or polyhedral) of the as-synthesized particles. In principle, this method involves two steps. In the first step, small-sized AuNPs seeds are prepared which are then in the second step added into a growth-solution containing $HAuCl_4$, stabilizing and reducing agents, respectively. As seeds, weakly passivated AuNPs, such as citrate-stabilized AuNPs are usually used as intermediates in further preparations of functionalization such as ligand substitution reaction and seed-growth-mediated synthesis due to the weak binding features of citric acid to gold. Mild reducing agents are commonly utilized in the second step, allowing a slow and control growth and on the other hand preventing possible formation of new seeds.[13,33–36]

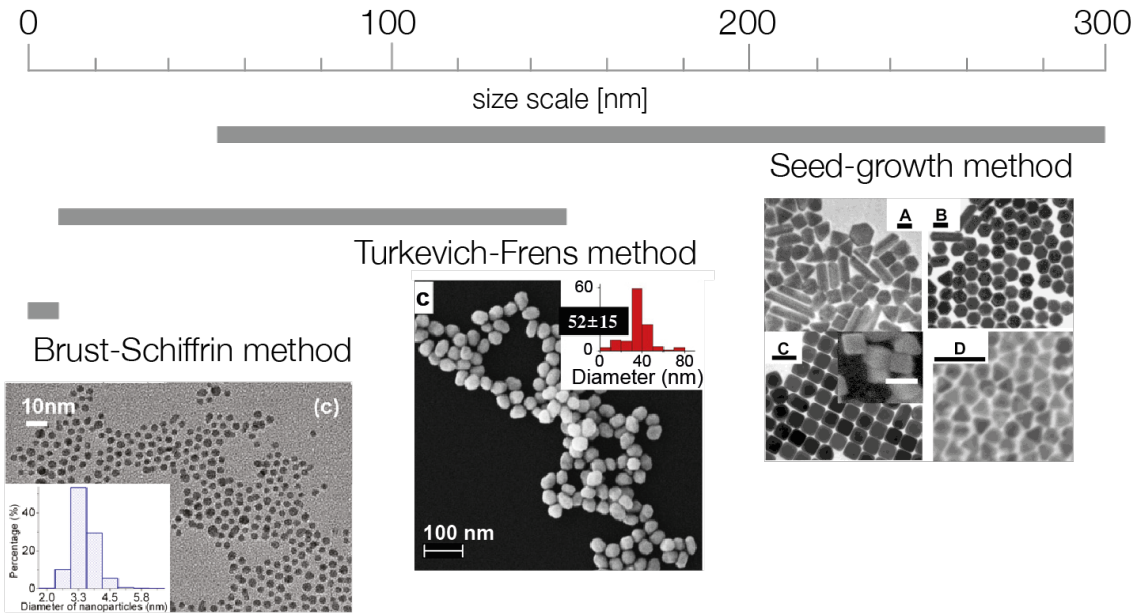

Figure 2: The three most important methods for the synthesis of gold nanoparticles for different sizes and shapes.

Top down approaches for the fabrication of AuNPs compared to the previously described *bottom up* approaches are scarcely present in literature. They start with a bulk gold substrate, usually film or pellet, followed by a nanoscale patterning procedure during which the major part of the gold film is removed, yielding AuNPs with predetermined scale and shape.[37] The most commonly used *top down* technique is the electron-beam method that results in the formation of multiple-shaped nanostructures with size control down to 100 nm.[38] Another well-known technique is the laser-based ablation method.[39–41]

1.2 Properties and Applications of Gold Nanoparticles

Gold nanoparticles exhibit exciting unique characteristics such as size- and shape-dependent optoelectronic properties, large surface-to-volume ratio, excellent biocompatibility and low toxicity.[42–45] An important physical property is the surface plasmon resonance (SPR). Spherical AuNPs exhibit a range of colors (*e.g.* brown, orange, red and purple) in solution as the core size increases from 1 to 100 nm, and generally show a size-relative absorption peak from 500 to 600 nm (Figure 3 b).[46,47]

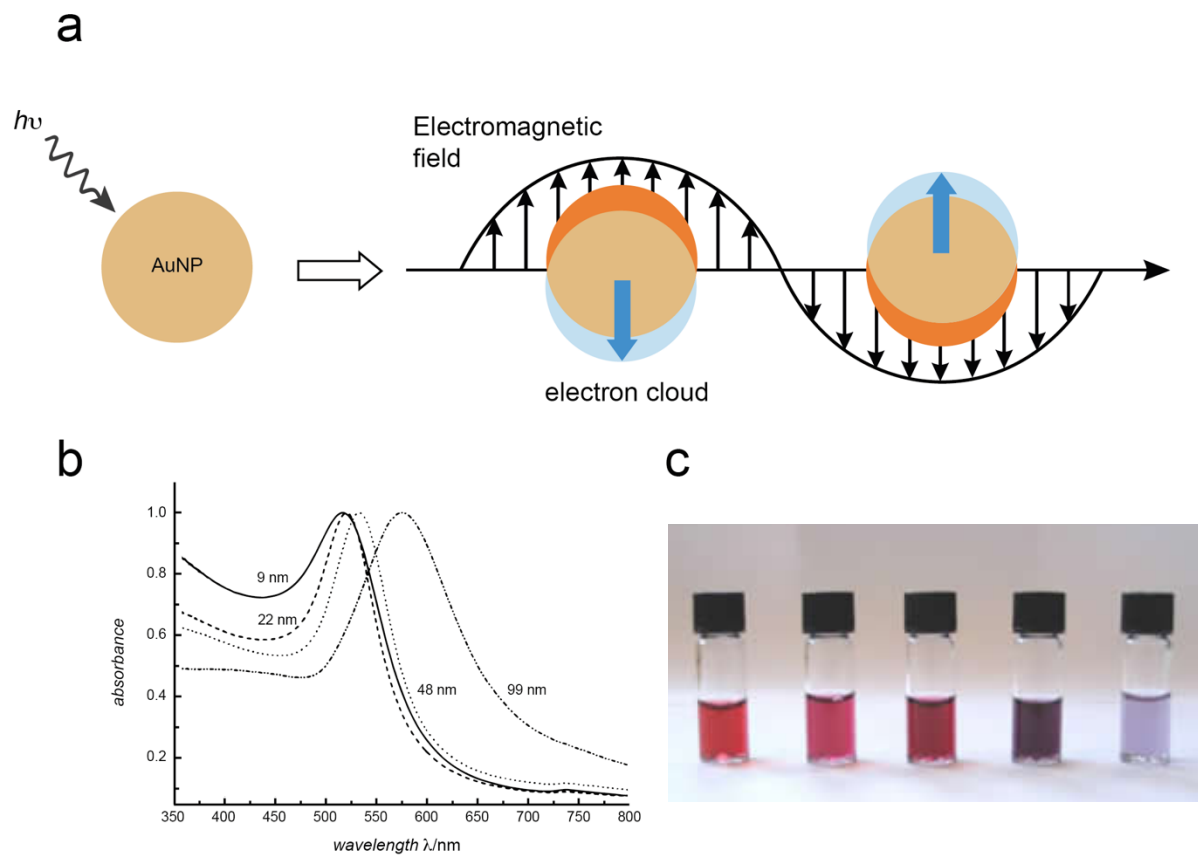

Figure 3: a) Schematic illustration of the plasmon oscillation of a gold nanoparticle.[48] b) UV-Vis absorption spectra of various-sized gold nanoparticles measured in water.[47] c) Aqueous solutions of gold nanoparticles with different sizes starting from 5 to 100 nm (left to right).[49]

This absorption band is visible in the UV-Vis spectra and is dominated by the collective oscillation of conduction electrons induced by an electric field of incoming light (Figure 3 a). This behavior is highly depending on size, shape and surrounding medium and determines the color of the solution (Figure 3 c). A dipole is induced in the nanoparticle by electromagnetic radiation resulting in a restoring force. However, this band is absent in both small nanoparticles (d<2 nm) and the bulk materials. This phenomenon is influenced by the size, shape, solvent, surface ligand, core charge, temperature and is even sensitive to the proximity of other NPs.[50–52] Aggregation of the nanoparticles in solution may result in significant red-shifting of the SPR frequency, broadening of surface plasmon band and changing the solutions' color from red to blue due to the interparticle plasmon coupling.[53] For many other metals the plasma frequency lies in the ultraviolet part of the spectrum and their solutions show no strong coloring effect. The plasma frequency in copper, silver and gold is pushed into the visible part of the spectrum due to d-d band transitions, as shown in (Figure 3 b).[47,54]

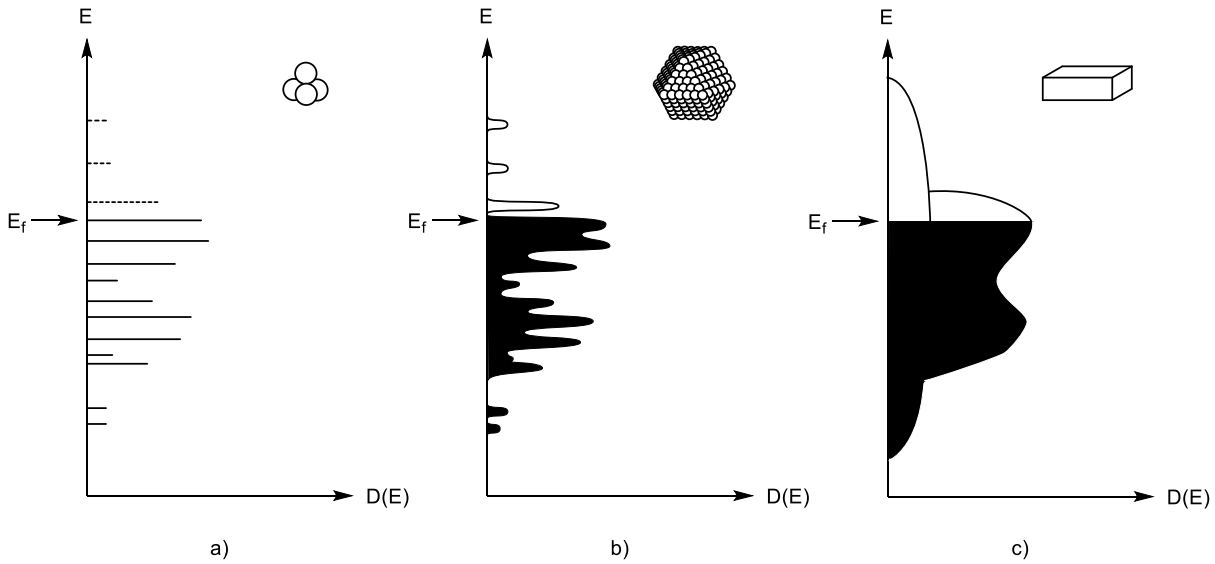

Figure 4: Distribution of energy states in a) clusters or molecules, b) nanoparticles and c) bulk metal. E_f = Fermi energy.[55]

Another interesting property of metal nanoparticles is the distribution of their energy states. At a sufficient small particle size the valence electrons are constrained and begin to occupy discrete energy levels. Figure 4 shows the electronic structures of a metal (plot of energy E versus the density of states D(E)) depending on the number of interacting atoms on the way from bulk metal with quasi delocalized valence electrons (a) *via* nanoparticles (b) to cluster with defined molecular orbitals similar to molecules. E_f denotes the Fermi level and the energy of the highest occupied molecular orbital. A particle of such size no longer follows classical physical laws and has to be described by the quantum mechanical rules. It can be considered as a particle in a box. Such small

pieces of metal exhibit different physical and chemical properties compared to bulk or molecules.[9,55] Thus, gold nanoparticles have become promising candidates for single electron devices which retain their scalability down to the molecular level in a field that was name *Single Electronics*.[56] For the fabrication of such devices, scalable methods for the directed assembly of nanoparticle units are required.[57–60]

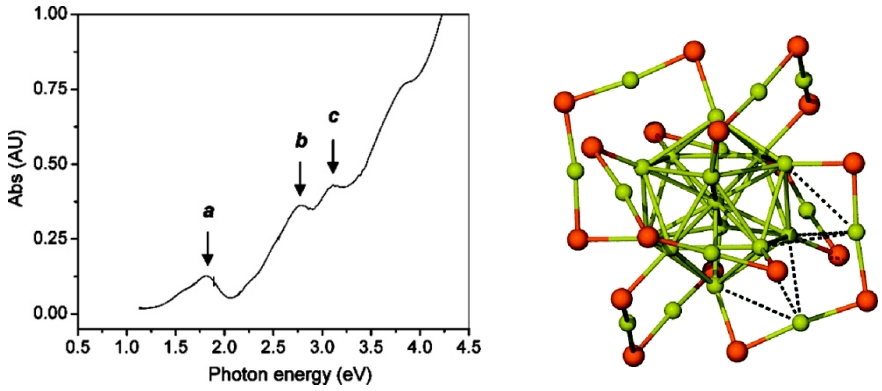

Figure 5: *Left:* UV-Vis spectrum of $Au_{25}(SR)_{18}$ cluster redissolved in toluene and *right:* its resolved crystal structure.[61]

As mentioned before, when AuNPs become extremely small (<2 nm in diameter), significant quantification may be observed to the conduction band. Such quantum-sized nanoparticles are often referred as ultrasmall nanoparticles, super atom complexes, monolayer-protected nanoclusters (MPCs) or if the crystal structure could be solved as nanocrystals.[62,63] They are mostly protected by thiolates and are thus denoted as $Au_n(SR)_m$, where *n* and *m* represent the number of gold atoms and thiolate ligands, respectively. In addition, they posses a so-called magic number of gold atoms, in which the core is *per se* more stable than others. The exceptional stability of these particles arises from the shell closure of the orbitals. A total electron count of n* = 2, 8, 18, 34, 58, 92, *etc.* must be given to fulfill this requirement.[64–66] Thiols and other ligands can electrochemically stabilize the gold cluster by delocalizing or withdrawing electrons from the core of the particle into covalent bonds. The requirement of an electrochemically closed shell super atom has to fulfill the requirement ($[Au_M(SR)_N]^Z$), which can be calculated by the equation: n* = M – N – Z. The shell-closure electron count (n*) of the gold core has to correlate to one of the shell-closure numbers mentioned above.[67] They commonly feature atomically precise composition and have, as a consequence, novel properties impaired by quantum size effects. They have discrete electronic energy levels and have shown multiple optical absorption peaks in the optical spectrum as opposed to the continuous band in spherical plasmonic nanoparticles.[68–75] Figure 5 shows such an optical spectrum, in which the step-like fine structure is clearly visible. The electronic transition at 1.85 eV (peak a; 670 nm) corresponds to the LUMO ← HOMO transition which is essentially an intraband

(sp ← sp) transition. The band at 2.76 eV (peak b; 450 nm) comes from the mixed intraband (sp ← sp) and interband (sp ← d) transitions. The transition at 3.10 eV (peak c; 400 nm) mainly arises from the interband (sp ← d) transition.[61] Interestingly, the ligand with which the NPs are passivated and protected plays a decisive role for this phenomenon. For instance, NPs passivated by phosphor ligands do not show these properties in the size range of 1.5 nm[76], however, for smaller phosphine-stabilized NPs (0.8 nm) the step-wise absorption is visible.[77,78] Nanoparticles enwrapped by oligothioether ligands with sizes around 1.1 nm (*vide infra*) do not show this phenomenon either.[79–84] Most likely due to the broader size distribution[61] and/or due to the weaker thioether-gold interactions, similar to the phosphine-stabilized NPs.[76] MCPs have also other properties like fluorescence, chirality and magnetic properties and partly due to their extraordinary chemical stability they can be found in various applications in biological sensing, catalysis and biomedicine.[1,33,85]

Another interesting aspect of gold nanoparticles is the possibility of functionalization with seemingly limitless ligands which is especially appealing in the fields of medicine and biology due to the remarkable amount of potential trendsetting applications.[86,87] Some examples of these applications are found in surface functionalized AuNPs - so called gold nanoconjugates - such as citrate[88], transferrin[89] and cetyltrimethyl-ammonium bromide[90] (CTAB) which are preferably used for the cell uptake processes; amines[91] are used for antiviral activity and drug delivery; oligonucleotides for mRNA[92] or cancer cell detection[93] and antibodies for imaging[94] and photothermal therapies[95]. As an examples, gold nanoparticles can be used for immunostaining, conjugated to specific antibodies for the molecule of interest serving as contrast agents for TEM investigations[96,97] and also for other sensing and labeling applications.[53,98,99] The interparticle-distance decrease to less than the particle radius causing a change in the plasmon resonance frequency due to dipolar coupling and causes a color change from red to purple in aggregated gold nanoparticles.[53,100] This phenomenon was used later by Mirkin and coworkers for the detection of DNA, where a short target DNA strand interlinked the oligonucleotide functionalized gold nanoparticles by complementary base pairing leading to a visible color change. Nowadays, this simple concept is widely used for standard diagnostics such as pregnancy tests.[101]

Another vastly growing field in the research with gold nanoparticles is catalysis. As mentioned before, Haruta's breakthrough showed with AuNPs immobilized on solid surface the efficient catalysts' capability for the oxidation of carbon by atmospheric air.[24] These conditions were then optimized by several research groups to perform at ambient conditions, which allowed the development of practical applications such as the use of supported AuNPs as additives in gas masks

or as sensors in analytical instruments.[102–108] Other industrially relevant reactions like the epoxidation of propene, the oxidation of glucose or the formation hydrogen peroxide were also found to be efficiently promoted by metal oxide supported AuNPs.[109] It is believed that the use of AuNPs as catalysts can lead to more efficient and therefore more environmentally friendly large scale industrial processes.[110] In addition, manifold reactions transformations with AuNPs supported on metal oxides can be performed nowadays such as oxophilic activation of epoxides, carbonyl compounds, and alcohols; alkyne activation for cyclizations; hydrosilane activations; dihydrogen activation; and C-C coupling reactions to name a few.[27]

Gold nanoparticles also play a special role in the field of nanoelectronics. Specifically, functional molecular switches on AuNPs are a growing branch still mainly focusing on fundamental research but already with a few practical applications.[111] This field of research requires the combination of the design and synthetic capabilities of both fields of research, supramolecular and materials chemistry. As potential switches azobenzenes[112], spiropyrans[113], dithienylethes[114], pseudorotaxanes[115], bistable catenanes[116] or bistable rotaxanes[117] are promising candidates. The ligands additionally comprise good anchoring units (depending on the metal; *e.g.* alkylated thiols or thiolanes for gold) for the binding and stabilization to form well-defined self-assembled monolayers (SAMs) on the metal nanoparticles.

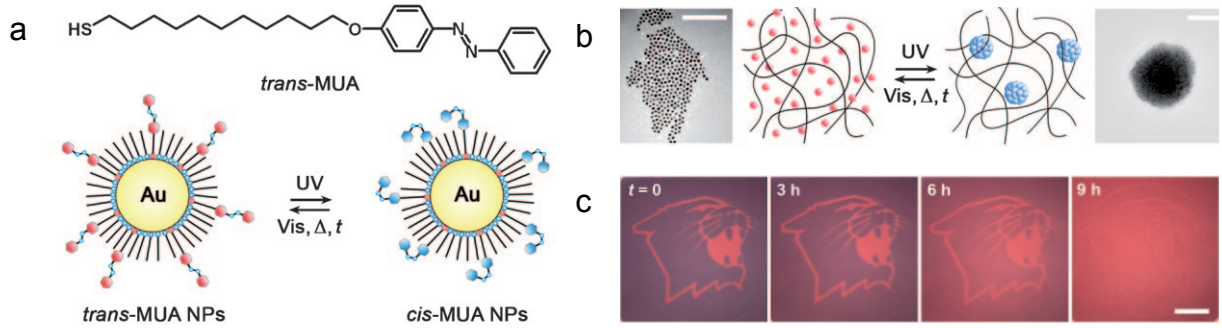

Figure 6: Reversible aggregation of photoactive nanoparticles. a) Structural formula of *trans*-4-(11-mercaptoundecanxy)-azobenzene (trans-MUA) and schematic illustration of the UV irradiation of causing trans-MUA to cis-MUA. b) Singly dispersed NPs (red) and aggregated NPs upon UV irradiation. c) Images created on AuNPs in a polymer gel by exposure through a transparency mask.[112]

These switches can be triggered by an external stimulus like light, chemically (redox) or by pH changes, depending on the switch, leading to modifications in the optical, electrical, magnetic, fluorescent, controlled release or aggregation properties of the NPs.[111] Note that rotaxanes or catenanes usually comprise electron-deficient moieties in the macrocycle and a rod comprising tetrathiafulvalenes (TTF, redox active) or dioxynaphtalenes (DNP, electron-efficient) as driving

forces, causing the threading or dethreading of the superstructures. An interesting example with potential application is shown by Klajn *et al.* where a metastable nanoparticle "ink" was used for writing self-erasing images.[112] Functional AuNPs were synthesized with *trans*-4-(11-mercaptoundecanxy)azobenzene (trans-MUA) and dodecylamine (DDA) as mixed SAM (Figure 6 a). Irradiation of the NPs with UV light or elevated temperature formed the cis-MUA, caused its aggregation into supraspherical assemblies within the film due to the created large dipole moment (Figure 6 b). They were embedded in thin, flexible organogel films and irradiated with a mask (Figure 6 c). The aggregated particles became bluish due to their increased plasmon resonance, whereas the apparent color depends on the duration of UV irradiation and the AuNP film self-erased in daylight within 9 hours.

Another exciting example of molecular switches on NPs with a potential application is shown by the group of Stoddart and coworkers, creating dynamic hook-and-eye nanoparticle sponges.[117] Redox active AuNPs stabilized by a mixture of electron-efficient diethyleneglycol-substituted TTF-moieties and triethyleneglycol dithiolanes (Figure 7 a). On the other hand, a polymer network with a crosslinked polymethacrylate backbone comprises the electron-deficient poly(cyclobis-paraquat-*p*-phenylene (PMMA-CBPQT^{4+}) side-chains.

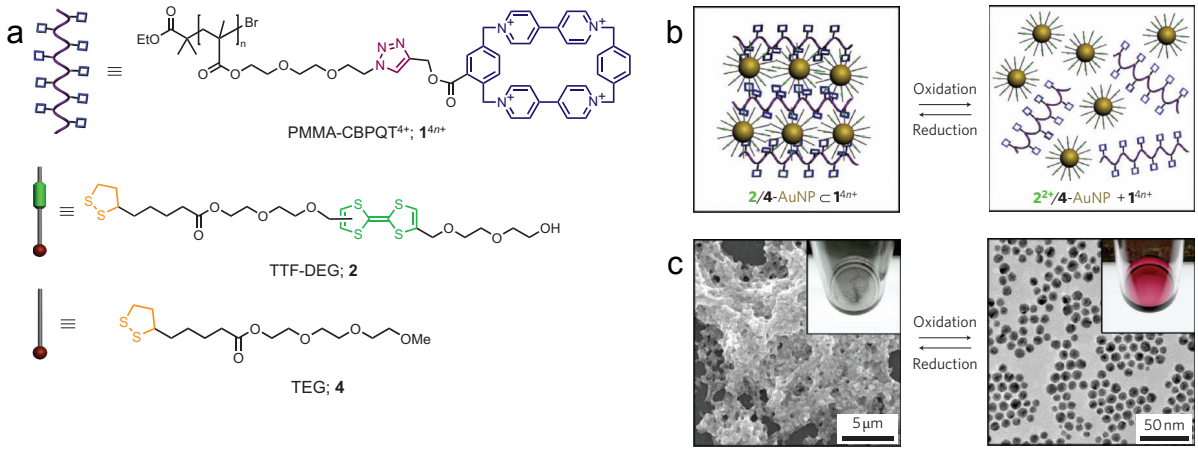

Figure 7: Complexation of electron-rich nanoparticles with an electron-deficient polymer. a) Chemical structures of the components. b) Schematic representation of the complexation and decomplexation *via* oxidation or reduction, respectively and c) SEM image (left) of the insoluble sponges due to formation of polymer-NP-superassemblies and TEM image (right) of the dispersed NPs in solution.[117]

By mixing both components with a distinct ratio (to avoid possible 'enveloping' of one over the other component) the superassembly crushes out of the solution as a sponge, while upon chemical oxidation of the TTF-moiety decorated on the NPs, both components become singly dispersed in solution (Figure 7 b and c). The interactions between the polymer and the NPs are mediated by the

reversible formation of polypseudorotaxanes *via* non-covalent bonding interactions. As a drawback for future applications, the polymer/NP sponges are limited to acetonitrile as solvent, since even minute addition of other polar solvents (*e.g.* water, dimethylformamide, or methanol) disrupt the hydrogen bonding within the pseudorotaxanes and causing their dissociation.

1.3 Thioether-Coated Nanoparticles and Previous Work

Thiolates are the most intensively investigated ligands since Brust and Schiffrin introduced their two-phase protocol.[30] Their main advantage is the high stabilization due to the strongly bound ligand shell to the NPs' surface. Long alkyl chains have been extensively used for this purpose.[1,32] However, when the objective is to give a functionality to the particles for further studies or applications, the use of these ligands could become disadvantageous, as many of these ligands are needed to stabilize an entire particle, leading to an uncontrolled number of functionalities on the NPs' surface. On the other hand, other functional groups which also show binding affinity to gold - albeit weaker than thiols - are phosphines[118], amines[119] and thioethers. Within this thesis, macromolecular multidentate thioethers are selected as the stabilizing ligands with the aim to reduce the number of ligands and control the number of functionalities per particle. Thioethers are found to bind less strong than thiols[120] but have in return the ability to bind in cooperative manner and still stabilize AuNPs sufficiently.[121] The importance of the cooperative stabilization of thioethers was already shown in 2001 by Reinhoudt and collaborators. Tetradentate alkyl thioethers showed a higher NP stability over the monodentate thioether ligand due to higher thioether denticity.[122] Since then, many other similar structures such as dendrimers[123–128] and polymers[129–131] comprising multidentate thioether-moieties were investigated for the synthesis of gold nanoparticles. The drawback of polymers is their large dispersity in molecular size and thus difficulties in tailoring the properties of the NPs. Dendrimer-structures, on the other hand, exhibit a precise structural entity that form tailor-made nanoparticles with a low integer number of ligands enwrapping the particles. However, this strategy remains challenging due to the synthetic complexity and the limited stability of the as-synthesized NPs due to insufficient repulsive units. The desire of long-term stable, monodisperse and monofunctional NPs for its applications in molecular electronics as stable building blocks or as sensing objects, keep researchers focus on this appealing fundamental research based on oligothioether ligand-stabilized NPs. In 2008 Peterle *et al.* investigated linear thioether oligomers to stabilize AuNPs.[80] Bi-, tetra-, hexa- and octadentate thioether ligands with a *m*-xylene comprising a *tert*-butyl backbone (Figure 8) were synthesized and studied. Interestingly, the longer octadentate ligand showed the highest NP stability features and smallest dispersity with a size of 1.1 ± 0.3 nm. The benzylic thioethers gave the essential flexibility

and the *tert*-butyl group decorated on the benzenes as bridges rendered a sufficiently large ligand shell to ensure long-term stability and redispersibility in common organic solvents.[80] This study supports the overall foundations for using thioether-based ligands: denticity, thioether flexibility and extention of the ligand shell are crucial characteristics to increase the stability and monodispersity of AuNPs. In addition, the fact that the NPs were stabilized by only two heptameric ligands led to appealing approaches to obtain bi-functionalized NPs (Figure 8).

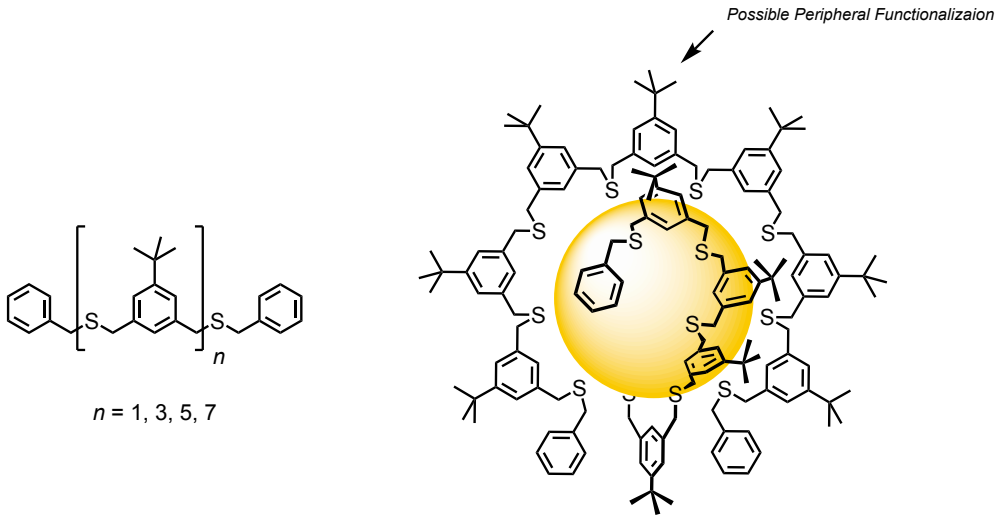

Figure 8: *Left:* Molecular structure of linear thioether ligands used to stabilize AuNPs. *Right:* Schematic illustration of two heptameric ligands enwrapping a NP and possible future functionalization.[80]

To this aim, modified ligands with one external functional group were prepared. Benzylic thioethers were assembled in linear oligomers to form octadentate ligands with the central benzene functionalized with an oligo(phenylene-ethynylene) (OPE) (Scheme 1).[79] Functional AuNPs were then obtained and the detailed investigation showed that the AuNPs are, on average, bifunctionalized with two terminal protected acetylenes with sizes of 1.1 ± 0.3 nm. These acetylenes were employed to covalently assemble the NP monomers and form NP organic-inorganic superstructures by an oxidative homocoupling protocol. Divalent NPs were also formed by Stellacci and coworkers, in which they selectively functionalized AuNPs by ligand exchange.[132] This exchange was found to be favored at diametrically opposed positions due to polar defects occurring when a curved NP surface is coated with an ordered monolayer. The divalent NPs were used to form 1D-chains with different NP distances depending on the diamine linker used for the assembly.[132] In the case of Peterle, the observed interparticle distances were considerably shorter than the full stretched length of the rigid functional linkers. The central benzene units of the ligands are likely to adopt a tilted arrangement with respect to the nanoparticle surface. This issue was later studied by Hermes and coworkers and could be overcome by the replacement of the central OPE-functionalized benzene unit by a pyridine-derivative. The pyridine-based ligands reflected the

calculated length of the rigid-rod spacer in their interparticle distances due to coordination of the pyridine's lone pair to the gold surface.[83]

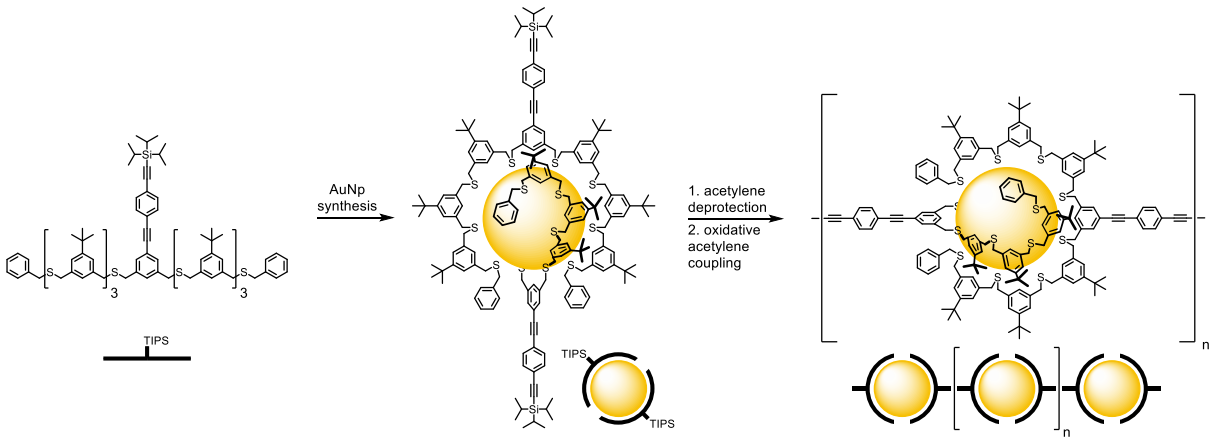

Scheme 1: The concept of using pre-functionalized ligands to introduce the desired functionality already within the NPs formation to form 'artificial molecules' as organic-inorganic oligomer or polymers.[79]

As this approach with linear oligothioether ligands exclusively gave bifunctional NPs, dendritic ligands with well-designed structures were envisaged proposed then to obtain monofunctionalized NPs.[81] The importance of the ligand shell rendering enhanced stability and redispersity feature was reported, as ethylene bridged dendrimers featured limited long-term stability compared to the *m*-xylene bridged thioether ligands. In addition, these *m*-xylene bridged dendrimer provided NPs with a narrow size distribution centered around a diameter of 1.2 nm and were enwrapped by a single ligand, optimal prerequisites for future monofunctionalized NPs.

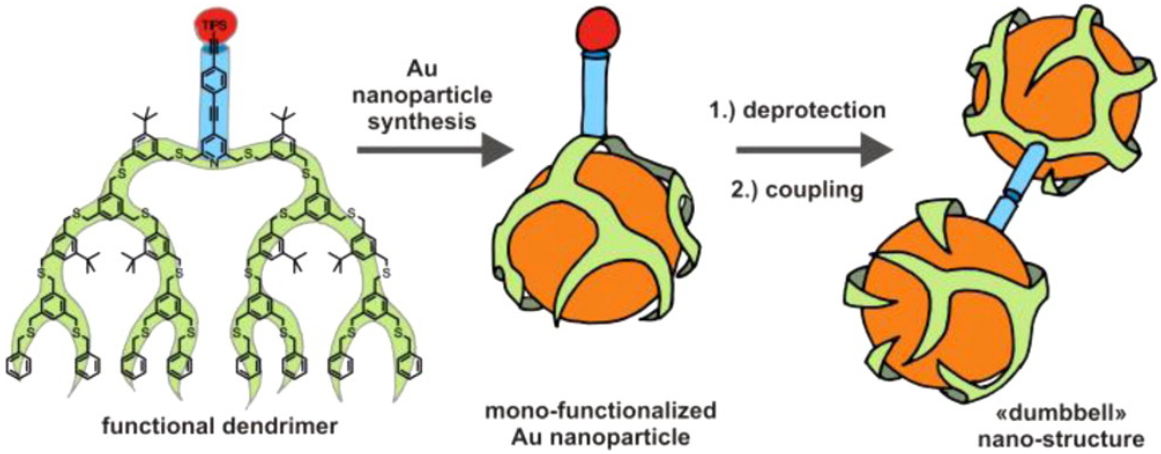

Scheme 2: General concept of forming ligand-stabilized AuNPs and NP-dimers.[82]

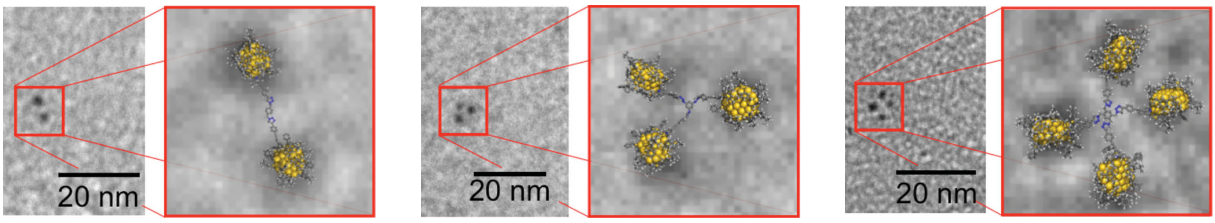

Scheme 3: Zoom with overlayed 3D sketches of the proposed structures.[84]

Based on the previous results, Hermes and coworkers synthesized a dendrimer structure comprising a central pyridine-unit for optimal peripheral arrangement of the functional OPE-rod (Scheme 2). The as-synthesized particles were as expected monofunctional with sizes around 1.3 ± 0.3 nm. The concept of forming dumbbell-like superstructures was then confirmed by using similar acetylene-homocoupling conditions as in the previous work.[82] Later, Sander *et al.* were able to form dimer, trimer and tetramer-superstructures *via* an acetylene-azide-cycloaddition click protocol together with di-, tri- and tetra-azide linker molecules (Scheme 3).[84] All formed superstructures lacked however on stability features needed for future applications.

2 Research Project and Concept

The aim of this project was to find a way how to precisely control and enlarge the size of small gold nanoparticles by using multidentate thioether-based ligands. Our strategy and design was based on previously reported benzylic thioether-based macrostructures (see *1. Introduction*). The scope of this field is geared, as a consequence, towards the synthesis of more complex systems with different bulkiness and exhibiting larger backbone-moieties (*i.e.* larger sulfur-sulfur distance); and the exploration of their feasibility in terms of size control and stability of the resulting AuNPs. We were interested in both: 1) AuNPs enwrapped by a low number of capping macromolecules, with a potential for mono-functionalization at their periphery for further wet chemical applications, and 2) size control of AuNPs, which will enable tuning of the physical and optical properties for future applications. As desired wet chemical processability requires long-term thermal stability of AuNPs and enhanced redispersibility features in common organic solvents, we focused mainly on the design and investigation of novel sterically bulky ligand structures.

This thesis is divided into three major parts, each describing the challenges of the ligands' synthesis and discussing the results of the as-synthesized AuNPs. The first part (*Chapter 3*) discusses linear oligomers with various backbone motifs of different bulky robustness and different length (sulfur-sulfur distance), and the influence of these parameters on the stability and size of the resulting AuNPs. The second part (*Chapter 4*) is based on tripodal dendritic molecular systems attached with various in length varying backbone-moieties, or cage-like structures with distinct cavity sizes and their ability to confine AuNPs. The last part (*Chapter 5*) describes a systematic study of two independent parameters and their effect on the size of the AuNPs enwrapped by various linear heptamers.

All the ligands can be described as a combination specific building blocks (BBs), shown in Scheme 4 a) that forms the backbone by their connection with a dimethyl sulfide moiety and which terminates with the end-capping ligand, 4-methylbenzyl group (grey parts in Scheme 4). Thus, a specific nomenclature is used throughout this thesis for an easy orientation of reader by helping to recognize all the final ligands with their different structural motifs just by reading their names instead of bare numbers (Scheme 4).

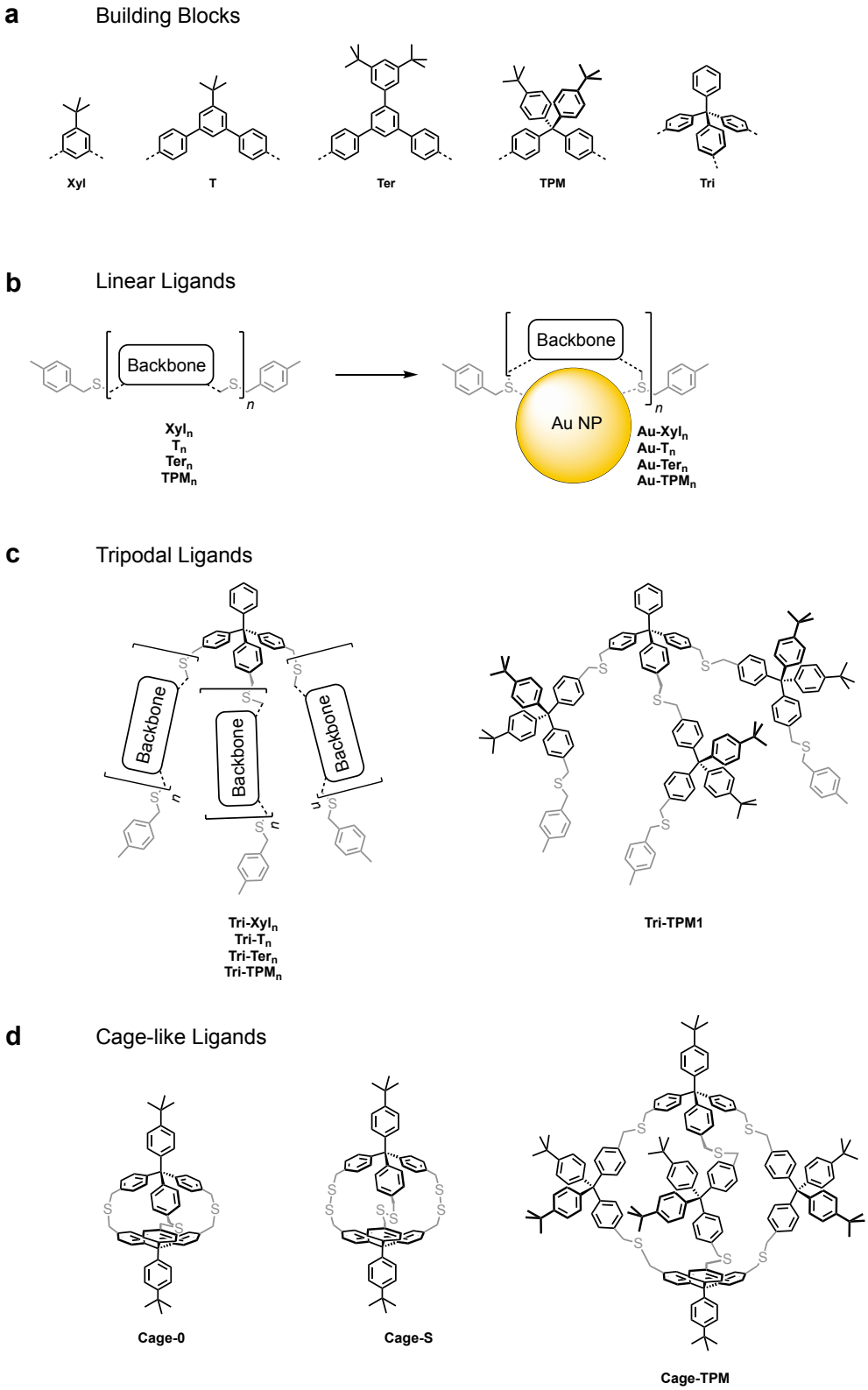

Scheme 4: Schematic illustration explaining the nomenclature used within this thesis. a) List of all the different building blocks and their corresponding abbreviations used for their names; b) nomenclature of linear oligomer and their corresponding name when stabilizing AuNPs (counts also for non-linear ligands); c) nomenclature of tripodal ligands with various in length varying side-arms. **Tri-TPM1** is shown here as an example. Note that "*n*" reflects the number of repeating units and is only here used in subscript, while the repeating numbers in the final names are written without subscripts; d) envisaged cage-like structures with their corresponding names.

The building blocks are abbreviated as follows (Scheme 4 a): **Xyl** for the *meta*-xylene-derivative, **T** for the terphenyl with a single *tert*-butyl moiety, **Ter** for the terphenyl with the additional di-*tert*-butyl phenyl group, **TPM** for the tetraphenylmethane-based derivative and **Tri** for the tripodal tetraphenylmethane-based derivative and **Cage** for cage-like derivatives.

The linear oligomers (Scheme 4 b) will be simply name by the abbreviation of the BBs followed by the number of repeating units. For example, the pentamer consisting of a backbone of five repeating tetraphenylmethane-based BBs will be named as **TPM5**, whereas the corresponding heptamer will be **TPM7**, and so on.

The dendritic tripodal-based ligands can be described as a central unit (the tetraphenylmethane BB, **Tri**) (Scheme 4 c), whose three arms are elongated by backbones based on different repetition units of BBs. Thus, these compounds will be identified by the abbreviation of the central unit (**Tri**) followed by the BB that forms the backbone and the number of repetition units. For instance, **Tri-TPM1**, will describe the dendritic tripodal ligand bearing only one tetraphenylmethane-unit per arm, and **Tri-TPM2** when tetraphenylmethane-dimers are linked as the backbone.

The cage-like structures (Scheme 4 d) are also based on tripodal tetraphenylmethane-based units bearing three symmetrical linkages. Compared to the tripodal units described before, the cage-like structures consist of a top and an identical bottom part, each with additional *tert*-butyl moieties likely to enhance their stability and redispersibility of the AuNPs. Depending on the linkages, their names will be formed accordingly: **Cage-0** when interlinked with dimethyl sulfides; **Cage-S** when interlinked with disulfides and **Cage-TPM** when the top and the bottom parts are interlinked with tetraphenylmethane-units.

Their corresponding NP stabilization will then be called **Au-TPM5**, **Au-TPM7**, **Au-Tri-TPM1** or **Au-Tri-TPM2**, **Au-Cage-0** and so on.

This doctoral thesis focuses on the synthesis of different ligands with a common focus towards the stabilization of differently sized gold nanoparticles. To maintain the central theme throughout the thesis, each chapter will start with a conceptual picture and a brief abstract in a grey box to summarize the main focus and achievements of this section, followed by a fundamental introductory motivation within the particular field.

3 Linear Ligand-Stabilized Gold Nanoparticles

3.1 Linear Terphenyl-Based Ligand Coated Gold Nanoparticles

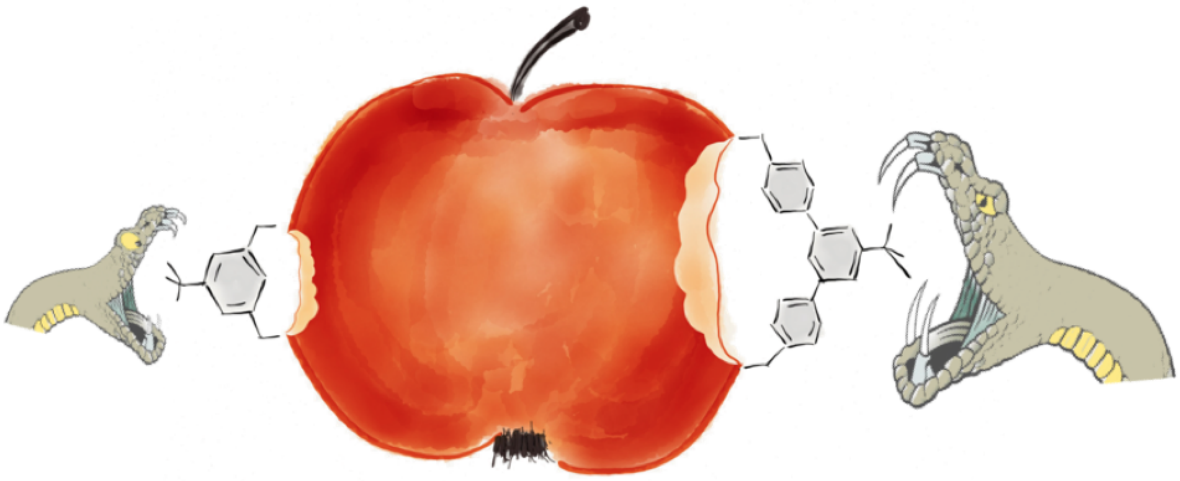

In this part, the design and the synthesis of linear multidentate terphenyl-based oligomers *via* an end-capping oligomerization strategy is presented. The spacing between neighboring sulfur atoms in the ligands backbone are increased compared to previously reported *meta*-xylene based oligomers (**Xyl**) It provides an insight of how the extension of the inter-sulfur bite-angle influences the dimensions of the synthesized gold nanoparticles. In addition, the electronic repulsion of the terphenylic oligomers comprising a bulkier di-*tert*-butyl moiety per terphenyl-backbone (**Ter**) is compared to their counterparts decorated with a single *tert*-butyl motif (**T**), and its influence on the stability of the resulting AuNPs is analyzed.

As was outlined in the introduction, the aim of this work is the systematic investigation of various parameters gearing towards increased stability and size of the synthesized gold nanoparticles. Small-sized nanoparticles (around 1.2 nm) are readily addressable by a small number of macromolecules like linear oligomers or dendrimers *via* surface coating, as it has been previously mentioned.[13] The weak interaction between a thioether moiety and the gold surface can amount considerable contribution by using multidentate oligothioether systems *e.g.* oligomers. It might even allow the macromolecule to self-rearrange for optimal conformation for the NPs coating. Inspired by this concept, various multidentate macromolecules like linear oligomers[80], and dendritic systems[81] for the stabilization of small NPs were successfully synthesized within our group. The low integer number of molecules per NPs decorated with a masked ethynyl moieties allowed the

selective formation of mono- or bifunctionalized NPs and its subsequent interconnection to create supramolecular dumbbells[82,84], trikes and quads[84] or linear pearl-necklace[79,83] hybrid materials *via* mild acetylene homo-coupling or acetylene/azide-click reactions. What all these macromolecules coated NPs have in common is that they all feature similar sizes around 1-1.3 nm with barely noticeable SPR-bands (UV-Vis). Therefore, their potential use for optical sensing applications is limited. Note that the reaction conditions were kept similar as possible throughout all the AuNPs-syntheses for better comparison along the different ligand structures. Even when comparing the dendritic ligands[81] with a fairly prior determined cage-like form, and the linear ligands[80] with no further predetermined curvature, the resulted NPs featured almost the same size. All these ligands have in common that their backbones feature the same *meta*-xylene moiety with the same the spacing between the sulfur atoms and thus the resulting bite-angle of the ligands is equal. This concept towards various-sized AuNPs by altering the distance between two sulfur motifs in a ligand was shown by Sakamoto and collaborators[133], with ligands based on pairs of interlinked thiophenols the dimensions of the stabilized NPs reflected the ligand's inter-sulfur distances. This trend has, however, never been studied on thioether ligands and we therefore wondered to which extent the ligand's design controls the dimensions of the formed NPs under otherwise the exact same applied conditions for the synthesis of AuNPs. For this purpose, two newly designed terphenyl-type oligomers (**T** and **Ter**), with increased spacing between the sulfur moieties compared to *meta*-xylene derivatives (Figure 9) were designed and synthesized. Both tailor-made terphenyl-derivatives comprise different steric repulsive groups, which will give further insight into the influence of the ligand shell systems of the AuNPs' stability (Figure 10).

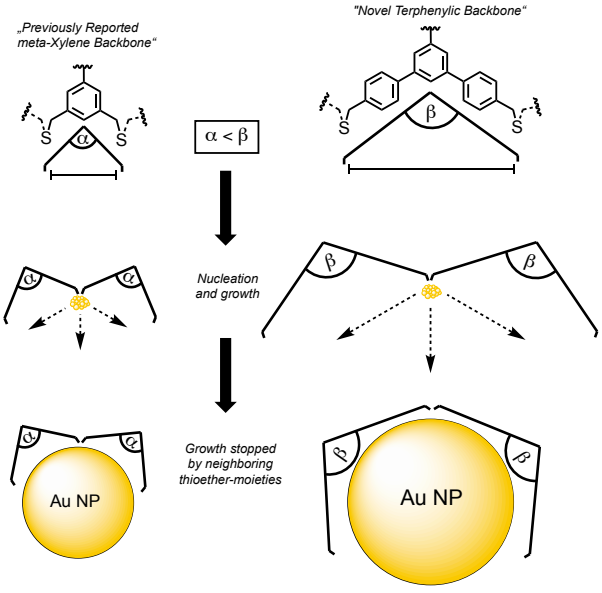

Figure 9: Representation of the increased sulfur-sulfur spacing (or bite-angle) from *meta*-xylene backbone over terphenylic backbone potentially controlling the size of the formed nanoparticles.

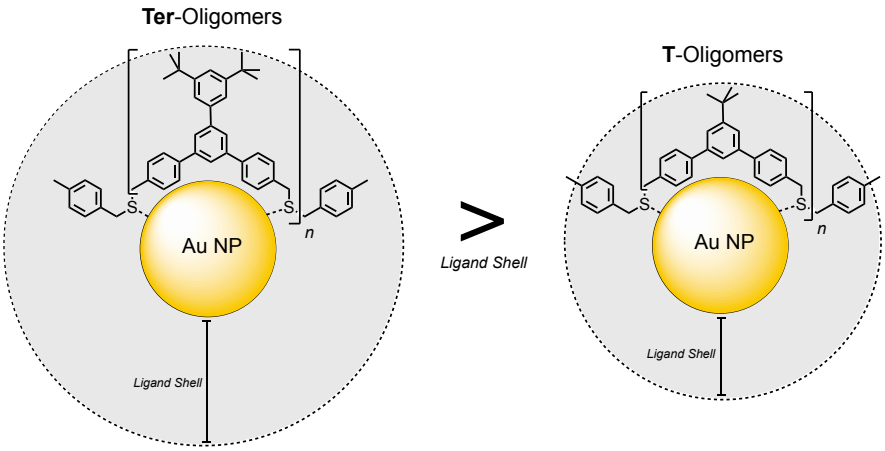

Figure 10: Illustration of the ligand shell between **Ter**- and **T**-Oligomers (n = 1, 3, 5, 7, 9).

The molecular design of the terphenylic backbone with **T** and **Ter** building blocks (BBs) combines both structural features and favorable features for the stabilization of AuNPs like the backbone's bulkiness for **Ter** oligomers provided by the 1,3-di-*tert*-butyl phenyl moiety mounted on the terphenyl linker. Furthermore, their increased spacing between the sulfur atoms (~12-14 Å, MM2 calculations) compared to the *meta*-xylene (~5-7 Å) might provide insights of how the extension of the inter-sulfur bite-angle influences the dimensions of the formed particles. The increased spacing between neighboring sulfur atoms results in more remote contact points of the multidentate ligand on the AuNPs' surface and thus, might favor the stabilization of particles of different dimensions, due to longer growth time until the NPs are fully enwrapped by the ligand. This influence is hardly considered in the literature[133] for thioether moieties and will further be investigated with the new oligomers **Ter** and **T**. Either the increased spacing influences the particle's size or it alters the arrangement of the ligand at the particle's surface, which holds the potential for new packaging motifs and ligand/particle ratios. The families of oligomers (*n* = 1, 3, 5, 7 and 9) for **Ter** and (*n* = 1, 3, 5, 7) **T** are obtained by an elaborated end-capping oligomerization strategy followed by isolation *via* automated recyclable gel permeation chromatography (GPC). Another interesting feature will be the processability and long-term stability of the AuNPs coated with the series of both oligomers **Ter** and **T**. As already mentioned in part *2. Research Project and Concept* (*vide supra*) the specific oligomers will be denoted with a number for convenience *e.g.* **Ter7** which corresponds to the heptamer of the ligand **Ter**.

3.1.1 Synthesis of the Ligands

The traditional stepwise elongation/deprotection strategy to synthesize different multidentate thioether oligomers was first proposed by Peterle *et al.* in 2008 and a sequence is depicted in Scheme 5.[80] This strategy is based on a S_N2 reaction of a dithiol derivative (*e.g.* compound **8**) and an

asymmetric trityl-protected bromo-derivative (*e.g.* compound **9**) usually at room temperature in tetrahydrofuran and sodium hydride as base to form a protected trimer (*e.g.* compound **14**). Heating would still be possible if the substitution reactions become too slow with larger, sterically more demanding nucleophiles. The next fundamental reaction within this sequence is the selective cleavage of the trityl protecting group in the presence of benzylic sulfides. The trityl group can be cleaved easily under acidic conditions in the presence of a cation scavenger, but stronger acidic conditions may also cleave the benzylic thioether.[134] It was found that triethylsilane can act as cation scavenger very efficiently, thus allowing for very fast deprotection reactions even at low concentrations of trifluoroacetic acid.[135] Dithiol trimer (*e.g.* compound **15**) can then either be elongated to form the trityl-protected pentamer (*e.g.* compound **16**) following the pathway to higher order oligomers, or end-capped (with for instance benzyl bromide) to form the final trimer.

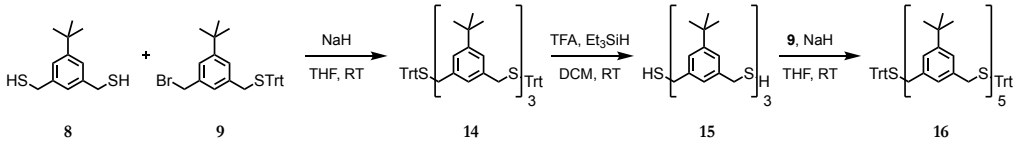

8 **9** **14** **15** **16**

Scheme 5: Sequence of the elongation/deprotection strategy proposed by Peterle and coworkers (Trt = trityl).

The usual high yields of these steps make this strategy appealing if large amounts of higher order oligomers are needed in the final AuNPs' synthesis. However, the multiple steps make this strategy to some extent laborious and mainly time consuming and large amounts of starting material are needed. We therefore sought for alternative strategies to form such oligomers more efficient, in order to quickly access oligomers with specific backbones for the investigation and synthesis towards stable gold nanoparticles. Thus, a one-pot end-capping oligomerization reaction was proposed, which is based on multiple reactions between two building blocks and the formed oligomers will eventually be end-capped with a suitable stopper. The formed oligomers are then separated and purified by size exclusion chromatography.

The one-pot end-capping oligomerization strategy has the advantage of making the entire family of oligomers in a single reaction. However, it also requires the subsequent separation of the individual members must be separated by chromatography, or more precisely automated recyclable gel permeation chromatography (GPC). This separation technique is based on the separation of different molecules according to their hydrodynamic radii. Note that this end-capping oligomerization reaction only provides odd-numbered oligomers (1, 3, 5, 7 *etc.*) as the use of the end-capping reagent defines the bisbenzylthiol (yellow backbone in Scheme 6) as terminal building block trapped at both ends of the oligomer chain. Furthermore, the formation of the oligomers is

expected to be sensitive to changes in the stoichiometry of BBs, which enables the tuning towards the formation of a specific oligomer. That means for example, if a heptamer is needed, which consists of seven building blocks as backbone (and two end-capping units), the reaction can be performed with 4:3 molar ratio between the dithiol precursor and the bromine precursor (or vinyl). If, however, the whole family of oligomers are needed, a 2:1 molar ratio between the precursors is likely to be best suited. In addition, 4-methylbenzyl bromide or 4-methylstyrene were chosen as possible end-capping units due to their characteristic ^{1}H-NMR signals simplifying the oligomers identification considerably. The protons residing on the methyl moiety as well as the upfield shifted AB-system recorded for the aromatic protons allows those signals to be used as internal standards to identify the particular member of the oligomer family by comparison of the integrals of the ^{1}H-NMR signals.

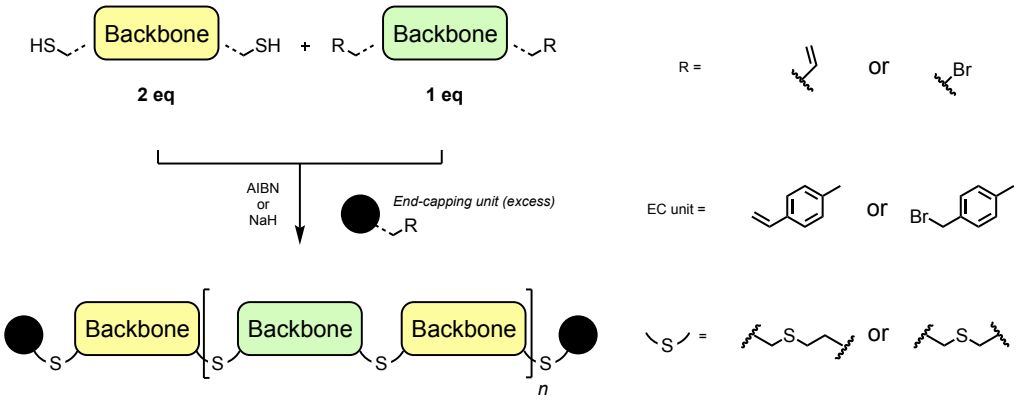

Scheme 6: Schematic illustration of the end-capping oligomerization strategy either *via* radical thiol-ene photopolymerization or S_N2-reaction initiated with azobisisobutyronitrile (AIBN) or sodium hydride (NaH), respectively (n = 0, 1, 2, 3 *etc.*).

Our first approach to obtain the desired oligomers focused on a one-pot end-capping oligomerization reaction based on radical-mediated thiol-ene polymerization reaction (Scheme 7). Thiol-ene polymerizations are well-known in literature since they are 1) highly efficient, 2) simple to execute and 3) proceed rapidly in high yields with almost no side-reactions.[136] The precursors **3** and **4** were synthesized as follows: standard Suzuki-Miyaura protocol was applied for 1,3-dibromo-5-(*tert*-butyl)benzene in tetrahydrofuran and water, either with *p*-tolylboronic acid to form compound **2**, or with 4-vinylbenzeneboronic acid to give precursor **5** in good yields, respectively. Wohl-Ziegler type bromination under mild conditions of compound **2** following the protocol of Peterle *et al.*[80], with *N*-bromosuccinimide as bromine source and azobisisobutyronitrile (AIBN) as radical starter in refluxing methyl formate yielded the dibromine derivative **3** in 84 %. Notably, the reaction had to be performed under argon atmosphere, as significant loss in yield was observed in

the presence of quenching oxygen. The dibromine-precursor **3** was then treated with thiourea as sulfur source in dimethyl sulfoxide (DMSO) for 15 hours at 40 °C. An excess of dichloromethane was added to precipitate the formed isothiouronium salt and washed with additional dichloromethane. The solid was then redissolved in degassed methanol and the reaction mixture was first hydrolyzed with a degassed aqueous solution of sodium hydroxide and then protonated with degassed aqueous hydrochloric acid, forming the dithiol-precursor **4** in a yield of 80 %.

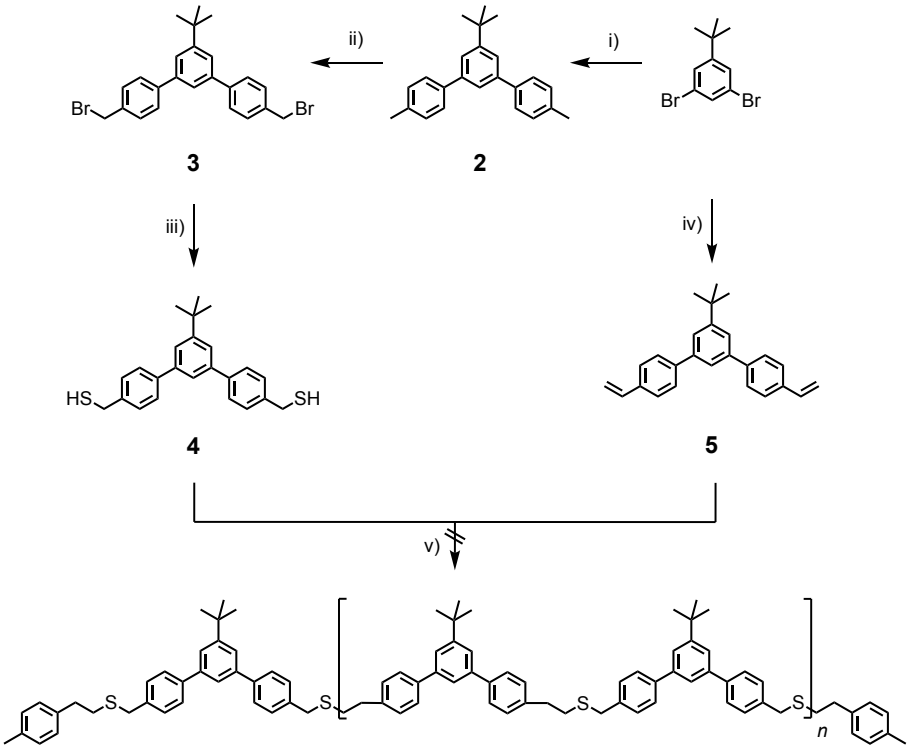

Scheme 7: Molecular structures and synthesis towards precursors **4** and **5**, and final end-capping oligomerization reaction *via* thiol-ene coupling (n = 0, 1, 3 *etc.*). i) *p*-Tolyl boronic acid, $Pd(PPh_3)_4$, K_2CO_3, THF/H_2O, reflux, 15 h, quant.; ii) *N*-bromosuccinimide (NBS), azobisisobutyronitrile (AIBN), methyl formate, hν, reflux, 84 %; iii) 1) thiourea, DMSO, 40 °C, 15 h, 2) DCM, 3) MeOH, 1 M aq. NaOH, 1 M aq. HCl, MeOH, 3 h, 80 %; iv) 4-vinylbenzeneboronic acid, $Pd(PPh_3)_4$, K_2CO_3, THF/H_2O reflux, 24 h, 82 %; v) 1) AIBN, THF, 15 min, 2) 4-methylstyrene, 15 h.

For the end-capping oligomerization *via* thiol-ene coupling, precursors **4** (14.8 mM) and **5** (7.4 mM) were dissolved in distilled tetrahydrofuran and the reaction mixture was degassed with argon for 10 minutes, in order to avoid major disulfide formations. Azobisisobutyronitrile were added and a UV-lamp used to initiate the oligomerization. After 15 minutes, an excess of 4-methylstyrene (29.6 mM) as end-capping unit was added to prevent further oligomerization and the reaction mixture was kept stirring overnight at room temperature. Precipitates were formed overnight that unfortunately were not soluble in organic solvents, and almost no compounds were left in solution that could be analyzed. It is likely that the oligomerization was too fast, forming insoluble polymers

before the end-capping unit could prevent longer chain formations. These results made us focus on a new strategy based on a one-pot end-capping *via* S_N2 oligomerization. This second approach has also the advantage of a higher symmetry in the final structure of the oligomers which facilitates the analysis of the desired products.

The synthetic plan (shown in Scheme 8) with the already synthesized precursors **3** and **4** leads to the formation of the oligomers $\mathbf{T_n}$. In addition, to improve the solubility of the target oligomers, and consequently, of the final AuNPs, new terphenyl compounds with an additional 1,3-di-*tert*-butylphenyl moiety was designed (precursors **21** and **22**), whose oligomerization *via* S_N2 leads to the oligomers $\mathbf{Ter_n}$. The precursors **21** and **22** were synthesized as follows: in the first step, mono-iodination of 1,3,5-tribromobenzene was achieved following the protocol of Lustenberger and coworkers[137] followed by a standard Suzuki-Miyaura protocol with 1,3-di-*tert*-butylphenylboronic acid in toluene and water giving compound **19** in yield of 60 % over two steps. Subsequent Suzuki coupling with **19** and *p*-tolylboronic acid in tetrahydrofuran (THF) and water gave compound **20** in 90 % yield. Bromination under mild conditions following the protocol of Peterle *et al.*[80], with *N*-bromosuccinimide as bromine source and azobisisobutyronitrile (AIBN) as radical starter in refluxing methyl formate yielded the dibromine-precursor **21** in 90 %. Again, the argon atmosphere was essential to minimize the amount of side-products. The dibromine-precursor **21** was then treated with thiourea as sulfur source in dimethyl sulfoxide (DMSO) for 15 hours at 40 °C. Upon addition of dichloromethane a precipitate (thiouronium salt) was formed, which was washed with additional dichloromethane and redissolved in degassed methanol. The solution was then first hydrolyzed with a degassed aqueous solution of sodium hydroxide and then protonated with degassed aqueous hydrochloric acid, forming dithiol-precursor **22** in acceptable yield of 56 %. This yield was considerably improved for precursor **22** (over two steps) with the following pathway: compound **21** was first reacted with an excess of trityl mercaptane and sodium hydride in tetrahydrofuran replacing both bromines with protected sulfurs (compound **23**, see *7. Experimental Part*), which were then easily cleaved with trifluoroacetic acid in presence of triethylsilane as cation scavenger in dichloromethane at room temperature, to give precursor **22** in 86 % yield. Both final end-capping oligomerization reactions were performed with one equivalent of the dibromine precursor **3** (23 mM) or **21** (18 mM), and two equivalents of the dithiol-precursor **4** (46 mM) or **22** (36 mM), respectively. In a typical procedure, the reactants were dissolved in distilled THF and the reaction mixture was degassed with argon for 10 minutes (preventing major disulfide formations) before adding sodium hydride (NaH) as base to initiate the oligomerization. After 15 minutes, an excess of 4-methylbenzyl bromide as end-capping unit was added to prevent further oligomerization and the reaction mixture was kept stirring overnight at room temperature.

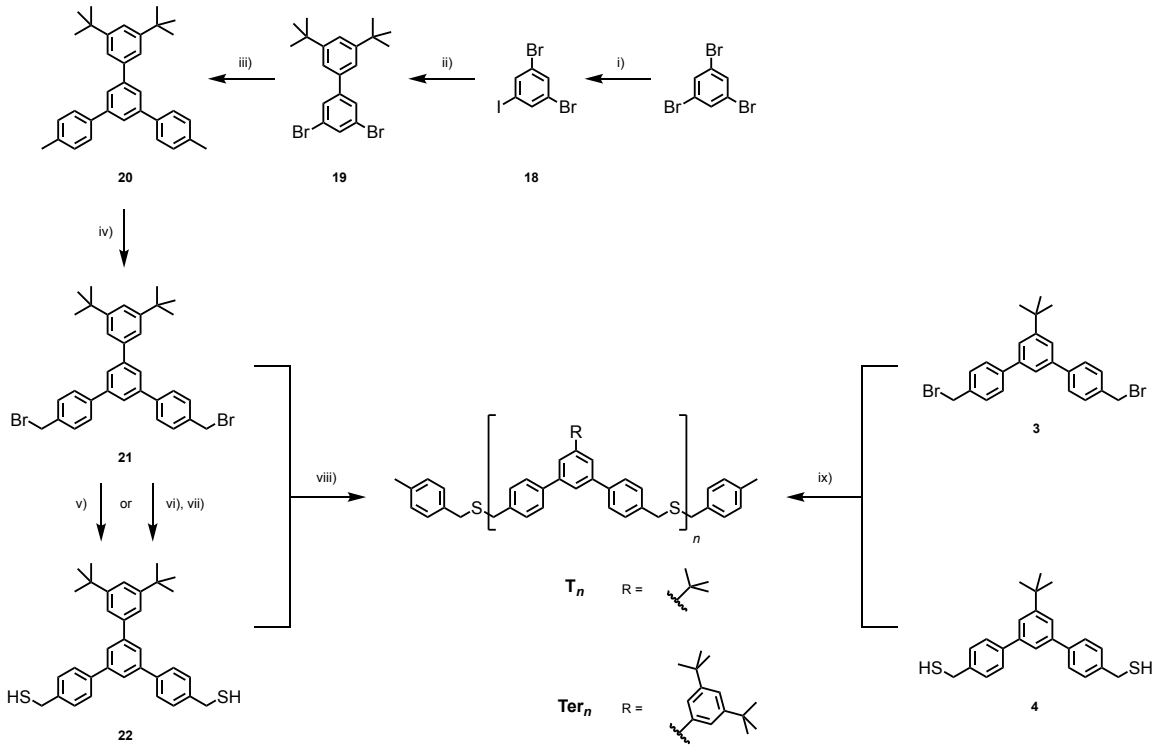

Scheme 8: Molecular structures and synthesis towards precursors **21** and **22**, and end-capping oligomerization reactions towards linear terphenyl-based thioether oligomers **Ter** and **T** (*n* = 1, 3, 5, 7 and for Ter including *n* = 9) i) 1) *n*-BuLi, Et_2O, -78 °C -> -20 °C, 1.5 h 2) I_2, -78 °C, 71 %; ii) (3,5-di-*tert*-butylphenyl)boronic acid, $Pd(PPh_3)_4$, K_2CO_3, toluene/H_2O, 90 °C, 15 h, 85 %; iii) *p*-tolyl boronic acid, $Pd(PPh_3)_4$, K_2CO_3, THF/H_2O, 80 °C, 24 h, 90 %; iv) *N*-bromosuccinimide (NBS), azobisisobutyronitrile (AIBN), methyl formate, hν, reflux, 90 %; v) 1) thiourea, DMSO, 40 °C, 15 h 2) DCM 3) MeOH, 1 M aq. NaOH, 1 M aq. HCl, 3 h, 56 %; vi) trityl mercaptane, sodium hydride (NaH), THF, RT, 3 h, 91 %; vii) **23**, trifluoroacetic acid, Et_3SiH, DCM, RT, 15 min; viii) and ix) 1) NaH, THF, 15 min 2) 4-methylbenzyl bromide, 15 h; **T1**: 41 %, **T3**: 22 %, **T5**: 7 %, **T7**: 4 %; **Ter1**: 50 %, **Ter3**: 12 %, **Ter5**: 3 %, **Ter7**: 2 %, **Ter9**: 1 %.

After a quick workup and filtration, the oligomers were isolated *via* automated recycling GPC in chloroform as eluent. This separation technique is based on the separation of different molecules according to their hydrodynamic radii. For each oligomer, more than 24 hours were required to separate them from the side-products exhibiting very similar hydrodynamic radii, which are probably oligomers comprising disulfide linkages caused by oxygen residues present in the reaction mixture. However, extensive degassing of the reaction mixture for a longer period of time did not lead to any further improvements. The oligomers of $\mathbf{T_n}$ and $\mathbf{Ter_n}$ could be separated and purified successfully by this method in following yields: monomer **T1** in 41 %, trimer **T3** in 22 %, pentamer **T5** in 7 % and heptamer **T7** in 4 %; and **Ter1** in 50 %, **Ter3** in 12 %, **Ter5** in 3 %, **Ter7** in 2 % and **Ter9** in 1 %. Note that the addition of the end-capping unit in a later point of time (*i.e.* >15 min) did not increase the isolable yield, but increased the amount of side-products. As mentioned

before, this one-pot end-capping oligomerization protocol is sensitive to changes in stoichiometry and was tested for heptamer **Ter7**: Since heptamer **Ter7** consists of seven building blocks (and two end-capping units), the reaction was performed with 4:3 molar ratio between the dithiol-precursor **22** (12.8 mM) and the dibromine-precursor **21** (10.3 mM). With this specific ratio, the yield of heptamer **Ter7** could be increased to 8 %.

3.1.2 Synthesis of the Gold Nanoparticles

The formation of AuNPs stabilized with the oligomers of $\mathbf{T_n}$ and $\mathbf{Ter_n}$ was carried out following the protocol of Brust *et al.*[30] with minor modifications. To ensure full comparability with former studies on thioether stabilized gold nanoparticles[79–84], a 1:1 molar ratio of thioether moieties to gold equivalents was maintained *i.e.* 8 molar equivalents Au(III) compared to 1 molar equivalent of the octadentate heptamer **Ter7**. In a typical procedure (Scheme 9), tetrachloroauric acid was first dissolved in deionized water and transferred to the organic phase upon addition of tetra-*n*-octylammonium bromide and stirred for 10 minutes. The ligand dissolved in dichloromethane was then added to the reaction mixture. After 15 minutes, the reduction of Au(III) to Au(0) was performed by adding an aqueous solution of sodium borohydride ($NaBH_4$) quickly to the two-phase system. For completion of the reducing process, stirring for another 15 minutes was required. After work up by precipitation of the formed AuNPs with ethanol, centrifugation and subsequent manual size exclusion chromatography, the obtained gold nanoparticles were analyzed by UV-Vis, transmission electron microscopy (TEM) and for **Ter7** and **Ter9** additional ^{1}H-NMR due to their increased stability.

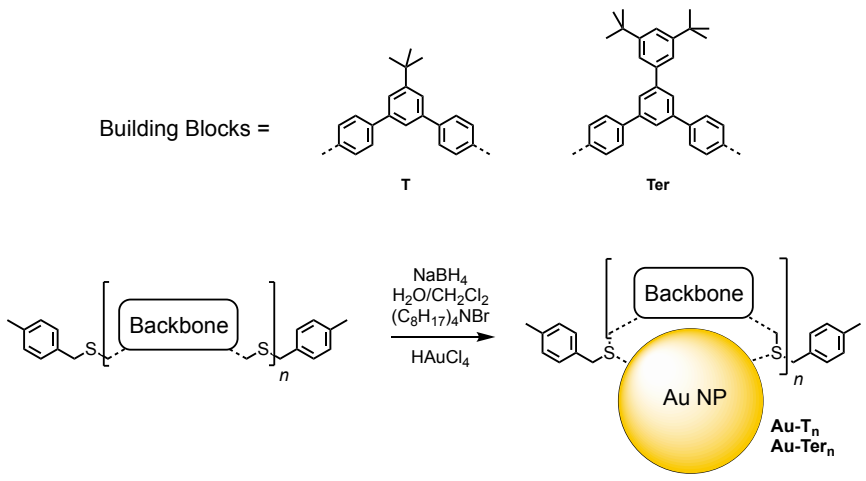

Scheme 9: Concept of AuNPs formation with the oligomers of **T** and **Ter** (n = 1, 3, 5 *etc.*).

3.1.3 Results and Discussion

Considering AuNPs coated by the terphenylic oligomers comprising just the *tert*-butyl group (**T1**, **T3**, **T5** and **T7**), the formed NPs readily precipitated out of the dark brown solution during their synthesis after about 3 minutes.

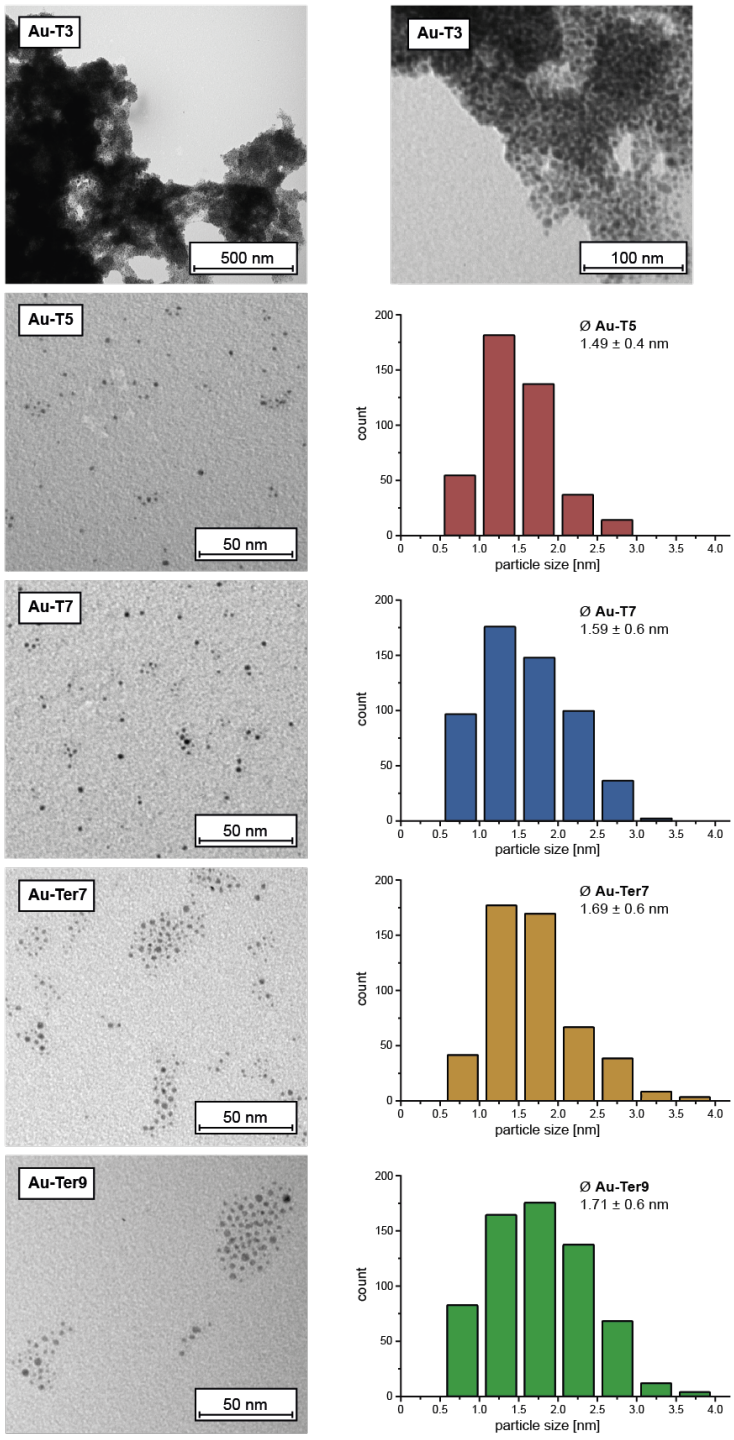

Figure 11: Left: Representative sections of the TEM micrographs for samples of oligomer-stabilized nanoparticles **Au-T3**, **Au-T5**, **Au-T7**, **Au-Ter7** and **Au-Ter9**. Right: size distribution of the particles observed in the TEM micrographs (except for **Au-T3**).

This could be observed by the naked eye as a black solid floated in the solution. Eventually, the dark brown solution turned colorless after approximately 7 minutes. The reason for the precipitation is due to coagulation of contacting NPs forming insoluble agglomerates. This indicates that the single *tert*-butyl motif on the terphenylic system does not offer enough steric repulsion; or in other words, the ligand shell of the NPs is too thin to prevent their coagulation even for higher order oligomers. Nevertheless, the black solids were washed with an excess of DCM, water and diethyl ether to get rid of remaining phase-transfer catalyst and residues of the base as well as excess ligands. Note that coagulation does not necessarily mean that the ligands are no longer binding to the AuNPs. Different attempts at trying to disperse the AuNPs by various common organic solvents failed. However, upon sonication in toluene for 15 minutes, a major part was indeed dispersed turning the solution dark brownish, allowing at least a few following measurements like UV-Vis absorption spectroscopy and TEM analysis. The concentration of dispersed AuNPs was too low for ^{1}H-NMR analysis, as no signals were observed even after longer sonication. **Au-T1** could not be redispersed by sonication; the solution of **Au-T3** was slightly colored, while fairly intense dark brownish solutions were observed in the case of **Au-T5** and **Au-T7**. TEM analysis (Figure 11) of **Au-T3** shows almost no singly dispersed NPs but large agglomerates discussed above, which - zoomed in - consists of single AuNPs. One can therefore assume that they are still enwrapped by the ligands, but size distribution calculations could therefore not be performed. Such large agglomerates were in fact also observable in the case of **Au-T5** and **Au-T7**. They were, however, a lot less numerous, and mostly single dispersed AuNPs could be observed. These findings are in agreement with the color intensities of previously discussed solutions. **Au-T5** feature a size distribution of 1.49 ± 0.4 nm, while for **Au-T7** a size distribution of 1.59 ± 0.6 nm was calculated, respectively. The UV-Vis spectra (Figure 12) confirm these results, as the absorption of **Au-T5** and **Au-T7** are very similar. However, a more prominent absorption peak around 520 nm was expected for these NPs with the calculated sizes, which might be attributed to the poorly dispersed nanoparticles.

The synthesis of the nanoparticles comprising the terphenylic ligands with the di-*tert*-butylphenyl motif (**Ter1**, **Ter3**, **Ter5**, **Ter7** and **Ter9**) performed - in contrast to the above stated ligands - much better, meaning that no precipitations was observed during the reaction. To our delight, the solutions featured a slight reddish hue, pointing towards larger AuNPs compared to previously reported NPs, which themselves were dark brown in solution.[79–84] This already shows at this stage that the bulkier di-*tert*-butylphenyl moieties provide a larger and therefore better ligand shell surrounding the nanoparticle compared to the single *tert*-butyl moiety per terphenylic unit. The organic phases were then transferred into falcon tubes and the solvent was reduced to a volume of

about 1 ml in a steady stream of nitrogen, followed by precipitation upon addition of ethanol and centrifugation. During this work up step, excess of possible TOAB potentially co-stabilizing the AuNPs was removed.[138] AuNPs stabilized by monomer **Au-Ter1** could however no longer be redispersed after this process, neither upon sonication in toluene. Gold nanoparticles **Au-Ter3** and **Au-Ter5** revealed their weak stabilizing ability as they got stuck on the manual size exclusion chromatography (Biobeads SX-1) eluting with dichloromethane and therefore no further analysis was possible.

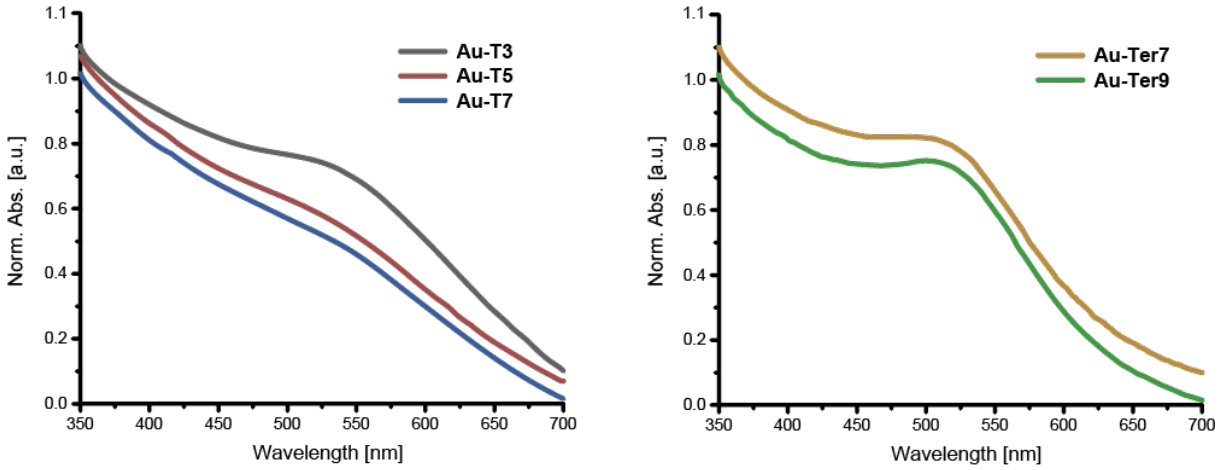

Figure 12: Normalized UV-Vis absorption spectra of the oligomers stabilized nanoparticles **Au-T3**, **Au-T5**, **Au-T7** (left; recorded in toluene) and **Au-Ter7** and **Au-Ter9** (right; recorded in dichloromethane). The individual absorption spectra are shifted vertically for clarity.

This purification-step usually serves to remove excessive ligands that did not stabilize the particles. For gold nanoparticles **Au-Ter7** and **Au-Ter9**, on the other hand, this purification step did work properly and the formed nanoparticles could further be analyzed. Both ligands, heptamer **Ter7** and nonamer **Ter9** stabilize AuNPs with similar sizes (Figure 11) of 1.69 ± 0.6 nm and 1.71 ± 0.6 nm and can also be observed on the UV-Vis absorption spectra, as the absorption of the plasmon resonance band around 520 nm are almost identical. As both **Au-Ter7** and **Au-Ter9** feature the same size, it shows that the length of the ligand is not responsible for the final size of AuNPs. The SPR bands for present AuNPs with the di-*tert*-butyl terphenylic ligand system are notably more prominent than for similar AuNPs in former studies[79–84] or the AuNPs stabilized by the terphenylic ligand system comprising the single *tert*-butyl motif. Interestingly, in all measured TEM micrographs for **Au-Ter7** and **Au-Ter9**, the AuNPs are mostly arranged in groups and hardly ever as single NP as was observed with the other terphenylic system discussed above. We therefore assume that the rather long ligands enwrap several gold nanoparticles in a mesh-like fashion, sharing the NPs' coverage and thus appear in randomly arranged groups, in stark contrast to former

studies where a small distinct number of ligands (1-2) stabilize a single gold nanoparticle. This is a possible explanation why the proton-signals in the ^{1}H-NMR (see Figure 39 and Figure 40 in *8. Appendix*) of the ligands covering the NPs do not appear broadened as much as we would expect in comparison to the naked ligands, since parts of the ligands are probably not actively involved in stabilizing the NPs. In fact, thermogravimetric analysis (see Figure 41 and Table 1 for calculations in *8. Appendix*) revealed that for **Au-Ter7** in average 3 ligands are stabilizing a single nanoparticle with above mentioned sizes and 2-3 ligands for **Au-Ter9**. The rather broad size distribution, *i.e.* large standard deviation, is thought to arise from this phenomenon as well. In addition, the rather moderate stability of the formed nanoparticles - *i.e.* after several weeks in dry state the NPs were only merely dispersible - can once more be tracked back arise from these findings and therefore results of the TGA analysis have to be interpreted with care. Nevertheless, based on the observed results, the hypothesis of creating larger gold nanoparticles by increasing the sulfur-sulfur spacing *via* extending the backbone of multidentate thioether ligands is verified and thus support the work of Sakamoto and coworkers.[133]

3.1.4 Summary and Conclusions

In summary, the synthesis of linear therphenylic multidentate thioether ligands bearing a single *tert*-butyl motif (**T1**, **T3**, **T5** and **T7**), as well as a bulkier di-*tert*-butylphenyl moiety (**Ter1**, **Ter3**, **Ter5**, **Ter7** and **Ter9**), *via* an efficient one-pot end-capping oligomerization-strategy, after initial investigations with radical thiol-ene coupling is reported. With particle sizes of 1.49 ± 0.4 nm and 1.59 ± 0.6 nm for **Au-T5** and **Au-T7**, and 1.69 ± 0.6 nm and 1.71 ± 0.6 nm for **Au-Ter7** and **Au-Ter9**, respectively, our primary aim of synthesizing larger AuNPs compared to previous work by extending the distance of the thioether moieties was achieved. The limited stability and broad size distribution of NPs comprising a single tert-butyl motif per backbone (**Au-T1**, **Au-T3, Au-T5** and **Au-T7**) can mainly be attributed to the insufficiently provided solvation shell covering the gold nanoparticles, as they become more stable with the bulkier di-*tert*-butylphenylic system ligands for **Au-Ter7** and **Au-Ter9**. These bulky ligands likely stabilize the AuNPs in a mesh-like fashion, *i.e.* a ligand is coating one or more AuNPs, or a NP is stabilized by multiple ligands. We believe that this mesh-like pattern weakens their arrangement significantly resulting in moderate stability features and may either arise from the applied conditions or from the limited ability of terphenylic ligands to enwrap the NPs.

3.2 Linear Tetraphenylmethane-Based Ligand Coated Gold Nanoparticles

In this part, the design and the synthesis of linear thioether-based ligand subunits with a tetraphenylmethane core for the stabilization of gold nanoparticles are presented. Mono- (**TPM 1**), tri- (**TPM3**), penta- (**TPM5**) and heptamers (**TPM7**) of the ligand have been synthesized and successfully used to stabilize AuNPs by enwrapping. With the exception of the monomer, all ligands proved to provide reliable long-term, thermal stability and redispersibility for the coated nanoparticle in common organic solvents. Despite variation of the oligomer length, all stable particles were of the same size in the case of the penta- or heptamer, passivated by a single ligand.

In order to use AuNPs as functional subunits for of hybrid materials[139] or as molecule-like building blocks[60,140] for the integration into larger architectures by wet chemical methods[1], the following features move into the focus of interest: 1) the particle's size and shape controlling its physical properties. Thus in an ideal sample, these dimensional and structural features should be as uniform as possible. 2) The chemical nature, the number and the spatial arrangement of functional groups exposed at the particles surface as connecting points addressed by wet chemistry. 3) The stability of the particle determining the harshness of applicable reaction conditions applied for their integration/decoration by wet chemistry protocols. And finally, 4) the NPs synthetic availability and purity.

While there is a whole plethora of reports on NPs stabilized by various thiolates[62], stabilization of NPs by thioether-based structures has only been reported on rare occasions. The weakness of the

interaction between the sulfur atom of a thioether motif and the NPs metal surface is particularly appealing, as 1) it can sum-up to a considerable contribution by using multidentate oligothioether systems, and 2) it might even allow for optimization of the arrangement of the coating structure by reversible ligand particle interactions. Inspired by the concept, we explored the potential of linear[80] as well as dendritic[81] multidentate thioether systems as passivating surface coatings of small AuNPs. The integer ratios between coating ligands and AuNPs even paved the way to stable, coated particles exposing an integer number of functional groups. In particular, the use of ligands comprising a central acetylene unit yielded in coated AuNPs exposing two ethynyl groups on opposed sides in the case of linear oligomeric thioether ligands,[79],[83] and even in AuNPs with a single ethynyl handle in the case of the dendritic ligand system.[82],[84] Oxidative acetylene homo coupling protocols enabled the assembly of organic-inorganic hybrid materials as "pearl necklace"-type arrays in the case of the bifunctionalized AuNPs,[79],[83] and as dumbbell-type structures in the case of monofunctionalized AuNPs.[82] The scope of wet chemical protocols profiting from these AuNPs as artificial molecules were further widened by applying azide-acetylene click-reaction protocols to decorate oligo-azide linkers with particles resulting in dumbbell-, trike- or squad-like superstructures.[84] In all these thioether ligand structures the sulfur atoms were interlinked by a *meta*-xylene motif and the importance of having a sterically demanding ligand shell covering the rather reactive surface of a AuNP became obvious during stabilizing studies with various dendritic systems.[81] While the second generation dendrimer stabilizing an entire particle and thereby providing mono-functionalized AuNPs were ideally suited for most of the applications we had in mind, the limited synthetic availability of the macromolecular ligand handicapped the further exploration of the system. We thus kept on seeking for alternative ligand motifs combining coordinating benzylic thioethers with bulkiness sterically protecting the coated ligand.

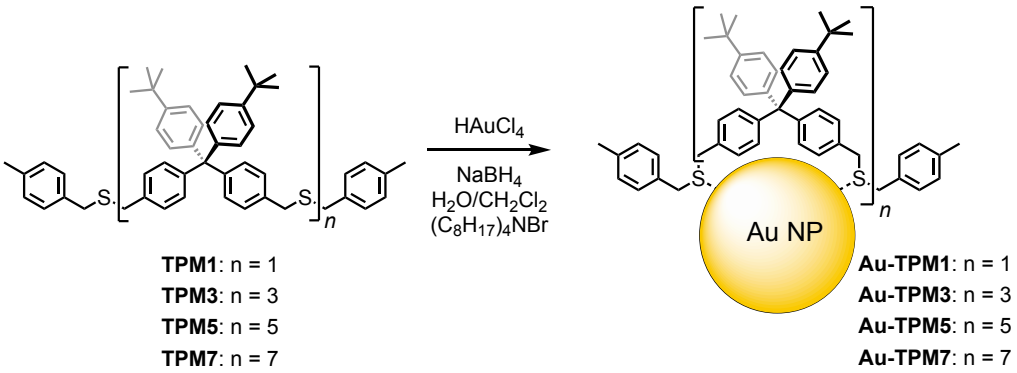

Scheme 10: Linear tetraphenylmethane-based thioether oligomers (**TPM1**, **TPM3**, **TPM5** and **TPM7**) and concept of their Au nanoparticle stabilization by surface coating.

Here, the synthetic route to the bulky tetraphenylmethane-based ligand theme and its excellent AuNPs stabilizing properties (Scheme 10) are reported. In particular, the obtained linear oligomers not only provide stable AuNPs with very good processability features, but also the pentamer **TPM5** and heptamer **TPM7** are both able to stabilize an entire particle and thus are interesting lead structures towards mono-functionalized AuNPs. The molecular design combines an increased bulkiness of the parent building block due to both, the two *tert*-butyl decorated phenyl rings and the three dimensional tetraphenylmethane core structure, with an increased spacing between both sulfur atoms compared to the *meta*-xylene motif. While the bulkiness is likely to provide solubility to both, the bare ligand as well as the coated particle, the increased spacing between neighboring sulfur atoms results in further remote contact points on the AuNPs, which should be reflected in the ligand/particle interactions. Either the increased spacing influences the particle's size as shown by the terphenylic oligomers (*vide supra*) or it alters the arrangement of the ligand at the particle's surface, which holds the potential for new packing motifs and ligand/particle ratios. The terminal sulfur atoms were again masked by 4-methylbenzyl-groups instead of the benzyl groups used so far, mainly to provide an easy to detect NMR signature of the subunit.

3.2.1 Synthesis of the Ligands

The key intermediate **33** consists of a rigid tetraphenylmethane core with two at its periphery attached *tert*-butyl moieties rendering improved solubility, and two methyl groups for further functionalization. Several routes towards this bulky precursor are summarized in the Scheme 11 and are based on electrophilic aromatic substitution reactions to forge the fourth benzene ring to - *via* double Grignard reaction synthesized - triphenylmethane alcohols.

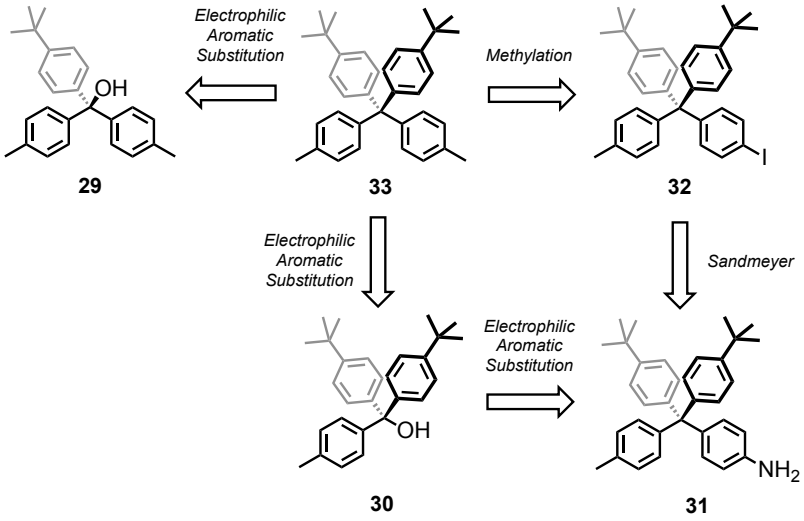

Scheme 11: Retrosynthetic pathways towards key intermediate **33**.

Both compounds **29** and **30** were synthesized *via* twofold Grignard reaction of 1-bromo-4-methylbenzene with methyl 4-(*tert*-butyl)benzoate, and 1-bromo-4-(*tert*-butyl)benzene and methyl 4-methylbenzoate, respectively, with solid magnesium in refluxing THF in good yields. Both electrophilic aromatic substitution reactions using the electron-rich *tert*-butyl benzene or toluene (also as solvent) in catalytic amounts of hydrochloric acid to directly synthesize compound **34** in one step failed. The traditional pathway was therefore chosen, by inserting first aniline followed by Sandmeyer iodination and methylation. More detailed, electrophilic aromatic substitution with aniline in glacial acetic acid and hydrochloric acid as catalyst led to compound **31** following a marginally modified literature protocol by Plietzsch and collaborators.[141] Subsequent one-pot Sandmeyer-type reaction delivered compound **32** by substitution of the amine by an iodine atom through preliminary *in situ* formation of its diazonium salt. Subsequent methylation with methyl lithium in THF yielded compound **33** with the completed carbon skeleton of the target structure in a yield of ~50 % over the four steps.

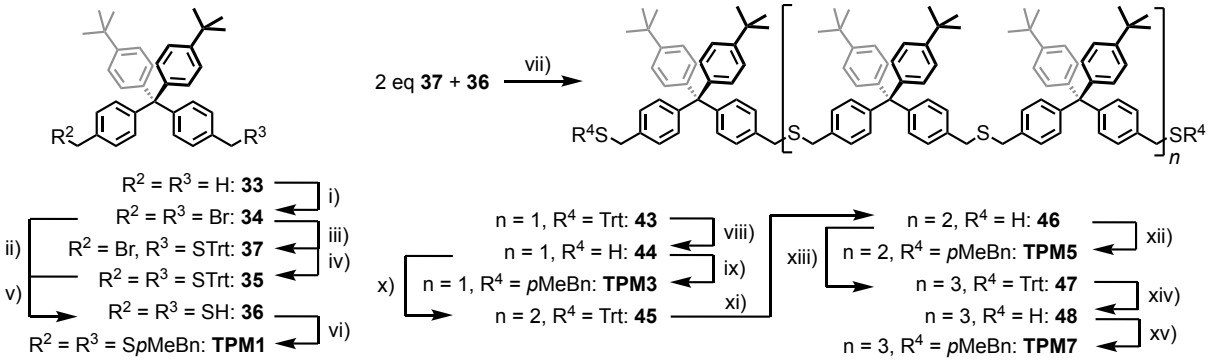

Scheme 12: Molecular structures and synthesis of ligands **TPM1**, **TPM3**, **TPM5** and **TPM7**. i) NBS, AIBN, methyl formate, hν, reflux, 15 h, 60 %; ii) 1) thiourea, DMSO, 40 °C, 15 h, 2) DCM, 3) 1 M aq. NaOH, 1 M aq. HCl, MeOH, 3 h, 51-93 %; iii) TrtSH, NaH, THF, RT, 15 h, 48 %; iv) TrtSH, NaH, THF, RT, 15 h, 48 %; v) $SiEt_3H$, TFA, DCM, RT, 1 h, quant. vi) 4-methylbenzyl bromide, NaH, THF, 5 h, 91 %; vii) NaH, THF, RT, 5 h, 88 %; viii) $SiEt_3H$, TFA, DCM, RT, 1 h, quant.; ix) 4-methylbenzyl bromide, NaH, THF, RT, 15 h, 89 %; x) **37**, NaH, THF, RT, 5 h, 83 %; xi) $SiEt_3H$, TFA, DCM, RT, 1 h, quant.; xii) 4-methylbenzyl bromide, NaH, THF, RT, 15 h, 77 %; xiii)) **37**, NaH, THF, RT, 5 h, 79 %; xiv) $SiEt_3H$, TFA, DCM, RT, 1 h, quant.; xv) 4-methylbenzyl bromide, NaH, THF, RT, 15 h, 72 %. Me = methyl, Bn = benzyl, Trt = trityl.

The key-precursors **34**-**36** were synthesized with slight modification of the protocol reported by Peterle *et al.*[80] and is displayed in Scheme 12: mild radical bromination of compound **33** upon illumination with a halogen lamp with *N*-bromosuccinimide (NBS) as bromine source in methyl formate gave the bis-benzylbromide derivative **34**. The bis-mercapto derivative **36** was obtained by treatment of the bromine precursor **34** with thiourea in dimethyl sulfoxide during 15 hours to form

its thiouronium salt, which was precipitated by an excess of dichloromethane. The precipitate was re-dissolved in methanol and treatment with aqueous sodium hydroxide (1 M), followed by reprotonation with aqueous hydrochloric acid (1 M) provided the desired bis-methylenemercapto tetraphenylmethane derivative **36** between 51 % (when upscaled) and 93 % yield. Continuous degassing of all solvents, aqueous solutions, and reaction mixtures in a steady stream of argon turned out to be crucial in order to avoid polymerization due to disulfide formations. The low yield for precursor **36** could be improved to 88 % (over two steps) with the following pathway: compound **34** was first reacted with an excess of trityl mercaptane and sodium hydride in tetrahydrofuran replacing both bromines with protected sulfurs to form compound **35** which were then easily cleaved with trifluoroacetic acid in presence of triethylsilane as cation scavenger in dichloromethane at room temperature. Preliminary attempts to synthesize all oligomers in one-pot by end-capping oligomerization, described for terphenylic oligomers (*vide supra*) with both key precursor **34** and **36** failed, and thus the traditional pathway reported by Peterle and coworkers was pursued.[80]

The monomeric ligand **TPM1** was isolated in good yields by column chromatography after treating the bis-mercapto precursor **36** with 4-methyl benzyl bromide and sodium hydride as base in THF at room temperature. The bifunctional compound **37**, made from the bis-bromine precursor **34** *via* a S_N2 reaction with trityl mercaptan and sodium hydride as base in THF, comprises one trityl masked thiol and a benzylic bromide as leaving group, and is therefore an ideal building block for the stepwise assembly of the longer oligomers **TPM3**, **TPM5** and **TPM7**. Elongation of the dithiol derivative **36** on both sides with **37** in THF at room temperature using sodium hydride as base gave the terminally trityl-protected trimer **43** in a good isolated yield of 88 %. Deprotection of **43** by treatment with trifluoroacetic acid and triethylsilane in dichloromethane gave quantitatively the trimer **44** exposing terminally free thiols. A similar elongation protocol enabled the transformation from the trimer **44** to the pentamer **45**, and from the free thiol pentamer **46** to the heptamer **47**. With 83 % for **45** and 79 % for **47**, the isolated yields decreased slightly the longer the oligomers became. Deprotections using the conditions described above for **43** provided the corresponding free dithiol trimer **44**, pentamer **46**, and heptamer **48** almost quantitatively. Subsequent end-capping of the dithiol oligomers was performed with similar conditions described above for the assembly of **TPM1** and provided the end-capped oligomers **TPM3**, **TPM5** and **TPM7** in good isolated yields.

3.2.2 Synthesis of the Gold Nanoparticles

The ability of these oligothioether type structures **TPM1**, **TPM3**, **TPM5** and **TPM7** to stabilize AuNPs was analyzed using a similar protocol already applied successfully for linear and dendritic multidentate ligand structures[79–84] and is sketched in Scheme 10 above. It basically consists of a variation of the AuNP synthesis reported by Brust *et al.*[30] in the presence of the multidentate ligand structure of interest. In a two-phase water/dichloromethane system comprising tetra-*n*-octyl-ammonium bromide (TOAB) as phase transfer catalyst, equal molar equivalents of gold and sulfur atoms were dissolved. In other words, 2 molar equivalents of the gold-salt $HAuCl_4$ were used for the bidentate ligand **TPM1**, 4 molar equivalents for the tetra-dentate ligand **TPM3**, and 6 respectively 8 molar equivalents of the gold-salt were used for the hexa- respectively the octa-dentate ligands **TPM5** and **TPM7**. After complete transfer of the gold-salt to the organic phase, the two-phase reaction mixture was vigorously stirred while an aqueous $NaBH_4$ solution was added. After another 10 minutes stirring at room temperature, the phases were allowed to separate and the intense dark brown colored DCM phase indicated the presence of AuNPs dissolved in the organic phase. Addition of excessive amounts of ethanol caused the precipitation of the AuNPs, which were centrifuged and dried *in vacuo*, before being redispersed in DCM. Interestingly, some of these particles were not only formed almost quantitatively (in fact the AuNPs were the only detectable form of gold), but also displayed very promising stability features, which depended on the length of the oligomer used to stabilize the AuNP.

3.2.3 Results and Discussion

Already with the monomeric ligand **TPM1**, no precipitation of gold was observed during the synthesis pointing at superior AuNPs stabilizing properties compared to the *meta*-xylene motif used by Peterle *et al.*, which caused precipitation of gold already during the particles synthesis.[80] In spite of these promising behavior during the synthesis, the ligand **TPM1** coated AuNPs (**Au-TPM1**) did not display suitable stability features agglomerating to larger AuNPs within hours in solution. The initially intense brown AuNPs solution already turned gradually reddish during work up, pointing at the formation of larger particles before agglomeration and precipitation. To our delight, the AuNPs **Au-TPM3**, **Au-TPM5** and **Au-TPM7** stabilized by the trimer **TPM3**, the pentamer **TPM5** and the heptamer **TPM7** displayed considerably improved stability features. These particles turned out to remain stable and soluble over several days without alteration of the UV spectra pointing at constant particle sizes. In the dried state, the particles were even stored over months without losing their redispersibility. These particles were easily redispersed in DCM allowing for repeated precipitation (with ethanol), centrifugation and redispersion cycles without loss of

material. Furthermore, these particles were stable enough to allow for purification by gel permeation chromatography, providing AuNPs samples of excellent purity. The extensively purified and *in vacuo* dried coated particles **Au-TPM3**, **Au-TPM5** and **Au-TPM7** were analyzed by UV-Vis- and ^{1}H-NMR-spectroscopy, transmission electron microscopy (TEM) and thermogravimetric analysis (TGA).

The ^{1}H-NMR spectra of the AuNPs **Au-TPM3**, **Au-TPM5** and **Au-TPM7** displayed broadening of all signals characteristic for particles due to reduced tumbling motion of the ^{1}H-labels in comparison to the free ligands (see Figure 42, Figure 43 and Figure 44 in *8. Appendix*). In spite of the reduced resolution of the ^{1}H-NMR signals, the spectra document clearly the successful separation of the AuNPs from both, the phase transfer catalyst TOAB and excess of oligomeric ligand due to purification by gel permeation chromatography.

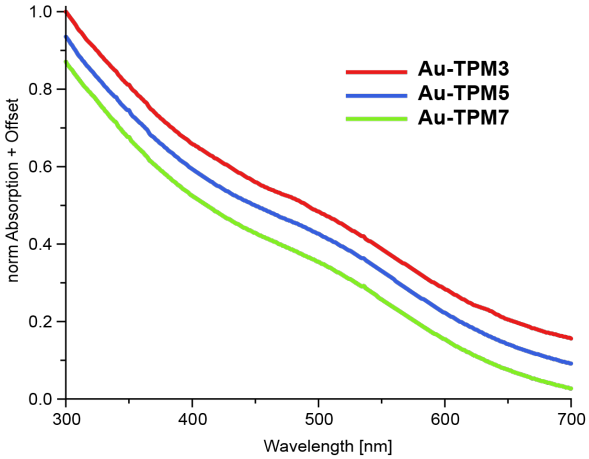

Figure 13: Normalized UV-Vis absorption spectra of the oligomers stabilized nanoparticles **Au-TPM3** (red), **Au-TPM5** (blue) and **Au-TPM7** (green) recorded in dichloromethane. The individual absorption spectra are shifted vertically for clarity (offset).

The UV-Vis absorption spectra of ligand stabilized particles **Au-TPM3**, **Au-TPM5** and **Au-TPM5** are very similar and are displayed in Figure 13. Eye-catching is the absence of a distinct surface plasmon resonance (SPR) band at around 520 nm pointing at AuNPs with diameters smaller than 2 nm.[142] To gain further information about the particles' sizes, TEM micrographs were recorded from samples spread over a carbon network covered TEM grid. Typical sections of the TEM micrographs for all particles are displayed in Figure 14. The gold particles observed in the TEM micrographs were analyzed using the software *ImageJ* (free online software) for particle counting and measuring, resulting in the size distributions. In agreement with the observations made in the UV-VIS spectra, all three ligands **TPM3**, **TPM5** and **TPM7** stabilize particles with diameters below 2 nm. The AuNPs obtained are very comparable for all three ligands even with very

comparable size distributions. In particular average particle sizes of 1.16 ± 0.32 nm were recorded for **Au-TPM3**, of 1.15 ± 0.30 nm for **Au-TPM5**, and of 1.17 ± 0.34 nm for **Au-TPM7** respectively. Thus the particle sizes obtained are comparable to the ones already reported using *meta*-xylene interlinked thioether oligomers (~1.1 nm).[79–84] This once again proves that not the length of the ligands is responsible for the final size of the NPs.

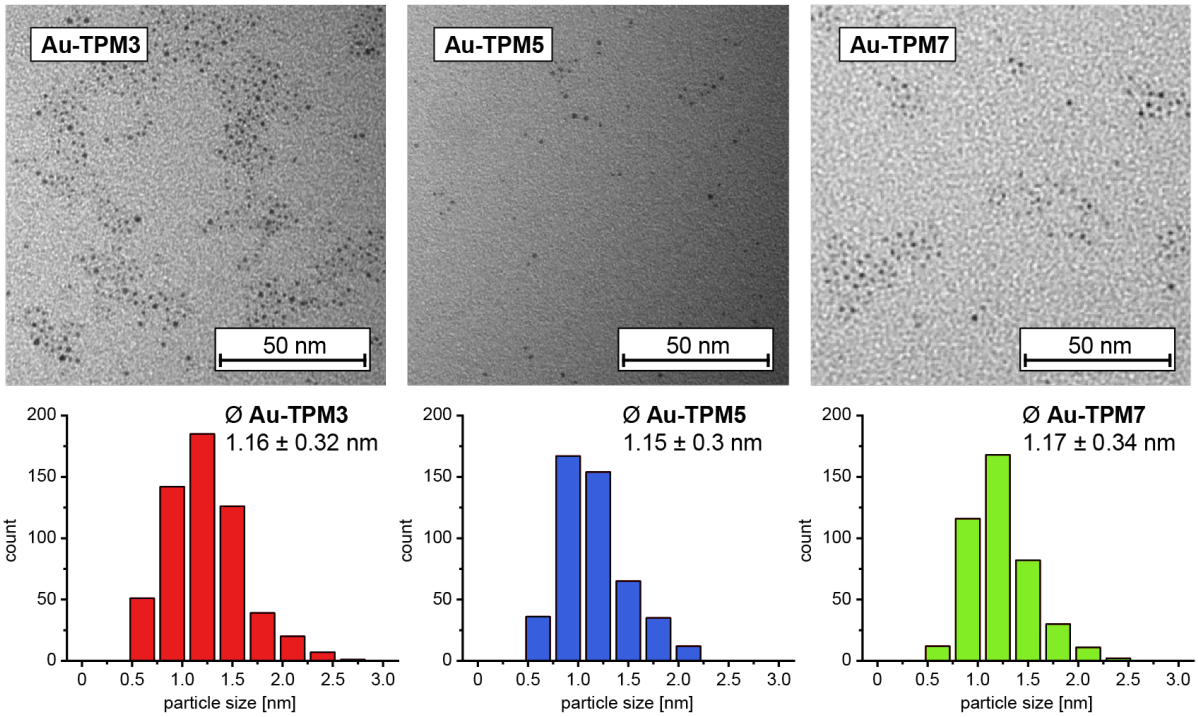

Figure 14: *Top*: Representative sections of the TEM micrographs for samples of the oligomer-stabilized nanoparticles **Au-TPM3**, **Au-TPM5** and **Au-TPM7**; *bottom*: corresponding size distributions of the particles observed in the TEM micrographs.

The purity of the coated AuNPs makes the thermogravimetric analysis (TGA) particularly interesting, allowing conclusions with respect of the ratio of organic ligand coating the AuNPs' surface. For all three AuNPs nanoparticles **Au-TPM3**, **Au-TPM5** and **Au-TPM7** the weight loss attributed to the decomposition of the organic coating starts at about 200 °C and levels out at about 600 °C (TGAs and the ligand-to-NP calculations are displayed in Figure 45 and Table 2 in *8. Appendix*). Weight losses of 26.5 %, 24.5 % and 32.1 % were recorded for **Au-TPM3**, **Au-TPM5** and **Au-TPM7** respectively. As the lost weight must arise from the coating ligands, the remaining weight must belong to the Au atoms forming the AuNPs. As the molecular weights of both, the coating ligand and of the Au atoms are known, the data even allow to determine the number of Au atoms per coating ligand.

In the case of **Au-TPM3** the remaining 73.5 % of the weight corresponds to 24.14 Au atoms per ligand **TPM3**. Assuming a spherical shape for the AuNP with the diameter of 1.16 nm obtained as average number by TEM analysis, the density of gold allows to calculate the average AuNP's mass and to determine the number of Au atoms involved. Applying these calculations to **Au-TPM3**, an average number of 48.27 Au atoms per particle is obtained corresponding to twice the number of Au atoms calculated per ligand. We thus conclude that two ligands **TPM3** are coating one particle, as it was already reported for *meta*-xylene based linear oligomers[79,83] and first generation dendritic ligands.[81] The analysis became even more exciting for the particles **Au-TPM5** and **Au-TPM7**: for **Au-TPM5** the TGA gave a ratio of 42.18 Au atoms per ligand **TPM5**, and the TEM based dimensional analysis of the particles pointed at 47.04 Au atoms per average AuNP. In the case of **Au-TPM7**, 39.49 Au atoms per ligand **TPM7** were calculated while the average particle was determined to consist of 49.54 Au atoms. In spite of the inaccuracy of these estimations of the number of Au atoms per ligand and particle, the obtained numbers clearly suggest that both ligand structures **TPM5** and **TPM7** are able to coat and stabilize an entire AuNP as single wrapping ligand. These oligomers seem to be flexible enough to wind around such small NPs and thus the increased sulfur-sulfur distance does not apply for this ligand-system with the applied conditions for the nanoparticle formation.

This 1:1 ratio of coating ligand per particle is particularly appealing for future developments towards particles exposing a single functional group as inorganic/organic hybrid macromolecules addressable by wet chemical protocols. Equally important for their use as "artificial macromolecules" is their thermal integrity in suspension limiting the range of potentially applicable reaction conditions. Thus suspensions of the particles **Au-TPM3**, **Au-TPM5** and **Au-TPM7** dispersed in toluene were gradually heated by steps of 10 °C and kept at the elevated temperature for one hour before optical analysis. For **Au-TPM3** a color change from brown to bluish accompanied by a black precipitation was observed above 90 °C, pointing at the thermal decomposition of the ligand coated **Au-TPM3**. Similar behavior at the same temperature was observed for **Au-TPM7**, pointing at comparable thermal stability of this AuNP coated by a single ligand. For **Au-TPM5** slightly lower decomposition temperatures were recorded, as the alteration in the UV-VIS spectra and precipitation was already observed above 80 °C. Our current working hypothesis is that the observed thermal stabilities might reflect the number of binding sites (*i.e.* thioether moieties) per particle. Consequently, the pentamer **TPM5** with 6 thioethers results in slightly less stable coatings than two molecules of the trimer **TPM3** or one heptamer **TPM7**, where in both cases 8 thioether units are connecting the coating to the particle's surface. For all three

coated particles **Au-TPM3**, **Au-TPM5** and **Au-TPM7** promising thermal stabilities were observed increasing their attraction as future ligand structure of inorganic/organic hybrid building blocks.

3.2.4 Summary and Conclusions

In conclusion, we present a new thioether-based oligomer motif with superior AuNP stabilizing properties. Despite the increased sulfur distance of the ligands' backbone did not increase the size of the NPs considerably as it was observed for the terphenylic ligands (*vide supra*), a new packaging motif was observed for parent ligands. The 1:1 ratio between coating ligands and AuNPs in combination with the improved synthetic accessibility of the linear oligomers **TPM5** and **TPM7** compared with the dendritic ligands reported so far and the thermal stability of the coated particles, makes these oligomers to very promising coatings for AuNPs with controlled exposure of functional groups. We attribute the superior stabilizing features mainly to the considerably enlarged bulkiness of the structure covering larger areas of the AuNPs' surface. In addition, the increased distance between thioether subunits lifts the interlinking structure from the coated gold surface, which might support the coating as well. In spite of the reduced number of coordinating thioether subunits per organic mass, these structures display promising thermal stability features in dispersion, pointing at an inferior role of the number of coordinating thioethers in the molecules design. This observation is to some extent supported by the work of McCaffrey *et al.*, who reported the stabilization of AuNPs in a rigid organic molecular cage, bearing only three thioether group as coordination point for the encapsulated AuNP.[143]

3.3 Acetylene-Functionalized Tetraphenylmethane-Type Pentamer

Within this chapter, the synthesis and the characterization of an acetylene-functionalized pentamer (**TPM5-Hog**) is reported, and is a consequential continuation of the tetraphenylmethane-based pentamer (**TPM5**), which showed a single ligand-to-NP stabilization by enwrapping. Albeit the limited stability of the formed NPs after unmasking the acetylene-moiety and subsequent coupling *via* Glaser-Hay conditions, major amounts of dimer dumbbell structures as organic-inorganic superstructures could be observed.

The coupling of AuNPs has been demonstrated in the past decade by different techniques, such as π-π interactions[144], H-bonding[145–147], host-guest interactions[111,112,116,117], Glaser-Hay acetylene homo-coupling[79,82,83], azide-click chemistry[84] or DNA recognition[86,148,149]. This concept to form organic-inorganic superstructures by wet chemical protocols in sight of future applications (*e.g.* labeling) remains however a challenge, as the resulting NPs should exhibit a crucial feature, stability, which is mainly given by the design and the architecture of the ligand stabilizing the NP. While its monofunctionalization can be and has been achieved for polymers and dendrimers in the before-mentioned examples, here we will discuss the first linear monofunctionalized ligand (**TPM5-Hog**) and its formation of dimer structure after deprotection and subsequent homo-coupling (Scheme 13). This will deliver further exploration of well-defined bulky structures coating AuNPs and will give an insight into their stability as organic-inorganic superstructures. It will further serve

as a proof-of-concept of the former work discussed in a chapter before (*vide supra*). The discrete number of coating ligands results in an equally well-defined number of peripheral masked acetylene functions per AuNP, and thus, the extent of surface functionalization per NP must be reflected in the connectivity of the NP subunits in the hybrid architectures obtained upon exposing them to acetylene coupling chemistry.

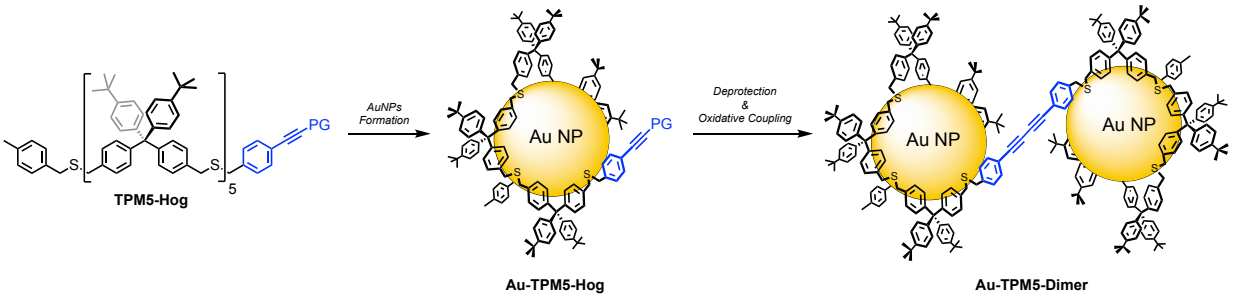

Scheme 13: General concept of forming ligand-stabilized AuNPs and NP dimers (functionality is highlighted in blue).

3.3.1 Synthesis of the Ligand

The fastest way to assemble acetylene-functionalized pentamer **TPM5-Hog** would probably be *via* end-capping of dithiol-pentamer **46** with 4-methylbenzyl bromide and an acetylene-functionalized benzyl bromide derivative (*e.g.* compound **50**) in one-pot. The subsequent separation of the formed statistical products would however be very tedious as several chromatography techniques would be needed. In addition, it is a statistical reaction, most of the formed end-capped pentamer would be purposeless, this strategy was not pursued. The retrosynthetic strategy towards acetylene-functionalized pentamer **TPM5-Hog** assembly *via* step-wise S_N2 of various building blocks is depicted in Scheme 14, and is synthesized with the asymmetric end-capped pentamer **55** and the thiol-derivative **52** comprising the masked acetylene as the functional unit. Note that (3-cyanoproply)diisopropylsilyl (CPDDIPS) was used for the protection of the acetylene-unit as it has a major advantage over the more commonly use triisopropylsilyl (TIPS). It was introduced by the group of Höger[150] and has an increased polarity compared to TIPS, resulting in an easier separation of its derivatives from the starting materials by flash column chromatography on silica. Otherwise, it comprises similar stability to temperature and to acidic and basic conditions and it can also be deprotected with a F^- source (*e.g.* tetra-*n*-butylammonium fluoride).[151]

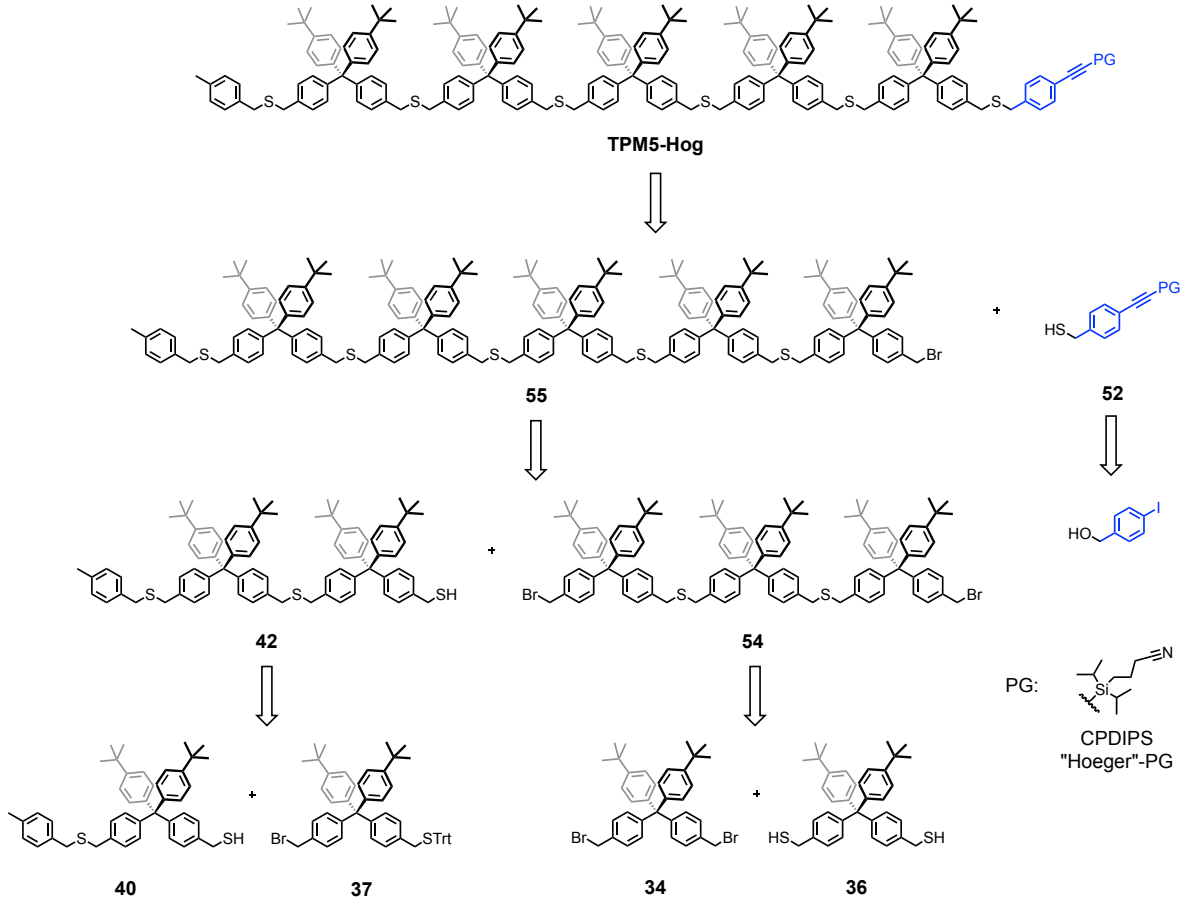

Scheme 14: Retrosynthetic strategy towards acetylene-functionalized pentamer **TPM5-Hog**.

Asymmetric bromide-pentameter **55** is based on a statistical reaction of asymmetric thiol dimer **42** and the dibromo-trimer **54**. For symplification, the synthesis towards dimer **42** will be describe in the next chapter about tridentate derivatives and bromo-trimer **54** is assembled with an excess of dibromo-precursor **34** with the dithiol-precursor **36**, both already described in the chapter before.

Noteworthy, the synthesis towards acetylene-functionalized pentamer **TPM5-Hog** was initially pursued by assembling first an asymmetric end-capped bromide tetramer synthesized with compound **40** and dibromo-trimer **54**, and then in the last step couple with an acetylene-functionalized building block comprising tetraphenylmethane backbone with a free thiol. However, the deprotection of compound **53** (Scheme 15) failed, which led to the strategy described before.

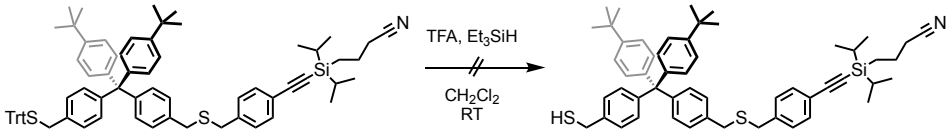

53

Scheme 15: Failed attempt of the deprotection of compound **53**.

The synthesis towards asymmetric bromo-pentamer **55** was performed as followed (Scheme 16): Dibromo-trimer **54** was obtained in a yield of 39 % after dropwise addition over one hour of dithiol-precursor **36** dissolved in THF into a solution of dibromo-precursor **34** and sodium hydride at room temperature. The moderate yield can mainly be attributed due to the formation of unwanted oligomers despite the careful addition *via* syringe pump. The synthesis of both precursors **34** and **36** were describe in the previous chapter. Note that the yield could not be improved when an excess of bromo-thiol compound **38** dissolved in THF was added dropwise into a solution of dibromo-precursor **34** and sodium hydride at room temperature. The asymmetric bromo-pentamer **55** was then obtained after statistical reaction of compound **42** (synthesis in *Chapter 4.1*) and dibromo-trimer **54** upon addition of sodium hydride in THF in an acceptable yield of 39 %. Acetylene-masked thiol-derivative **52** was furnished as followed: the acetylene functionality was introduced *via* Sonogashira reaction starting with a degassed mixture of 4-iodobenzyl alcohol, bis(triphenylphosphine)palladium(II) dichloride and copper(I) iodide dissolved in triethylamine as base and tetrahydrofuran as solvent, after which 3-cyanoproply)diisopropylsilyl acetylene was added. The reaction was kept constant at 40 °C for 12 hours in order to obtain compound **49** in quantitative yield. Subsequent substitution of the alcohol with a bromide *via* S_N2 reaction of the benzylic alcohol of compound **49** and phosphorus tribromide in THF gave compound **50** in quantitative yield. Note that compound **50** is very labile likely due to its electronic conjugation, and thus would convert to benzylic chloride upon contact with chlorinated solvents (*e.g.* DCM or chloroform). This reaction is commonly performed in dichloromethane but in this case, it had to be strictly avoided for the reaction, workup and analysis. Compound **50** was then treated with trityl mercaptane in THF to obtain compound **51**, which was then deprotected to the thiol-precursor **52** with trifluoroacetic acid and triethylsilane as cation scavenger in a yield of 85 % over two steps. Acetylene-functionalized pentamer **TPM5-Hog** was finally obtained in 71 % by treatment of compound **55** and a slight excess of compound **52** with sodium hydride in THF.

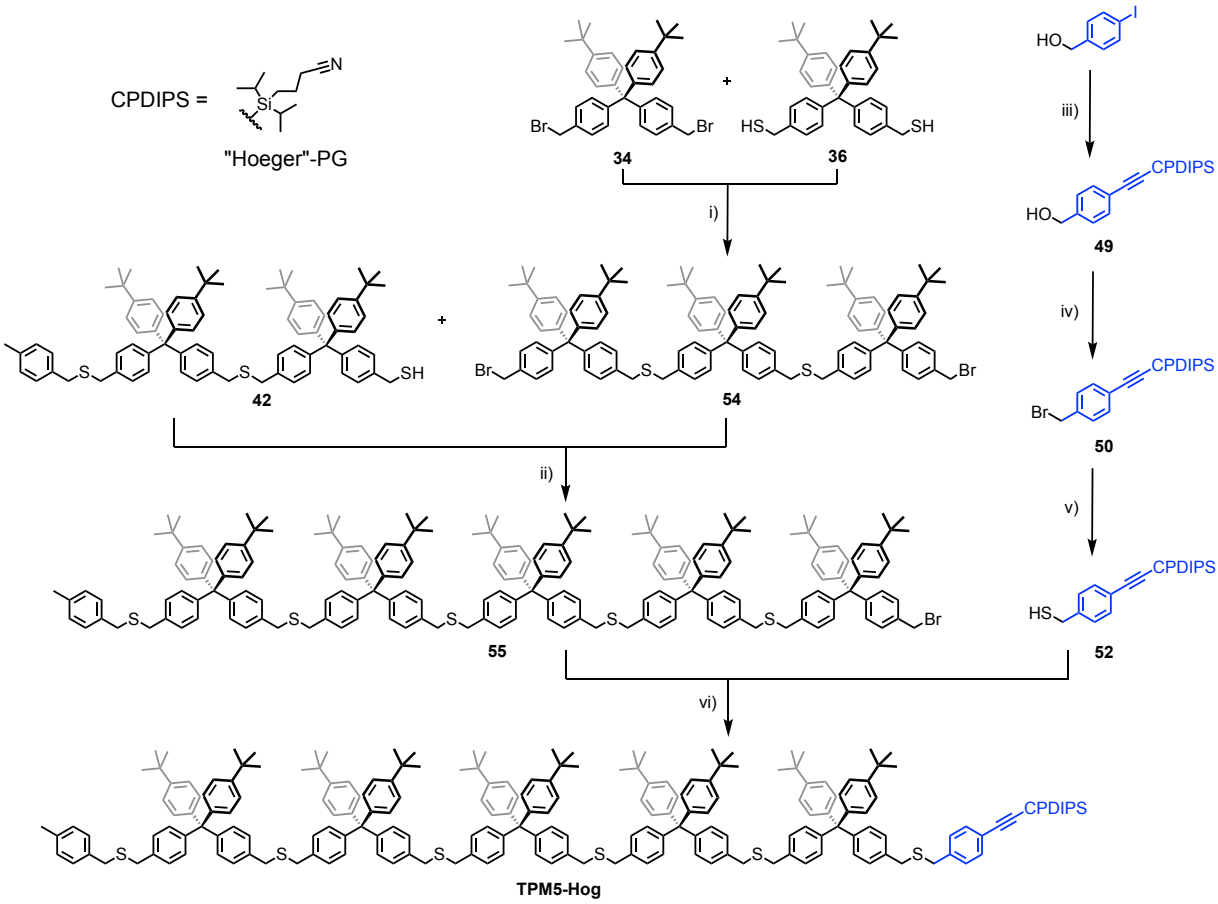

Scheme 16: Molecular structures and synthesis of acetylene-functionalized pentamer **TPM5-Hog**. i) NaH, THF, RT, 16 h, 39 %; ii) NaH, THF, RT, 15 h, 39 %; iii) (3-cyanoproply)diisopropylsilyl acetylene, $PdCl_2(PPh_3)_2$, CuI, Et_3N, THF, 40 °C, 12 h, quant.; iv) PBr_3, THF, 0 °C, 3 h, quant.; v) 1) TrtSH, NaH, THF, RT, 15 h, 88 %, 2) $SiEt_3H$, TFA, DCM, RT, 1 h, quant.; vi) NaH, THF, RT, 15 h, 71 %. Trt = trityl.

3.3.2 Synthesis of the Gold Nanoparticles, Deprotection and Coupling Conditions

The ability of the acetylene-functionalized pentamer **TPM5-Hog** to stabilize AuNPs was analyzed using a similar protocol already applied successfully for linear and dendritic multidentate ligand structures[79–84] and is sketched in Scheme 17. It basically consists of a variation of the AuNP synthesis reported by Brust *et al.*[30] in the presence of the multidentate ligand structure of interest. In a two-phase water/dichloromethane system comprising tetra-*n*-octylammonium bromide (TOAB) as phase transfer catalyst, equal molar equivalents of gold and sulfur atoms were dissolved. In other words, 6 molar equivalents of the gold-salt $HAuCl_4$ were used for the hexadentate ligand **TPM5-Hog**. After complete transfer of the gold-salt to the organic phase, the two-phase reaction mixture was vigorously stirred while an aqueous $NaBH_4$ solution was added. After another 10 minutes stirring at room temperature, the phases were allowed to separate and the intense dark brown colored DCM phase indicated the presence of AuNPs dissolved in the organic phase. Addition of excessive amounts of ethanol caused the precipitation of the AuNPs, which were

centrifuged. This process was repeated three times in order to remove excess of TOAB before the excess of ligand was removed by gel-permeation chromatography (Biobeads SX-1). The as-synthesized nanoparticles were then analyzed by UV-Vis and TEM before subjecting to further wet chemical treatment.

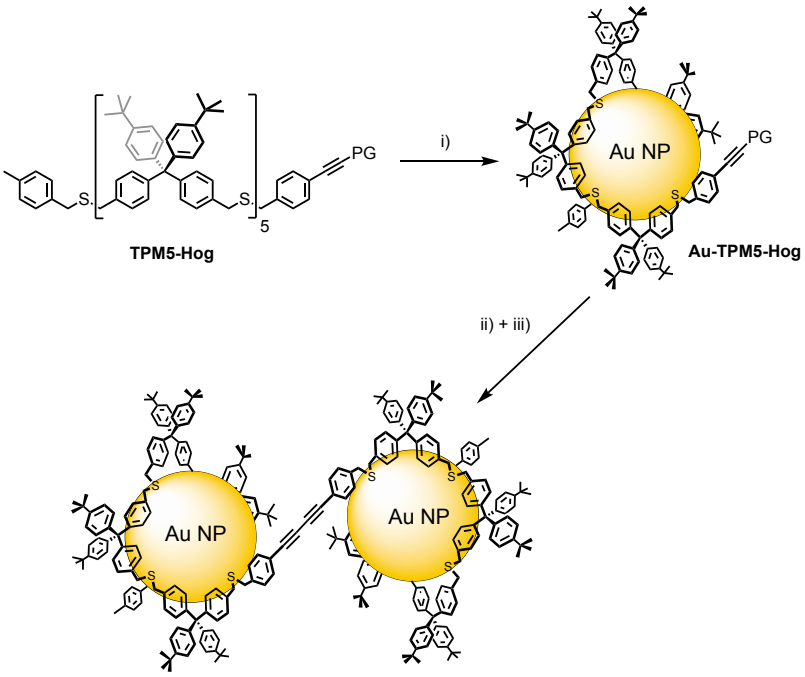

Scheme 17: General concept of forming ligand-stabilized AuNPs and NPs-dimers. i) AuNPs formation: $HAuCl_4$, TOAB, $NaBH_4$, H_2O/DCM; ii) deprotection: TBAF, DCM; iii) oxidative coupling: CuCl, TMEDA, O_2 (ambient conditions).

For better comparison, the deprotection and oxidative coupling conditions were kept similar to the protocols reported in literature[79,82,84] and is based on a modified Glaser-Hay[152] wet chemical oxidative acetylene coupling protocol. The acetylene functionalized Au NPs were dispersed in dichloromethane and tetra-*n*-butylammonium fluoride was added for the removal of CPDIPS-protecting group. The mixture was left stirring for 1 hour, and quenched with water, extracted with DCM and dried with magnesium sulfate. After filtration, the solution was concentrated and *N,N,N',N'*-tetramethylethylenediamine and copper(I) chloride were added under ambient conditions to provide the needed oxygen for the oxidative coupling. The dimerization reaction was left stirring for 3 hours and then quenched with a saturated solution of ammonium chloride, extracted with dichloromethane and dried with magnesium sulfate. After filtration and aqueous workup, the solution was concentrated and investigated by TEM on carbon coated copper grids.

3.3.3 Results and Discussion

The synthesis towards **Au-TPM5-Hog** did work without any indication of precipitation and also during the - sometimes - critical purification step by manual size exclusion chromatography confirmed their expected enhanced stability, similar to the unfunctionalized pentamer (**TPM5**) discussed before (*vide supra*). Before the final deprotection and coupling procedure, the as-synthesized NPs were analyzed by UV-Vis and TEM.

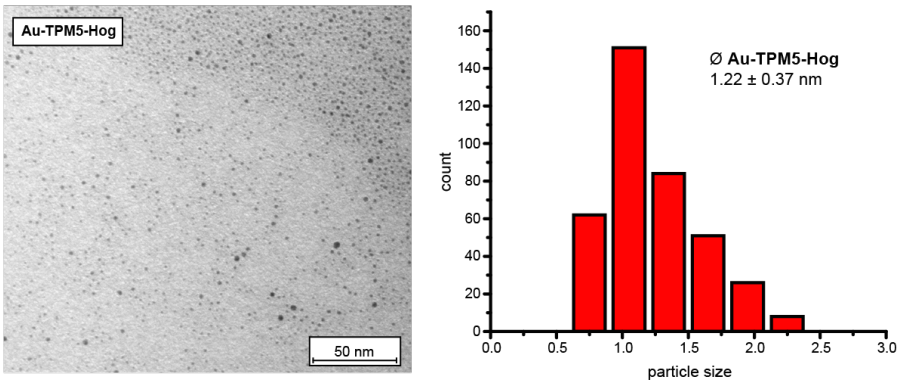

Figure 15: *Left:* Representative section of the TEM micrographs for samples of the oligomer-stabilized nanoparticles **Au-TPM5-Hog**; *right*: corresponding size distribution of the particles observed in the TEM micrographs.

The micrographs (Figure 15) showed small AuNPs (1.22 ± 0.37 nm) with a narrow size distribution and are, as expected, comparable to the unfunctionalized pentamer, which exhibited a size of 1.15 ± 0.3 nm. The UV-Vis spectra shown below (Figure 16, black curve) confirmed their small sizes, as almost no SPR-band can be observed at 520 nm. In addition, the rise towards a peak below 300 nm can be attributed to the delocalized oligo(phenylene-ethylene) (OPE) present in this system.[82,84] The confirmation of monofunctionalized AuNPs by TGA was not performed as both, the size distribution and the UV-Vis were very similar to the functionalized pentamer **TPM5-Hog**. On the other hand, the disintegration of the precious particles by TGA, would require a larger amount of ligand. During the deprotection with TBAF, no precipitation of the particles were visible and after a brief aqueous workup the deprotected particles were directly exposed to Glaser-Hay protocol discussed before. After 3 hours, no precipitation of the AuNPs was observed during this time unlike the smaller of the two dendrimeric ligands reported by Hermes and collaborators.[82] After the workup, the particles were analyzed again by UV-Vis and TEM. For the latter, highly diluted solutions were used for deposition on the grids to avoid accidental proximity of not covalently linked NPs.

Figure 16 shows the representative UV-Vis spectra of the NPs **Au-TPM5-Hog** before and after the coupling. The expected red-shift of the OPE-band around 300 nm after the coupling is an

indication of an enlarged OPE-system. Surprisingly, the SPR-band at 520 nm has shifted as well to higher frequency, much in contrast to former studies.[82,84] This could either mean that the plasmon resonance does favor and electronic communication between the NPs as a plasmonic coupling, or the ligand does not sufficiently stabilize the NPs enabling the agglomeration to larger NPs, or both. Note that during the syntheses precipitation of the particles could however not be observed.

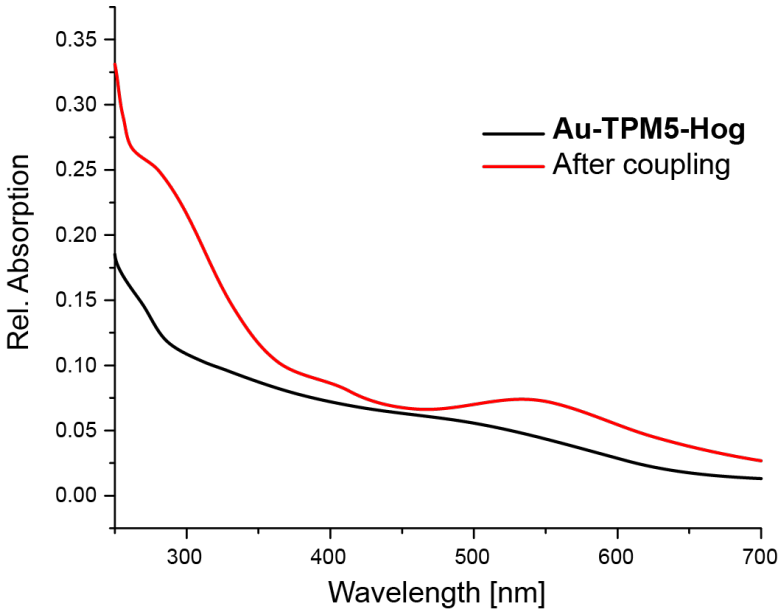

Figure 16: UV-Vis spectra of AuNPs before (black) and after the acetylene coupling (red).

TEM analysis indeed showed the presence of partially larger NPs (> 2 nm), however also formation of - mostly - dimers, few trimers but also uncoupled small NPs, as shown in a crude TEM image displayed in Figure 17 (top). Out of about thirty TEM images, unreacted monomers, coupled dimers and trimers or higher order oligomers were counted. Mostly unreacted NPs (~60 %) are visible, followed by a great amount of dimers (~31 %) and only a few formed trimers or higher architectures (~9 %) can be observed. The observed red-shift of the SPR-band is more likely due to the simultaneously formation of agglomerated larger AuNPs than a SPR-coupling of dimers and trimers, as this SPR-coupling could not be observed either in former reports.[79,82–84] The formation of trimers and higher order oligomers can be explained such, as the deprotected acetylene-moiety can also interact with the gold-core of another AuNP which was also observed in the literature[82] or that some particles can also be stabilized by two ligands. Interparticle distances were not measured, as this distance may vary due to different packaging motifs of the linear pentamer and the AuNP with the acetylene-moiety attached at the end of the strand.

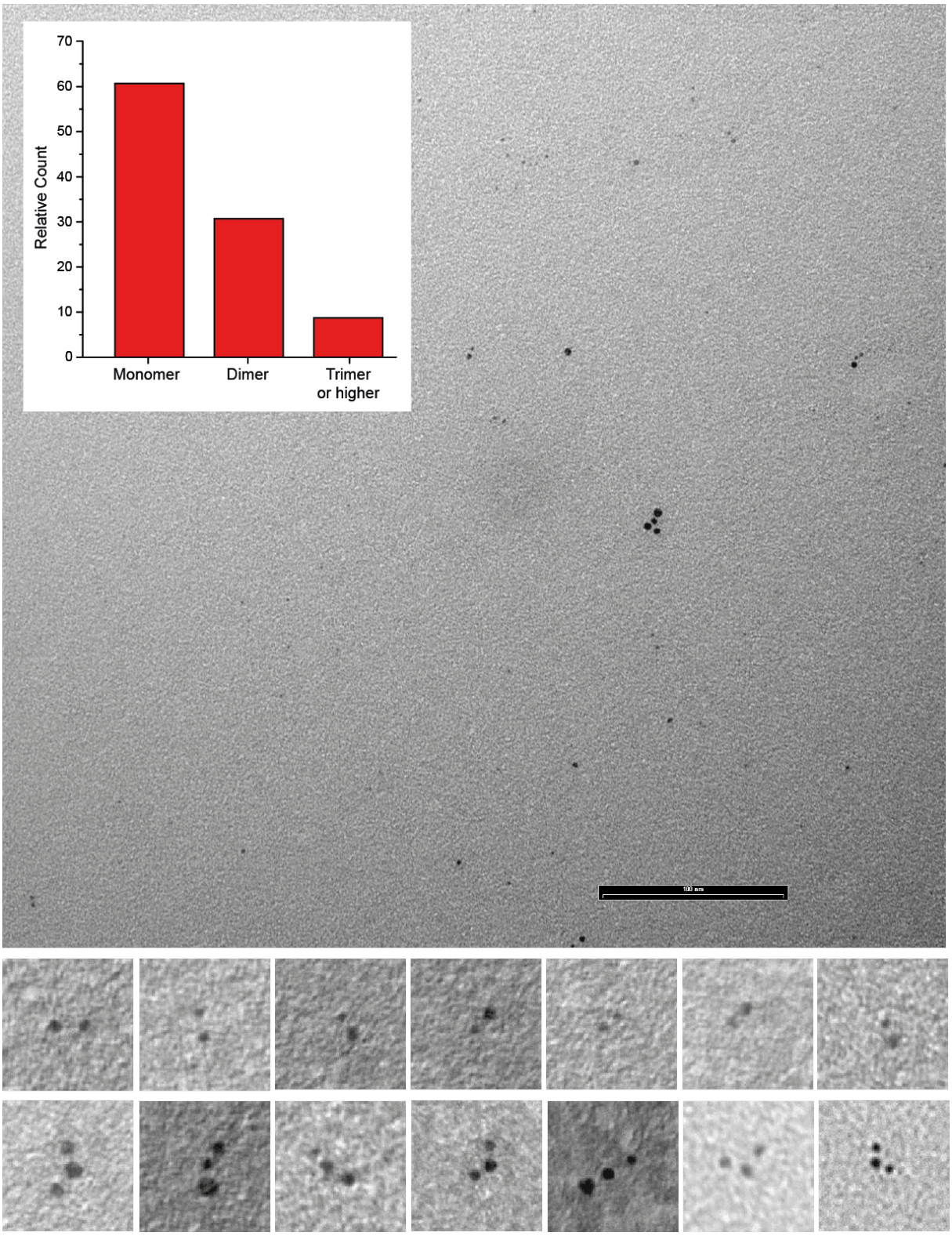

Figure 17: *Top:* Crude TEM image after the deprotection and coupling of **Au-TPM5-Hog** displaying partially larger NPs, and small uncoupled NPs, dimers and trimers. Scale bar corresponds to 100 nm. Inserted overlay of the relative counts of uncoupled monomers, coupled dimers, coupled trimers or higher order oligomers. *Bottom:* Representative TEM images of diluted solutions of **Au-TPM5-Hog** dimers and trimers. Each image has a width of 22 nm.

Nevertheless, formation of mostly dimer architectures could be observed with the applied coupling conditions. The design with the masked acetylene-moiety at the end of the linear pentamer strand may be suboptimal, compared to formed studies since, which had their functionality pointing outwards of the AuNP sphere as 1) the freely moving acetylene-moiety likely results in an increased competing interaction of the acetylene with an adjacent and may therefore also weaken their stability allowing fuse to larger NPs and 2) the interparticle distances cannot be measured to verify the correct distance between the coupled organic-inorganic architectures due to different possible arrangements of the functionalized pentamer **TPM5-Hog**. Note that further processing like size exclusion chromatography remained challenging due to their weak stability resulting in precipitation on the column, similar to former studies.[79,82–84]

3.3.4 Summary and Conclusions

In summary, the synthesis and characterization towards linear acetylene-monofunctionalized tetraphenylmethane-based pentamer (**TPM5-Hog**) and its ability to successfully stabilize AuNPs by enwrapping is reported. The concept of homo-coupling the functionalized particles *via* wet chemical Glaser-Hay conditions was demonstrated by forming mostly dimer over trimer or higher order oligomer architectures. The limited stability of the formed organic-inorganic hybrid superstructures is likely to arise from the linear pentamer with the functionalization at its end, allowing an unhindered moving of its functionalized tail, weakening the arrangement of the ligand-to-NP, resulting in partially larger dimensions of the particles.

4 Tripodal Thioether-Coated Gold Nanoparticles

4.1 Tripodal Dendritic-Based Ligand Coated Gold Nanoparticles

This part focuses on the design and the synthesis of a tetraphenylmethane-based central tripodal subunit able to link three oligomeric thioether-bridged side-chains. The novel dendritic coverage on the gold nanoparticles enables readily particles which are enwrapped by a single ligand, being interesting for future functionalization at its periphery. Depending on the nature of the attached side-chains (**Xyl**, **TPM**, **Ter**) the as-synthesized gold nanoparticles exhibit different stability features with almost similar sizes.

This work is based on the linear tetraphenylmethane-based oligomers described before (*vide supra*) with the aim of using this moiety as a tripodal central unit, by the attachment with various side-chains, in order to investigate and explore their ability to enwrap gold nanoparticles.

Tripodal chemical structures comprising sulfurs as anchoring points for the adsorption on gold surfaces have been studied in the past decade, amongst others as self-assembled monolayers (SAMs)[153–155] or for the investigation concerning their spatial arrangement[156–160] on the surface mainly *via* scanning tunneling microscope (STM). In most of the reported publications of tripodal structures, the tetraphenylmethane-based subunit is used and studied as this bulky group benefits from its robustness and well-defined arrangement on the metal surface.[157,158] The voluminous

tetraphenylmethane core forces the unoccupied phenyl ring to an orientation perpendicular to the metal surface[161,162] which is favorable for the exposure and availability of functional moieties for further modification as has been shown with similar tetraphenylmethane-based tripod structures deposited gold surfaces[163]. Furthermore, its occupied surface area can be expected on the basis of their structural dimensions, substantially greater than that of mono- or bipodal structures.[153] In fact, linear *meta*-xylene based oligomers tend to lean towards the gold likely due to π-Au interactions[79] and was redesigned with an additional nitrogen - as pyridine unit - with the lone-pair coordinating to the gold as a third hook[164] in order to obtain perpendicular functionalization.[82–84] However, formation of gold nanoparticles using the tripodal tetraphenylmethane as a central subunit has not been considered in the literature and are thus worthy candidates owning the promising features described before.

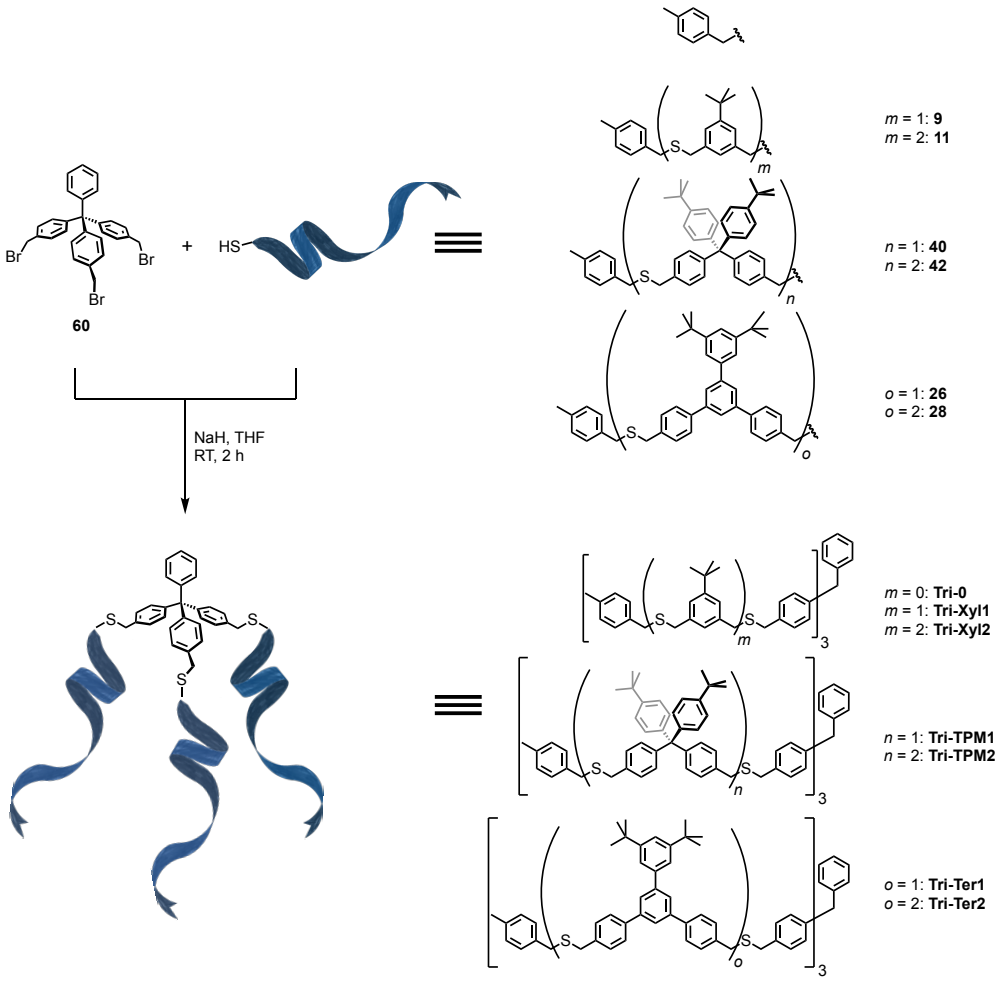

Scheme 18: Overview over the ligand concept. The tripodal central linking unit **60** offers a free phenyl moiety for future functionalization and reacts with oligomeric thioether side-chain thiols *via* S_N2 to give ligands: **Tri-0** end-capped with *p*-methylbenzylthiol; **Tri-Xyl1** and **Tri-Xyl2** as *meta*-xylene-based side-chains; **Tri-TPM1** and **Tri-TPM2** as tetraphenylmethane-based side-chains; and **Tri-Ter1** and **Tri-Ter2** as terphenyl-based side-chains.

In this part, a tripodal tetraphenylmethane-derivate central subunit (**60**) which readily connects three oligomeric, thioether-based side-chains attached to the benzylic *para* position of three of the four phenyls, is presented (Scheme 18), which are attached to the benzylic *para* position of three of the four phenyls. The unoccupied phenyl allows future functionalization on the in upright position in respect to the Au surface. The side-chains are based on earlier work and showed remarkable stability features - for *meta*-xylene-based[80] and tetraphenylmethane-based oligomers (described in the *chapter 3.2*) - whereas the terphenyl-based oligomers with their considerably increased bite-angle offered larger AuNPs (describe in *chapter 3.1*). We were therefore wondering to which extent these features have similar impact on the resulting gold nanoparticles when connected to the tripodal tetraphenylmethane-based subunit. And on the other hand, possible mono-ligand stabilized particles are expected, benefiting from the ligands' nature to enwrap - like the claw machine grabbing a toy - similar to dendrimer-type[81] enwrapping of AuNPs.

4.1.1 Synthesis of the Ligands

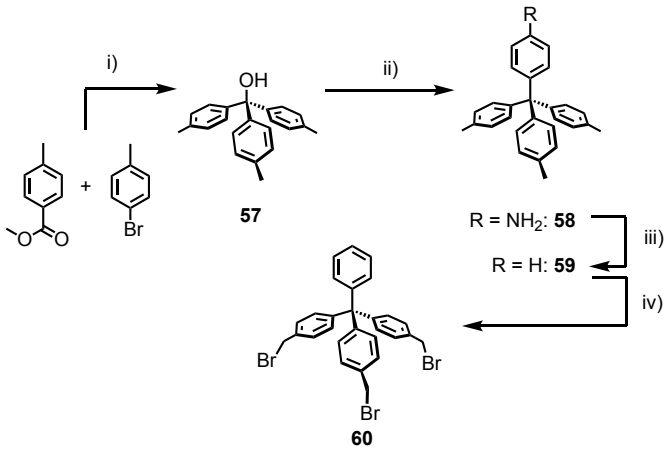

Scheme 19: Molecular structures and synthesis of tripodal central linking subunit **60**: i) 1) Mg, THF, reflux, 24 h, 2) H_2O, sat. NH_4Cl, 98 %; ii) aniline, HCl, AcOH, 140 °C, 3 h, 66 %; iii) 1) BF_3OEt_2, *t*$BuNO_2$, THF, -10 °C, 2 h, 2) $FeSO_4$, DMF, 2.5 h, 3) H_2O, 0 °C, 80 %; iv) NBS, AIBN, hν, methyl formate, reflux, 15 h, 50 %.

The central linking subunit **60** (Scheme 19) was synthesized as follows: triphenylmethanol derivative **57** was obtained *via* twofold Grignard reaction of the Grignard reagent obtained from 1-bromo-4-methylbenzene and solid magnesium in tetrahydrofuran with methyl *p*-toluate. Subsequent electrophilic aromatic substitution with aniline in glacial acetic acid with hydrochloric acid as catalyst gave tetraphenylmethane-derivative **58**. Defunctionalization of the amine moiety towards compound **59** was carried out *via in situ* formation of the diazonium salt in dichloromethane of the prior and subsequent treatment with iron sulfate in dimethylformamide. We chose the two-step

detour *via* introduction of aniline over the aromatic substitution to benzene to benefit from a readily functionalization of the amine moiety for the future course of the work and to prevent potential twofold substitution to the benzene, leading to unwanted side-products. The central subunit **60** was obtained *via* mild bromination of compound **59** with *N*-bromosuccinimide (NBS) as a bromine source and azobisisobutyronitril (AIBN) as a radical starter in methyl formate, exploiting the solvent's low boiling point and therefore hindering overbromination of the benzylic position upon illumination with a halogen lamp. Over four steps, a moderate yield of 26 % was obtained.

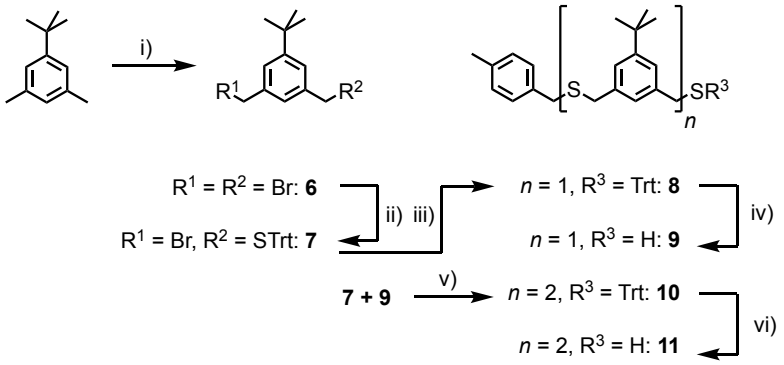

Scheme 20: Molecular structures and synthesis of mono- and dimeric side-chains **9** and **11**: i) NBS, AIBN, hν, methyl formate, reflux, 15 h, 65 %; ii) TrtSH, NaH, THF, RT, 2 h, 38 %; iii) *p*-methylbenzylthiol, NaH, THF, RT, 2 h, 91 %); iv) Et_3SiH, TFA, DCM, RT, 1 h, 91 %; v) NaH, THF, RT, 2 h, 79 %; vi) Et_3SiH, TFA, DCM, RT, 1 h, 77 %. Trt = trityl.

Mono- and dimeric side-chains **9** and **11** were obtained from a modified protocol previously reported by Peterle *et al.*[80] (Scheme 20), comprising slight changes: benzylic bromination of 1-tert-butyl-3,5-dimethylbenzene was performed, as stated above, upon illumination with a halogen lamp in presence of *N*-bromosuccinimide and azobisisobutyronitrile as radical starter to give dibromo-compound **6**. In order to have control over the side-chain length, the following stepwise deprotection-elongation strategy was chosen. Statistic substitution of one bromine site with trityl mercaptan in tetrahydrofuran *via* S_N2-reaction upon addition of sodium hydride gave the monoprotected compound **7**. To prevent polymerization in subsequent reaction steps, the free bromine moiety was end-capped with *p*-methylbenzylthiol using the same conditions to yield compound **8**. Subsequent deprotection by treatment with trifluoroacetic acid trifluoroacetic acid and triethylsilane as cation scavenger in dichloromethane gave monomeric side-chain **9** in an overall yield of 20 %. The S_N2-reaction of compounds **7** and **9** in tetrahydrofuran in presence of sodium hydride yielded the protected dimeric side-chain **10**. Dimeric side-chain **11** was obtained from precursor **10** using the same deprotection conditions as before, giving an overall yield of 12 %.

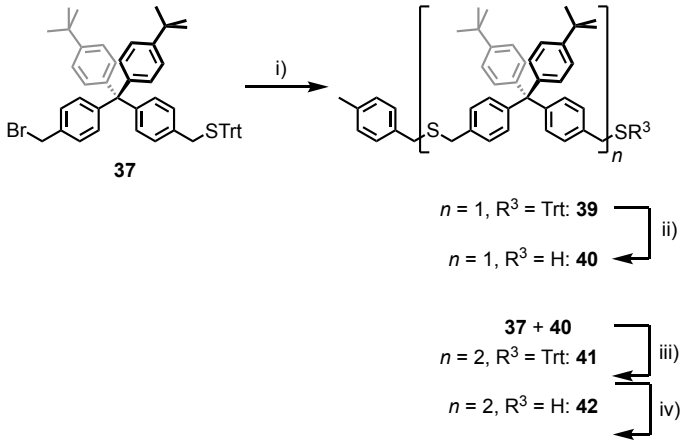

Scheme 21: Molecular structures and synthesis of mono- and dimeric side-chains **40** and **42**: i) *p*-methylbenzylthiol, NaH, THF, RT, 2 h, 93 %; ii) Et_3SiH, TFA, DCM, RT, 1 h, quant.; iii) NaH, THF, RT, 2 h, 85 %; iv) Et_3SiH, TFA, DCM, RT, 1 h, 89 %.

In order to obtain side-chains **40** and **42**, the same elongation-deprotection strategy as used for side-chains **9** and **11** was carried out (Scheme 21): end-capping of **37** with *p*-methylbenzylthiol under the same conditions gave precursor **39**. Note that the synthesis towards **37** was discussed in *chapter 3.2* (*vide supra*). Monomeric side-chain **40** was obtained *via* deprotection in dichloromethane with triethylsilane as cation scavenger and trifluoroacetic acid as a proton source in an overall yield of 14 %. Elongation with compound **37** and sodium hydride in tetrahydrofuran gave dimer **41**, and subsequent deprotection with trifluoroacetic acid and triethylsilane in dichloromethane gave dimeric side-chain **42** in an overall yield of 10 %.

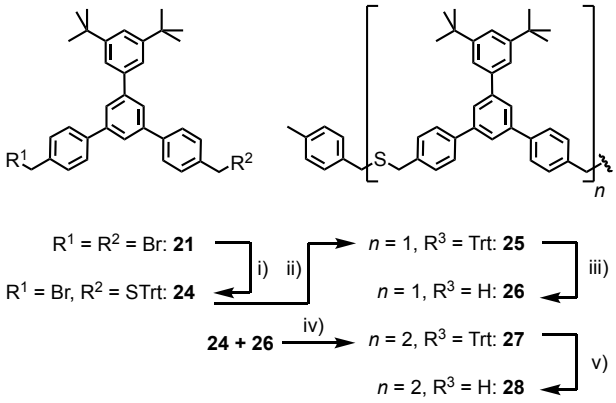

Scheme 22: Molecular structures and synthesis of mono- and dimeric side-chains **26** and **28**: i) TrtSH, NaH, THF, RT, 2 h, 39 %; ii) *p*-methylbenzylthiol, NaH, THF, RT, 2 h, 88 %); iii) Et_3SiH, TFA, DCM, RT, 1 h, 94 %; iv) NaH, THF, RT, 2 h, 90 %; v) Et_3SiH, TFA, DCM, RT, 1 h, 70 %. Trt = trityl.

In order to obtain side-chains **26** and **28**, the same elongation-deprotection strategy as used for side-chains **9** and **11** was carried out (Scheme 22): Dibromo-compound **21** was treated with trityl mercaptane with sodium in tetrahydrofuran to give asymmetric protected compound **24**. Note that the synthesis towards **24** was discussed in *chapter 3.1* (*vide supra*). End-capping of **24** with *p*-methylbenzylthiol under the same conditions gave precursor **25**. Monomeric side-chain **26** was obtained *via* deprotection in dichloromethane with triethylsilane as cation scavenger and trifluoroacetic acid as a proton source in an overall yield of 17 %. Elongation with compound **24** and sodium hydride in tetrahydrofuran gave dimer **27**, and subsequent deprotection with trifluoroacetic acid and triethylsilane in dichloromethane gave dimeric side-chain **28** in an overall yield of 11 %.

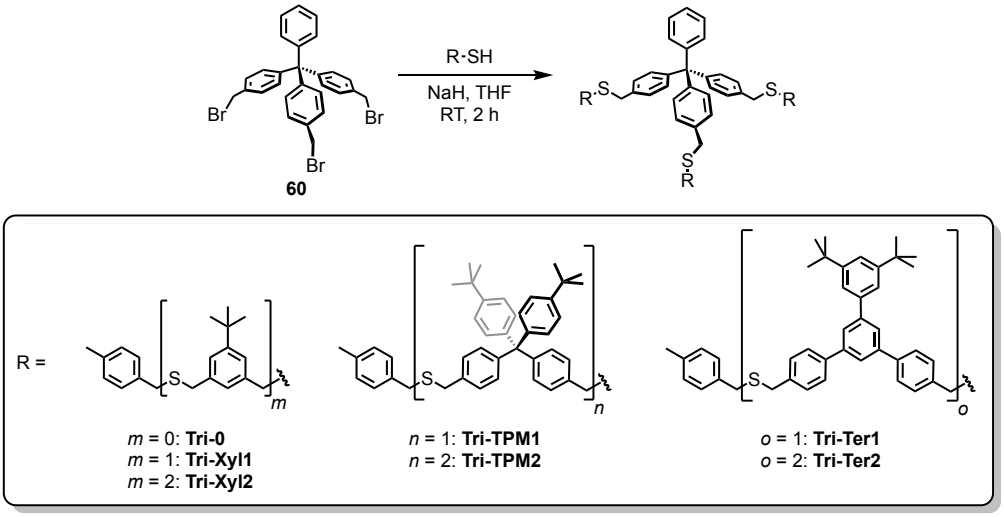

Scheme 23: Synthesis of all final ligands from central linking unit **60**.

All ligands **Tri-0**, **Tri-Xyl1**, **Tri-Xyl2**, **Tri-TPM1**, **Tri-TPM2**, **Tri-Ter1** and **Tri-Ter2** were synthesized under closely similar conditions using **60** as the central linking unit, *p*-methylbenzylthiol as a side-chain for **Tri-0** or the respective side-chain thiols **9** and **11** for ligands **Tri-Xyl1** and **Tri-Xyl2**, side-chain thiols **40** and **42** for ligands **Tri-TPM1** and **Tri-TPM2**, side-chain thiols **26** and **28** for ligands **Tri-TPM1** and **Tri-TPM2**, allowing the S_N2-reactions to start by addition of NaH as base (Scheme 23).

4.1.2 Synthesis of the Gold Nanoparticles

AuNP syntheses from all seven ligands **Tri-0**, **Tri-Xyl1**, **Tri-Xyl2**, **Tri-TPM1**, **Tri-TPM2**, **Tri-Ter1** and **Tri-Ter2** (Scheme 24) was carried out following a previously successfully implemented protocol[79–84] based on a variation of the AuNP synthesis proposed by Brust and coworkers.[165] In

the aqueous phase of a biphasic system, one molar equivalent of gold-salt ($HAuCl_4$) for each sulfur atom in the ligand, dissolved in the organic phase (DCM), was added. This means that 3 molar equivalents of $HAuCl_4$ were used for the tridentate ligand **Tri-0**, 6 molar equivalents of the gold-salt for the hexadentate ligands **Tri-Xyl1**, **Tri-TPM1** and **Tri-Ter1**, and 9 molar equivalents of gold for the nonadentate ligands **Tri-Xyl2**, **Tri-TPM2** and **Tri-Ter2**. The transfer of the gold-salt from the aqueous to the organic phase was achieved by addition of tetra-*n*-ammonium bromide (TOAB) to the organic phase. Nucleation of the AuNPs was induced *via* reduction by addition of an aqueous solution of sodium borohydride ($NaBH_4$). The effectiveness of which was observed by an immediate change in color of the organic phase from bright red to opaque dark brown. After rigorous stirring for 15 minutes, the phases were separated and the particles were allowed to precipitate by addition of excess ethanol. Separation and purification of the AuNPs from excess TOAB, $NaBH_4$ and ligand molecules was achieved by centrifugation and subsequent size-exclusion chromatography (Biobeads SX-1).

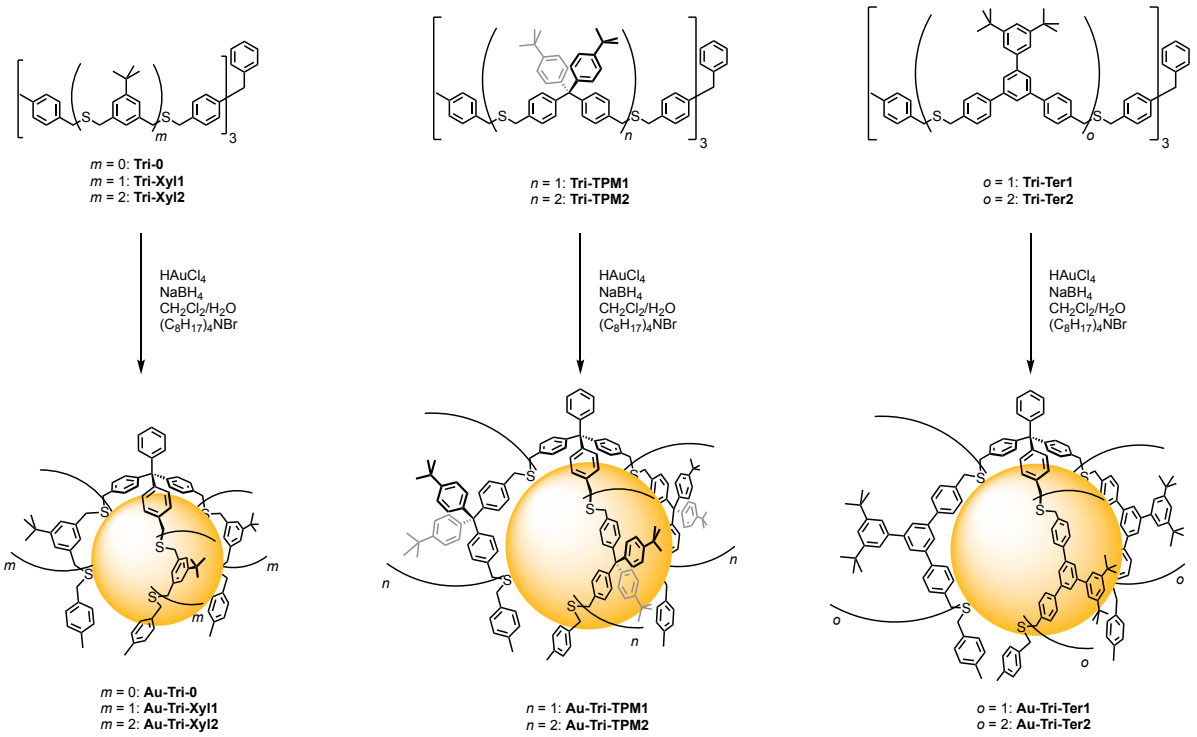

Scheme 24: Syntheses of AuNPs formations with the tripodal tetraphenylmethane-based thioether derivatives (**Tri**) with three different side-chains (**Xyl$_m$**, **TPM$_n$** or **Ter$_o$**) and concept of their Au nanoparticle stabilization by surface coating.

4.1.3 Results and Discussion

During AuNPs synthesis with the ligands **Tri-0** and **Tri-Xyl1** (**Au-Tri-0** and **Au-Tri-Xyl1**) no precipitation was observed, but after a few hours at room temperature an insoluble black solid was

formed, disabling further analysis. For ligand **Tri-Ter1** even during the process of AuNPs formation, black precipitate was formed, already pointing towards the moderate ability of the terphenyl-type backbone to stabilize the NPs for shorter linear terphenyl-type oligomers as discussed in a *chapter 3.1*. Particles passivated with ligand **Tri-Xyl2** and **Tri-Ter2** (**Au-Tri-Xyl2** and **Au-Tri-Ter2**) were stable for days in both dry state and redispersed in dichloromethane with no signs of alteration in the UV-Vis absorption spectrum, giving evidence consistency in particle size and stability. Moreover, we hereby further confirm the assumption that a longer ligand chain comprising more thioether moieties gives greater stability of the AuNPs, since a stronger overall anchoring of the ligand to the particles can be achieved for the same ligand system, as has already been proposed in earlier works within the field of multidentate thioether stabilized AuNPs.[80,81] Both, however, showed signs of decomposition after several days when deposit of the same indispersible black powdery residue was observed for **Au-Tri-0** and **Au-Tri-Xyl1** was found, indicating a rather limited long-term stability of **Au-Tri-Xyl2** as well as for **Au-Tri-Ter2**. For this reason, no thermal stability experiments were conducted with **Au-Tri-Xyl2** and **Au-Tri-Ter2**, as they clearly showed their limited stability at room temperature already. In the case of AuNPs stabilized by the ligands **Au-Tri-TPM1** and **Au-Tri-TPM2** (**Au-Tri-TPM1** and **Au-Tri-TPM2**), however, no such stability issues as well as no alteration of their UV-Vis absorption spectra were observed over weeks during which time the particles were stored, analyzed, dispersed and re-dried in vacuo multiple times, showing the ligands' excellent stabilization abilities similar to the linear tetraphenylmethane-based oligomer discussed in the chapter before (*vide supra*). The particles with moderate to excellent stabilities were analyzed and characterized by UV-Vis absorption spectroscopy and transmission electron microscopy (TEM), while only for **Au-Tri-Xyl2**, **Au-Tri-TPM1** and **Au-Tri-TPM2** further characterization by TGA and ^{1}H-NMR were performed.

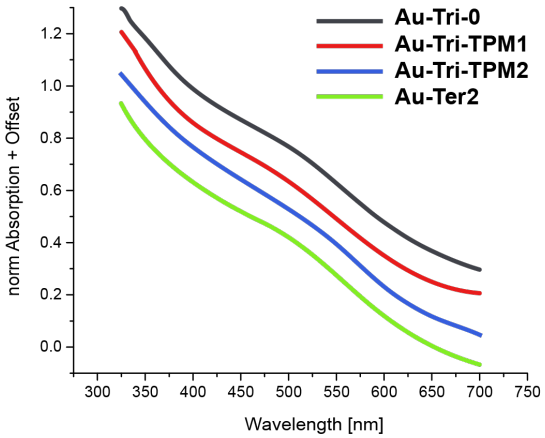

Figure 18: Normalized UV-Vis absorption spectra of the ligands stabilized nanoparticles **Au-Tri-Xyl2** (black), **Au-Tri-TPM1** (red), **Au-Tri-TPM2** (blue) and **Au-Tri-Ter2** (green) recorded in dichloromethane. The individual absorption spectra are shifted vertically for clarity (offset).

The UV-Vis absorption spectra (Figure 18) of all ligand stabilized AuNPs show an absence of a discrete plasmon resonance band (SPR) at around 520 nm, indicating sizes below 2 nm.[166] Almost similar sizes for present AuNPs can be assumed, as the absorption bands display similar curvature, despite the different side-chains. Size determination of the AuNPs by TEM analysis indeed revealed almost similar mean sizes within error boundaries (Figure 19): 1.24 ± 0.3 nm for **Au-Tri-Xyl2**, 1.05 ± 0.3 nm for **Au-Tri-TPM1**, 1.17 ± 0.3 nm for **Au-Tri-TPM2** and 1.27 ± 0.4 for **Au-Tri-Ter2**. The distribution of **Au-Tri-Ter2** show a trend to slightly larger sizes with a main size (bar with highest population) around 1.4 nm with slightly increased error boundary. This could be induced due to the increased spacing of the sulfur atoms of the spacing. The main size for **Au-Tri-Xyl2** is 1.1 nm, for **Au-Tri-TPM1** is 0.9 nm and for **Au-Tri-TPM2** is 1.2 nm. That the main size is slightly off the mean size is however likely due to the limited resolution of the TEM device for such minute sizes of AuNPs. Therefore, these data are probably not very accurate and high-resolution TEM analysis would be helpful here, as pictures with a higher resolution have higher contrast and thus can easier be processed and analyzed with the analysis program (*ImageJ* - free online software), resulting in a more accurate Gaussian distribution. Nevertheless, the fact that the UV-Vis for all present particles show no plasmon resonance with similar curvature, the influence of the side-chains architecture seems less dictating and the size is likely to be determined from the central linking unit. That the tetraphenylmethane-type side-chains - also with a slightly increased spacing compared to the *meta*-xylene-type side-chains - give NPs with small sizes was also observable for their linear counterparts discussed in *chapter 3.2* (*vide supra*) and is thus not very surprising. Also, their increased stability features, so far observed during several drying and redispersing cycles with no signs of precipitation is very similar to their linear ligands.

In the ^{1}H-NMR spectra of the AuNPs **Au-Tri-Xyl1**, **Au-Tri-TPM1** and **Au-Tri-TPM2**, the characteristic broadening of all ligand signals due to the reduced tumbling motion of the ^{1}H-labels in comparison to the free ligands is clearly visible, giving evidence of the successful stabilization of the NPs by their respective ligands (see Figure 46, Figure 47 and Figure 48 in *8. Appendix*). Note that the broadening of the protons of **Au-Tri-Xyl2** is not as pronounced as for **Au-Tri-TPM1** and **Au-Tri-TPM2**, likely due to the limited stability features. The spectra further prove the successful separation and purification of the AuNPs from both the phase transfer catalyst TOAB and the excess ligand by repeated centrifugation and size-exclusion chromatography.

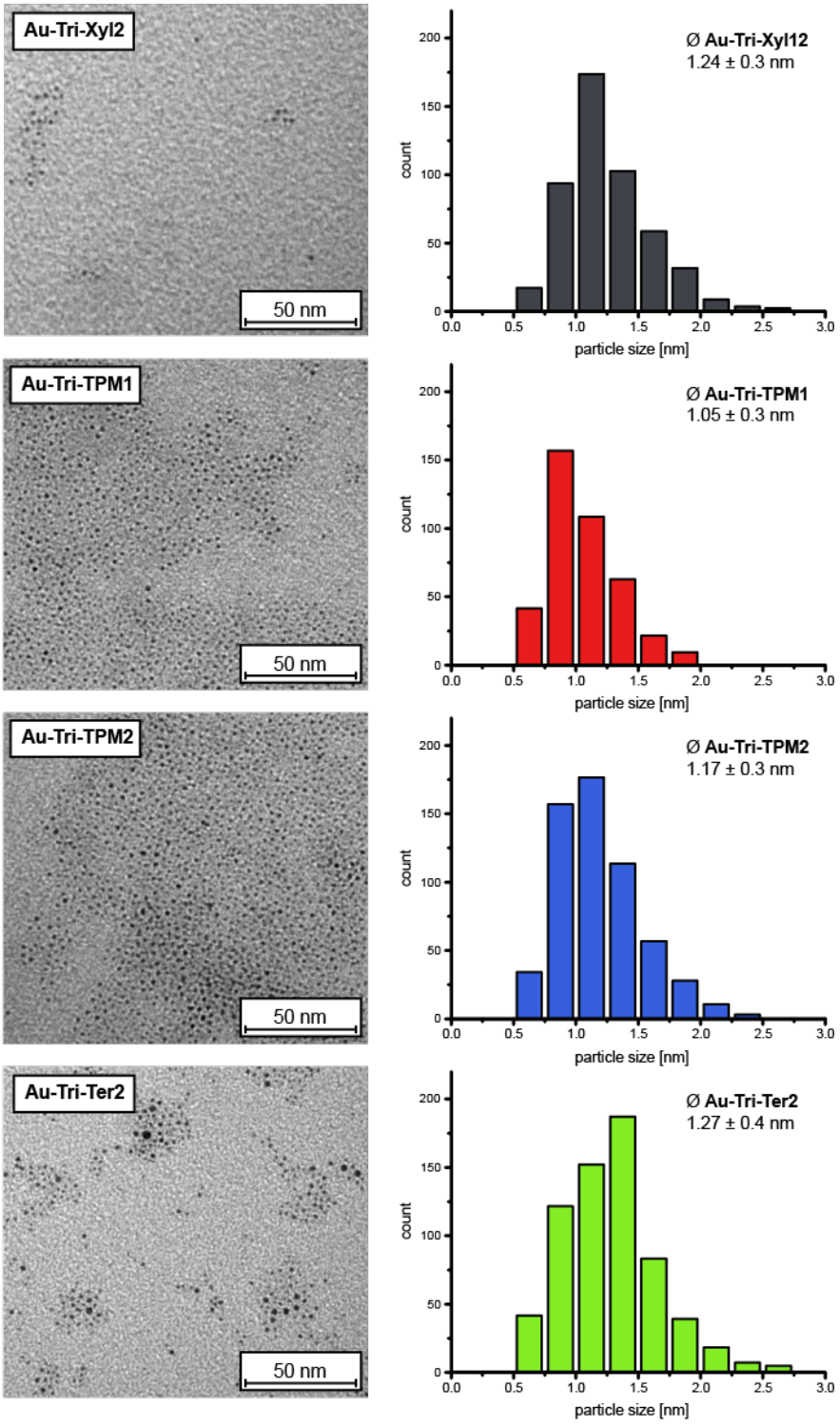

Figure 19: *Left*: Representative sections of the TEM micrographs for samples of the ligand-stabilized nanoparticles **Au-Tri-Xyl2**, **Au-Tri-TPM1**, **Au-Tri-TPM2** and **Au-Tri-Ter2**; *right*: corresponding size distributions of the particles observed in the TEM micrographs.

In order to determine the ligand-to-particle ratio, TGA was performed with **Au-Tri-Xyl2**, **Au-Tri-TPM1** and **Au-Tri-TPM2**. All three AuNPs prove consistent behavior by starting to decompose at slightly below 100 °C. The steady loss of material was measured at a constant temperature

increment of 10 °C per minute and was found to flatten out at 600 °C (see Figure 49 and Table 3 in *8. Appendix*). The respective mass losses due to ligand decomposition were 43.91 % for **Au-Tri-Xyl2** which corresponds to 15.11 Au atoms per molecule of **Tri-Xyl2**, 29.72 % in the case of **Au-Tri-TPM1**, giving a ratio of 35.06 Au atoms per molecule of **Tri-TPM1** and finally 30.71 % for **Au-Tri-TPM2**, corresponding to 42.35 atoms stabilized by one ligand **Tri-TPM2**. From these findings, the average size for the respective AuNPs and the bulk density of gold, the ligand-to-particle ratio was calculated. For **Au-Tri-Xyl2**, an average particle was calculated to contain 59.97 atoms, implying a coverage of 3.97 ligands per particle, thus highly exceeding the desired single-ligand enwrapping. This finding has however to be interpreted with caution, as the **Au-Tri-Xyl2** are not very stable compared to the tetraphenylmethane-type counterparts and possible co-stabilization is involved. Important to note here is that short-chained *meta*-xylene-based linear ligands (trimer and pentamer) have reportedly yielded likewise unstable particles.[80] Yet it is imperative to keep in mind that the side-chains which differ fundamentally in their architecture play the major role in the stabilization of the AuNPs. Contrarily, both **Au-Tri-TPM1** and **Au-Tri-TPM2** displayed a lot more promising properties, as their average particle sizes suggest AuNPs composed of 35.80 and 49.53 atoms covered by 1.02 molecules **Tri-TPM1** and 1.17 molecules **Tri-TPM2**, respectively. From this, we conclude that both generate AuNPs covered by a single ligand and thus prove our assumption that these ligands can enwrap a single NP like the claw machines grabbing a toy.

4.1.4 Summary and Conclusions

We have synthesized a central tripodal building block allowing introduction of three oligomeric thioether-based side-chains for reliable monofunctionalization of AuNPs comprising one freely accessible site for the introduction of functional groups. All successfully synthesized AuNPs are of the same size within error tolerance despite variation of the side-chains, indicating that not the side-chains or the distance between two thioether moieties, yet rather the conformation of the central building unit dictates the curvature and thus the dimensions of the nanoparticles. Both ligands comprising tetraphenylmethane-based side-chains with different length (**Tri-TPM1** and **Tri-TPM2**) enwrap the particles with enhanced stability features in a ligand-to-NP ratio of 1:1, suitable for monofunctionalized NPs for future wet chemical approaches. Further, these two ligands stand in line with similar previously presented and discussed ligands in regard of stability dependence on number of thioethers binding to the gold as well as to their bulkiness.

4.2 Tripodal Tetraphenylmethane-Based Cages

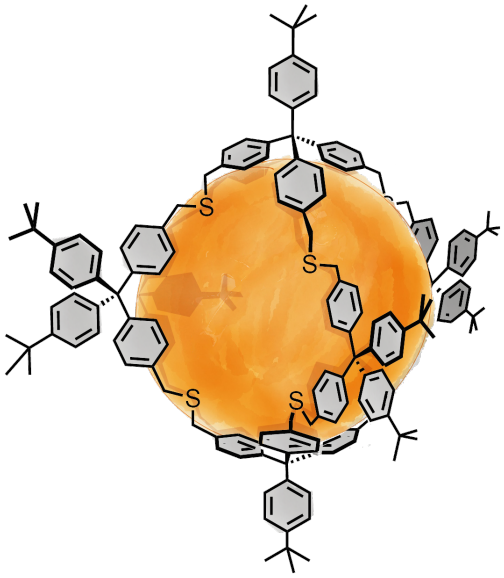

Within this chapter, the synthesis of cage-like compounds consisting of tetraphenylmethane-type structures and their passivation of AuNPs with a particular attention on their stability is discussed. This work is a consequential continuation of the before-discussed tripodal compounds, which exhibited excellent AuNP stability when linked with tetraphenylmethane-type side-arms. As a major advantage, cage-like compounds should deliver exclusively monofunctionalized NPs when decorated with suitable functionality at its periphery.

Formation of AuNPs with well-defined and monodisperse sizes in a controlled manner is crucial for future applications.[1] Therefore, cage-like compounds have recently attracted increased attention, allowing controlled templated synthesis of AuNPs with tailor-made properties given by their structural design. Only a few examples are however reported so far in literature, as the synthesis of such cage-molecules are challenging to realize with the attention to their future AuNPs' stability. A DNA-origami cage is reported by Zhang and coworkers which swallows gold nanoparticles with a size range from 3-5 nm separated by gel electrophoresis.[167] Another example of DNA-origami AuNPs is described shown by Liu *et al.* where particle size up to 15 nm can be furnished. Recently McCaffrey *et al.* reported the first example of controlled AuNP synthesis, templated in a well-defined, discrete organic cage with a size of 1.9 nm.[143] An interesting aspect of that work is the fact that only a few thioether groups are used for the nucleation of the AuNPs, whereas the bare organic aromatic cage-like backbone is stabilizing the entire particle and dictating

their sizes. Another example of cage-templated synthesis to stable and monodisperse NPs is reported by Mondal *et al.* with various sizes up to 3.7 nm.[168] A possible disadvantage of the two latter examples may lie in the long-term stability and the inherent limited processability for future applications as the ligand shell consists of a bare aromatic ligand shell with almost no steric repulsion.

A major advantage of cage-like molecules lies in the NPs' surface functionalization, as they can label the NP with a single copy of a functional moiety. On the basis of our previous work on tripodal tetraphenylmethane-based dendritic molecules, which offered great AuNP stability properties, we were wondering whether it will be possible to make similar cage-like structures. For this purpose, we designed novel structures (Figure 20) with different cavity sizes, each interlinked *via* three strands.

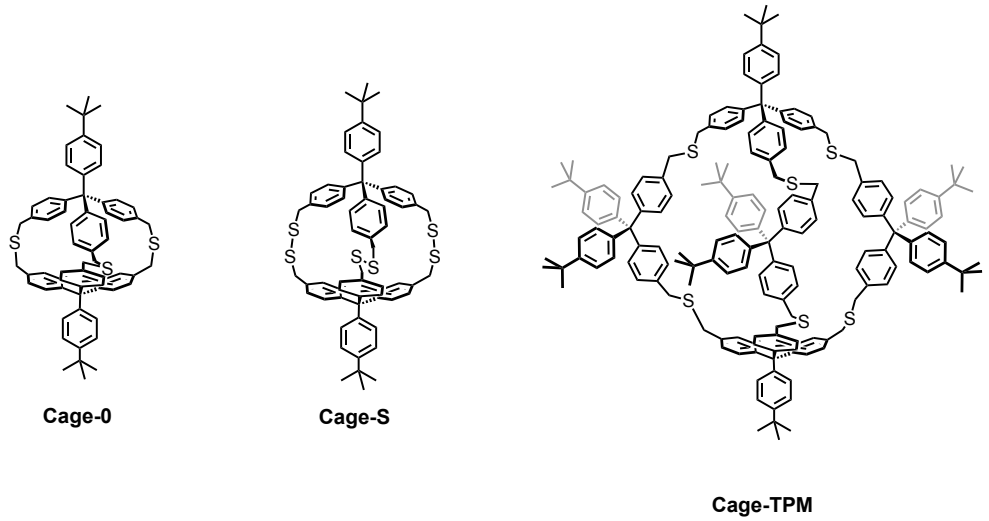

Figure 20: Cage-like compounds **Cage-0**, **Cage-S** and **Cage-TPM**.

The additional *tert*-butyl groups attached on their periphery compared to the tripodal derivatives (*e.g.* **Tri-TPM1**) should render increased stability and redispersibility for future wet chemical applications. Furthermore, a facile functionalization on one side of the periphery would give both: monofunctionalized AuNPs with well-defined and monodisperse sizes with enhanced stability due to their structural features.

4.2.1 Synthesis of the Ligands

As mentioned in the introduction, tripodal derivatives consisting of a tetraphenylmethane-based backbone, discussed in *chapter 4.1* (*vide supra*) are ideal precursors to form cage-like compounds. In Scheme 25, three possible target molecules are suggested which are likely to be readily synthesized

out of the corresponding bromo- or thiol-precursors, respectively, and are formed *via* S_N2 reactions in the case of **Cage-0** and **Cage-TPM**, or *via* oxidative thiol-homo-coupling in the case of **Cage-S**. The concentration of the reaction with which these cage-compounds are closed is assumed to play a major role, for 1) the closing itself and 2) minimize the amount of side-products such as oligomers, which are however inevitable. The formed products and side-products would be then purified by flash column chromatography and purified by automated recyclable gel permeation chromatography (GPC), benefiting from their decreased hydrodynamic radii compared to the formed oligomers.

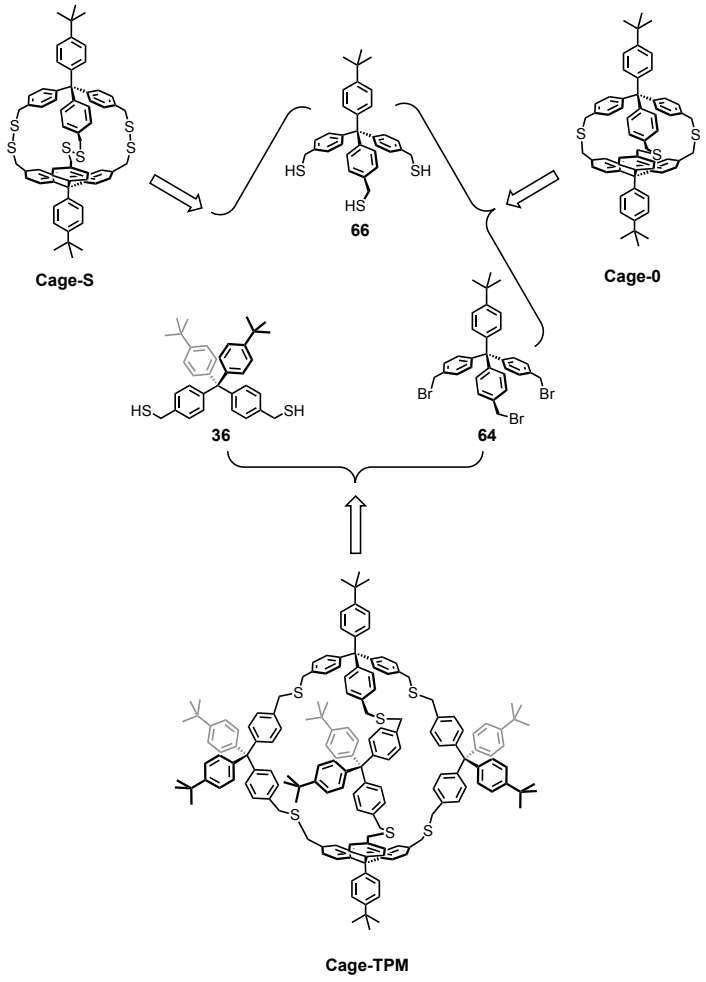

Scheme 25: Retrosynthetic pathways of cage-like compounds: **Cage-0**, **Cage-S** and **Cage-TPM**.

The tris-thiol compound **66**, precursor of the target **Cage-S** and **Cage-0**, and the tris-bromo precursor **64** of **Cage-TPM**, are synthesized as follows (Scheme 26): Compound **29** was obtained *via* twofold Grignard reaction and was already described in *chapter 3.2* (*vide supra*). Subsequent electrophilic aromatic substitution with aniline in glacial acetic acid with hydrochloric acid as catalyst gave tetraphenylmethane-derivative **61**. Subsequent one-pot Sandmeyer-type reaction delivered compound **62** by substitution of the amine by an iodine atom through preliminary *in situ*

formation of its diazonium salt. Subsequent methylation with methyl lithium in THF yielded compound **63** with the completed carbon skeleton of the target structure in a yield of ~18 % over the four steps. The tripodal bromo-precursor **64** was obtained in 65 % yield *via* mild bromination of compound **63** with *N*-bromosuccinimide (NBS) as a bromine source and azobisisobutyronitril (AIBN) as a radical starter in methyl formate, exploiting the solvent's low boiling point and therefore hindering overbromination of the benzylic position upon illumination with a halogen lamp. The synthesis towards tripodal thiol-precursor **66** could not be accomplished by direct reaction using thiourea as sulfur source due to solubility issues and thus, a two-step route was chosen: compound **64** was first reacted with an excess of trityl mercaptane and sodium hydride in tetrahydrofuran replacing both bromines with protected sulfurs to form compound **65** which were then easily cleaved with trifluoroacetic acid in presence of triethylsilane as cation scavenger in dichloromethane at room temperature with a yield of 80 % over both steps.

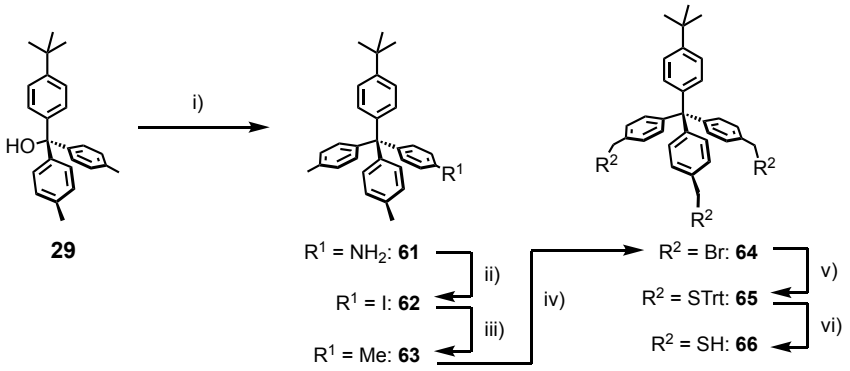

Scheme 26: Molecular structures and synthesis of tripodal precursors **64** and **66**: i) aniline, HCl, AcOH, 140 °C, 3 h, 49 %; ii) 1) BF_3OEt_2, *t*$BuNO_2$, DCM, -10 °C, 2 h, 2) I_2, KI, RT, 20 h, 55 %; iii) MeLi, THF, -78 °C, 2 h, 81 %; iv) NBS, AIBN, hν, methyl formate, reflux, 15 h, 65 %; v) TrtSH, THF, RT, 15 h, 88 %; vi) Et_3SiH, TFA, DCM, RT, 1 h, 91 %. Me = methyl, Trt = trityl.

Cage-like compound **Cage-S** was obtained as follows (Scheme 27): a solution of tripodal thiol-compound **66** (2.34 mM) and sodium hydride in tetrahydrofuran was vigorously stirred under ambient conditions. After preliminary flash column chromatography to exclude major side-products, the crude was subjected to automated recyclable GPC affording **Cage-S** in 52 % yield after few cycles. Note that the progress of these cage-like compounds could fortunately be monitored by MALDI-ToF mass spectrometry. Figure 21 shows the ^{1}H-NMR spectra of **Cage-S** with a zoomed section of the benzylic region. One can recognize that the molecule is highly symmetric (D_{3h}) in solution and thus the benzylic protons appear as single peak. Moreover, this peak appears despite the adjacent disulfide moieties at 3.68 ppm and is thus very similar to benzylic protons of linear tetraphenylmethane-based oligomers. This slight upfield shift compared to linear

benzylic disulfide derivatives may arise due to the constrained cage-like system. Note that the signals of both *tert*-butyl protons appear as a singlet at 1.30 ppm and the adjacent major peak at 1.26 ppm belongs to residual grease either from the deuterated solvent or from the cage-like features.

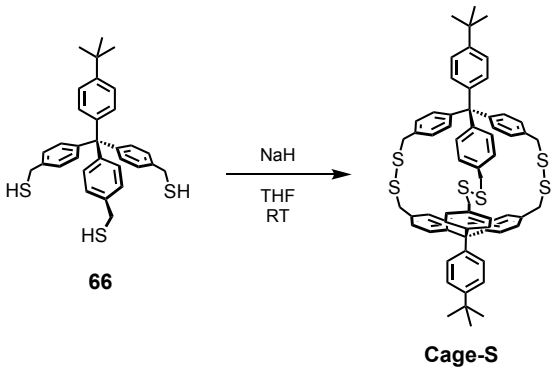

Scheme 27: Synthesis of cage-like compound **Cage-S** with tripodal thiol-derivative **66**.

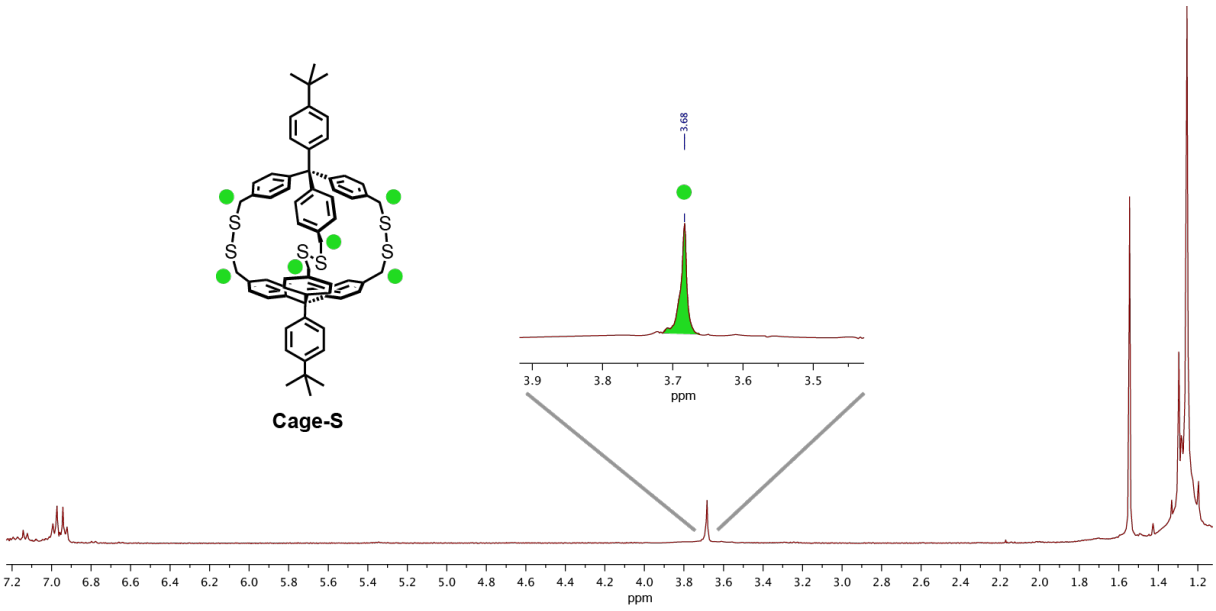

Figure 21: ^{1}H-NMR spectra of compound **Cage-S** and zoomed benzylic region measured in chloroform-*d*.

The synthesis towards the cage-like molecule **Cage-0** is depicted in Scheme 28. Tripodal bromo-derivative **64** (970 µM) and tris-thiol derivative (970 µM) were dissolved in freshly distilled and argon-purged tetrahydrofuran. For all final closings, tetrahydrofuran was always freshly distilled and degassed for at least 15 minutes (depending on the amount of solvent used) and before the addition of sodium hydride, the reaction mixture was degassed as well for at least 10 minutes in order to avoid unwanted disulfide formations, which would significantly lower the yield and complicate the purification. The reaction process could also be monitored by MALDI-ToF mass

spectrometry. After preliminary flash column chromatography to exclude major side-products the product was obtained after a few cycles on the automated recyclable GPC in a yield of 61 %. The ^{1}H-NMR in Figure 22 shows similar features like for cage-like molecule **Cage-S** discussed before. The symmetry of **Cage-0** (D_{3h}) also shows one set of signal as singlet for the benzylic protons. The distinctive upfield shift of the benzylic protons (3.81 ppm) is rather unusual compared to linear tetraphenylmethane-based oligomers and is likely due to the constraint system. The signals for both *tert*-butyl protons (1.28 ppm) appear also here as singlet and are next to the less prominent grease peak (1.26 ppm). It however might be that these cage-like molecules are prone to trap grease from the solvent due to their cage-like features.

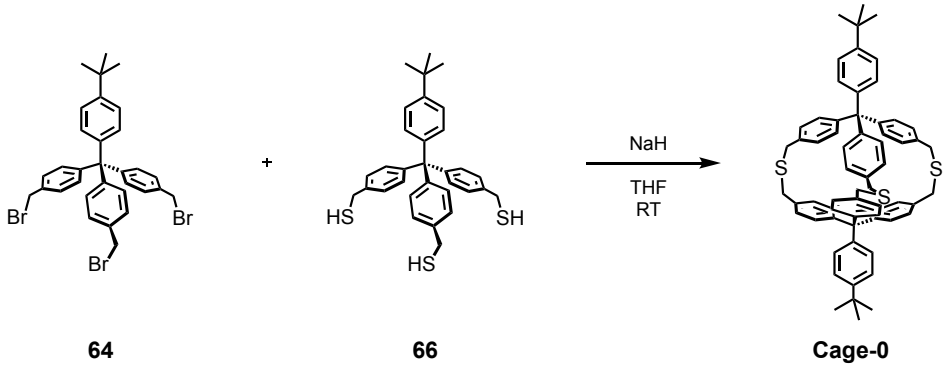

Scheme 28: Synthesis of cage-like compound **Cage-0** with tripodal bromo-derivative **64** and thiol-derivative **66**.

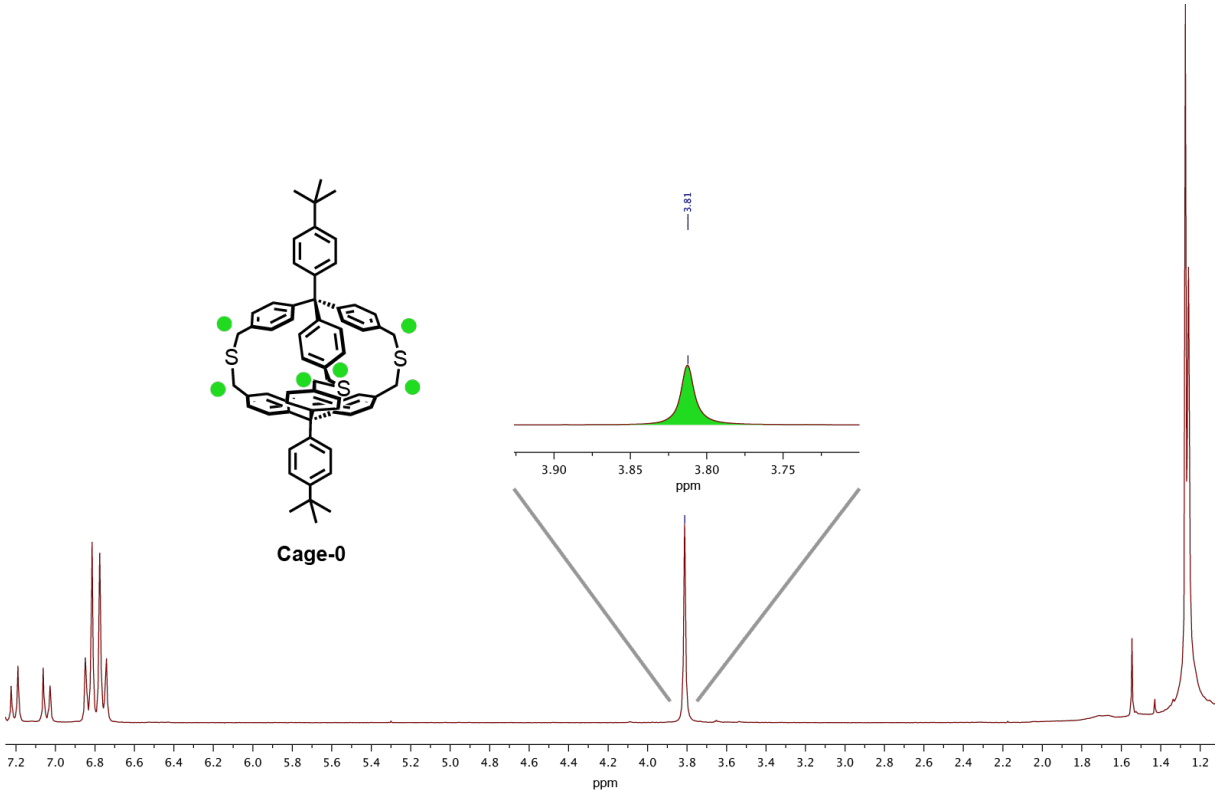

Figure 22: ^{1}H-NMR spectra of compound **Cage-0** and zoomed benzylic region measured in chloroform-*d*.

The synthesis towards **Cage-TPM** was performed as follows (Scheme 29): Two molar equivalent of tripodal bromo-derivative **64** (30.6 mM) and three molar equivalent of dithiol-derivative **36** (45.8 mM) were dissolved in freshly distilled and argon-degassed tetrahydrofuran. The reaction mixture was degassed before the addition of sodium hydride at room temperature. To our delight the mass of the product could be observed after a few hours of reacting, which unfortunately did not correspond to the wanted cage-like compound **Cage-TPM**.

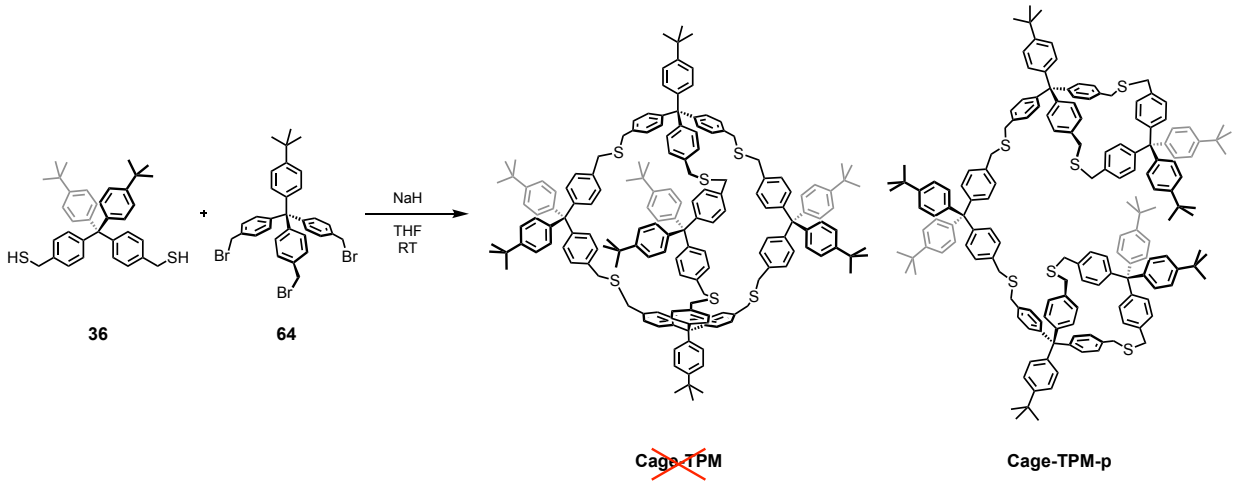

Scheme 29: Synthesis of pseudo cage-like compound **Cage-TPM-p** instead of **Cage-TPM** with tripodal bromo-derivative **64** and dithiol-derivative **36**.

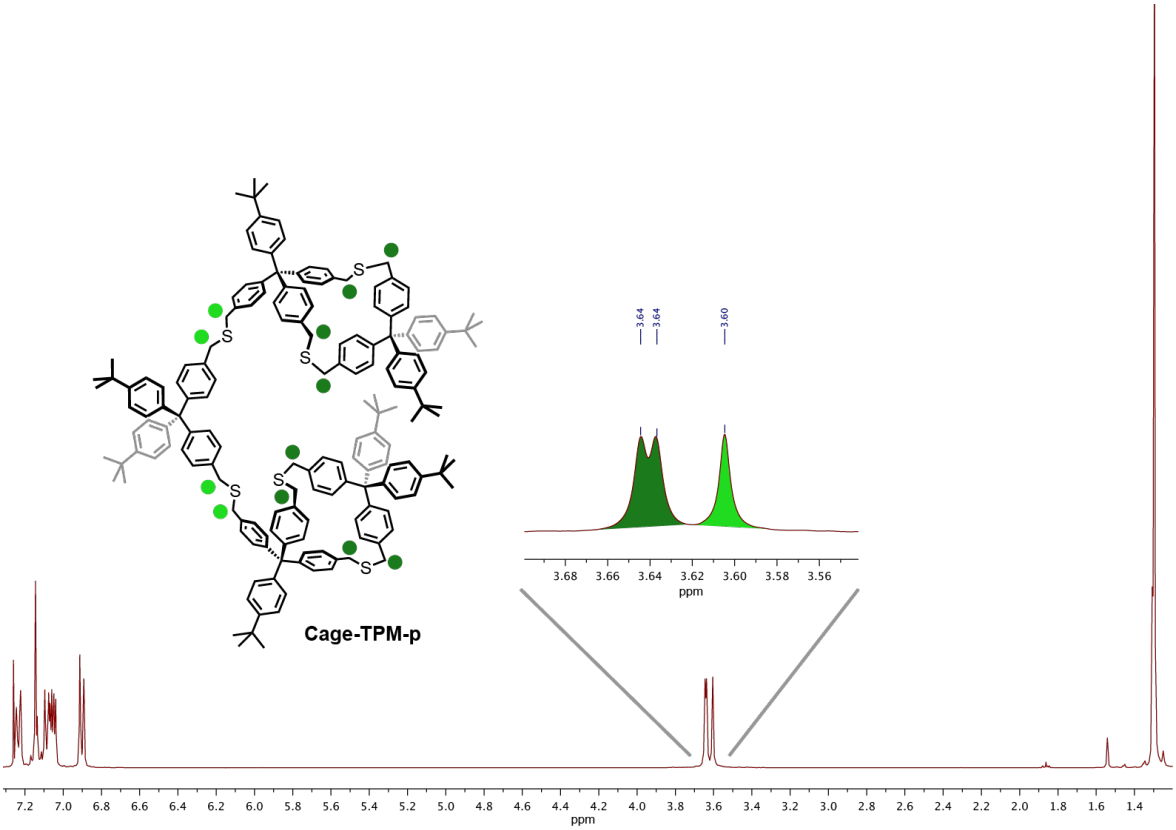

Figure 23: ^{1}H-NMR spectra of compound **Cage-TPM-p** and zoomed benzylic region measured in chloroform-*d*.

The ^{1}H-NMR depicted in Figure 23 shows for the benzylic protons three sets of singlets (3.60-3.64), two of which are overlapping, and a singlet which is slightly downfield shifted. There findings would rather correspond to a structure suggested as the "pseudo cage-like" structure **Cage-TPM-p** with a C_{2v}-symmetry. As **Cage-TPM** would most likely have a symmetry of D_{3h}, two singlets are thus expected for the benzylic protons. Also, the signals for the *tert*-butyl groups around ~1.30 ppm (see *7. Experimental Part*) appear as two singlets with similar integrals and a larger singlet with double the integral, which would point towards the **Cage-TPM-p** structure. It therefore seems that the reaction of the dithiol-derivative (compound **36**) is more favored when the two bromides belong to the same molecule rather than when the reaction involves two molecules of compound **64**. Interestingly, by lowering the temperature, increasing the concentration or even under addition with pseudo-high dilution (syringe pump), not any different result was obtained.

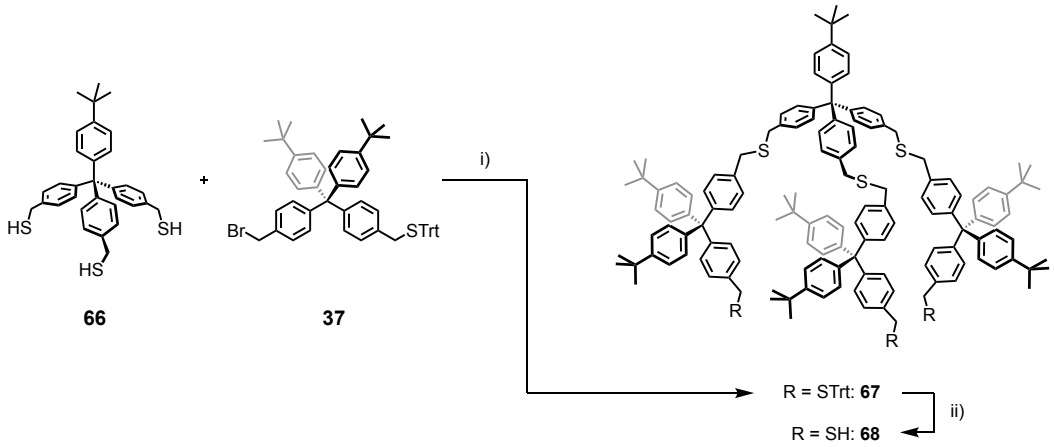

Scheme 30: Stepwise pathway to compound **68** to avoid the intramolecular substitution.

To avoid the intramolecular substitution, describe above, a stepwise pathway was therefore chosen (Scheme 30). The synthesis to the tripodal compound **68** comprising elongated thiol side-chains was performed as follows: tripodal thiol-derivative **66** was enlarged with an excess of the asymmetric S-trityl-protected bromo-derivative **37** in tetrahydrofuran using sodium hydride as base to form compound **67** in a yield of 61 %. The synthesis towards compound **37** was described in *chapter 3.2* (*vide supra*). Subsequent deprotection with trifluoroacetic acid and triethylsilane as cation scavenger gave precursor **66** in 85 %.

The final closing towards the cage-like molecule **Cage-TPM** was then performed similar to the protocols described before (Scheme 31): in a typical reaction, one molar equivalent of bromo-precursor **64** (2.02 mM) and one molar equivalent of tripodal thiol-precursor 67 (2.02 mM) were dissolved freshly distilled and argon-degassed tetrahydrofuran. Before the addition of sodium

hydride, the reaction mixture was degassed for at least 10 minutes (depending on the amount of THF), to avoid major disulfide formations which would lower the yield significantly and to avoid side-products with similar hydrodynamic radii impeding the separation and purification of the product. After preliminary flash column chromatography to exclude major side-products the product was obtained after a few cycles on the automated recyclable GPC in a yield of 61 % (mixture).

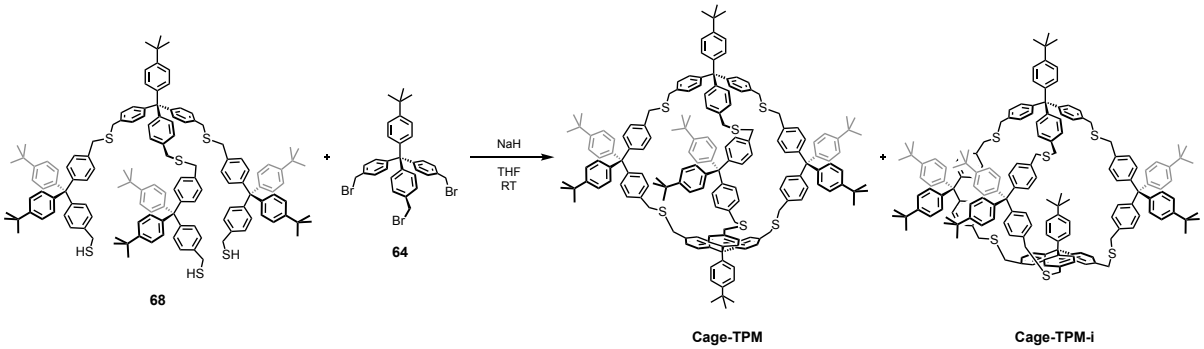

Scheme 31: Final closing of compound **68** with **64** to afford both: **Cage-TPM** and unwanted side-product **Cage-TPM-i**.

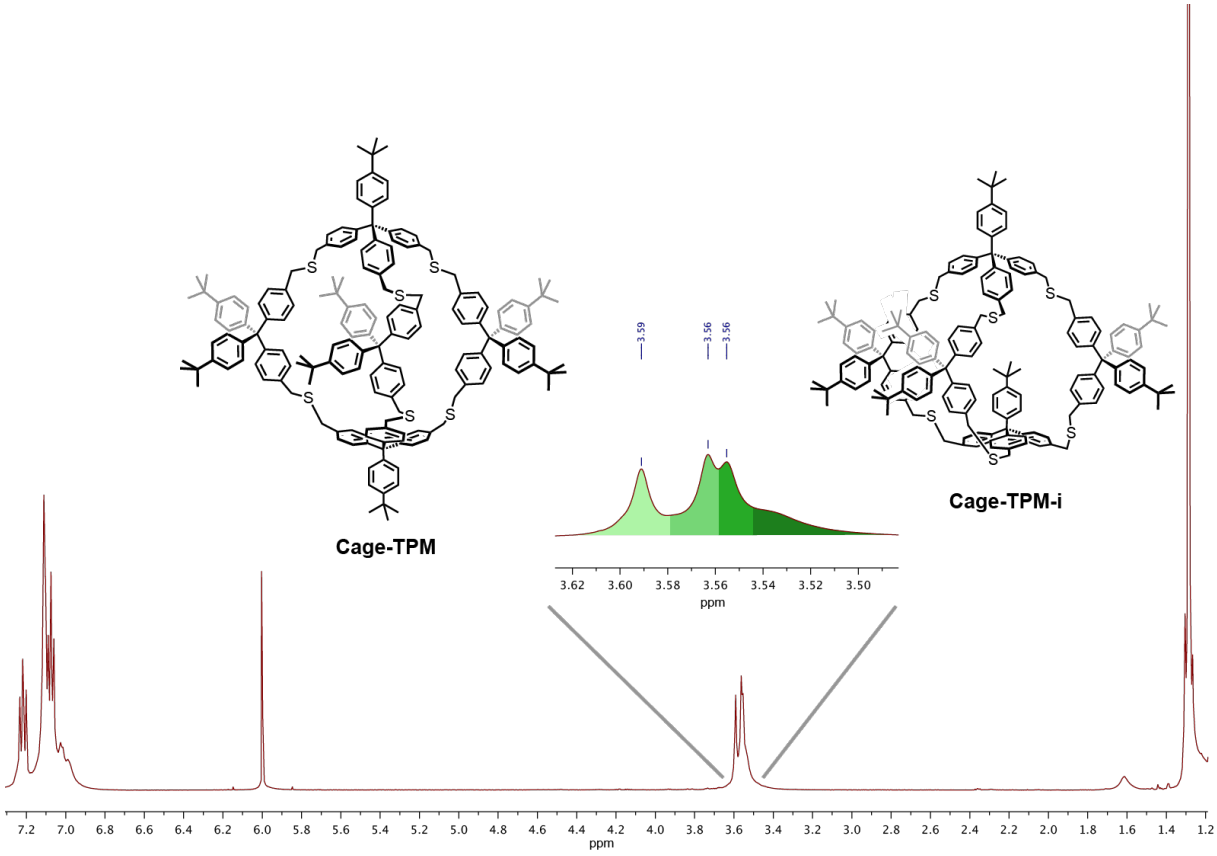

Figure 24: ^{1}H-NMR spectra of a mixture of cage-like molecules **Cage-TPM** and **Cage-TPM-i** and zoomed benzylic region measured in 1,1,2,2-tetrachloroethane-d_2.

Although the peak appeared as single peak after several cycles on the GPC the ^{1}H-NMR (Figure 24) revealed a mixture of compounds. As mentioned before, two singlets would be expected in the benzylic region due to the symmetry of **Cage-TPM**. However, in the spectra, three prominent and a broad singlet are clearly observable (see four shades of greens in Figure 24), pointing to - most likely - two compounds. This, and the fact that there was a single peak visible in the GPC, *i.e.* with the same hydrodynamic radii together with the mass-peaks only belonging to the product let us assume the presence of two compounds. It could be explained by two different ways of closing the cage by one of the tripodal tetraphenylmethane-based bromo-compound **64** involved in the reaction: 1) with the *tert*-butylbenzene unit pointing outwards, which gives **Cage-TPM** and 2) with the *tert*-butylbenzene unit pointing inwards, giving its inversed cage-like molecule **Cage-TPM-i**.

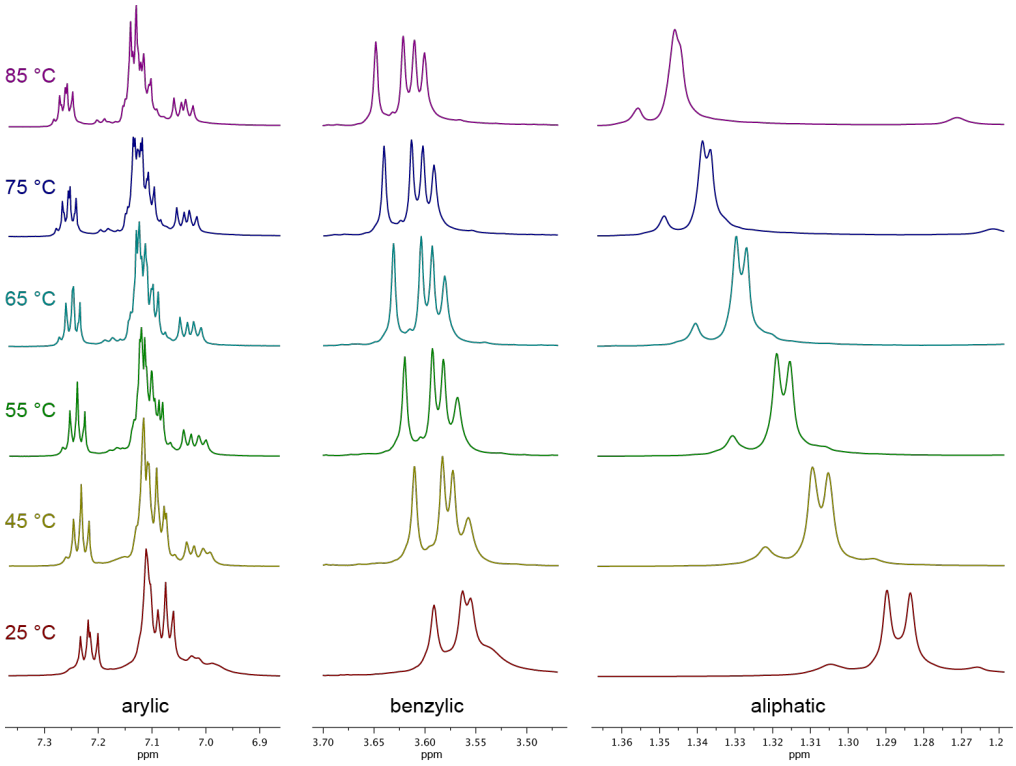

Figure 25: Temperature-dependent ^{1}H-NMR starting from 25 °C up to 85 °C for the arylic, benzylic and the aliphatic region of the mixture of **Cage-TPM** and **Cage-TPM-i** measured in 1,1,2,2-tetrachloroethane-d_2. Note that the various regions (arylic, benzylic and aliphatic) are cut apart and zoomed independently for clarity and can thus not be compared with each other on that figure.

To further analyze the mixture of **Cage-TPM** and **Cage-TPM-i**, temperature-dependent ^{1}H-NMR were measured and are summarized in Figure 25. The upfield shift of the aliphatic protons (~0.062 ppm) appears relatively strong within that figure for higher temperatures and is due to the different zooming, and is in fact similar to the shift of the benzylic protons (~0.058 ppm), and for

the arylic protons the upfield shift is slightly lower (~0.046 ppm). The signals of the *tert*-butyl moieties move closely together with higher temperature until at 85 °C appear almost as singlet. Interestingly, the before-mentioned broad shoulder, which appears in the benzylic region at room temperature becomes more distinct with higher temperature until at 85 °C when all four signals - probably two of **Cage-TPM** and two of **Cage-TPM-i** - appear as four singlets. Our current working hypothesis of why a set of protons appears such broadened is likely arising from the inverted cage-like compound **Cage-TPM-i**, which hinders a part of the molecule to freely rotate and thus, reduces its tumbling motion resulting in a broad peak. The signals for the protons in the arylic region show similar behavior. With increasing temperatures, the more distinct the peaks can be observed. However, for full NMR characterization, furhter purification and separation of the cages would be required.

As in the previous case, altering the temperature or the concentration did no alter these findings. In addition, the reaction was repeated with a large excess of C_{60}, or the unfunctionalized tetraphenylmethane derivative **33**, respectively, in order to fill the bowl-shaped derivative **68** such that the tripodal bromo-derivative **64** is forced to close the cage while pointing outwards. However, in both cases, the product could not be isolated in the GPC due to the minute amount of formed product (detected with MALDI-ToF) and due to the larger amounts of side-products with similar hydrodynamic radii were formed. Note that various attempts to separate this mixture with the cage-like molecules by HPLC with classical solvent mixtures failed as well, due to their expected similar polarity. Thus, further investigation either in varying the conditions or trying more exotic solvent mixtures for HPLC would probably be helpful here. Nonetheless, AuNP formation of the mixture will still be performed, as **Cage-TPM-i** is predicted to be less stable than **Cage-TPM**, as a *tert*-butyl benzene moiety points inside the cavity of the cage and is expected to crush out of the solution.

For a better spatial imagination of **Cage-TPM**, a geometry optimized model was calculated and is displayed in Figure 26. The calculated symmetry was C_1, instead of previously expected D_{3h}, probably since thioether moieties are too flexible and thus responsible for the distortion within the molecule. One could therefore assume that the benzylic protons in the ^{1}H-NMR of **Cage-TPM** are not symmetrical and appear as shown in Figure 24, suggesting the presence of just the desired molecule. HMBC and HMQC studies confirmed however the presence of two species, which have the same hydrodynamic radii as proven by DOSY experiments. Calculations were carried out using the Gaussian09 suite of codes,[169] on the B3LYP level of theory using a mixed basis set. C, H and S atoms were treated with 6-31G** basis set.[170]

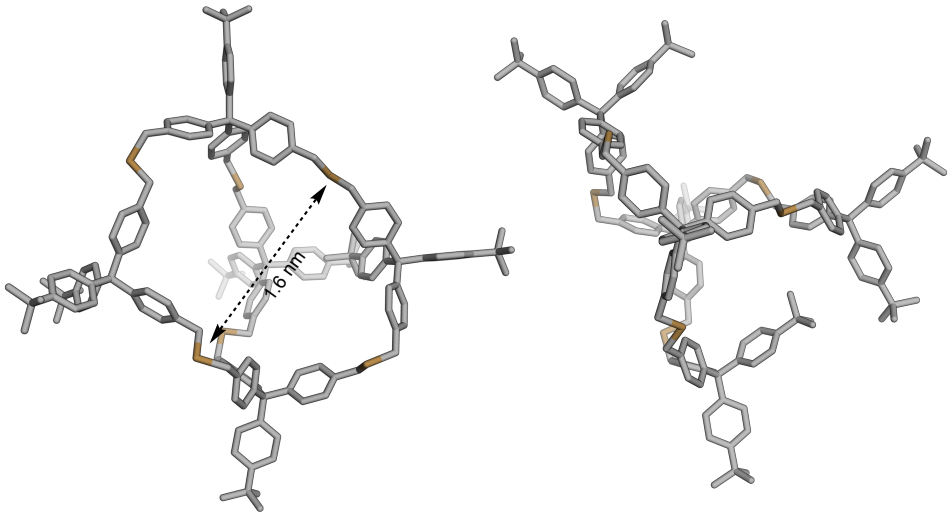

Figure 26: Geometry optimized model of **Cage-TPM** in side-view (*left*) and top-view (right). The cavity inside the cage (diagonal thioether distance) has roughly a diameter of 1.6 nm.

4.2.2 Synthesis of the Gold Nanoparticles

AuNP syntheses from the ligands **Cage-0**, **Cage-S**, **Cage-TPM-p**, and the mixture of **Cage-TPM** and **Cage-TPM-i** (Scheme 32) was carried out following a previously successfully implemented protocol[79–84] based on a variation of the AuNP synthesis proposed by Brust and coworkers.[165] In the aqueous phase of a biphasic system, one molar equivalent of gold-salt ($HAuCl_4$) for each sulfur atom in the ligand, dissolved in the organic phase (DCM), was added. This means that 3 molar equivalents of $HAuCl_4$ were used for the tridentate cage **Cage-0** as well as for **Cage-S** with the three disulfides motifs, and 6 molar equivalents of the gold-salt for the hexadentate pseudo-cage **Cage-TPM-p**, as well as for the mixture of **Cage-TPM** and **Cage-TPM-i**, which both also contain 6 thioether moieties. Note that **Cage-TPM-i** is predicted to be less stable than **Cage-TPM**, as a *tert*-butyl benzene moiety points inside the cavity of the cage and is expected to crush out of the solution. The transfer of the gold-salt from the aqueous to the organic phase was achieved by addition of tetra-*n*-ammonium bromide (TOAB) to the organic phase. Nucleation of the AuNPs was induced *via* reduction by addition of an aqueous solution of sodium borohydride ($NaBH_4$). The effectiveness of which was observed by an immediate change in color of the organic phase from bright red to opaque dark brown. After rigorous stirring for 15 minutes, the phases were separated and the particles were allowed to precipitate by addition of excess ethanol. Separation and purification of the AuNPs from excess TOAB, $NaBH_4$ and ligand molecules was achieved by centrifugation and subsequent size-exclusion chromatography (Biobeads SX-1).

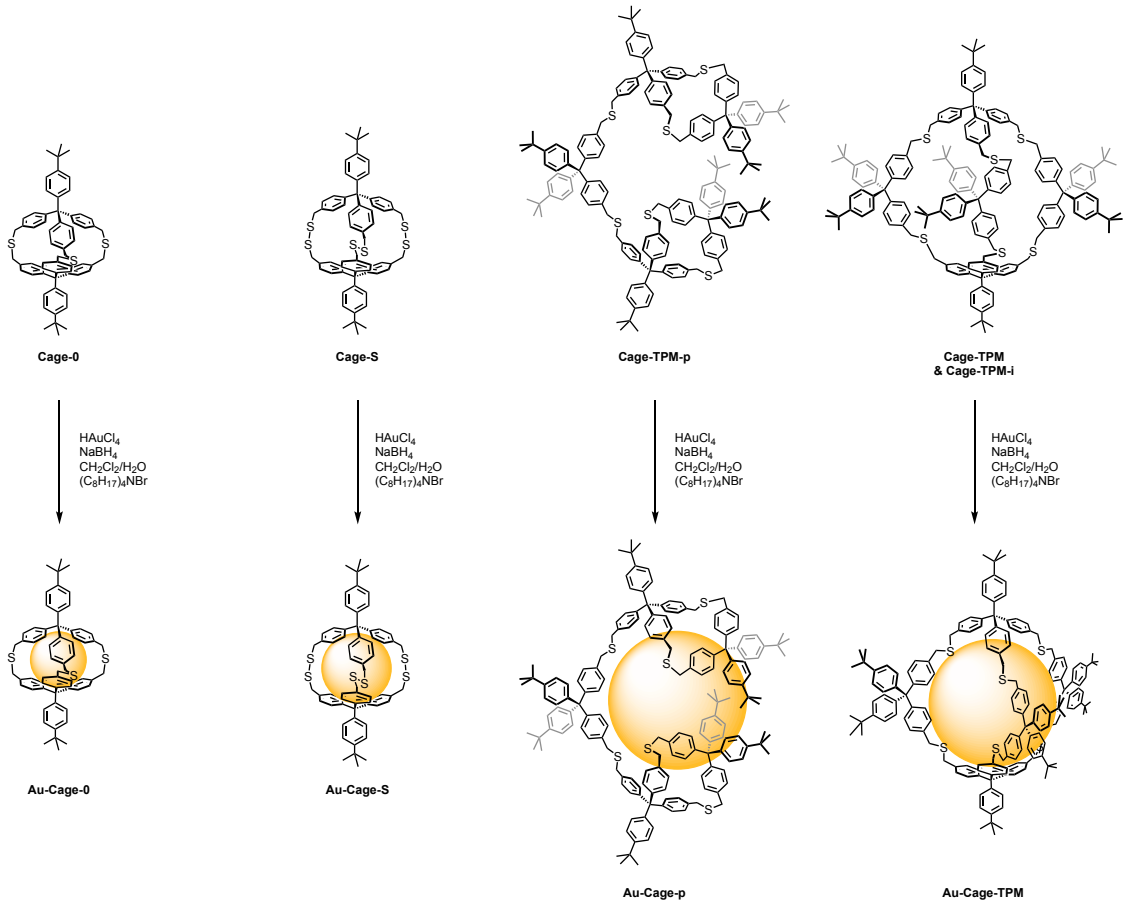

Scheme 32: Syntheses of AuNPs formations with the cage-like compounds **Cage-0**, **Cage-S**, **Cage-TPM-p**, and the mixture of **Cage-TPM** and **Cage-TPM-i**, and concept of their Au nanoparticle stabilization by surface coating. The AuNP stabilization of **Cage-TPM-i** is not depicted, as the resulting particles are not expected to be stable.

4.2.3 Results and Discussion

Although during the AuNP syntheses with the ligands **Cage-0** and **Cage-S** no precipitation of gold was visible, **Au-Cage-0** and **Au-Cage-S** revealed their limited stability while purifying by manual size exclusion chromatography. Indeed, after drying, several attempts to disperse them in common organic solvents failed and remained completely insoluble. The lack of sufficient protection, given by those cages with each only two *tert*-butyl group pointing in opposite directions and no protection in the "equatorial" region of the NP may be a reasonable explanation. Or in other words, the ligand shell did not offer enough steric repulsion to prevent the particles from coagulation. Similar behavior was observed for the pseudo cage-like ligand **Cage-TPM-p**. The limited motion likely hindered the ligand from an optimal arrangement to fully cover and protect the AuNP, as could be observed for the tripodal ligands (*e.g.* **Tri-TPM1**, *vide supra*). **Au-Cage-TPM-p** thus remained completely insoluble after drying. The solutions' colors of the mentioned particles were in all cases dark brown, indicating a size around 1 nm, however UV-Vis (and other

characterizations) were not performed for **Au-Cage-0**, **Au-Cage-S** and **Au-Cage-TPM-p**, due to the lack of stability. In contrast, AuNP formation as well as the subsequent purification steps for the mixture of **Cage-TPM** and **Cage-TPM-i** worked surprisingly well with any signs of precipitation, as **Cage-TPM-i** was expected to be less stable, sooner or later crushing out of the solution. In fact, particles passivated with this mixture were stable for days in both dry state and redispersed in dichloromethane with no signs of alteration in the UV-Vis absorption spectrum, giving evidence consistency in their stability. In addition, the solution during the AuNP synthesis appeared unexpectedly reddish, strongly pointing to a size around 2 nm, as 1) the sizes of **Au-Tri-TPM1** which were formed with the exact same amount of gold-salt resulted in a size of ~1.2 nm, and 2) the calculated diameter of the cavity inside **Cage-TPM** (diagonal thioether distance) is approximately 1.6 nm. The difference in AuNP size between the mixture of cage-like ligands and the previously described tripodal derivative **Au-Tri-TPM1** (*vide supra*) becomes even more obvious in the UV-Vis trace displayed in Figure 27.

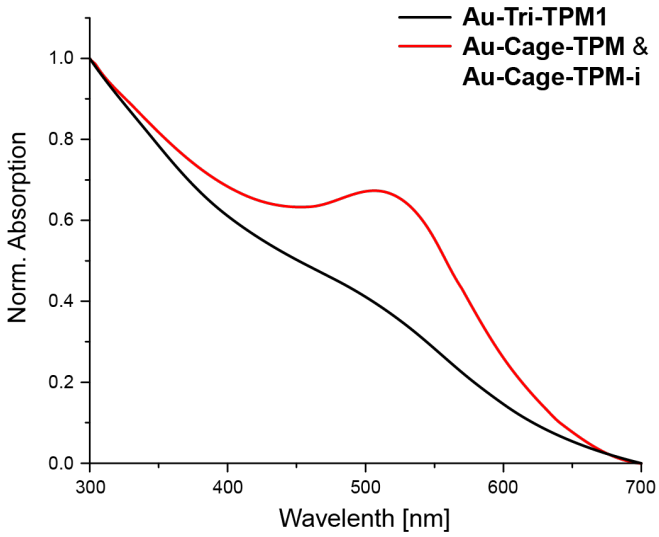

Figure 27: Normalized UV-Vis spectra of the mixture of cage-like **Au-Cage-TPM** and **Au-Cage** (red curve) and previously described tripodal derivative **Au-Tri-TPM1** (black curve).

While **Au-Tri-TPM1** with its size of 1.05 ± 0.3 nm feature almost no SPR-band, the mixture of Au-**Cage-TPM** and **Au-Cage-TPM-i** exhibits a distinct SPR-band at 520 nm. Size determination of the AuNPs by TEM analysis (Figure 28) indeed revealed a substantial larger mean sizes within error boundaries of 2.37 ± 0.95 nm for the mixture of **Au-Cage-TPM** and **Au-Cage-TPM-i**. Again, as the exact same amount of gold-salt was used for the AuNP synthesis, either similar sizes were expected or at least a maximum size of approximately 1.6 nm. Interestingly, the figure with the size distribution feature a rather flat descent on the left side of the maxima (smaller NPs) and steep descent towards larger NPs, as if it would contain a shoulder at the smaller size regime. It is

therefore tempting to say that this size distribution has to some extent a bimodal distribution, one with a maxima lover than 2 nm (appearing from **Au-Cage-TPM**), and the visible maxima at around 2.5 nm (appearing from **Au-Cage-TPM-i**), which would also explain the broad size distribution error of ± 0.95 nm.

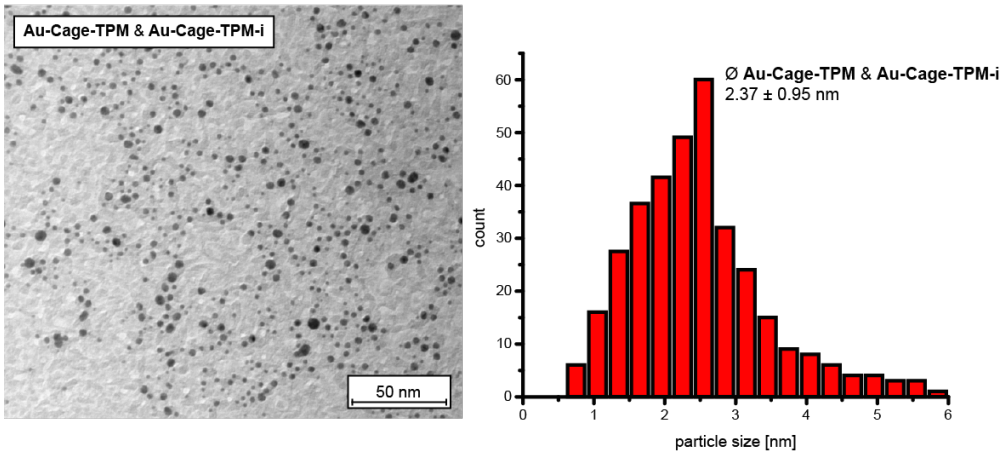

Figure 28: *Left*: Representative section of the TEM micrographs for samples of the ligand-stabilized nanoparticles of **Au-Cage-TPM** and **Au-Cage-TPM-i** (mixture); *right*: corresponding size distributions of the particles observed in the TEM micrographs.

As the ^{1}H-NMR of the mixture (see Figure 50 in *8. Appendix*) shows the typical broadening of the ligands' protons and no major impurities thermogravimetric analysis (TGA) could be measured. TGA results (see Figure 51 and Table 4 in *8. Appendix*) of the mixture further revealed that in average a NP with a size of 2.37 nm is surrounded by almost 7 ligands. This result has to be interpreted with caution however, as we have a mixture of two species with the same mass, which each obviously stabilize the particles in a different manner. While we assume that **Cage-TPM** is only able to stabilize one particle in its cavity, *i.e.* a single cage is stabilizing an entire particle with a size of approximately 1.6 nm. **Cage-TPM-i** on the other hand is not able to stabilize a particle in its cavity, but rather stabilizes with its outer tripodal arrangement a particle with larger sizes (>1.6 nm) by multiple ligands. Therefore, we conclude that after the reduction of the gold-salt the particle grows in the cavity of **Cage-TPM** until a maximum is reached (~1.6 nm) and all ligands of that kind are "filled", and the rest of the particles continues growing until they are fully capped by several ligands of **Cage-TPM-i** (at least 2-3 ligands for 2.5 nm and more for larger NPs). In addition, **Cage-TPM-i** could probably stabilize even larger particles, by using a larger amount of ligands, which would be aggregated similar as the fragments of a berry as it has compared to other discussed ligands an enormous ligand shell (Figure 29). However, this interpretation can only be confirmed if both ligands could be separated and analyzed independently.

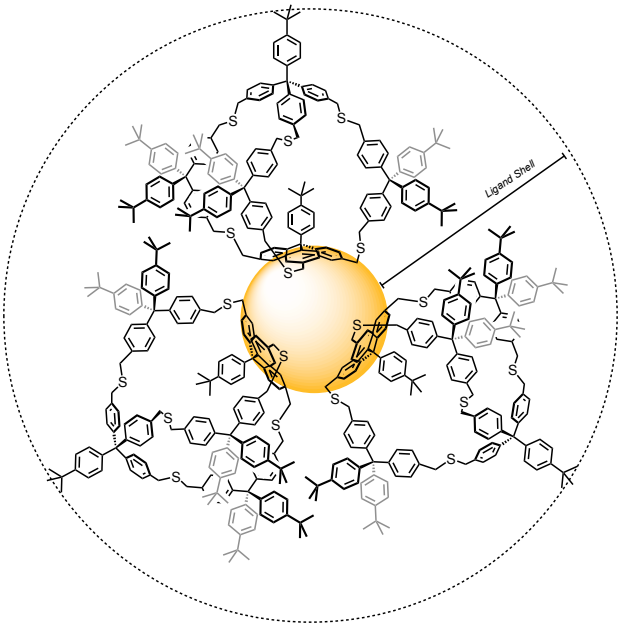

Figure 29: Schematic illustration of **Cage-TPM-i** stabilizing a NP and the bulky ligand shell.

4.2.4 Summary and Conclusions

A series of cage-like compounds were synthesized and characterized. While the synthesis of **Cage-0** and **Cage-S** were rather straightforward, the synthesis towards **Cage-TPM** appeared more troublesome: when applying a direct synthesis with **36** and **64** as precursors, a pseudo cage-like form **Cage-TPM-p** was exclusively formed. To avoid this issue, a step-wise synthesis was chosen *via* the precursor **68**, which already contains the side-arms and has to be closed with precursor **64**. This closing step, however, gave a mixture of compound **Cage-TPM** and the unexpected **Cage-TPM-i**, with the *tert*-butyl phenyl of **64** pointing inwards the cavity. This mixture appeared to be inseparable by automated recyclable GPC and HPLC with common solvent mixtures. Various attempts of closing the cage, in presence of an additive ligand (*e.g.* C_{60}) with the purpose to fill the cavity, forcing the *tert*-butyl group facing outwards failed. Gold nanoparticle syntheses were performed with all the obtained ligands. The smaller cages **Cage-0** and **Cage-S** did not stabilize particles efficiently, likely due to their rather weak ligand shell, while pseudo cage **Cage-TPM-p** failed to arrange itself such, to prevent the AuNPs from coagulation. On the other hand, the mixture of **Cage-TPM** and **Cage-TPM-i** gave, albeit unexpectedly large, also very stable NPs. As we believe that **Cage-TPM** only stabilizes NPs with a size approximately of 1.6 nm in its cavity, the larger dimensions of the particles most likely arise from **Cage-TPM-i** with its tripodal outer form, allowing an ideal arrangement and protection for larger AuNPs (>2 nm).

5 Size Control Study with Three Linear Heptamers

In this chapter, the systematic investigation of two independent parameters, potentially steering the size of linear octadentate heptamer-coated gold nanoparticles is presented; being 1) the chemical structure (*i.e.* sulfur-sulfur distance or bite angle) of the coating thioether heptamer ligand and in combination with 2) the ratio of ligand to tetrachloroauric acid ($HAuCl_4$) reduced during the formation of the AuNPs. For this purpose, three already presented heptamers with increasing distance between neighboring sulfur atoms in the ligand backbone: the *meta*-xylene based heptamer **Xyl7**, the tetraphenylmethane-based heptamer **TPM7**, and the terphenyl-based ligand **Ter7**, are selected and analyzed. While for both investigated parameters a clear trend to various-sized NPs is shown, a stronger influence in the resulting sizes is observed by alteration of ligand-to-gold ratio. Remarkable processability - and long-term stability-features - were observed for AuNPs stabilized by the bulky tetraphenylmethane-heptamer **TPM7**.

Since the seminal work of Brust and Schiffrin[30] in the last century, the number of publications based on the synthesis of "small" nanoparticles (*i.e.* 1-10 nm) has been growing vastly.[13] Within this small size regime, nanoparticles exhibit different electronic and optical properties[1] which paved the way for new scientific fields of research. With sizes of 5 nm and below, gold nanoparticles (AuNPs) offer quantum dot like behavior[62] or atom-mimicry features[171] allowing their integration as stable building blocks[60] in nanoelectronic devices.[58,172] For sensing applications the size-trend goes into the opposite directions, benefiting from their optical properties offering larger plasmonic resonance bands (SPR).[173–175] For this purpose, AuNPs should have diameters

starting from at least 2 nm[142], making them however more challenging to synthesize, especially if coated by a small integer number of ligands. Given these unique properties with different sizes, it is therefore imperative to be able to precisely control their sizes.

A concept for controlling the AuNPs size has been proposed by Hostetler and coworkers.[176] They showed that by altering the molar ratio between the ligand (dodecanethiols) and the gold-salt ($HAuCl_4$), and even the temperature or the rate at which the reduction is conducted, AuNPs between 1.5 to 5.2 nm can be synthesized. Since then, many different modifications of the two-phase Brust-Schiffrin method[30] focusing on different sizes by altering ligand/Au ratio[130,177–180] were published as well as by altering the pH-value[181,182]. In addition, the work of Hussain and collaborators shows that not only said ratio but the nature of the ligand itself can play a decisive role for resulting sizes, as different thioether polymers gave different sizes while maintaining the same reaction conditions.[130] Recently McCaffrey *et al.* reported the first example of controlled AuNPs synthesis, templated in a well-defined, discrete organic cage with a size of 1.9 nm.[143] Another example of cage-templated synthesis to stable and monodisperse NPs is reported by Mondal *et al.* with sizes up to 3.7 nm.[168] While a recent study showed the mechanistic insights of the Brust-Schiffrin method for thiol derivatives[183], the precise role of thioethers during the synthesis of AuNPs is a topic of current investigations.

Smaller sized nanoparticles (1.2 nm) are readily addressable by a small number of macromolecules like linear oligomers or dendrimers *via* multidentate thioether surface coating, as has been described -albeit scarcely- in literature.[13] The weak interaction between a thioether moiety and the gold surface can amount considerable contribution to the stability of the NPs by using multidentate oligothioether systems *e.g.* oligomers, and might even allow the macromolecule to self-rearrange for optimal conformation for the NPs coating. Inspired by this concept, we explored various multidentate macromolecules like linear oligomers[80], and dendritic systems[81] for the stabilization of small NPs. The low integer number of molecules per NPs decorated with a masked ethynyl moieties allowed mono- or bifunctionalized NPs to create supramolecular dumbbell[82,84], trikes and quads[84] or linear pearl-necklace[79,184] hybrid materials *via* mild acetylene homo-coupling or acetylene/azide-click reactions. What is strikingly conspicuous however is the fact that all these macromolecule-coated NPs feature almost the same sizes around 1-1.3 nm with barely noticeable SPR-bands (UV-Vis), and have thus limited potential for optical sensing applications. Note that the reaction conditions were kept as similar as possible throughout all the AuNPs-synthesis for better comparison along the different ligand structures. Even when comparing the dendritic ligands[81] with a fairly prior determined cage-like form, and the linear ligands[80] with no further

predetermined curvature, the resulted NPs featured almost the same size. Also the spacing between the thioether sulfur atoms in the oligomeric ligand seems to have only a minor influence on the dimension of the stabilized nanoparticle, as demonstrated by the very comparable dimensions of nanoparticles stabilized by linear heptamers based either on a *m*-xylene-based motif[79] and the more bulky tetraphenylmethane-based ligand described in a chapter before (*vide supra*) with an increased spacing between the sulfur atoms. Only for thioether oligomers interconnected with the terphenyl-based ligands showed a trend towards larger gold nanoparticles with a distinct absorption band in the UV-Vis was observed so far, when the same conditions were applied, with somehow limited stability features. While the AuNPs on the other hand showed promising stability features for both octadentate ligands (**Xyl7** and **TPM7**), the major difference was the heptamer/NP ratio required, as two ligands of the xylene-derivative coated one NP while a single tetraphenylmethane-based ligand was able to enwrap an entire NP. These results were to some extent unexpected as with ligands based on pairs of interlinked thiophenols the dimensions of the stabilized NPs reflected the ligand's inter-sulfur distances.[133]

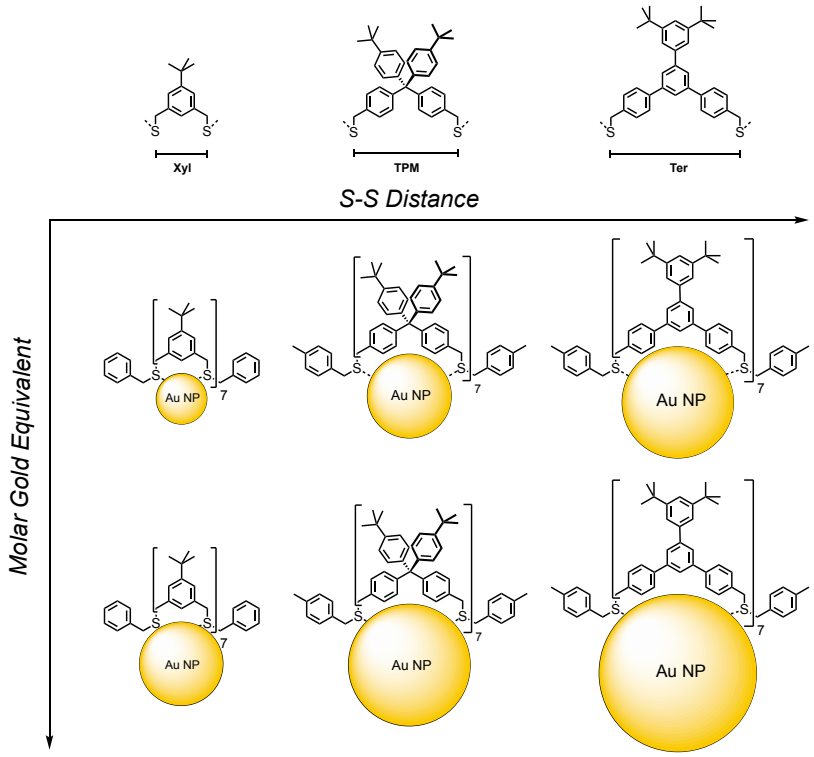

Figure 30: Representation of the two parameters potentially controlling the size of the formed nanoparticles. Namely the coating benzylic thioether heptamers with increasing sulfur-sulfur spacing from **Xyl** over **TPM** to **Ter**, and the molar amount of the gold formed during the nanoparticle synthesis. Note that heptamer **Xyl** was used with benzyl-groups as described in literature[80] instead of 4-methylbenzyl as endcapping groups.

We therefore wondered to which extent the ligand's design controls the dimensions of the formed NPs and perhaps the conditions under which the NPs are formed play a more important role with

respect to the dimension of the formed AuNPs. We are interested in both, AuNPs enwrapped by a low integer number of capping macromolecules with distinct designs for potential functionalization at its periphery for further wet chemical applications, and on the other hand, NPs large enough exhibiting prominent SPR-bands suitable for optical sensing purposes. We thus decided to systematically vary the parameters space to investigate the ligands' correlation with the size of the obtained NPs. As parameters, we focus in particular on the amount of used gold-salt during the AuNPs synthesis and on increasing the distance between sulfur-moieties by changing the ligand system, as sketched in Figure 30.

Here we report the systematic investigation of two parameters potentially steering the size of the thioether coated AuNPs. Namely the chemical structure of the coating thioether heptamer ligand and the ratio of ligand to the gold-salt reduced during the formation of the AuNPs. Concerning the structure of the thioether ligands, the three different linear heptamers *m*-xylene[80] (**Xyl**), tetraphenylmethane (**TPM**), and the terphenyl-type derivative (**Ter**) are studied, as they previously showed best stability features within each family of oligomers. The molecular design of the terphenylic heptamer **Ter** comprises structural features with favorable features for the stabilization of AuNPs like the backbone's bulkiness provided by the 1,3-di-*tert*-butyl phenyl moiety mounted on the terphenyl linker. Furthermore, its increased spacing between both sulfur atoms (~12-14 Å**)** compared to the heptamers **Xyl** (~5-7 Å) and **TPM** (~10-12 Å)[1] might provide inside to what extent the inter-sulfur bite-angle influences the dimensions of the formed particles in combination with increasing gold-salt. The increased spacing between neighboring sulfur atoms results in more remote contact points of the multidentate ligand on the AuNP's surface and thus might favor the stabilization of particles of alternative dimensions.

5.1 Synthesis of the Gold Nanoparticles

An adapted protocol of the two-phase Brust-Schiffrin method[80] was used to synthesize AuNPs stabilized by the here investigated heptamers (**Xyl7**, **TPM7** and **Ter7**, see Scheme 33). The main difference to our former studies on thioether stabilized gold nanoparticles[79–84] was that the molar ratio of ligand to gold-salt was varied. So far we kept the growth conditions for the particles as uniform as possible enabling the comparison of stabilization features due to the ligands design and thus, a 1:1 molar ratio of thioether moieties to gold equivalents (*e.g.* 8 equivalents Au(III) per octadentate ligand) was used. In this new study an exponential series of molar gold equivalents 8, 16, 32 and 64 (512 and 1024 only for heptamer **TPM7**) was investigated to fully exhaust the scope

[1] MM2 Calculations in Chem3D, **n.d.**

of each ligand's stabilization ability. In a typical procedure, tetrachloroauric acid was first dissolved in deionized water, transferred to the organic phase upon addition of tetra-*n*-octylammonium bromide and stirred for several minutes until the completion of the phase transfer was indicated by a colorless aqueous phase. The ligand dissolved in DCM was then added to the reaction mixture. After 15 minutes, the reduction of Au(III) to Au(0) was triggered by addition of an aqueous solution of sodium borohydride ($NaBH_4$) to the two-phase system. For completion of the reducing process, stirring for another 15 minutes was required. As work up, the volume of the organic phase was reduced by steady stream of argon to approximately 0.5 ml and then centrifuged upon addition of ethanol. The supernatant was discarded and the precipitated particles were redispersed in dichloromethane and subjected to manual size exclusion chromatography (Biobeads SX1 in DCM) for the separation of excess ligand. The as-synthesized AuNPs were finally analyzed by UV-Vis spectroscopy, and transmission electron microscopy (TEM). For **Au-TPM-16**, **-32** and **-64**, which displayed the required stability as coated particles, their characterization was complemented by ^{1}H-NMR spectra and thermogravimetric analyses (TGA).

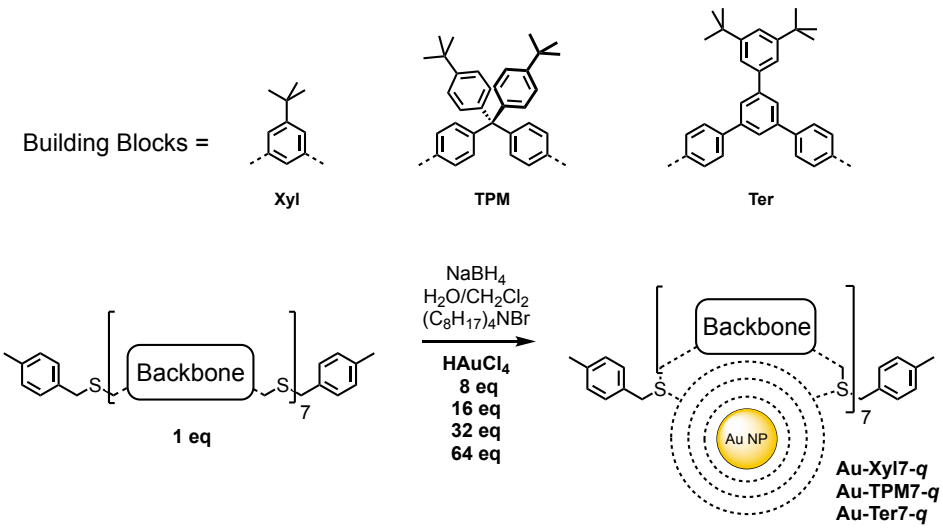

Scheme 33: Concept of AuNPs formation with the heptamers **Xyl7**, **TPM7** and **Ter7** bearing different core length by varying the Lig/Au-ratio. Note that "*q*" is used for simplifying the names and corresponds to number of molar equivalents $HAuCl_4$ used for the reaction compared to one molar equivalent of ligand. Note that heptamer **Xyl7** was used with benzyl-groups described in literature[80] instead of 4-methylbenzyl as endcapping groups.

To clearly separate the influence of the different parameters, we first discuss the development of the NPs sizes as a function of the gold equivalents used during their syntheses for each ligand system individually. And only in the second part, the influence of structural features of the different ligand designs on the dimensions of the stabilized NPs will be compared.

5.2 Results and Discussion

5.2.1 AuNPs Stabilized by Heptamer **Xyl7**

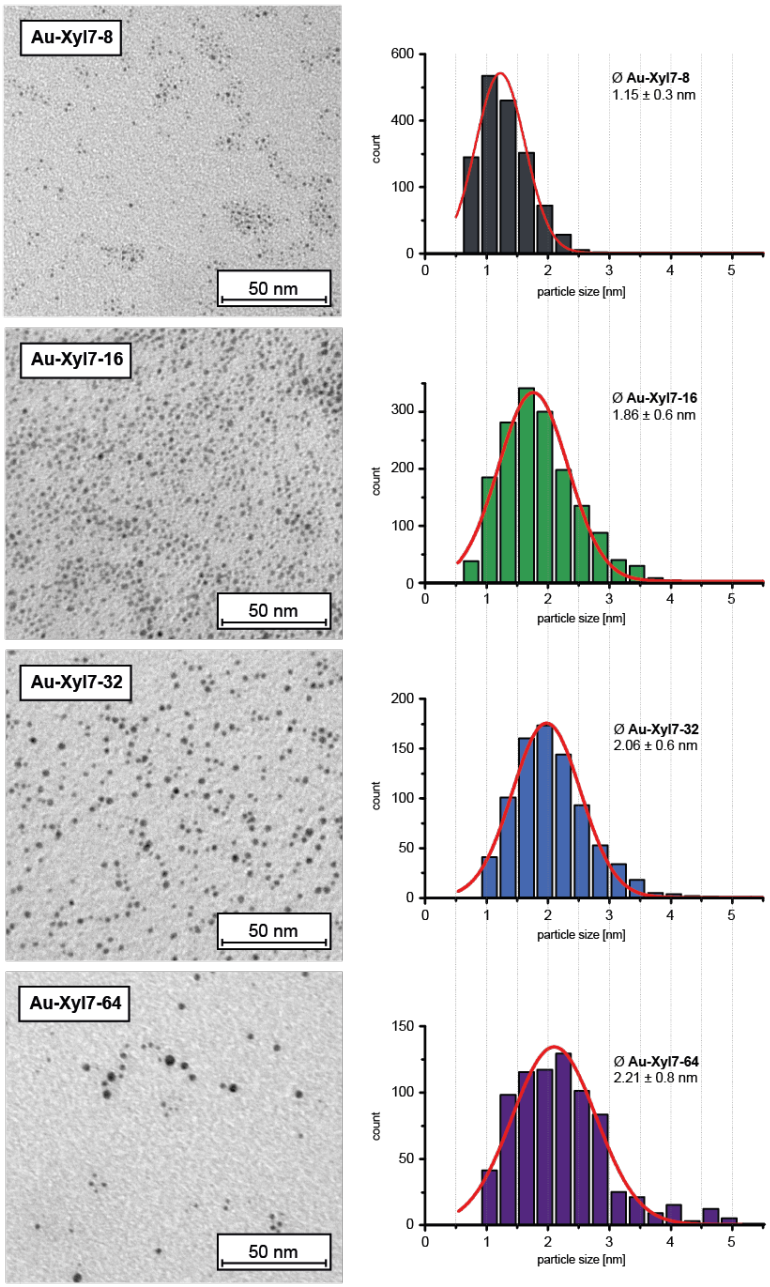

Figure 31: (Left) Representative sections of the TEM micrographs for samples of **Au-Xyl7-8**, **-16**, **-32** and **-64** and (right) their corresponding size distributions with calculated Gaussian curves (red). The vertical grid is implemented for better comparison.

Considering the synthesis towards AuNPs coated by heptamer **Xyl7**, the more gold-salt used for the reaction (8, 16, 32 and 64 equivalents), the more reddish the solution appeared, while in the case of 16 equivalents still a dark brownish hue was visible similar to 8 equivalent of gold-salt used as reported by Peterle and coworkers.[80] This reddish color already is a promising indication that

larger NPs were formed with this octadentate ligand. Although during the progress of the synthesis for all entries comprising 16 equivalents or more of the gold-salt, a black precipitation floating in the solution was observed by naked eye while the intense color remained throughout the syntheses. The precipitation were insoluble agglomerates of coagulated NPs, which either pointed at a poor stabilization/protection of the NP provided by the surrounding ligand shell, or indicated that all ligands were already involved in the stabilization of the AuNPs and thus the remaining gold precipitated. The organic phases were then transferred into falcon tubes and the solvent was reduced to a volume of about 1 ml in a steady stream of nitrogen, followed by precipitation upon addition of ethanol and centrifugation. During this work up step potentially remaining excess of TOAB, which might also co-stabilize the AuNPs, was removed.[138] The particles were further purified by manual gel permeation chromatography (GPC, Biobeads SX1 eluted with DCM) to remove potentially remaining excess of ligand. On the GPC column the NP samples obtained by applying 16, 32 or 64 gold equivalents smeared which is indicative for a limited stabilization of the NP by the ligand shell. Another indicator for the rather poor stabilization provided by the ligand was the fact that these NPs could no longer be redispersed after several drying/redispersing attempts. This poor processing behavior also made their characterization by ^{1}H-NMR spectroscopy and TGA impossible. To still analyze these NPs, the solutions were directly used to perform UV-Vis spectroscopy and to prepare samples suitable for transmission electron microscopy (TEM) analyses. TEM analysis (see Figure 31) shows for **Au-Xyl7-8** a size of 1.15 ± 0.3 nm,[80] **Au-Xyl7-16** a size of 1.86 ± 0.6 nm (1.62 x), for **Au-Xyl7-32** a size of 2.06 ± 0.6 nm (1.11 x) and for **Au-Xyl7-64** a size of 2.21 ± 0.8 nm (1.07 x). This increasing dimensions of the NPs shows that the size is dependent on the ratio between the ligand and gold-salt. Probably as a consequence of the increased sizes, a clear trend to wider size-distributions with larger NPs is observed with **Au-Xyl7-64** featuring a broad variation of ± 0.8 nm compared to the rather narrow distribution of ± 0.3 nm recorded for **Au-Xyl7-8**. While **Au-Xyl7-8** are enwrapped by two ligands per particle[80], more ligands are probably involved in the stabilization of the larger NPs. While heptamer **Xyl7** with the *meta*-xylene derivatives showed very promising stabilization features for the 1.15 nm-sized NPs, this was obviously less the case for larger NPs. Most likely the rather slim backbone of the octadentate heptamer **Xyl7** exposing a single *tert*-butyl group per linking unit can neither be arranged in a compact coating covering the NPs surface efficiently nor provide sufficient steric repulsion to separate larger NPs.

5.2.2 AuNPs Stabilized by Heptamer **TPM7**

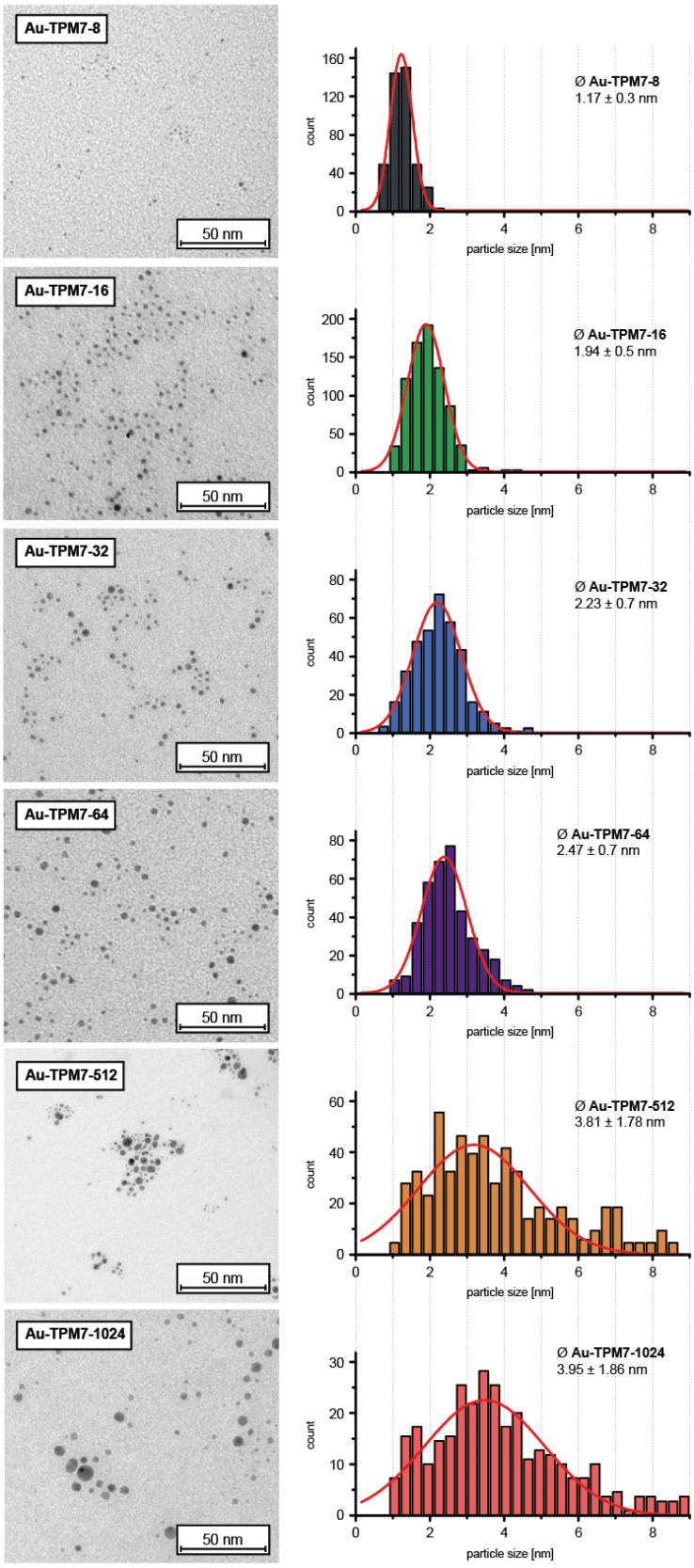

Figure 32: (Left) Representative sections of the TEM micrographs for samples of **Au-TPM7-8**, **-16**, **-32**, **-64**, **-512** and **-1024** and (right) their corresponding size distributions with calculated Gaussian curves (red). The vertical grid is implemented for better comparison.

During the AuNPs synthesis with heptamer **TPM7** no precipitation was detected when 16 and 32 equivalents of gold-salt were used and only in the case of 64 equivalents a few black pieces were observed, but far less than while during particle synthesis with heptamer **Xyl7**. This already shows at this stage that the bulkier tetraphenylmethane-based ligand provides a thicker and therefore better protection shell covering the nanoparticles compared to the heptamer **Xyl7**. The colors observed during the synthesis were very similar to the ones observed during the syntheses described above using **Xyl7** with comparable equivalents of the gold-salt, pointing at comparable sizes of the stabilized NPs. Also during the subsequent purification by precipitation and redispersion cycles and GPC no signs of particle coagulation were observed for the **TPM7**-coated NPs. In contrast to the **Xyl7**-coated NPs, the GPC column charged with **TPM7** stabilize NPs remained white, pointing at complete wash-out of the particle fractions from the column, further corroborating the excellent stability features of the **TPM7**-coated particles. Indeed, the as-synthesized **Au-TPM7-16**, **-32** and **-64** were stable enough for further processing, allowing in particular repetitive drying and redispersion. Therefore, additionally to TEM and UV-Vis analysis, TGA, ^{1}H-NMR and thermal-stability experiments were successfully performed.

The ideal behavior of the heptamer **TPM7** in the syntheses up to 64 equivalents of gold-salt per thioether (8 equivalents per octadentate **TPM7**) raised questions concerning the limits of its stabilization ability. In order to explore the limit of the stabilization features of **TPM7** we performed additional AuNP syntheses with 512 and 1024 molar gold equivalents. For these two NP syntheses considerable amounts of precipitates were detected in the dark red solutions. And in similarity to the larger AuNPs stabilized by heptamer **Xyl7** described before, the **TPM7** stabilized AuNPs obtained by using excessive amounts of gold salt were no longer dispersible after purification by GPC. The dimensions of the **TPM7**-coated AuNPs obtained from the various reaction conditions were again analyzed by TEM and the analyses are displayed in Figure 32. With diameters of 1.17 ± 0.3 nm for **Au-TPM7-8** (described in *chapter 3.2* (*vide supra*)), 1.94 ± 0.5 nm for **Au-TPM7-16**, 2.23 ± 0.7 nm for **Au-TPM7-32**, 2.47 ± 0.7 nm for **Au-TPM7-64**, 3.81 ± 1.8 nm for **Au-TPM7-512**, and 3.95 ± 1.9 nm for **Au-TPM7-1024** a similar trend to larger NPs and broader size distributions with increasing equivalents of the gold salt deployed during the synthesis was observed. As first approximation the diameter of the NP is expected to grow with the third radical of the mass, and thus, an increase of the particle diameter by the factor $\sqrt[3]{2} = 1.26$ would be expected for doubling the amount of gold equivalents. The observed increases in dimensions of successive NP syntheses from **Au-TPM7-8** to **Au-TPM7-64** were with 1.66, 1.15, and 1.11 within the expected dimensions but also point at alternative boundary conditions, like the dimension and the structure of the oligomer present, which control the sizes of the NPs. For the

two samples prepared with excessive amounts of gold salt **Au-TPM7-512** and **Au-TPM7-1024** the observed increase was less than expected. **Au-TPM7-512** was only 1.58 times larger than **Au-TPM7-64** and **Au-TPM7-1024** was only 1.01 times larger than **Au-TPM7-512**, while increases by factors 2 (= $\sqrt[3]{8}$) and 1.26 respectively would have been expected. The lack of increase might be rationalized by the loss of gold during their syntheses by precipitation. However, the size distributions of these two samples was very broad further questioning the level of size control remaining during these reaction conditions.

^{1}H-NMR spectra of **Au-TPM7-16**, **-32**, **-64** (see Figure 52, Figure 53 and Figure 54 in *8. Appendix*) showed the characteristic broadening of the signals (aliphatic and aromatic) in comparison to the pure ligand. The signals appear rather weak and might arise from the enlarged nanoparticles. However only a small amount of ligand was used in each case for the synthesis of the AuNPs compared to the enormous amounts of gold. Thermogravimetric analysis (see Figure 55 and Table 5 for calculations in *8. Appendix*) revealed an increased amount of ligands per particle participating in the stabilization with increasing size of the NP. While **Au-TPM7-8** with a size of 1.17 ± 0.34 nm is enwrapped in average by a single heptamer, calculated in a chapter before (*vide supra*), the weight loss during the thermogravimetrical analysis pointed at two (1.96) and three (2.96) heptamers which are in average stabilizing **Au-TPM7-16** and **Au-TPM7-64**, respectively. That the ratio between coating ligand and NP is no longer strictly an integer but that we encounter NPs stabilized by different numbers of ligands is displayed by **Au-TPM7-32**, for which an average ratio between heptamer and NP of 2.33 has been recorded.

Another important factor for AuNPs is their thermal stabilities in suspension, limiting the range of potentially applicable reaction conditions. For this purpose, suspensions of the particles **Au-TPM7-16**, **-32**, **-64** dispersed in toluene were gradually heated stepwise by 10 °C and kept at the elevated temperature for one hour before the integrity of the sample was analyzed by UV-Vis spectroscopy (see Figure 56, Figure 57 and Figure 58 in *8. Appendix*). For **Au-TPM7-16**, no decomposition of the particles was observed in toluene up to 110 °C. Due to the boiling point of toluene (111 °C), a further increase in temperature was only possible by replacing toluene by *p*-xylene and indeed, a color change from brown-red to bluish accompanied by formation of a black precipitate was observed at 120 °C indicating thermal decomposition of the particles. The decompositions temperatures recorded for **Au-TPM7-32** and **Au-TPM7-64** were with 90-100 °C in a similar range as observed for **Au-TPM7-8**. For both samples an initial increase of the SPR-band was observed at 100 °C pointing at the formation of larger agglomerates, followed by complete disappearance of the SPR-band at 110 °C due to crushing out of the Au(0) species. It is

tempting to hypothesize that the stoichiometric match between two heptamers **TPM7** per NP in **Au-TPM7-16** is reflected in the increased thermal stability.

5.2.3 AuNPs Stabilized by Heptamer **Ter7**

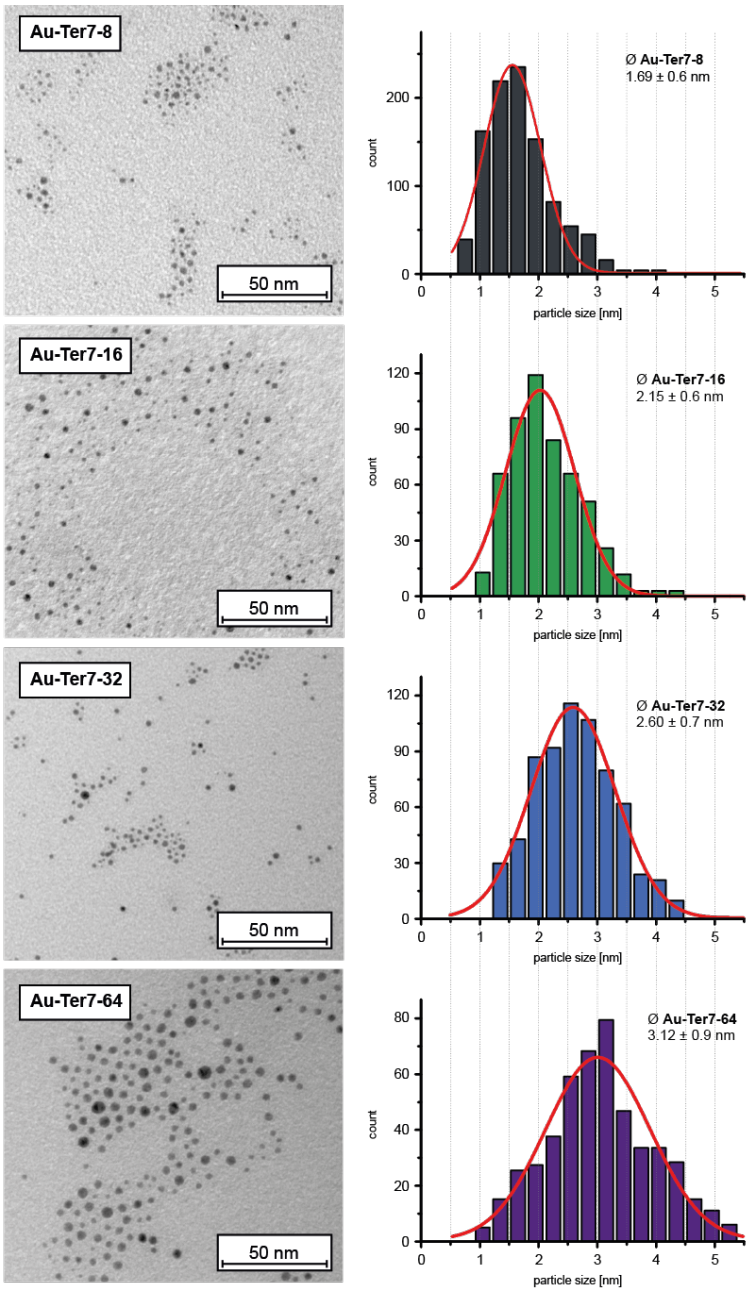

Figure 33: (Left) Representative sections of the TEM micrographs for samples of **Au-Ter7-8**, **-16**, **-32** and **-64**, and (right) their corresponding size distributions with calculated Gaussian curves (red). The vertical grid is implemented for better comparison.

The NP syntheses in the presence of the heptamer **Ter7** resembled the ones with **Xyl7**. Also here major precipitations were detected during the syntheses even though the reaction solution remained red-colored. As described in *chapter 3.1* (*vide supra*), the reaction with 8 equivalents of the

gold salt featured a slight reddish hue, pointing towards larger AuNPs compared to previously reported NPs[79–84], which themselves were - with 8 equivalents of gold-salt - dark brown in solution. It thus seems that the reaction conditions are not solely steering the dimensions of the NPs but that the chemical structure of the heptamer present has some influence as well. Despite all formed nanoparticles with this ligand were stable during the workup steps, they featured limited stability while drying and redispersing. While **Au-Ter7-16**, **-32** and **-64** were completely indispersible, **Au-Ter7-8** showed only moderate redispersibility.

The TEM investigations (Figure 33) revealed sizes of 1.69 ± 0.6 nm for **Au-Ter7-8**, 2.15 ± 0.6 nm for **Au-Ter7-16**, 2.60 ± 0.7 nm for **Au-Ter7-32**, and 3.12 ± 0.9 for **Au-Ter7-64**. Again, the trend to larger particles with an increased amount of gold salt used during their syntheses was observed for the terphenylic heptamer **Ter7**. Interestingly the observed size increases with **Au-Ter7-16** having a 1.27 times larger diameter than **Au-Ter7-8**, **Au-Ter7-32** with a 1.21 times the diameter of **Au-Ter7-16**, and **Au-Ter7-64** having 1.2 time the one of **Au-Ter7-32** match almost perfectly the increase by the factor $\sqrt[3]{2} = 1.26$ expected for the diameter upon doubling the mass of the particle. Compared to both other heptamer systems **Xyl7** and **TPM7**, which provided stable particles with a narrow size distribution when 8 equivalents of gold salt were used, the NPs obtained with **Ter7** displayed limited stability features and were in general larger with broader size distributions, also if only 8 equivalents of the gold salt were deployed. In spite of the two bulky *tert*-butyl groups, the heptamer **Ter7** seems neither to be able to stabilize AuNPs of particular dimensions nor do these NPs display reasonable processability. We thus concluded that the structural motif is not suited for the development of functional coatings making NPs addressable by wet chemistry.

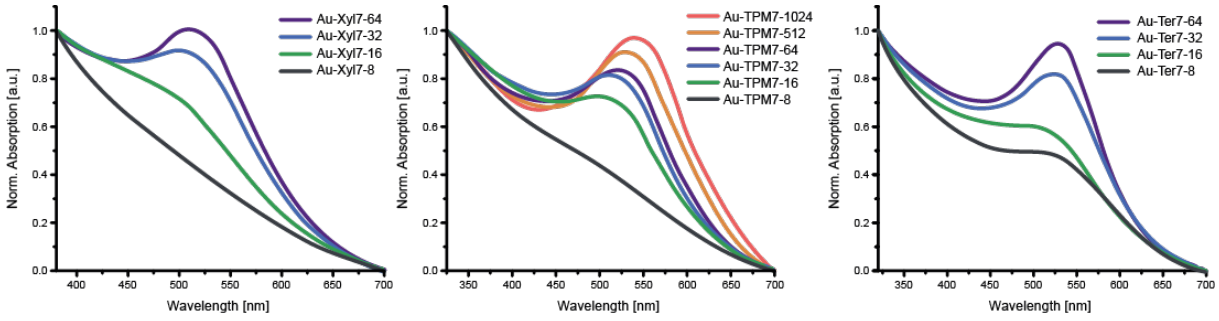

Figure 34: Normalized UV-Vis spectra of heptamers **Xyl7** (left), **TPM7** (middle) and **Ter7** (right) stabilized AuNPs recorded in CH_2Cl_2. Note that each molar gold equivalent features the same color code.

The UV-Vis spectra recorded for each heptamer system corroborate the size trends observed by TEM analyses and are displayed in Figure 34. For each ligand system a more prominent SPR-band

was recorded the more gold-salt (8 eq., 16 eq., 32 eq., 64 eq. *etc.*) was used for the synthesis of the AuNPs. Also a slight red-shift[13] of the SPR-band was observed for every ligand system when the obtained particles were getting larger. This effect is particularly apparent for the heptamer **TPM7** due to the complementation of the series by **Au-TPM7-512** and **Au-TPM7-1024** to explore the limits of the stabilization potential of the ligand system. As described in *chapter 3.1* (*vide supra*) the increased size of **Au-Ter7-8** (1.69 ± 0.6 nm) in the series of NPs synthesized with 8 equivalents of gold-salt (black lines), for which a SPR-band was visible, while **Au-Xyl7-8** (1.15 ± 0.3 nm) and **Au-TPM7-8** (1.17 ± 0.3 nm) did not display a SPR-band as expected for their tiny dimensions. While for thiolate-protected[67,71,73] NPs typically stepwise UV-Vis absorption bands between 300 and 800 nm were observed within this minute size-regime, we do not observe similar bands in the UV-Vis for **Au-Xyl7-8** and **Au-TPM7-8**. This may either arise from the broad size distribution[68] and/or due to the weaker thioether-gold interactions, similar to phosphine-stabilized[65] NPs. For the next series of NPs synthesized with 16 equivalents of gold-salt (green line) a SPR-band was visible for all three members, even though the intensity of the band recorded for **Au-Xyl7-16** (1.86 ± 0.6 nm) was unexpected weak considering the particles' sizes determined by TEM. AuNPs synthesized with 32 (blue lines) and 64 (purple lines) gold equivalents featured for every ligand system remarkable SPR-bands. Note that the shape of the SPR-band does not only depend on the particles' sizes but also on their shapes, morphologies, and their distributions.[13]

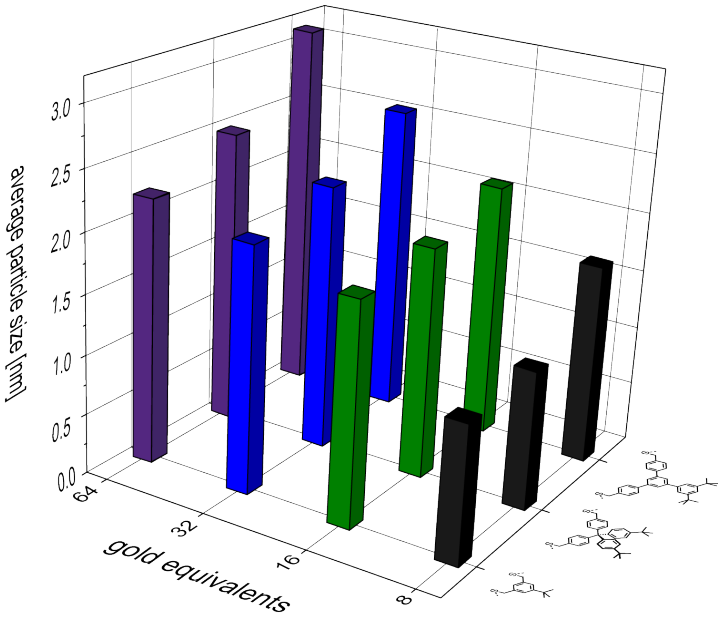

Figure 35: 3D-graph displaying the average sizes of AuNPs stabilized by heptamer **Xyl7** (front row), **TPM7** (middle row) and Ter7 (back row) synthesized from various amounts of gold salt. The color codes the gold equivalents used during the NP syntheses.

So far we have seen that for all three heptameric ligands investigated, with increasing amounts of gold-salt used the nanoparticles became larger, the size-distributions became broader, and their tendency to precipitate increased. There are however also clear differences mainly in the stability, solubility, and thus also processability of the heptamer-coated particles and we wondered to which extent structural features of the ligands are reflected in the obtained NPs. Our initial working hypothesis was that an increased spacing between both sulfur atoms of a bridging motif might result in larger particles. The here investigated series of heptamers was an ideal model system to challenge this hypothesis, as the spacing between neighboring thioether sulfur atoms increases steadily from 4.6 Å for the **Xyl**, over 9.6 Å for **TPM**, to 12 Å for the **Ter** backbone, as has been estimated from simple MM2 modeling. Figure 35 displays the recorded average particle's sizes of the AuNPs stabilized by the heptamers **Xyl7**, **TPM7**, and **Ter7** with 8, 16, 32, and 64 equivalents of gold-salt used enabling the comparison of the NP dimensions between the different ligand systems. All the size distributions for each ligand family with increasing amount of gold-salt used for their NP syntheses are additionally merged in Figure 36 below.

The 3D-graph (Figure 35) and the 2D-graph (Figure 36) clearly show both trends, the increased dimensions of the particles due to the increased amount of gold present during the synthesis and the size increase due to the ligand structure used. While the order of the size increase due to the ligand structure supports the hypothesized correlation with the spacing between neighboring sulfur atoms, the amount of NP size increase is neither proportional to, nor another obvious function of the increase in S-S distance in the ligand system. It however remains questionable to which extent the dimensions of the NPs reflect directly structural features of the arrangement of the coating ligand at the NP surface or other physicochemical properties depending on the coating like stability and solubility features influencing concentrations and growth kinetics. Eye-catching in both presentation of the entire collection of particles are the surprising small dimensions of the AuNPs synthesized from 8 equivalents of gold salt with the two heptamers **Xyl7** and **TPM7**. Both particles **Au-Xyl7-8** and **Au-TPM7-8** displayed good stability and processability features, were characterized by a narrow size distribution, and an integer average number of ligand per NP. It is thus tempting to interpret their small sizes as a consequence of a compact coating shell by 2 heptamers **Xyl7**, in the case of **Au-Xyl-8**[80], and by a single molecule **TPM7** in **Au-TPM7-8**, as has already been described in a chapter before (*vide supra*). Also it is not surprising that the heptamer **Ter7** is less suited to stabilize small particles, as the considerably increases S-S spacing results in more remote contact points disfavoring the adaption of the coating ligand shell to spherical objects with too small radii.

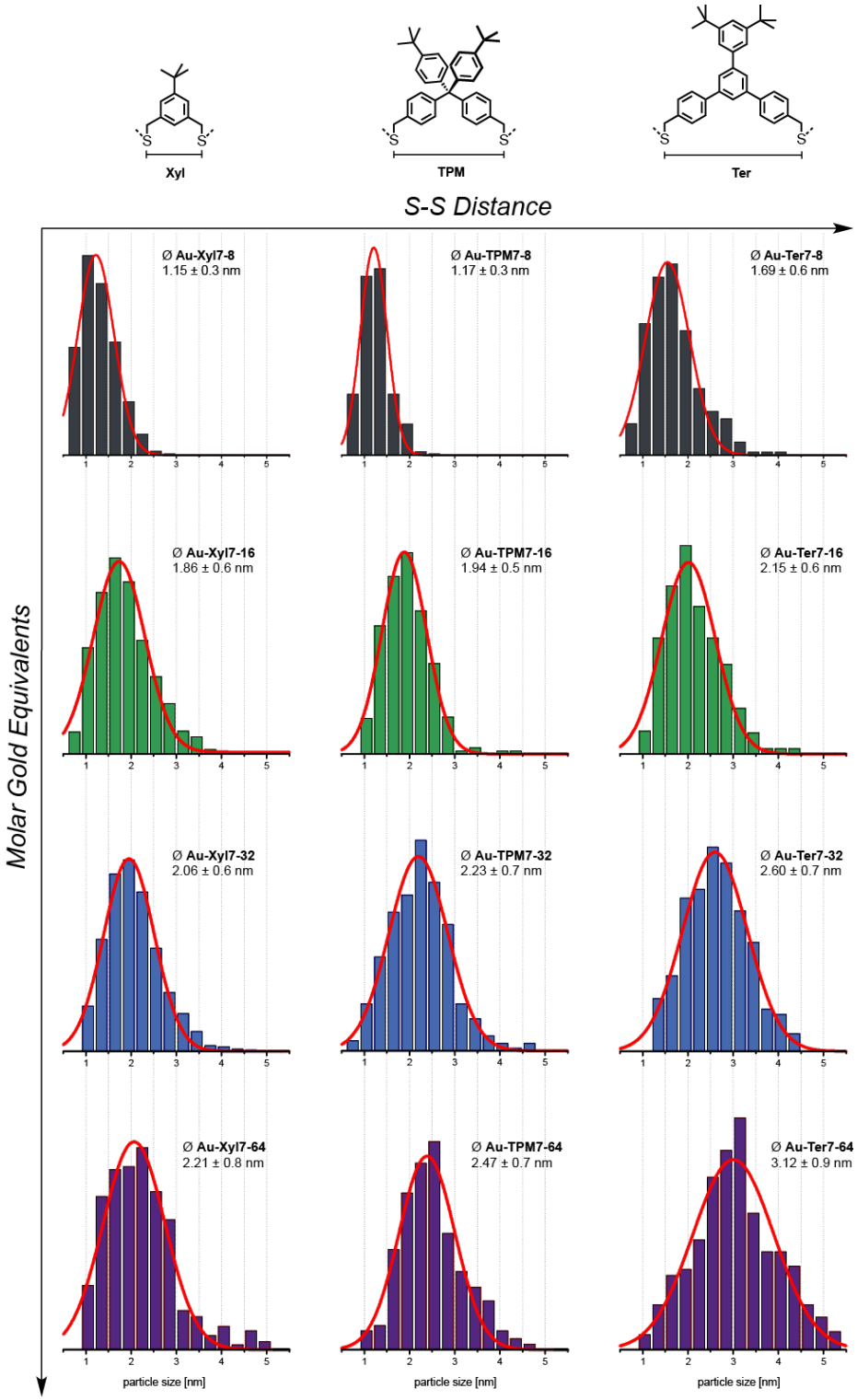

Figure 36: Merged size distributions of all heptamer-stabilized AuNPs (left column: **Xyl7**; middle column: **TPM7**; and right column: **Ter7**) with increasing gold-salt equivalents used for their NP syntheses (first row: 8 eq.; second row: 16 eq.; third row: 32 eq.; and fourth row: 64 eq.).

5.3 Summary and Conclusions

A systematic study identifying parameters and boundary conditions controlling the dimensions of ligand coated gold nanoparticles is presented. For that purpose, the series of heptameric ligand structures comprising eight benzylic thioether linkages as coordination sites for the gold particles was analyzed with the heptamers **Xyl7**, **TPM7** and **Ter7**, each with different distance between neighboring sulfur atoms in the ligand backbone. The three linear heptameric ligand systems were present during the reductions of various concentration of gold salts to investigate their AuNP stabilizing properties. For all three ligand systems the average sizes of the NPs grew with an increased concentration of the gold salt reduced. In addition, the sizes of the NPs also depend on the dimensions of the coating ligand with a trend reflecting the spacing between the sulfur atoms in the individual bridging motifs. Also the different ligand motifs displayed considerable differences in the stability and processability of the coated particles. While **Au-Xyl7-*q*** only provided stable and redispersible NPs with low concentration of gold salt yielding in **Au-Xyl7-8** with a well-defined ratio of two ligands coating the NP, larger amounts of gold salts provided larger NPs with reduced stability properties. All **Ter7** coated particles (**Au-Ter-*q***) only showed very limited stability and solubility features, while the entire **Au-TPM7-*q*** series clearly displayed superior thermal stability and processability properties compared to the other two ligand systems. It seems that the increased bulkiness of the bridging motif in **TPM7** favors these desired physical-chemical characteristics.

6 Summary and Outlook

A series of linear, tripodal and cage-like multidentate thioether ligands for the ligand-controlled synthesis and surface functionalization of gold nanoparticles (AuNPs) was developed. The properties of these thioether ligands, regarding their influence on sizes, stability and dispersity of the resulting AuNPs were investigated. It was shown that the size of the as-synthesized AuNPs depends on various parameters, such as the structural motif of the ligands and the conditions with which the NPs are assembled. Furthermore, the bulkiness of these ligands and their spatial arrangement enabling superior enwrapping of the particles, play a crucial role in stabilizing AuNPs, an essential factor for future wet chemical processing.

Initial experiments were geared towards the formation of larger NPs compared to previously reported NPs (~1.1 nm) also stabilized by multidentate benzylic thioether ligands. The idea was to increase the bite-angle of the ligands by enlarging the sulfur-sulfur distance of the linear thioether oligomers (Figure 37 a). Therefore, a series of linear oligomeric structures (Figure 37 b) was synthesized and subjected to the two-phase protocol of Brust and Schiffrin[30] to create AuNPs.

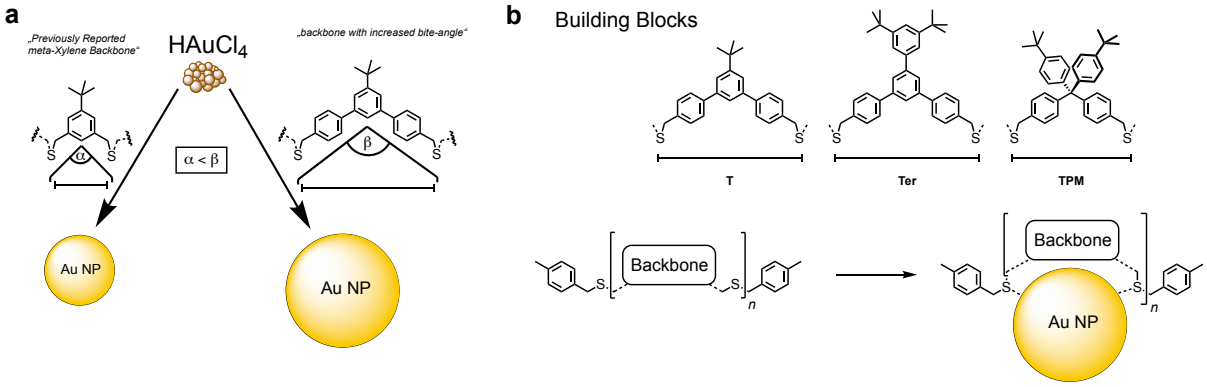

Figure 37: a) Concept of the ligands' bite-angle to the AuNP; b) oligomers consisting of various building blocks forming the corresponding backbones for the AuNP syntheses.

The terphenylic-based oligomers indeed enabled an increase of the size up to ~1.7 nm. On the other hand, the formed AuNPs featured limited stability, as indicated by their non-redispersibility in common organic solvents after a few days. Nonetheless, the ligand shell surrounding the NPs has an influence in the stability, as **Au-Ter$_n$** (with a bulkier design) displayed for longer oligomers (**Ter5** and **Ter7**) a greater stability over **Au-T$_n$**. Interestingly, despite the increased sulfur-sulfur distance of tetraphenylmethane-based oligomers **TPM$_n$** over the *meta*-xylene-based oligomers **Xyl$_n$**, they did not increase the sizes of the resulting NPs (~1.2 nm) substantially as expected, but revealed new packaging motifs. Due to their flexibility, a single-ligand-per-NP stabilization was observed

for **TPM5** and **TPM7**, while the shorter **TPM3** revealed a two-ligand-per-NP stabilization, similar to the reported *meta*-xylene-based heptamers by Peterle and coworkers.[80] In addition, due to the bulkiness of tetraphenylmethane with its spatial arrangement, all the linear oligomers **TPM$_n$** showed excellent long-term NP-stabilization even at elevated temperature up to 90 °C. This fact together with the mono-ligand enwrapping, enabled the pathway for new monofunctionalized NPs based on linear ligands.

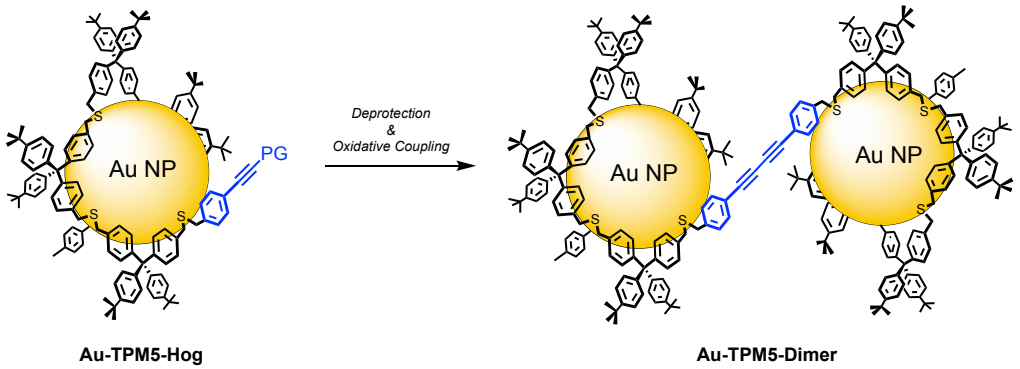

Scheme 34: Concept of **TPM5-Hog**-stabilized AuNPs and the dimer formation upon deprotection and oxidative coupling (PG: protecting group).

For this purpose, the linear pentamer **TPM5-Hog** was synthesized, exhibiting a CPDIPS-masked acetylene-moiety on one end of the oligomer strand. After AuNP synthesis, **Au-TPM5-Hog** was deprotected and subsequently subjected to Glaser-Hay oxidative coupling conditions (Scheme 34). The size increase of the NPs during the homo-coupling, visible in the UV-Vis spectra, is mainly attributed to the ligands arrangement on the NP, which became weaker after the coupling, likely by ripping of the ligand. It therefore seems that a peripheral decorated functionality as reported by Hermes and Sander may be superior.[82,84] Nevertheless, TEM analysis revealed almost a third of all analyzed images to be NP-dimers, and a small amount to trimers or larger superstructures.

The great NP stability, featured by tetraphenylmethane-based ligands in general, in combination with their spatial tetrahedral shape of tetraphenylmethane, led to further designs like the tripodal ligands. Therefore, a central tripodal building block was synthesized allowing the introduction of three oligomeric thioether-based side-chains. As side-chains, monomers and dimers of previously reported *meta*-xylene-based (**Xyl**), tetraphenylmethane-based (**TPM**) and terphenyl-based ligands (**Ter**) were chosen to further explore their ability to stabilize when attached to a central tripodal linker. All successfully synthesized AuNPs were - unexpectedly - of the same size within error tolerance (~1.1 nm) despite variation of the side-chains. It indicates that neither the side-chains nor the distance between two thioether moieties, yet rather the conformation of the central building

unit dictates the curvature and thus the dimensions of the nanoparticles. Again, both ligands comprising tetraphenylmethane-based side-chains with different length (**Tri-TPM1** and **Tri-TPM2**) enwrap the particles with enhanced stability features in a ligand-to-NP ratio of 1:1, suitable for monofunctionalized NPs for future wet chemical approaches.

Another elegant way to tune the size of a NP is by the templated synthesis within cage-like molecules. The cavity inside the cage dictates the final size of the NP and, thus, monodisperse distribution can be expected. Based on the tripodal ligands, cage-like molecules were designed and synthesized, each consisting of three bridging strands (Figure 38).

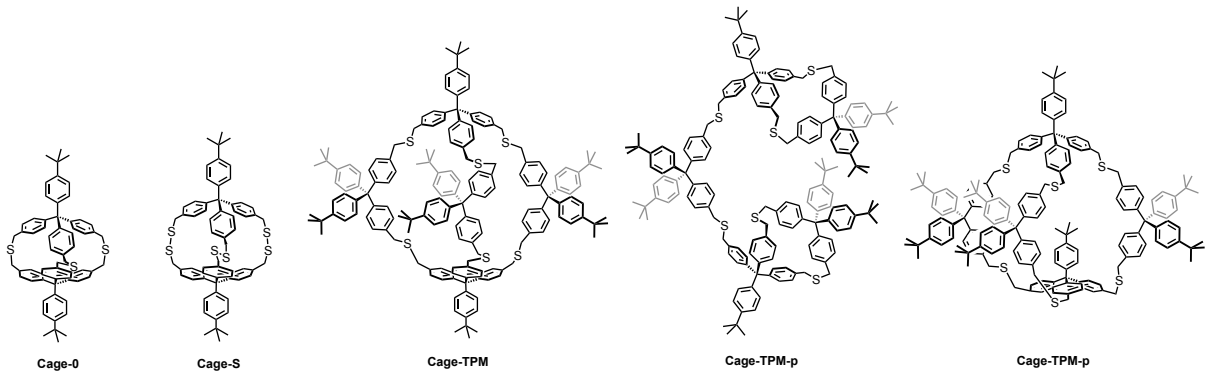

Figure 38: Cage-like compounds **Cage-0**, **Cage-S** and **Cage-TPM**, and side-products **Cage-TPM-p** and **Cage-TPM-i**.

While the synthesis of **Cage-0** and **Cage-S** worked well, the synthesis of **Cage-TPM** turned out to be more challenging. When applying a direct one-pot synthesis, the pseudo cage-like **Cage-TPM-p** was formed exclusively, which was then avoided by a stepwise synthesis *via* a tripodal precursor. The final closing step gave, according to NMR studies, a mixture of compound **Cage-TPM** and the unexpected **Cage-TPM-i**, with the *tert*-butyl phenyl pointing inwards the cavity. This mixture appeared to be inseparable by automated recyclable GPC and HPLC with common solvent mixtures. Gold nanoparticle syntheses were performed with all the obtained ligands. The smaller cages **Cage-0** and **Cage-S** did not stabilize particles efficiently, likely due to their rather weak ligand shell, while pseudo cage **Cage-TPM-p** failed to arrange itself such that it would prevent the AuNPs from coagulation. On the other hand, the mixture of **Cage-TPM** and **Cage-TPM-i** gave unexpectedly large and also very stable NPs. As we believe that **Cage-TPM** only stabilizes NPs with a size approximately of 1.6 nm inside its cavity, the larger dimensions of the particles most likely arise from **Cage-TPM-i** with its tripodal outer form, allowing an ideal arrangement and protection for larger AuNPs (>2 nm). Separation of both compounds would be interesting, to have an insight in their ability to stabilize NPs separately.

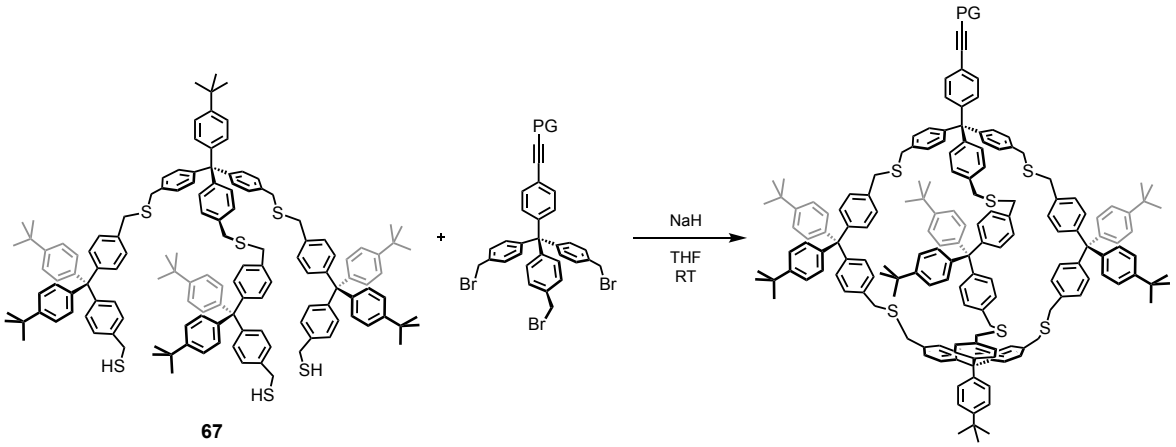

Scheme 35: Final closing step of **67** with a protected acetylene decorated on a tri-bromo precursor, allowing the formation of a functionalized cage-derivative.

A possible idea to overcome the mentioned issue is shown in Scheme 35. The tripodal precursor **67** can be closed with a functionalized tri-bromo precursor containing an acetylene, which should be masked with bulky protecting group. This protected phenylethynyl moiety should be sufficient to avoid the closing while pointing inward the cage due to steric hindrance.

Finally, we was found that as-synthesized AuNPs were much larger with the same ligand, when more gold-salt was used during the synthesis. For that purpose, a systematic investigation with the already described linear heptamers **Xyl7**, **TPM7** and **Ter7**, each with different distance between neighboring sulfur atoms in the ligand backbone was performed. The three linear heptameric ligand systems were present during the reductions of various concentration of gold-salts to investigate their AuNP stabilizing properties. For all three ligand systems, the average sizes of the NPs grew with an increased concentration of the gold-salt reduced. In addition, the sizes of the NPs also depend on the dimensions of the coating ligand with a trend reflecting the spacing between the sulfur atoms in the individual bridging motifs, as already shown before with **Ter7**. Also the different ligand motifs displayed considerable differences in the stability and processability of the coated particles. While **Au-Xyl7-*q*** only provided stable and redispersible NPs with low concentration of gold-salt, larger amounts of gold-salts provided larger NPs with reduced stability properties. All **Ter7** coated particles only showed very limited stability and solubility features, while the entire **Au-TPM7-*q*** series clearly displayed superior thermal stability and processability properties compared to the other two ligand systems.

TGA analysis revealed for the series of **Au-TPM7-*q*** that with increasing AuNP size, an increased amount of ligands is participating in the stabilization of a single NP. It seems that the increased bulkiness of the bridging motif in **TPM7** favors these desired physical-chemical characteristics. This method in particular allows to screen various ligand-to-gold ratio with a specific ligand, to quickly see with which concentration the ligand offers best NP-stability and on the other hand explore the potential size limit.

In summary, within this work, different thioether ligands were synthesized and their ability to enwrap the AuNPs influencing their size was systematically tested. The designed ligands have in general a weaker impact in the resulting AuNPs' sizes, when compared to changes in reaction conditions. However, their structural motifs have a great influence in the long-term stability and processability of the as-synthesized nanoparticles. These promising results help the tuning of stable AuNPs with distinct sizes for its further use as "molecular" components in nanodevices or scalable objects for optical sensing applications.

7 Experimental Part

7.1 Materials and Methods

Reagents and Solvents: All reagents and solvents were obtained either from *Sigma-Aldrich*, *Acros Organics*, *Fluorochem*, *Alfa Aesar*, *VWR*, *Fluka*, *ABCR*, *Apollo Scientific* or *TCI* and were used as received unless otherwise stated. Dry solvents used for reactions corresponded to the quality puriss, p. a., abs., over Molecular Sieves from *Fluka*. For an inert atmosphere Argon 4.8 from *PanGas* was used. Oxygen-free solvents were obtained from commercial sources or *via* degassing with argon. Technical grade solvents were use for extraction and column chromatography.

UV/Vis spectroscopy: UV/Vis spectra were recorded on a *Shimadzu* UV spectrometer UV-1800 using optical 1115F-QS *Hellma* cuvettes (10 mm light path). The wavelength of maxima absorption maxima (λ_{max}) are reported in nm.

NMR spectroscopy: Nuclear magnetic resonance (NMR) spectra were recorded using a *Bruker* DPX-NMR (400 MHz for ^{1}H and 101 MHz for ^{13}C), a *Bruker* DRX-500 (500 MHz for ^{1}H and 125 MHz for ^{13}C) or a *Bruker* Ascend Avance III HD (600 MHz for ^{1}H and 151 MHz for ^{13}C) spectrometer at ambient temperature in the solvents indicated. Solvents for NMR were obtained from *Cambridge Isotope Laboratories* or *Sigma Aldrich*. Chemical shifts are given in ppm relative to trimethylsilane (TMS) or the residual proton signal of the deuterated solvent ($CDCl_3$: 7.26 ppm, CD_2Cl_2: 5.33 ppm, DMSO-d6: 2.49 ppm) for ^{1}H spectra or the carbon signal of the solvent ($CDCl_3$: 77.0 ppm, CD_2Cl_2: 55.8 ppm, DMSO-d6: 39.5 ppm) for ^{13}C spectra. The coupling constants (J) are given in Hertz (Hz), the multiplicities are denoted as: *s* (singlet), *d* (duplet), *t* (triplet), *q* (quartet), *m* (multiplet) and *br* (broad).

Mass Spectrometry: Electron spray mass spectrometry was measured by Dr. Heinz Nadig on a *Bruker* amaZon^{TM} X for electrospray ionization (ESI). MALDI-ToF mass spectra were performed on a *Bruker microflex*™ mass spectrometer, calibrated with CsI_3, and α-cyano-4-hydroxycinnamic acid (unless stated differently) was used as matrix. Important signals are given in m/z. Gas chromatography-mass spectrometry (GC-MS) was performed on a *Shimadzu GCMS-QP2010 SE* gas chromatography system with a ZB-5HT inferno column (30 m x 0.25 m x 0.25 m), at 1 ml/min He-flow rate (split =20:1) with a *Shimadzu* mass detector (EI 70 eV). Direct analysis in real time mass spectrometry (DART-MS) was measured on a IonSense DART-SVP100 (He, 450 °C) connected to a *Shimadzu* LC-2020. High-resolution mass spectra (HRMS) were measured as HR-ESI-ToF-MS with a *Bruker* Maxis 4G instrument or HR-MALDI-FTICR with a *Bruker* solariX 94.

Gel permeation chromatography (GPC) was performed for the purification of gold nanoparticles using *Bio-Rad Bio-Beads* S-X1 Beads (operating range 600 - 14000 g/mol) with DCM or toluene as solvent (manual GPC). Recyclable, automated GPC was performed on a *Shimadzu* Prominence System with SDV preparative columns from *Polymer Standards Service* with chloroform (analytical: two SDV columns in series, 7.5 mm x 30 cm each, exclusion limit: 70'000 and 400'000 g/mol; preparative: two Showdex columns in series, 20 mm x 60 cm each, exclusion limit: 30'000 g/mol).

Elementary analysis was performed by Sylvie Mittelheisser on a *Vario Micro Cube*.

Thin layer chromatography (TLC) was performed on 0.25 mm precoated glass plates (silica gel 60 F_{254}) from *Merk*. Compounds were detected at 254 nm by fluorescence quenching or at 366 nm by self-fluorescence. If necessary, the plates were stained with $KMnO_4$, vanillin, cerium or ninhydrin.

Column chromatography purifications were carried out on *SilicaFlash® P60* (particle size 40 - 63 μm) from *SiliCycle*.

Thermogravimetric Analysis (TGA) was performed by Annika Büttner or Cedric Wobill on a *Mettler Toledo TGA/SDTA851e* with a heating rate of 10 °C/minute.

Transmission Electron Microscopy (TEM) was performed on a *Philips CM100* transmission electron microscope at 80 kV. The particles were deposited by carefully putting a drop of the nanoparticles dispersion on top of a thin carbon film that spanned a perforated carbon support film covering a copper microscopy grid from *Pacific Grid Tech*.

7.2 Synthetic Procedure

7.2.1 Terphenyl **T**-Ligands

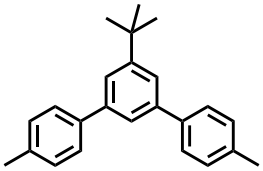

1

$C_{24}H_{26}$
314.47 g/mol

5'-(*tert*-Butyl)-4,4''-dimethyl-1,1':3',1''-terphenyl (1): 1,3-Dibromo-5-*tert*-butylbenzene (7.13 g, 24.4 mmol), *p*-tolylboronic acid (8.89 g, 65.4 mmol) and potassium carbonate (12.3 g, 89.1 mmol) were subsequently added to a 500 ml argon-purged two-necked flask. Dry THF (150 ml) and water (50 ml) were added and the reaction mixture was degassed with argon for 15 minutes. $Pd(PPh_3)_4$ (570 µg, 490 µmol) was added and the mixture was refluxed for 15 hours. The resulting mixture was poured into water and extracted three times with EtOAc. The combined organic fractions were dried over $MgSO_4$, filtrated and the volatile was evaporated to dryness. The yellow solid was subjected to column chromatography on silica eluting with *c*-hexane/EtOAc (10:1) to afford compound **1** as a white solid (7.62 g, quant.).

^{1}H NMR (400 MHz, Chloroform-*d*): δ 7.59 – 7.52 (m, 7H), 7.26 (dd, *J* = 8.0, 0.9 Hz, 4H), 2.40 (s, 6H), 1.41 (s, 9H).

^{13}C NMR (101 MHz, Chloroform-*d*): δ 152.00, 141.48, 139.04, 137.01, 129.48, 127.28, 123.30, 123.09, 35.00, 31.53, 21.16.

GC-MS (EI, 70 eV): *m*/*z* (%) = 299.3 (100), 314.3 (92), 315.3 (22), 300.3 (21), 135.6 (13), 269.2 (8), 257.15 (8), 255.15 (8), 127.1 (7), 271.2 (7).

EA: found: C 91.60 %, H 8.13 %; required: C 91.67 %, H 8.33 %.

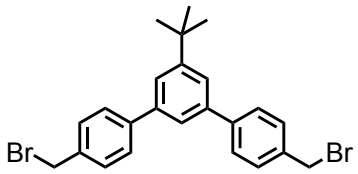

2

$C_{24}H_{24}Br_2$
472.26 g/mol

5'-(*tert*-Butyl)-4,4''-dibromomethyl-1,1':3',1''-terphenyl (2): Compound **1** (500 mg, 1.59 mmol) and *N*-bromosuccinimide (1.14 g, 6.36 mmol) were added to an argon-purged 100 ml three-necked flask and suspended in methyl formate (50 ml) and degassed with argon for 20 minutes. After addition of AIBN (13.3 mg, 80 µmol) the reaction mixture was illuminated by a 500 W halogen lamp and refluxed overnight. The solvent was removed by distillation and the residue was redissolved in DCM. The mixture was washed once with a saturated aqueous solution of sodium thiosulfate ($Na_2S_2O_3$), twice with a saturated aqueous solution of sodium bicarbonate ($NaHCO_3$), once with water and brine. The organic phase was dried over $MgSO_4$, filtrated and the solvent was removed *in vacuo*. The residue was subjected to column chromatography eluting with *c*-hexane/DCM (10:1) to afford compound **2** as a white solid (630 mg, 84 %).

^{1}H NMR (400 MHz, Chloroform-*d*): δ 7.64 – 7.55 (m, 7H), 7.51 – 7.48 (m, 4H), 4.57 (s, 4H), 1.42 (s, 9H).

^{13}C NMR (101 MHz, Chloroform-*d*): δ 152.35, 141.86, 140.93, 136.88, 129.53, 127.82, 123.73, 123.49, 35.04, 33.40, 31.49.

MS (DART, positive, 350 °C): *m/z* (%) = 471.8 (67.4), 470.8 (27.0), 470.2 (33.9).

HRMS (MALDI-ToF): *m/z* calculated for $C_{24}H_{23}Br_2$: 469.0161 $[M\text{-}1H]^+$; found: 469.0161 $[M\text{-}1H]^+$.

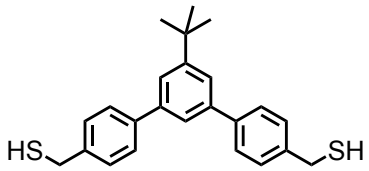

3

$C_{24}H_{26}S_2$
378.59 g/mol

(5'-(*tert*-Butyl)-[1,1':3',1''-terphenyl]-4,4''-diyl)dimethanethiol (3): A solution of **2** (500 mg, 1.06 mmol) and thiourea (814 mg, 10.6 mmol) in dry dimethyl sulfoxide (15 ml) was left stirring for 15 hours at 40 °C under an atmosphere of argon. The mixture was diluted with DCM (30 ml) and the formed white precipitate (isothiouronium salt) filtrated and washed with additional DCM. The white solid was added into a 1 L round bottom flask, purged with argon and dissolved in methanol (100 ml). The reaction mixture was degassed with argon for 30 minutes and then a degassed aqueous solution of 1 M NaOH (200 ml) was added into the reaction mixture and stirred for 1.5 hours followed by addition of a degassed aqueous solution of 1 M HCl (250 ml) and stirred for another 1.5 hours. The reaction mixture was washed three times with DCM (3 x 150 ml), the combined organic phases were dried over $MgSO_4$, filtrated and the volatile was removed *in vacuo* and if needed, purified by flash column chromatography eluting with *c*-hexane/DCM (2:1) to afford compound **3** as white solid (322 mg, 80 %).

^{1}H NMR (400 MHz, Chloroform-*d*): δ 7.63 – 7.54 (m, 7H), 7.45 – 7.38 (m, 4H), 3.81 (d, *J* = 7.6 Hz, 4H), 1.81 (t, *J* = 7.6 Hz, 2H), 1.42 (s, 9H).

^{13}C NMR (101 MHz, Chloroform-*d*): δ 152.18, 141.12, 140.58, 140.24, 128.45, 127.68, 123.42, 115.61, 34.99, 31.47, 28.70.

HRMS (ESI-ToF, negative): *m*/*z* calculated for $C_{24}H_{25}S_2^-$: 377.1400 [M-1H]$^-$; found: 377.1403 [M-1H]$^-$.

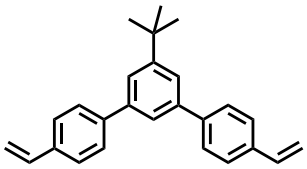

4

$C_{26}H_{26}$
338.49 g/mol

5'-(*tert*-Butyl)-4,4''-divinyl-1,1':3',1''-terphenyl (4): 1,3-Dibromo-5-*tert*-butylbenzene (500 mg, 171 mmol), 4-vinylbenzeneboronic acid (659 mg, 4.45 mmol) and tetrakis(triphenylphosphine)-palladium(0) (99.9 mg, 80 µmol) were dissolved in THF (10 ml). After adding 3 ml of 2 M aqueous K_2CO_3 (861 mg, 6.16 mmol), the reaction mixture was refluxed for 24 hours under ambient conditions. The reaction mixture was allowed to cool to room temperature and extracted with EtOAc (3 times). The combined organic fractions were washed with brine and dried over $MgSO_4$. The solvent was removed and the crude was purified by flash column chromatography eluting with c-hexane/dichloromethane (20:1) to give **4** as a white solid (477 mg, 82 %).

^{1}H NMR (400 MHz, Chloroform-*d*): δ 7.65 – 7.58 (m, 7H), δ 7.54 – 7.48 (m, 4H), δ 6.78 (dd, *J* = 17.6, 10.8 Hz, 2H), δ 5.84 – 5.77 (m, 2H), δ 5.28 (dt, *J* = 10.9, 0.6 Hz, 2H), δ 1.43 (s, 9H).

^{13}C NMR (101 MHz, Chloroform-*d*): δ 152.28, 141.52, 140.58, 140.24, 138.32, 129.45, 127.78, 124.44, 123.72, 114.77, 31.57, 28.60.

MS (MALDI-ToF, positive): *m*/*z* 361.30 $[M+Na]^+$.

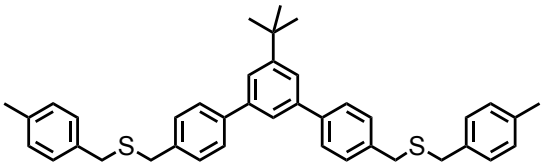

T1

$C_{40}H_{42}S_2$
586.90 g/mol

Monomer T1: For the final "end-capping oligomerization" reaction, compound **2** (437 mg, 920 µmol) and **3** (700 mg, 1.84 mmol) were dissolved in freshly distilled and degassed THF (40 ml) and the reaction mixture was degassed with argon for 20 minutes. The oligomerization was initiated by addition of sodium hydride (370 mg, 9.24 mmol) and let react for 15 minutes at room temperature, after which 4-methylbenzyl bromide (698 mg, 3.70 mmol) was added. After 15 hours, the reaction mixture was quenched by addition of water, extracted three times with methyl *tert*-butyl ether (MTBE) and dried over $MgSO_4$. The volatile was removed *in vacuo* and the crude product was subjected to a short column chromatography eluting with *c*-hexane/EtOAc (1:1) and then purified on automated recyclable gel permeation chromatography (GPC) obtaining the monomer **T1** as colorless oil (444 mg, 41 %).

^{1}H NMR (400 MHz, Chloroform-*d*): δ 7.62 – 7.57 (m, 7H), 7.38 (d, *J* = 8.2 Hz, 4H), 7.21 (d, *J* = 8.0 Hz, 4H), 7.16 – 7.11 (m, 4H), 3.65 (s, 4H), 3.62 (s, 4H), 2.35 (s, 6H), 1.43 (s, 9H).

^{13}C NMR (101 MHz, Chloroform-*d*): δ 152.14, 141.18, 140.42, 137.36, 136.63, 135.00, 129.41, 129.19, 128.92, 127.44, 123.37, 123.33, 35.35, 35.25, 35.01, 31.50, 21.13.

EA: found: C 81.99 %, H 7.13 %; required: C 81.86 %, H 7.21 %.

HRMS (MALDI-ToF): *m/z* calculated for $C_{40}H_{42}S_2$: 609.2620 $[M+Na]^+$, 625.2360 $[M+K]^+$; found: 609.2620 $[M+Na]^+$, 625.2362 $[M+K]^+$.

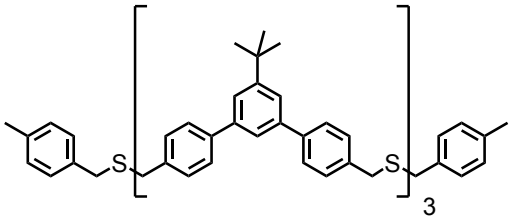

T3

$C_{88}H_{90}S_4$
1275.93 g/mol

Trimer T3: For the final "end-capping oligomerization" reaction, compound **2** (437 mg, 920 µmol) and **3** (700 mg, 1.84 mmol) were dissolved in freshly distilled and degassed THF (40 ml) and the reaction mixture was degassed with argon for 20 minutes. The oligomerization was initiated by addition of sodium hydride (370 mg, 9.24 mmol) and let react for 15 minutes at room temperature, after which 4-methylbenzyl bromide (698 mg, 3.70 mmol) was added. After 15 hours, the reaction mixture was quenched by addition of water, extracted with methyl *tert*-butyl ether (MTBE) and dried over $MgSO_4$. The volatile was removed *in vacuo* and the crude product was subjected to a short column chromatography eluting with *c*-hexane/EtOAc (1:1) and then purified on automated recyclable gel permeation chromatography (GPC) obtaining the trimer **T3** as colorless oil (260 mg, 22 %).

^{1}H NMR (400 MHz, Chloroform-*d*): δ 7.72 – 7.65 (m, 21H), 7.48 (d, *J* = 8.2 Hz, 8H), 7.45 – 7.42 (m, 4H), 7.25 (d, *J* = 7.9 Hz, 4H), 7.19 (d, *J* = 7.5 Hz, 4H), 3.78 (s, 8H), 3.72 (s, 4H), 3.68 (s, 4H), 2.38 (s, 6H), 1.49 (s, 27H).

^{13}C NMR (101 MHz, Chloroform-*d*): δ 152.31, 152.30, 141.33, 141.30, 141.28, 140.65, 140.55, 137.50, 137.37, 136.76, 135.14, 129.59, 129.55, 129.32, 129.06, 127.63, 127.57, 123.50, 123.47, 35.50, 35.47, 35.39, 35.15, 31.64, 21.27.

HRMS (MALDI-ToF): *m/z* calculated for $C_{88}H_{90}S_4$: 1297.5818 $[M+Na]^+$; found: 1297.5809 $[M+Na]^+$.

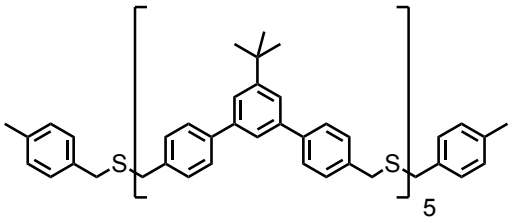

T5

$C_{136}H_{138}S_6$
1964.96 g/mol

Pentamer T5: For the final "end-capping oligomerization" reaction, compound **2** (437 mg, 920 μmol) and **3** (700 mg, 1.84 mmol) were dissolved in freshly distilled and degassed THF (40 ml) and the reaction mixture was degassed with argon for 20 minutes. The oligomerization was initiated by addition of sodium hydride (370 mg, 9.24 mmol) and let react for 15 minutes at room temperature, after which 4-methylbenzyl bromide (698 mg, 3.7 mmol) was added. After 15 hours, the reaction mixture was quenched by addition of water, extracted with methyl *tert*-butyl ether (MTBE) and dried over $MgSO_4$. The volatile was removed *in vacuo* and the crude product was subjected to a short column chromatography eluting with *c*-hexane/EtOAc (1:1) and then purified on automated recyclable gel permeation chromatography (GPC) obtaining the pentamer **T5** as colorless oil (84.8 mg, 7 %).

^{1}H NMR (400 MHz, Chloroform-*d*): δ 7.61 – 7.53 (m, 35H), 7.39 – 7.31 (m, 20H), 7.16 – 7.13 (d, *J* = 8.0 Hz, 4H), 7.10 – 7.06 (d, *J* = 7.6 Hz, 4H), 3.67 (s, 16H), 3.61 (s, 4H), 3.57 (s, 4H), 2.27 (s, 6H), 1.37 (s, 45H).

^{13}C NMR (101 MHz, Chloroform-*d*): δ 152.30, 152.28, 141.32, 141.29, 141.27, 140.63, 140.53, 137.49, 137.36, 136.73, 135.12, 129.58, 129.54, 129.31, 129.05, 127.61, 127.56, 123.49, 123.45, 35.48, 35.45, 35.37, 35.13, 31.63, 21.26.

HRMS (MALDI-ToF): *m/z* calculated for $C_{136}H_{138}S_6$: 1985.9015 $[M+Na]^+$; found: 1985.9014 $[M+Na]^+$.

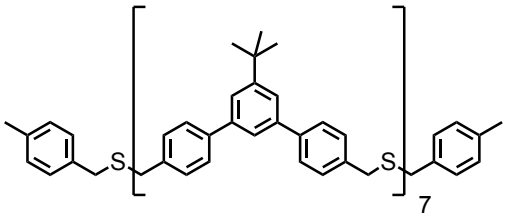

T7

$C_{184}H_{186}S_8$
2653.99 g/mol

Heptamer T7: For the final "end-capping oligomerization" reaction, compound **2** (437 mg, 920 μmol) and **3** (700 mg, 1.84 mmol) were dissolved in freshly distilled and degassed THF (40 ml) and the reaction mixture was degassed with argon for 20 minutes. The oligomerization was initiated by addition of sodium hydride (370 mg, 9.24 mmol) and let react for 15 minutes at room temperature, after which 4-methylbenzyl bromide (698 mg, 3.7 mmol) was added. After 15 hours, the reaction mixture was quenched by addition of water, extracted with methyl *tert*-butyl ether (MTBE) and dried over $MgSO_4$. The volatile was removed *in vacuo* and the crude product was subjected to a short column chromatography eluting with *c*-hexane/EtOAc (1:1) and then purified on automated recyclable gel permeation chromatography (GPC) obtaining the heptamer **T7** as colorless oil (24.4 mg, 4 %).

^{1}H NMR (400 MHz, Chloroform-*d*): δ 7.60 – 7.53 (m, 47H), 7.40 – 7.28 (m, 30H), 7.13 (d, *J* = 8.0 Hz, 4H), 7.07 (d, *J* = 7.6 Hz, 4H), 3.66 (s, 24H), 3.60 (s, 4H), 3.56 (s, 4H), 2.27 (s, 6H), 1.36 (s, 63H).

^{13}C NMR (101 MHz, Chloroform-*d*): δ 152.32, 152.30, 141.33, 141.30, 141.28, 140.65, 140.55, 137.50, 137.38, 136.77, 135.14, 129.59, 129.55, 129.32, 129.06, 127.63, 127.57, 123.51, 123.47, 35.49, 35.39, 35.15, 31.65, 21.27.

MS (MALDI-ToF, positive): broad peak at *m/z* 2676 $[M+Na]^+$.

7.2.2 Xylene **Xyl**-Ligands

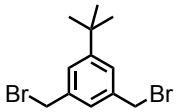

5

$C_{12}H_{16}Br_2$
320.07 g/mol

1,3-Bis(bromomethyl)-5-*tert*-butylbenzene (5):[80] 5-*tert*-Butyl-*m*-xylene (6.09 g, 36.4 mmol) and *N*-bromosuccinimide (13.8 g, 77.3 mmol) were dissolved in methyl formate (400 ml). Azobisisobutyronitrile (AIBN) (34.0 mg, 200 µmol) was added and the reaction mixture was stirred overnight illuminated by a 500 W halogen lamp. After cooling to room temperature the reaction was quenched with saturated aqueous sodium thiosulfate solution. The organic layer was separated and evaporated to dryness. The residue was dissolved in DCM (30 ml), washed with saturated aqueous sodium hydrogen carbonate solution, water, dried over magnesium sulfate, filtered and evaporated to dryness. The residue was recrystallized from cyclohexane three times to give dibromo-derivative **5** as white solid (7.02 g, 60 %).

^{1}H NMR (400 MHz, Chloroform-*d*): δ 7.33 (d, *J* = 1.7 Hz, 2H), 7.25 (t, *J* = 1.7 Hz, 1H), 4.47 (s, 4H), 1.32 (s, 9H).

^{13}C NMR (101 MHz, Chloroform-*d*): δ 153.0, 138.4, 127.3, 126.7, 35.2, 33.9, 31.6.

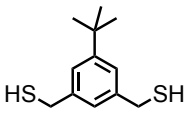

6

$C_{12}H_{18}S_2$
226.40 g/mol

(5-*tert*-Butyl-1,3-phenylene)dimethanethiol (6):[80] A solution of compound **5** (1.60 g, 5.00 mmol) and thiourea (2.00 g, 26.0 mmol) in dry dimethyl sulfoxide (20 ml) was stirred at 50 °C overnight under an atmosphere of argon. The reaction mixture was poured into DCM (500 ml). The white precipitate was filtered off and dissolved in methanol (25 ml). This solution was poured into an ice cooled 1 M aqueous sodium hydroxide solution (25 ml), which was acidified with 1 M hydrochloric acid. The mixture was extracted with DCM and the combined organic fractions were washed with water, dried over magnesium sulfate, filtered and evaporated to dryness to give dithiol-compound **6** as a colorless solid (715.8 mg, 63 %).

^{1}H NMR (400 MHz, Chloroform-*d*): δ 7.21 (br, 2H), 7.13 (br, 1H), 3.74 (d, *J* = 7.5, 4H), 1.77 (t, *J* = 7.5, 2H), 1.32 (s, 9H).

^{13}C NMR (101 MHz, Chloroform-*d*): δ 152.1, 141.1, 124.8, 123.8, 34.7, 31.3, 29.1.

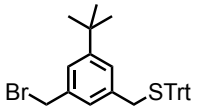

7

$C_{31}H_{31}BrS$
515.55 g/mol

(3-(Bromomethyl)-5-*tert*-butylbenzyl)(trityl)sulfane (7):[80] Dibromo-derivative **5** (3.00 g, 9.37 mmol) and trityl thiol (2.00 g, 7.02 mmol) were dissolved in dry THF (60 ml). Sodium hydride (560 mg, 14.0 mmol) was added and the mixture was stirred at room temperature for 12 hours. Afterwards water (300 ml) was carefully added to quench the reaction and the mixture was extracted with methyl-*tert*-butylether (MTBE) (3 x 150 ml). The combined organic fractions were washed with brine, dried over magnesium sulfate, filtered and evaporated to dryness. After purification by flash column chromatography eluting with *c*-hexane/DCM (4:1), compound **7** was obtained as white solid (2.20 g, 61 %).

^{1}H NMR (400 MHz, Chloroform-*d*): δ 7.49 – 7.44 (m, 6H), 7.33 – 7.20 (m, 10H), 7.02 (br, 1H), 6.96 (br, 1H), 4.42 (s, 2H), 3.32 (s, 2H), 1.27 (s, 9H).

^{13}C NMR (101 MHz, Chloroform-*d*): δ 152.12, 144.80, 137.65, 137.61, 129.80, 128.09, 126.97, 126.88, 126.45, 124.97, 67.76, 37.12, 34.81, 34.11, 31.3.

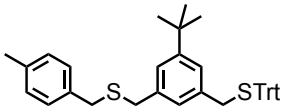

8

$C_{39}H_{40}S_2$
572.87 g/mol

1-(*p*-Tolylmethylthiomethyl)-3-(tritylthiomethyl)-5-(*tert*-butyl)benzene (8): In a dry, degassed 25 ml Schlenk-tube, compound **7** (693 mg, 1.34 mmol) and *p*-tolylmercaptane (273 µl, 2.02 mmol) were dissolved in 7 ml dry, degassed THF. NaH (60 % dispersed in mineral oil, 268 mg, 6.70 mmol) was added to the solution which was then allowed to stir at room temperature for 15 hours. The reaction mixture was quenched with water, then extracted three times with MTBE, washed once with brine, dried over $MgSO_4$ and the solvent removed *in vacuo*. The crude product was subjected to column chromatography eluting with *c*-hexane/DCM (4:1) to yield a pale solid (698 mg, 91 %).

^{1}H NMR (400 MHz, Chloroform-*d*): δ 7.50 – 7.45 (m, 6H), 7.33 – 7.07 (m, 14H), 6.98 (d, *J* = 1.8 Hz, 1H), 6.88 (d, *J* = 1.7 Hz, 1H), 3.52 (d, *J* = 2.9 Hz, 4H), 3.31 (s, 2H), 2.32 (s, 3H), 1.27 (s, 9H).

^{13}C NMR (101 MHz, Chloroform-*d*): δ 151.51, 144.83, 137.99, 136.49, 135.11, 129.16, 127.98, 126.74, 124.93, 67.56, 37.25, 35.62, 35.27, 34.65, 31.38, 21.16.

HRMS (ESI-ToF): *m/z* calculated for $C_{39}H_{40}S_2$: 590.2915 $[M+NH_4]^+$, 595.2469 $[M+Na]^+$, 611.2208 $[M+K]^+$; found: 590.2910 $[M+NH_4]^+$, 595.2464 $[M+Na]^+$, 611.2203 $[M+K]^+$.

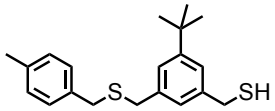

9

$C_{20}H_{26}S_2$
330.55 g/mol

1-(*p*-Tolylmethylthiomethyl)-3-(mercapto)-5-(*tert*-butyl)benzene (9): In a dry, degassed 10 ml Schlenk-tube, precursor **8** (698 mg, 1.22 mmol) was dissolved in 6 ml dry DCM, and was degassed with argon for 15 minutes. Thriethylsilane (590 µl, 3.66 mmol) and trifluoroacetic acid (240 µl, 4 % of DCM volume) were added to the solution. An immediate color change to yellow, fading after 5 minutes was observed. The mixture was stirred for another hour at room temperature before quenching upon addition of saturated aqueous sodium bicarbonate. The aqueous phase was extracted three times with MTBE and the combined organic phases were washed once with brine, dried over $MgSO_4$, filtrated and the solvent removed *in vacuo*. The crude product was subjected to column chromatography eluting with *c*-hexane/DCM (8:1) to yield compound **9** as a colorless oil (368 mg, 91 %).

^{1}H NMR (400 MHz, Chloroform-*d*): δ 7.21 – 7.10 (m, 6H), 7.07 (t, *J* = 1.6 Hz, 1H), 3.72 (d, *J* = 7.5 Hz, 2H), 3.57 (s, 4H), 2.33 (s, 3H), 1.76 (t, *J* = 7.5 Hz, 1H), 1.31 (s, 9H).

^{13}C NMR (101 MHz, Chloroform-*d*): δ 151.78, 140.92, 138.26, 136.60, 135.08, 129.18, 128.95, 125.88, 125.00, 123.73, 35.73, 35.46, 34.73, 31.39, 29.18, 21.16.

HRMS (ESI-ToF): *m/z* calculated for $C_{20}H_{26}S_2$: 331.1554 $[M+H]^+$, 353.1374 $[M+Na]^+$; found: 331.1549 $[M+H]^+$, 353.1368 $[M+Na]^+$.

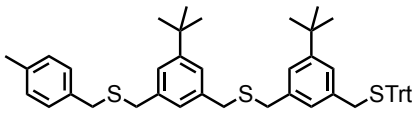

10

$C_{51}H_{56}S_3$
765.19 g/mol

Compound 10: In a dry, degassed 10 ml Schlenk-tube, precursor **9** (56.2 mg, 170 μmol) and precursor **7** (87.4 mg, 170 μmol) were dissolved in 3 ml dry THF and degassed with argon for 15 minutes. NaH (60 % dispersion in mineral oil, 17.1 mg, 428 μmol) was added to the mixture, which was then stirred for 15 hours at room temperature, and then quenched by addition of water. The aqueous phase was extracted three times with MTBE, and the combined organic fractions were washed three times with water, dried over $MgSO_4$ and the solvent was removed *in vacuo*. The crude product was subjected to flash column chromatography eluting with *c*-hexane/DCM (4:1) to afford compound **10** as a pale yellowish solid (103 mg, 79 %).

^{1}H NMR (400 MHz, Chloroform-*d*): δ 7.53 – 7.41 (m, 6H), 7.36 – 7.01 (m, 17H), 6.99 (s, 1H), 6.91 (s, 1H), 3.55 (d, J = 2.2 Hz, 8H), 3.31 (s, 2H), 2.31 (s, 3H), 1.30 (s, 9H), 1.27 (s, 9H).

^{13}C NMR (101 MHz, Chloroform-*d*): δ 151.61, 151.52, 144.82, 138.05, 138.03, 138.00, 137.11, 136.55, 135.14, 129.74, 129.19, 128.98, 127.98, 126.86, 126.84, 126.74, 124.90, 124.85, 124.70, 67.61, 37.26, 35.97, 35.84, 35.46, 34.70, 34.68, 31.46, 31.42, 21.18.

HRMS (ESI-ToF): m/z calculated for $C_{51}H_{56}S_3$: 782.3888 $[M+NH_4]^+$, 787.3442 $[M+Na]^+$, $[M+K]^+$; found: 782.3882 $[M+NH_4]^+$, 787.3436 $[M+Na]^+$, 803.3181 $[M+K]^+$.

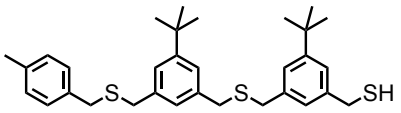

11

$C_{32}H_{42}S_3$
522.87 g/mol

Compound 11: In a dry, degassed 15 ml three-necked flask, precursor **10** (103 mg, 134 µmol) was dissolved in 5 ml dry DCM and degassed with argon for 15 minutes, then triethylsilane (200 µl, 1.26 mmol) and trifluoroacetic acid (200 µl, 4 % of DCM volume) were added to the mixture. The reaction mixture was allowed to stir at room temperature for 15 hours, and was then quenched by addition of saturated aqueous sodium bicarbonate. The aqueous phase was extracted three times with DCM, dried over $MgSO_4$ and the solvent was removed *in vacuo*. The crude product was subjected to flash column chromatography eluting with *c*-hexane/DCM (3:1) to afford compound **11** as a colorless oil (51.5 mg, 73 %).

^{1}H NMR (400 MHz, Chloroform-d): δ 7.20 (dt, *J* = 3.4, 1.7 Hz, 4H), 7.17 – 7.11 (m, 4H), 7.11 – 7.06 (m, 2H), 3.72 (d, *J* = 7.5Hz, 2H), 3.61 – 3.57 (m, 8H), 2.34 (s, 3H), 1.77 (t, *J* = 7.5 Hz, 1H), 1.32 (s, 2H), 1.32 (s, 9H).

^{13}C-NMR (101 MHz, Chloroform-*d*): δ 151.90, 151.55, 140.96, 138.28, 138.00, 136.57, 135.11, 129.19, 128.96, 126.86, 125.90, 124.94, 124.86, 124.70, 123.80, 35.99, 35.89, 35.85, 35.50, 34.76, 34.70, 31.44, 31.43, 29.18, 21.17.

HRMS (ESI-ToF): *m/z* calculated for $C_{51}H_{56}S_3$: 523.2527 $[M+H]^+$, 540.2792 $[M+NH_4]^+$, 545.2346 $[M+Na]^+$, 561.2086 $[M+K]^+$; found: 523.2521 $[M+H]^+$, 540.2787 $[M+NH_4]^+$, 545.2341 $[M+Na]^+$, 561.2080 $[M+K]^+$.

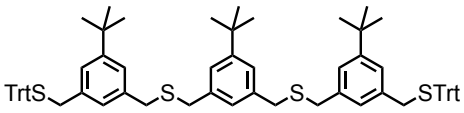

12

$C_{74}H_{78}S_4$
1095.68 g/mol

Trityl-protected trimer 14:[80] Compound **6** (340 mg, 1.50 mmol) and compound **7** (1.70 g, 3.30 mmol) were dissolved in dry THF (80 ml) under an atmosphere of argon. Sodium hydride (60 % in mineral oil, 300 mg, 7.50 mmol) was added and the mixture was stirred at room temperature for 3 hours. The reaction was quenched with water and extracted with MTBE. The combined organic fractions were washed with brine, dried over magnesium sulfate, filtered and evaporated to dryness. After purification by flash column chromatography eluting with *c*-hexane/DCM (3:2), the trityl-protected trimer **12** was obtained as colorless foam (1.30 g, 80 %).

^{1}H NMR (400 MHz, Chloroform-*d*): δ 7.48 – 7.44 (m, 12H), 7.32 – 7.27 (m, 12H), 7.24 – 7.19 (m, 6H), 7.16 (br, 2H), 7.13 (br, 2H), 7.05 (br, 1H), 6.98 (br, 2H), 3.55 (s, 4H), 3.54 (s, 4H), 3.30 (s, 4H), 1.29 (s, 9H), 1.26 (s, 18H).

13C NMR (101 MHz, Chloroform-*d*): δ 151.55, 144.76, 138.00, 137.92, 137.01, 129.68, 127.92, 126.77, 126.68, 124.80, 67.54, 37.19, 35.93, 34.61, 31.41, 31.35.

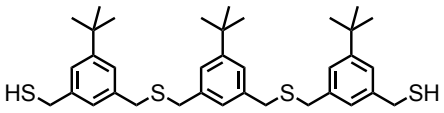

13

$C_{36}H_{50}S_4$
611.04 g/mol

Dithiol-trimer 13:[80] The trityl-protected trimer **12** (960 mg, 880 µmol) was dissolved in DCM (15 ml) and triethylsilane (380 µl, 2.36 mmol) was added, followed by trifluoroacetic acid (600 µl, 4 % of the DCM volume). The reaction mixture immediately turned yellow and decolorized after approximately 2 minutes. After additional 10 minutes the reaction was quenched with saturated aqueous sodium hydrogen carbonate. The two phases were separated and the aqueous phase was washed with DCM. The combined organic fractions were dried over magnesium sulfate, filtered and evaporated to dryness. After purification by flash column chromatography eluting with *c*-hexane/DCM (1:1) the dithiol trimer **13** was obtained as a white solid (535 mg, quant.).

^{1}H NMR (400 MHz, Chloroform-*d*): δ .7.22 – 7.18 (m, 6H), 7.09 – 7.07 (m, 3H), 3.72 (d, *J* = 7.5, 4H), 3.61 (s, 4H), 3.60 (s, 4H), 1.76 (t, *J* = 7.5, 2H), 1.33 (s, 9H), 1.31 (s, 18H).

^{13}C NMR (101 MHz, Chloroform-*d*): δ 151.68, 151.62, 140.89, 138.19, 137.94, 126.80, 125.83, 124.80, 124.73, 123.77, 35.97, 35.88, 34.69, 34.65, 31.39, 31.35, 29.11.

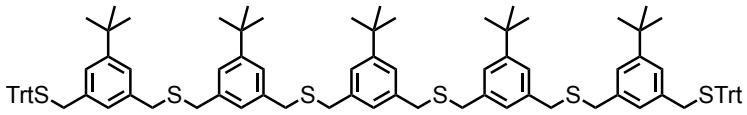

14

$C_{98}H_{110}S_6$
1480.32 g/mol

Trityl-protected pentamer 14:[80] Dithiol-trimer **13** (610 mg, 1.00 mmol) and compound **7** (1.10 g, 2.13 mmol) were dissolved in dry THF (60 ml) under an atmosphere of argon. Sodium hydride (60 % in mineral oil, 160 mg, 4.00 mmol) was added and the mixture was stirred at room temperature for 3 hours. The reaction was quenched with water and extracted with MTBE. The combined organic fractions were washed with brine, dried over magnesium sulfate, filtered and evaporated to dryness. After purification by flash column chromatography eluting with *c*-hexane/DCM (3:2), the trityl-protected pentamer **14** was obtained as colorless foam (1.10 g, 75 %).

^{1}H NMR (400 MHz, Chloroform-*d*): δ 7.48 – 7.44 (m, 12H), 7.32 – 7.27 (m, 12H), 7.24 – 7.17 (m, 10H), 7.16 (br, 2H), 7.14 (br, 2H), 7.09 – 7.06 (m, 3H), 6.98 (br, 2H), 6.91 (br, 2H), 3.58 (s, 8H), 3.56 (s, 4H), 3.55 (s, 4H), 3.31 (s, 4H), 1.31 - 1.29 (m, 27H), 1.27 (s, 18H).

^{13}C NMR (101 MHz, Chloroform-*d*): δ 151.5, 144.7, 138.0, 137.9, 137.0, 129.7,127.9. 126.8, 126.7, 126.6, 124.8, 124.7, 67.5, 37.2, 36.0, 35.9, 34.6 (2x), 31.3 (2x).

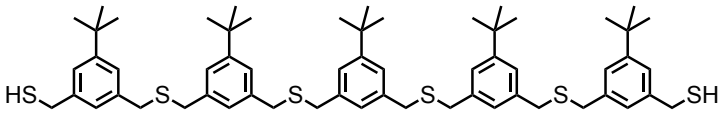

15

$C_{60}H_{82}S_6$
995.68 g/mol

Dithiol-pentamer 15:[80] The trityl-protected pentamer **14** (400 mg, 270 µmol) was dissolved in DCM (5 ml) and triethylsilane (113 µl, 82.5 mg, 700 µmol) was added, followed by trifluoroacetic acid (170 µl, 4 % of the DCM volume). The reaction mixture immediately turned yellow and decolorized after approximately 2 minutes. After additional 10 minutes the reaction was quenched with saturated aqueous sodium hydrogen carbonate. The two phases were separated and the aqueous phase was washed with DCM. The combined organic fractions were dried over magnesium sulfate, filtered and evaporated to dryness. After purification by flash column chromatography eluting with *c*-hexane/DCM (1:2) the dithiol pentamer **15** was obtained as a white solid (250 mg, 93 %).

^{1}H NMR (400 MHz, Chloroform-*d*): δ 7.21 – 7.18 (m, 10H), 7.10 – 7.06 (m, 5H), 3.71 (d, *J* = 7.5, 4H), 3.63 – 3.58 (m, 16H), 1.76 (t, *J* = 7.5, 2H), 1.34 – 1.29 (m, 45H).

^{13}C NMR (101 MHz, Chloroform-*d*): δ 151.8, 151.6, 140.9, 138.2, 138.0, 126.8, 125.8, 124.8, 124.7, 123.8, 36.0 (2x), 35.9, 34.7, 34.6, 31.4 (2x), 29.1.

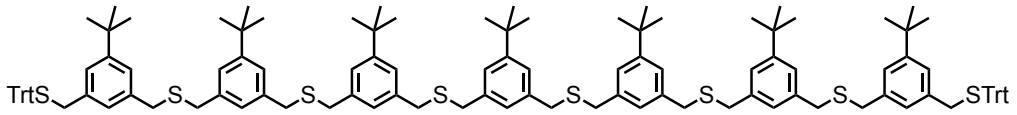

16

$C_{122}H_{142}S_8$
1864.96 g/mol

Trityl-protected heptamer 16:[80] The dithiol pentamer **15** (140 mg, 140 µmol) and compound **7** (159 mg, 310 µmol) were dissolved in dry THF (10 ml) under an atmosphere of argon. Sodium hydride (60 % in mineral oil, 22.4 mg, 560 µmol) was added and the mixture was stirred at room temperature for 3 hours. The reaction was quenched with water and extracted with MTBE. The combined organic fractions were washed with brine, dried over magnesium sulfate, filtered and evaporated to dryness. After purification by flash column chromatography eluting with *c*-haxane/DCM (3:2), the trityl-protected heptamer **16** was obtained as colorless foam (232 mg, 89 %).

^{1}H NMR (400 MHz, Chloroform-*d*): δ 7.48 – 7.44 (m, 12H), 7.32 – 7.27 (m, 12H), 7.24 – 7.13 (m, 19H), 7.10 – 7.06 (m, 4H), 6.98 (s, 2H), 6.90 (s, 2H), 3.62 – 3.53 (m, 24H), 3.30 (s, 4H), 1.31 – 1.26 (m, 63H, H).

^{13}C NMR (101 MHz, Chloroform-*d*): δ 151.55, 144.76, 138.02, 137.04, 129.69, 127.92, 126.79, 126.68, 124.79, 124.72, 35.98, 34.65, 31.41, 31.35.

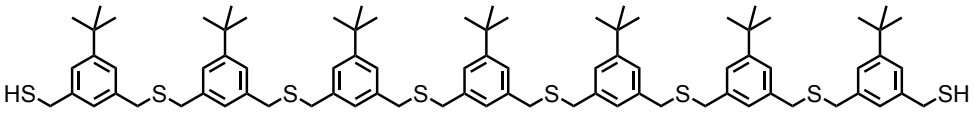

17

$C_{84}H_{114}S_8$
1380.32 g/mol

Dithiol-heptamer 17:[80] The trityl-protected heptamer **16** (298 mg, 160 µmol) was dissolved in DCM (3 ml) and triethylsilane (103 µl, 75.2 mg, 640 µmol) was added, followed by trifluoroacetic acid (200 µl, 4 % of the DCM volume). The reaction mixture immediately turned yellow and decolorized after approximately 2 minutes. After additional 10 minutes the reaction was quenched with saturated aqueous sodium hydrogen carbonate. The two phases were separated and the aqueous phase was washed with DCM. The combined organic fractions were dried over magnesium sulfate, filtered and evaporated to dryness. After purification by flash column chromatography eluting with *c*-hexane/DCM (1:2) the dithiol-heptamer **17** was obtained as a white solid (200 mg, 91 %).

^{1}H NMR (400 MHz, Chloroform-*d*): δ 7.21 – 7.17 (m, 14H), 7.10 – 7.06 (m, 7H), 3.71 (d, *J* = 7.5, 4H), 3.62 – 3.57 (m, 24H), 1.75 (t, *J* = 7.5, 2H), 1.32 – 1.29 (m, 63H).

^{13}C NMR (101 MHz, Chloroform-*d*): δ 151.8, 151.6, 140.9, 138.0, 138.0, 126.8, 125.8, 124.8, 124.7, 123.8, 36.0, 35.9, 34.7, 34.6, 31.4, 29.1.

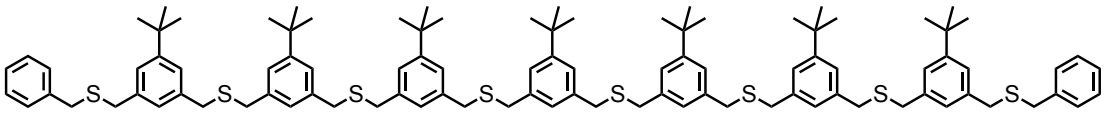

Xyl7

$C_{98}H_{126}S_8$
1560.57 g/mol

Heptamer Xyl7: Dithiol heptamer **17** (203 mg, 150 µmol) and benzyl chloride (41.1 mg, 320 µmol) were dissolved in dry degassed THF (10 ml) under an atmosphere of argon. Sodium hydride (60 % in mineral oil, 73.0 mg, 1.83 mmol) was added and the mixture was stirred for 1.5 hours at room temperature. The reaction was quenched with water and extracted with MTBE three times. The combined organic fractions were washed with brine, dried over magnesium sulfate and evaporated to dryness. Purification of the crude product was achieved by flash column chromatography eluting with c-hexane/DCM (2:3) to yield heptamer **Xyl7** as colorless solid (198 mg, 87 %).

^{1}H NMR (400 MHz, Dichloromethane-*d*): δ 7.34 – 7.05 (m, 31H), 3.61 (br, 28H), 3.59 (s, 4H), 1.31 (m, 63H).

^{13}C NMR (101 MHz, Chloroform-*d*): δ 151.6, 151.5 (2x), 138.2, 138.0, 137.8, 129.0, 128.4, 126.9, 126.8, 124.9, 124.7 (2x), 36.0, 35.9, 35.8, 35.7, 34.6, 31.4 (2x).

7.2.3 Terphenyl **Ter**-Ligands

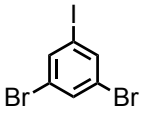

18

$C_6H_3Br_2I$
361.80 g/mol

1,3-Dibromo-5-iodobenzene (18):[137] 1,3,5-Tribromobenzene (2.00 g, 6.23 mmol) in dry diethyl ether (80 ml) at -78 °C, *n*-BuLi (1.6 M in hexane; 3.97 ml, 6.35 mmol) was added *via* syringe pump over 30 min, and the obtained solution was stirred for 1.5 hour. The reaction mixture was cooled to -78 °C and iodine (1.66 g, 6.54 mmol) was dissolved in dry diethyl ether (10 ml) and added *via* syringe pump and the mixture was then slowly warmed to room temperature. The organic phase was extracted twice with saturated aqueous solution of sodium thiosulfate ($Na_2S_2O_3$), once with brine, dried over magnesium sulfate and evaporated *in vacuo*. Recrystallization from ethanol (3 times) afforded compound **18** as white needles (1.60 g, 71 %).

^{1}H NMR (400 MHz, Chloroform-*d*): δ 7.64 (d, *J* = 1.6, 2H); 7.90 (t, *J* = 1.6, 1H).

^{13}C NMR (101 MHz, Chloroform-*d*): δ 94.46; 123.45; 133.74; 138.61.

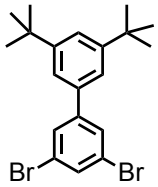

19

$C_{20}H_{24}Br_2$
424.22 g/mol

3,5-Dibromo-3',5'-di-*tert*-butyl-1,1'-biphenyl (19): 1,3-Dibromo-5-iodobenzene (**18**) (5.84 g, 16.1 mmol), 1,3-di-*tert*-butylphenyl boronic acid (3.97 g, 17.0 mmol) and potassium carbonate (13.5 g, 96.9 mmol) were subsequently added to a 1000 ml argon-purged two-necked flask. Toluene (500 ml) and water (100 ml) were added and the reaction mixture was degassed with argon for 15 minutes. $Pd(PPh_3)_4$ (377 mg, 323 µmol) was added and the mixture was refluxed for 15 hours. The resulting mixture was poured into water and extracted with EtOAc. The combined organic fractions were dried over magnesium sulfate, filtrated and the volatile was evaporated to dryness. The yellow crude was subjected to column chromatography on silica eluting with *c*-hexane/DCM (10:1) yielding compound **19** as a white solid (5.80 g, 85 %).

^{1}H NMR (400 MHz, Chloroform-*d*): δ 7.63 (s, 3H), 7.48 (t, *J* = 1.8 Hz, 1H), 7.32 (d, *J* = 1.8 Hz, 2H), 1.38 (s, 18H).

^{13}C NMR (101 MHz, Chloroform-*d*): δ 151.59, 146.14, 137.90, 132.25, 129.25, 123.08, 122.60, 121.54, 35.03, 31.49.

GC-MS (EI, 70 eV): *m*/*z* (%) = 57.1 (100), 409 (32), 411 (16), 407 (15), 424.05 (8), 89.05 (7), 410 (6), 103.1 (5), 426 (5), 422.05 (5), 58.1 (4), 101.1 (4), 94.6 (4), 408.05 (4), 412 (3), 142.6 (3), 102.05 (3), 191.1 (3), 55.1 (3).

EA: found: C 56.95 %, H 5.53 %; required: C 56.63 %, H 5.70 %.

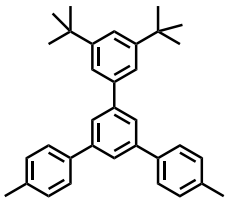

20

$C_{34}H_{38}$
446.68 g/mol

5'-(*tert*-Butyl)-4,4''-dimethyl-1,1':3',1''-terphenyl (20): 1,3-Dibromo-5-*tert*-butylbenzene (**19**) (7.13 g, 24.4 mmol), *p*-tolylboronic acid (8.89 g, 65.4 mmol) and potassium carbonate (12.3 g, 89.1 mmol) were subsequently added to a 500 ml argon-purged two-necked flask. Tetrahydrofuran (150 ml) and water (50 ml) were added and the reaction mixture was degassed with argon for 15 minutes. $Pd(PPh_3)_4$ (570 µg, 490 µmol) was added and the mixture was refluxed for 15 hours. The resulting mixture was poured into water and extracted with EtOAc. The combined organic fractions were dried over $MgSO_4$, filtrated and the volatile was evaporated to dryness. The yellow solid was subjected to column chromatography on silica eluting with *c*-hexane/EtOAc (10:1) to afford compound **20** as a white solid (7.62 g, quant.).

^{1}H NMR (400 MHz, Chloroform-*d*): δ 7.59 – 7.52 (m, 7H), 7.26 (dd, *J* = 8.0, 0.9 Hz, 4H), 2.40 (s, 6H), 1.41 (s, 9H).

^{13}C NMR (101 MHz, Chloroform-*d*): δ 152.00, 141.48, 139.04, 137.01, 129.48, 127.28, 123.30, 123.09, 35.00, 31.53, 21.16.

GC-MS (EI, 70 eV): m/z (%) = 299.3 (100), 314.3 (92), 315.3 (22), 300.3 (21), 135.6 (13), 269.2 (8), 257.15 (8), 255.15 (8), 127.1 (7), 271.2 (7).

EA: found: C 91.60 %, H 8.13 %; required: C 91.67 %, H 8.33 %.

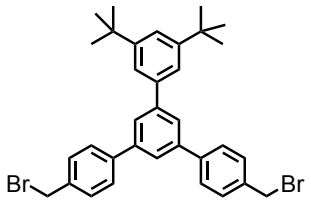

21

$C_{34}H_{36}Br_2$
604.47 g/mol

4''-(Bromomethyl)-5'-(4-(bromomethyl)phenyl)-3,5-di-*tert*-butyl-1,1':3',1''-terphenyl (21): Compound **20** (3.91 g, 8.75 mmol) and *N*-bromosuccinimide (6.29 g, 35.0 mmol) were added to an argon-purged 500 ml three-neck flask and suspended in methyl formate (250 ml) and degassed with argon for 20 minutes. After addition of AIBN (147 mg, 870 µmol) the reaction mixture was illuminated by a 500 W halogen lamp and refluxed overnight. The solvent was removed by distillation and the residue was redissolved in DCM. The mixture was washed once with a saturated aqueous solution of $Na_2S_2O_3$, twice with a saturated aqueous solution of $NaHCO_3$, once with water and brine. The organic phase was dried over $MgSO_4$, filtrated and the solvent was removed *in vacuo*. The residue was subjected to column chromatography eluting with *c*-hexane/DCM (10:1) to afford compound **21** as a white solid (4.78 g, 90 %).

^{1}H NMR (400 MHz, Chloroform-*d*): δ 7.76 – 7.72 (m, 3H), 7.69 – 7.64 (m, 4H), 7.54 – 7.47 (m, 7H), 4.58 (s, 4H), 1.40 (s, 18H).

^{13}C NMR (101 MHz, Chloroform-*d*): δ 151.51, 144.11, 144.06, 141.72, 141.52, 140.61, 137.27, 129.76, 127.97, 125.95, 124.98, 122.01, 35.19, 33.44, 31.70.

HRMS (MALDI-ToF): *m/z* calculated for $C_{34}H_{35}Br_2$: 601.1100 $[M-H]^+$; found: 601.1099 $[M-H]^+$.

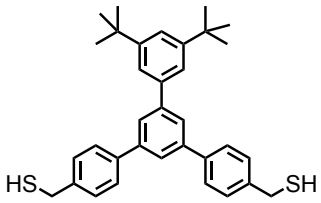

22

$C_{34}H_{38}S_2$
510.80 g/mol

(5'-(3,5-Di-*tert*-butylphenyl)-[1,1':3',1''-terphenyl]-4,4''-diyl)dimethanethiol (22): The trityl-protected compound **24** (616 mg, 610 µmol) was dissolved in DCM (15 ml) and triethylsilane (300 µl, 1.85 mmol) was added, followed by trifluoroacetic acid (600 µl, 4 % of the DCM volume). The reaction mixture immediately turned yellow and decolorized after approximately 2 minutes. After additional 10 minutes the reaction was quenched with saturated aqueous sodium hydrogen carbonate. The two phases were separated and the aqueous phase was washed with DCM. The combined organic fractions were dried over magnesium sulfate, filtered and evaporated to dryness. After purification by flash column chromatography eluting with *c*-hexane/DCM (1:1) compound **22** was obtained as a white solid (296 mg, quant.).

or:

(5'-(3,5-Di-*tert*-butylphenyl)-[1,1':3',1''-terphenyl]-4,4''-diyl)dimethanethiol (22): A solution of **23** (1.00 g, 1.65 mmol) and thiourea (630 mg, 8.27 mmol) in dry dimethyl sulfoxide (10 ml) was left stirring for 15 hours at 40 °C under an atmosphere of argon. The mixture was diluted with DCM (50 ml) and the formed white precipitate (isothiouronium salt) filtrated and washed with additional DCM. The white solid was added into a 1 L round bottom flask, purged with argon and dissolved in methanol (200 ml). The reaction mixture was degassed with argon for 30 minutes and then a degassed aqueous solution of 1 M NaOH (200 ml) was added into the reaction mixture and stirred for 1.5 hours. Then, a degassed aqueous solution of 1 M HCl (250 ml) was added and stirred for 1.5 hours. The reaction mixture was washed three times with DCM. The combined organic phases were dried over $MgSO_4$, filtrated and the volatile was removed *in vacuo* to afford compound **22** as white solid (420 mg, 56 %).

^{1}H NMR (400 MHz, Chloroform-*d*): δ 7.75 (s, 3H), 7.67 (d, *J* = 8.2 Hz, 4H), 7.56 – 7.42 (m, 7H), 3.83 (d, *J* = 7.6 Hz, 4H), 1.84 (t, *J* = 7.6 Hz, 2H), 1.42 (s, 18H).

^{13}C NMR (101 MHz, Chloroform-*d*): δ 151.32, 143.86, 141.81, 140.65, 140.54, 140.11, 128.59, 127.72, 125.55, 124.78, 121.90, 121.78, 35.06, 31.59, 28.73.

HRMS (MALDI-ToF): *m/z* calculated for $C_{34}H_{38}S_2$: 508.2253 $[M-2H]^{2-}$, 509.2331 $[M-1H]^-$; found: 508.2253 $[M-2H]^+$, 509.2332 [M-1H].

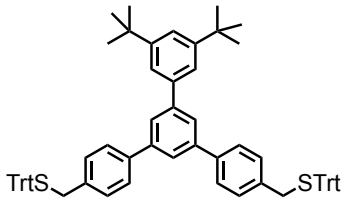

23

$C_{72}H_{66}S_2$
995.44 g/mol

((5'-(3,5-Di-tert-butylphenyl)-[1,1':3',1''-terphenyl]-4,4''-diyl)bis(methylene))bis(tritylsulfane) (23): Compound **21** (525 mg, 870 µmol) and trityl thiol (743 mg, 2.61 mmol) were dissolved in dry degassed THF (30 ml) under an atmosphere of argon. Sodium hydride (60 % in mineral oil, 348 mg, 8.69 mmol) was added and the mixture was stirred at room temperature for 3 hours. The reaction was quenched with water and extracted with MTBE. The combined organic fractions were washed with brine, dried over magnesium sulfate, filtered and evaporated to dryness. After purification by flash column chromatography eluting with *c*-hexane/DCM (3:2) compound **23** was obtained as colorless foam (788 mg, 91 %).

^{1}H NMR (400 MHz, Chloroform-*d*): δ 7.67 (m, 3H), 7.58 – 7.53 (m, 4H), 7.52 – 7.43 (m, 15H), 7.35 – 7.29 (m, 12H), 7.26 – 7.22 (m, 10H), 3.38 (s, 4H), 1.38 (s, 18H).

^{13}C NMR (101 MHz, Chloroform-*d*): δ 151.39, 144.83, 141.99, 140.20, 136.51, 135.18, 129.77, 129.72, 128.12, 128.08, 128.06, 127.65, 127.65, 126.87, 125.58, 122.02, 67.65, 66.65, 36.84, 35.16, 31.69.

MS (MALDI-ToF, positive): *m/z* 751.35 [M-Trt].

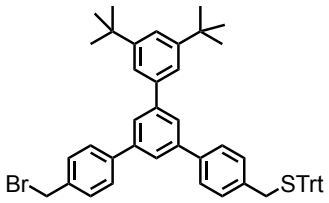

24

$C_{53}H_{51}BrS$
799.96 g/mol

((5'-(4-(Bromomethyl)phenyl)-3'',5''-di-tert-butyl-[1,1':3',1''-terphenyl]-4-yl)methyl)(trityl)sulfane (24): Compound **21** (231 mg, 380 µmol) and trityl thiol (65.3 mg, 230 µmol) were dissolved in dry degassed THF (30 ml) under an atmosphere of argon. Sodium hydride (60 % in mineral oil, 76.4 mg, 1.91 mmol) was added and the mixture was stirred at room temperature for 3 hours. The reaction was quenched with water and extracted with MTBE. The combined organic fractions were washed with brine, dried over magnesium sulfate, filtered and evaporated to dryness. After purification by flash column chromatography eluting with *c*-hexane/DCM (3:2) compound **24** was obtained as colorless foam (120 mg, 39 %).

^{1}H NMR (400 MHz, Chloroform-*d*): δ 7.73 – 7.63 (m, 6H), 7.59 – 7.45 (m, 13H), 7.36 – 7.23 (m, 10H), 4.58 (s, 2H), 3.38 (s, 2H), 1.39 (s, 18H).

^{13}C NMR (101 MHz, Chloroform-*d*): δ 151.31, 144.69, 141.48, 141.46, 129.63, 129.63, 129.61, 129.58, 127.98, 127.94, 127.92, 127.83, 127.51, 127.27, 126.74, 121.87, 67.73, 67.53, 36.71, 35.03, 33.35, 31.56, 24.88.

MS (MALDI-ToF, positive): *m/z* 821.11 $[M+Na]^+$.

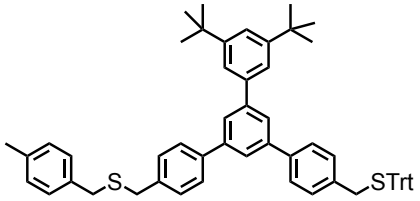

25

$C_{61}H_{60}S_2$
857.27 g/mol

((3'',5''-Di-*tert*-butyl-5'-(4-(((4-methylbenzyl)thio)methyl)phenyl)-[1,1':3',1''-terphenyl]-4-yl)methyl)(trityl)sulfane (25): In a dry, degassed 25 ml Schlenk-tube, compound **24** (150 mg, 180 µmol) and *p*-tolylmercaptane (52.0 mg, 380 µmol) were dissolved in 5 ml dry, degassed THF. NaH (60 % dispersed in mineral oil, 150 mg, 3.76 mmol) was added to the solution which was then allowed to stir at room temperature for 15 hours. The reaction mixture was quenched with water, then extracted three times with MTBE, washed once with brine, dried over $MgSO_4$ and the solvent removed *in vacuo*. The crude product was subjected to column chromatography eluting with *c*-hexane/DCM (4:1) to yield compound **25** as a pale solid (141 mg, 88 %).

^{1}H NMR (400 MHz, Chloroform-*d*): δ 7.90 – 7.73 (m, 10H), 7.68 (d, *J* = 8.2 Hz, 2H), 7.63 – 7.48 (m, 12H), 7.43 – 7.28 (m, 7H), 7.22 (d, *J* = 7.5 Hz, 2H), 3.76 (s, 2H), 3.73 (s, 2H), 3.48 (s, 2H), 2.42 (s, 3H), 1.47 (s, 18H).

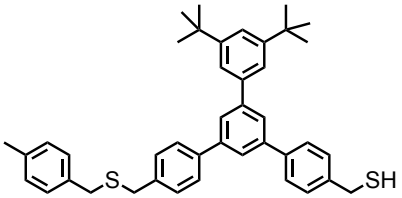

26

$C_{42}H_{46}S_2$
614.95 g/mol

(3'',5''-Di-*tert*-butyl-5'-(4-(((4-methylbenzyl)thio)methyl)phenyl)-[1,1':3',1''-terphenyl]-4-yl)methanethiol (26): In a dry, degassed 10 ml Schlenk-tube, precursor **25** (147 mg, 170 µmol) was dissolved in 6 ml dry DCM, and was degassed with argon for 15 minutes. Thriethylsilane (41.4 µl, 260 µmol) and trifluoroacetic acid (240 µl, 4 % of DCM volume) were added to the solution. An immediate color change to yellow, fading after 5 minutes was observed. The mixture was stirred for another hour at room temperature before quenching upon addition of saturated aqueous sodium bicarbonate. The aqueous phase was extracted three times with MTBE and the combined organic phase was washed once with brine, dried over $MgSO_4$, filtrated and the solvent removed *in vacuo*. The crude product was subjected to column chromatography eluting with *c*-hexane/DCM (8:1) to yield compound **26** as a colorless oil (99.0 mg, 94 %).

^{1}H NMR (400 MHz, Chloroform-*d*): δ 7.79 – 7.73 (m, 7H), 7.71 – 7.63 (m, 7H), 7.49 – 7.39 (m, 5H), 7.23 (d, *J* = 8.0 Hz, 2H), 7.16 (d, *J* = 7.6 Hz, 2H), 3.70 (d, *J* = 7.5 Hz, 2H), 3.82 (s, 2H), 3.68 (s, 2H), 3.65 (s, 2H), 1.84 (t, *J* = 7.6 Hz, 1H), 1.42 (s, 18H).

MS (MALDI-ToF, negative): *m*/*z* 613.11 $[M-H]^-$.

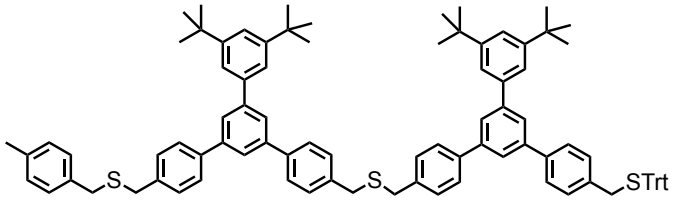

27

$C_{95}H_{96}S_3$
1333.99 g/mol

Compound 27: In a dry, degassed 25 ml Schlenk-tube, compound **26** (78 mg, 130 µmol) and compound **24** (151 mg, 190 µmol) were dissolved in 5 ml dry, degassed THF. NaH (60 % dispersed in mineral oil, 30.0 mg, 1.26 mmol) was added to the solution which was then allowed to stir at room temperature for 15 hours. The reaction mixture was quenched with water, then extracted three times with MTBE, washed once with brine, dried over $MgSO_4$ and the solvent removed *in vacuo*. The crude product was subjected to column chromatography eluting with *c*-hexane/DCM (3:1) and if necessary to automated recyclable GPC to yield compound **27** as a colorless solid (151 mg, 90 %).

^{1}H NMR (400 MHz, Chloroform-*d*): δ 7.90 – 7.73 (m, 12H), 7.68 (d, *J* = 8.2 Hz, 2H), 7.63 – 7.48 (m, 17H), 7.43 – 7.28 (m, 14H), 7.22 (d, *J* = 7.5 Hz, 2H), 3.81 (s, 4H), 3.74 (s, 2H), 3.71 (s, 2H), 3.48 (s, 2H), 2.42 (s, 3H), 1.50 (s, 18H), 1.49 (s, 18H).

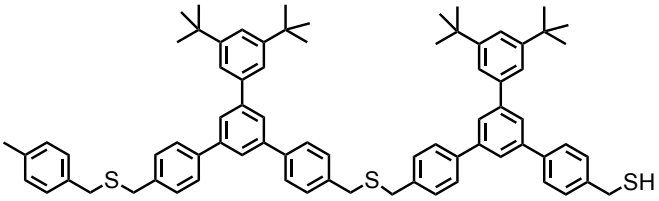

28

$C_{76}H_{82}S_3$
1091.67 g/mol

Compound 28: In a dry, degassed 10 ml Schlenk-tube, precursor **27** (151 mg, 140 µmol) was dissolved in 5 ml dry DCM, and was degassed with argon for 15 minutes. Thriethylsilane (33.4 µl, 210 µmol) and trifluoroacetic acid (200 µl, 4 % of DCM volume) were added to the solution. An immediate color change to yellow, fading after 5 minutes was observed. The mixture was stirred for another hour at room temperature before quenching upon addition of saturated aqueous sodium bicarbonate. The aqueous phase was extracted three times with MTBE and the combined organic phase was washed once with brine, dried over $MgSO_4$ and the solvent removed *in vacuo*. The crude product was subjected to column chromatography eluting with *c*-hexane/DCM (1:1) to yield compound **28** as a colorless solid (105 mg, 70 %).

^{1}H NMR (400 MHz, Chloroform-*d*): δ 7.85 – 7.78 (m, 4H), 7.73 – 7.69 (m, 4H), 7.58 – 7.54 (m, 4H), 7.53 – 7.44 (m, 8H), 7.36 – 7.30 (m, 4H), 7.28 – 7.22 (m, 4H), 7.20 – 7.15 (m, 5H), 3.85 (d, *J* = 7.5 Hz, 2H), 3.78 (s, 4H), 3.70 (s, 2H), 3.68 (s, 2H), 2.39 (s, 3H), 1.86 (t, *J* = 7.6 Hz, 1H), 1.46 (s, 18H), 1.45 (s, 18H).

MS (MALDI-ToF, negative): *m*/*z* 1089.12 $[M-H]^-$.

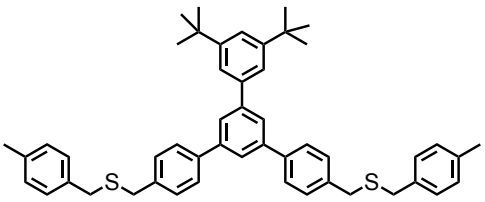

Ter1

$C_{50}H_{54}S_2$
719.10 g/mol

Monomer Ter1: For the final "end-capping oligomerization" reaction, compound **21** (233 mg, 360 µmol) and **22** (393 mg, 720 µmol) were dissolved in freshly distilled and degassed THF (20 ml) and the reaction mixture was degassed with argon for 20 minutes. The oligomerization was initiated by addition of sodium hydride (154 mg, 3.85 mmol) and let react for 15 minutes at room temperature, after which 4-methylbenzyl bromide (294 mg, 1.54 mmol) was added. After 15 hours, the reaction mixture was quenched by addition of water, extracted with MTBE and dried over $MgSO_4$. The volatile was removed *in vacuo* and the crude product was subjected to a short column chromatography eluting with *c*-hexane/EtOAc (1:1) and then purified on automated recyclable gel permeation chromatography (GPC) obtaining monomer **Ter1** as a colorless oil (139 mg, 50 %).

^{1}H NMR (400 MHz, Chloroform-*d*): δ 7.78 – 7.74 (m, 3H), 7.68 – 7.63 (m, 4H), 7.50 (q, J = 1.2 Hz, 3H), 7.43 – 7.39 (m, 4H), 7.25 – 7.20 (m, 4H), 7.16 – 7.12 (m, 4H), 3.67 (s, 4H), 3.64 (s, 4H), 2.35 (s, 6H), 1.41 (s, 18H).

^{13}C NMR (101 MHz, Chloroform-*d*): δ 151.42, 141.98, 140.84, 140.08, 137.81, 136.80, 135.12, 129.65, 129.34, 129.07, 127.60, 125.58, 124.89, 122.03, 35.56, 35.40, 35.19, 31.72, 21.27.

HRMS (MALDI-ToF): m/z calculated for $C_{50}H_{54}S_2$: 719.3740 $[M+1H]^+$, 741.3559 $[M+Na]^+$, 763.3379 $[M-H+2Na]^+$; found: 719.3753 $[M+1H]^+$, 741.3558 $[M+Na]^+$, 763.3387 $[M-H+2Na]^+$.

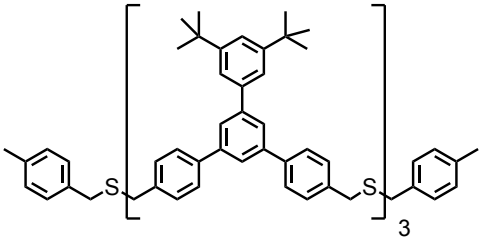

Ter3

$C_{118}H_{126}S_4$
1672.55 g/mol

Trimer Ter3: For the final "end-capping oligomerization" reaction, compound **21** (233 mg, 360 μmol) and **22** (393 mg, 720 μmol) were dissolved in freshly distilled and degassed THF (20 ml) and the reaction mixture was degassed with argon for 20 minutes. The oligomerization was initiated by addition of sodium hydride (154 mg, 3.85 mmol) and let react for 15 minutes at room temperature, after which 4-methylbenzyl bromide (294 mg, 1.54 mmol) was added. After 15 hours, the reaction mixture was quenched by addition of water, extracted with MTBE and dried over $MgSO_4$. The volatile was removed *in vacuo* and the crude product was subjected to a short column chromatography eluting with *c*-hexane/EtOAc (1:1) and then purified on automated recyclable gel permeation chromatography (GPC) obtaining monomer **Ter3** as a colorless oil (76.4 mg, 12 %).

^{1}H NMR (400 MHz, Chloroform-*d*): δ 7.80 – 7.74 (m, 10H), 7.72 – 7.63 (m, 12H), 7.49 (p, *J* = 1.7 Hz, 8H), 7.45 (d, *J* = 8.1 Hz, 8H), 7.40 (d, *J* = 8.2 Hz, 4H), 7.21 (d, *J* = 8.0 Hz, 4H), 7.13 (d, *J* = 7.6 Hz, 4H), 3.73 (s, 8H), 3.65 (s, 4H), 3.63 (s, 4H), 2.34 (s, 6H), 1.40 (s, 54H).

^{13}C NMR (101 MHz, Chloroform-*d*): δ 151.43, 143.98, 140.83, 140.20, 140.07, 137.64, 129.69, 129.34, 129.06, 128.12, 127.67, 127.59, 125.62, 124.89, 122.03, 121.88, 35.57, 35.41, 35.18, 31.72, 29.86

MS (MALDI-ToF, positive): *m*/*z* 1695.11 $[M+Na]^+$.

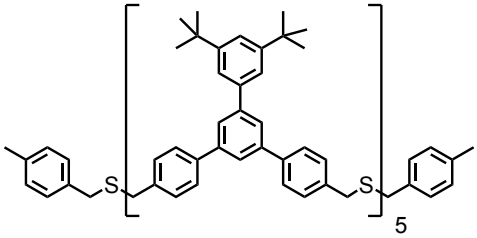

Ter5

$C_{186}H_{198}S_6$
2625.99 g/mol

Pentamer Ter5: For the final "end-capping oligomerization" reaction, compound **21** (233 mg, 360 μmol) and **22** (393 mg, 720 μmol) were dissolved in freshly distilled and degassed THF (20 ml) and the reaction mixture was degassed with argon for 20 minutes. The oligomerization was initiated by addition of sodium hydride (154 mg, 3.85 mmol) and let react for 15 minutes at room temperature, after which 4-methylbenzyl bromide (294 mg, 1.54 mmol) was added. After 15 hours, the reaction mixture was quenched by addition of water, extracted with MTBE and dried over $MgSO_4$. The volatile was removed *in vacuo* and the crude product was subjected to a short column chromatography eluting with *c*-hexane/EtOAc (1:1) and then purified on automated recyclable gel permeation chromatography (GPC) obtaining monomer **Ter5** as a colorless oil (15.4 mg, 3 %).

^{1}H NMR (400 MHz, Chloroform-*d*): δ 7.83 – 7.76 (m, 16H), 7.72 – 7.65 (m, 20H), 7.53 – 7.45 (m, 24H), 7.41 (d, *J* = 8.2 Hz, 4H), 7.22 (d, *J* = 8.0 Hz, 4H), 7.15 (d, *J* = 7.9 Hz, 4H), 3.74 (s, 16H), 3.67 (s, 4H), 3.64 (s, 4H), 2.35 (s, 6H), 1.41 (s, 90H).

^{13}C NMR (101 MHz, Chloroform-*d*) δ 151.42, 143.99, 141.96, 140.82, 140.20, 137.64, 129.69, 129.33, 129.06, 128.20, 127.67, 127.59, 125.62, 124.89, 122.03, 121.88, 77.48, 35.56, 35.41, 35.18, 31.72, 29.87.

HRMS (MALDI-ToF): *m/z* calculated for $C_{186}H_{198}S_6$: 2646.3710 $[M+Na]^+$; found: 2646.3728 $[M+Na]^+$.

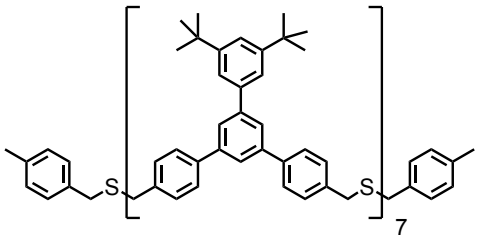

Ter7

$C_{254}H_{270}S_8$
3579.43 g/mol

Heptamer Ter7: For the final "end-capping oligomerization" reaction, compound **21** (233 mg, 360 μmol) and **22** (393 mg, 720 μmol) were dissolved in freshly distilled and degassed THF (20 ml) and the reaction mixture was degassed with argon for 20 minutes. The oligomerization was initiated by addition of sodium hydride (154 mg, 3.85 mmol) and let react for 15 minutes at room temperature, after which 4-methylbenzyl bromide (294 mg, 1.54 mmol) was added. After 15 hours, the reaction mixture was quenched by addition of water, extracted with MTBE and dried over $MgSO_4$. The volatile was removed *in vacuo* and the crude product was subjected to a short column chromatography eluting with *c*-hexane/EtOAc (1:1) and then purified on automated recyclable gel permeation chromatography (GPC) obtaining monomer **Ter7** as a colorless oil (10.8 mg, 2 %).

or; for heptamer **Ter7** optimized ratio of dibromine- **21** and dithiol-derivative **22**:

Heptamer Ter7: For the final "end-capping oligomerization" reaction, compound **23** (18.6 mg, 30.7 μmol) and **25** (19.6 mg, 38.4 μmol) were dissolved in freshly distilled and degassed THF (20 ml) and the reaction mixture was degassed with argon for 20 minutes. The oligomerization was initiated by addition of sodium hydride (12.3 mg, 123 μmol) and let react for 15 minutes at room temperature, after which 4-methylbenzyl bromide (294 mg, 1.54 mmol) was added. After 15 hours, the reaction mixture was quenched by addition of water, extracted with MTBE and dried over $MgSO_4$. The volatile was removed *in vacuo* and the crude product was subjected to a short column chromatography eluting with *c*-hexane/EtOAc (1:1) and then purified on automated recyclable gel permeation chromatography (GPC) obtaining monomer **Ter7** as a colorless oil (2.8 mg, 8 %).

^{1}H NMR (400 MHz, Chloroform-*d*): δ 7.78 – 7.74 (m, 22H), 7.70 – 7.66 (m, 24H), 7.50 – 7.48 (m, 26H), 7.45 (d, *J* = 8.2 Hz, 26H), 3.72 (s, 24H), 3.65 (s, 4H), 3.62 (s, 4H), 2.34 (s, 6H), 1.40 (s, 126H).

^{13}C NMR (101 MHz, Chloroform-*d*): δ 151.28, 143.84, 141.81, 140.68, 140.05, 137.50, 129.55, 129.51, 129.19, 128.91, 127.52, 127.45, 125.48, 124.75, 121.88, 121.74, 35.41, 35.38, 35.26, 35.03, 31.57.

HRMS (MALDI-ToF): *m/z* calculated for $C_{254}H_{270}S_8$: 3598.8785 $[M+Na]^+$, 3614.8525 $[M+K]^+$; found: 3598.8740 $[M+Na]^+$, 3614.8480 $[M+K]^+$.

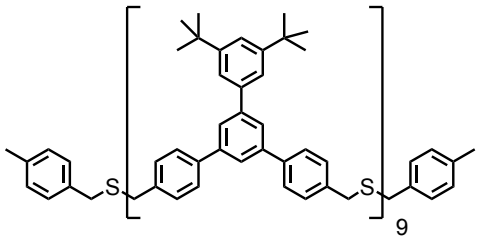

Ter9

$C_{322}H_{342}S_{10}$
4532.88 g/mol

Nonamer Ter9: For the final "end-capping oligomerization" reaction, compound **21** (233 mg, 360 μmol) and **22** (393 mg, 720 μmol) were dissolved in freshly distilled and degassed THF (20 ml) and the reaction mixture was degassed with argon for 20 minutes. The oligomerization was initiated by addition of sodium hydride (154 mg, 3.85 mmol) and let react for 15 minutes at room temperature, after which 4-methylbenzyl bromide (294 mg, 1.54 mmol) was added. After 15 hours, the reaction mixture was quenched by addition of water, extracted with MTBE and dried over $MgSO_4$. The volatile was removed *in vacuo* and the crude product was subjected to a short column chromatography eluting with *c*-hexane/EtOAc (1:1) and then purified on automated recyclable gel permeation chromatography (GPC) obtaining monomer **Ter9** as a colorless oil (4.4 mg, 1 %).

^{1}H NMR (400 MHz, Chloroform-*d*): δ 7.81 – 7.72 (m, 27H), 7.72 – 7.61 (m, 35H), 7.51 – 7.37 (m, 64H), 7.21 (d, *J* = 8.0 Hz, 4H), 7.13 (d, *J* = 7.9 Hz, 4H), 3.72 (s, 32H), 3.65 (s, 4H), 3.62 (s, 4H), 2.34 (s, 6H), 1.39 (s, 162H).

MS (MALDI-ToF, positive): broad peak *m*/*z* 4554 $[M+Na]^+$.

7.2.4 Tetraphenylmethane **TPM**-Ligands

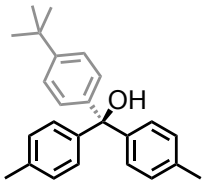

29

$C_{25}H_{28}O$
344.50 g/mol

Bis(*p*-tolyl)-(4-(*tert*-butyl)phenyl)methanol (29):[185] In a dry degassed 500 ml two-necked flask equipped with rubber septum, reflux condenser and addition funnel, Mg turnings (1.58 g, 65.0 mmol) were suspended in dry degassed THF (20 ml) under argon atmosphere. 4-Bromtoluene (11.1 g, 65 mmol) dissolved dry degassed THF (20 ml) were added dropwise to the reaction mixture. In order to activate the Grignard reagent, one pellet of iodine was added to the mixture, which was subsequently stirred for 3 hours. Methyl *p*-toluate (4.72 ml, 26.0 mmol) dissolved in dry degassed THF (20 ml) and was added to the mixture, which was then refluxed for 24 hours. After cooling to room temperature, the reaction mixture was quenched with saturated aqueous NH_4Cl solution. The aqueous phase was washed with MTBE. The combined organic phases were washed twice with water, dried over magnesium sulfate and the solvent was evaporated *in vacuo*. The crude product was subjected to column chromatography eluting with *c*-hexane/DCM (5:1) to obtain compound **29** as a white solid (7.29 g, 81 %).

^{1}H NMR (400 MHz, Chloroform-d): δ 7.30 (m, 2H), 7.19 – 7.14 (m, 6H), 7.12 – 7.07 (m, 4H), 2.70 (s, 1H), 2.33 (s, 6H), 1.30 (s, 9H).

^{13}C NMR (101 MHz, Chloroform-d): δ 149.92, 144.42, 144.24, 136.69, 128.58, 127.88, 127.63, 124.81, 81.64, 34.50, 31.43, 21.11.

GC-MS (EI, 70 eV): *m*/*z* (%) = 344.1 (12), 327.1 (29), 326.1 (70), 312.1 (14), 311.1 (34), 254.1 (15), 253.1 (72), 224.1 (21), 211.0 (30), 182.1 (15), 161.1 (27), 134.1 (14), 119.1 (100), 91.0 (32), 57.1 (34).

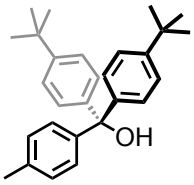

30

$C_{28}H_{34}O$
386.58 g/mol

Bis(4-(*tert*-butyl)phenyl)(*p*-tolyl)methanol (30): In a dry degassed 500 ml two-necked flask equipped with rubber septum, reflux condenser and addition funnel, magnesium turnings (4.00 g, 167 mmol) were suspended in 100 ml dry degassed THF under argon atmosphere. 1-Bromo-4-tert-butylbenzene (29.1 ml, 167 mmol) dissolved in 100 ml dry, degassed THF was added dropwise. In order to activate the *Grignard* reagent, one pellet of iodine was added to the mixture which was subsequently stirred for 3 hours. Methyl *p*-toluate (10.0 g, 66.7 mmol) was dissolved in 100 ml dry, degassed THF and was added to the mixture which was then refluxed for 22 hours. After cooling to room temperature, saturated aqueous ammonium chloride and water were added and the aqueous phase was extracted with MTBE. The combined organic phases were washed twice with water, dried over magnesium sulfate, filtrated and the solvent was evaporated. The crude product was subjected to column chromatography eluting with *c*-hexane/DCM (1:1) to obtain compound **30** as a white solid (22.5 g, 87 %).

^{1}H NMR (400 MHz, Chloroform-*d*): δ 7.34 – 7.27 (m, 4H), 7.22 – 7.14 (m, 6H), 7.14 – 7.07 (m, 2H), 2.69 (s, 1H), 2.34 (s, 3H), 1.31 (s, 18H).

^{13}C NMR (101 MHz, Chloroform-*d*): δ 149.87, 144.33, 144.16, 136.62, 128.49, 127.76, 127.53, 124.74, 81.54, 34.45, 31.36, 21.05.

EA: found: C 87.11 %, H 9.20 %; required: C 87.00 %, H 8.87 %.

GC-MS (EI, 70 eV): *m*/*z* (%) = 57.1 (100), 91.1 (31), 105.1 (17), 118.1 (18), 119.1 (74), 141.2 (20), 146.1 (10), 161.1 (69), 178.1 (27), 209.1 (10), 224.1 (25), 237.1 (24), 252.1 (14), 253.2 (85), 254.1 (18), 266.2 (11), 279.2 (11), 295.2 (52), 296.2 (13), 339.15 (13), 353.2 (24), 354.2 (42), 355.2 (14), 368.25 (50), 369.25 (49), 370.2 (16), 386.2 (18).

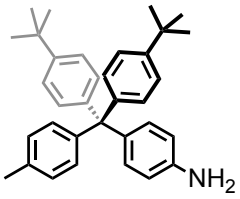

31

$C_{34}H_{39}N$
461.69 g/mol

4-(Bis(4-(*tert*-butyl)phenyl)(*p*-tolyl)methyl)aniline (31):[141] To a solution of freshly distilled aniline (22.7 ml, 249 mmol) and conc. HCl (21 ml) in 150 ml glacial acetic acid in a 500 ml two-necked flask, precursor **30** (20.1 g, 52.3 mmol) was gradually added. The reaction mixture was refluxed and stirred at 140 °C for 15 hours. After cooling to room temperature, the acetic acid was evaporated by distillation. The solid was dissolved in DCM, washed with water, dried over magnesium sulfate, filtrated and the solvent evaporated. The crude product was subjected to column chromatography eluting with *c*-hexane/ EtOAc (5:1 and 1 % Et_3N) to afford compound **31** as a white solid (17.0 g, 71 %).

^{1}H NMR (400 MHz, Chloroform-*d*): δ 7.21 (d, *J* = 8.7 Hz, 4H), 7.12 – 7.06 (m, 6H), 7.04 – 7.00 (m, 2H), 6.96 (d, *J* = 8.6 Hz, 2H), 6.56 (d, *J* = 8.6 Hz, 2H), 3.58 (s, 2H), 2.31 (s, 3H), 1.29 (s, 18H).

^{13}C NMR (101 MHz, Chloroform-*d*): δ 148.89, 147.98, 144.17, 143.68, 134.78, 131.88, 130.87, 130.48, 127.71, 123.86, 113.86, 90.21, 63.12, 34.11, 31.22, 20.76.

EA: found: C 88.38 %, H 8.76 %, N 2.93 %; required: C 88.45 %, H 8.51 %, N 3.03 %.

MS (MALDI-ToF, positive): *m/z* 361.30.

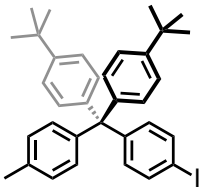

32

$C_{34}H_{37}I$
572.57 g/mol

4,4'-((4-Iodophenyl)(*p*-tolyl)methylene)bis(*tert*-butylbenzene) (32): To a dry, degassed 1000 ml three-necked flask equipped with thermometer and rubber septa, boron trifluoride diethyl etherate (8.23 ml, 65.0 mmol) was added and the flask was cooled to -10 °C. Compound **31** (15.0 g, 32.5 mmol) dissolved in 200 ml dry, degassed DCM was added dropwise. *tert*- Butyl nitrite (7.58 ml, 56.9 mmol) was dissolved in 200 ml dry, degassed THF and added dropwise. The mixture was allowed to stir for 3 hours. Potassium iodide (8.00 g, 48.7 mmol) and iodine (10.9 g, 42.2 mmol) were added to the mixture. The reaction mixture was allowed to gradually warm up to room temperature and was stirred for 15 hours and then quenched with saturated aqueous sodium thiosulfate solution. A pale solid precipitated which was filtrated over hyflo, and redissolved in DCM. The organic phase was washed three times with water, dried over magnesium sulfate, filtrated and the solvent was removed *in vacuo*. The crude product was subjected to column chromatography (*c*-hexane) to afford compound **32** as a pale yellow solid (15.7 g, 84 %).

^{1}H NMR (400 MHz, Chloroform-*d*): δ 7.60 – 7.51 (m, 2H), 7.25 – 7.20 (m, 4H), 7.12 – 7.03 (m, 8H), 7.00 – 6.93 (m, 2H), 2.31 (s, 3H), 1.29 (s, 18H).

^{13}C NMR (101 MHz, Chloroform-*d*): δ 148.60, 147.34, 143.68, 143.38, 136.35, 135.41, 133.28, 130.93, 130.58, 128.16, 124.32, 91.50, 63.58, 34.34, 31.39, 20.96.

EA: found: C 71.42 %, H 6.52 %; required: C 71.32 %, H 6.51 %.

MS (MALDI-ToF, positive): *m/z* 572.43.

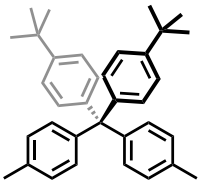

33

$C_{35}H_{40}$
460.71 g/mol

Bis(4-(*tert*-butyl)phenyl)di-*p*-tolylmethane (33): Under inert atmosphere, precursor **32** (16.0 g, 27.9 mmol) was dissolved in dry and degassed THF (250 ml). The solution was cooled to -60 °C and methyl lithium (1.6 M solution in hexane, 52.3 ml, 83.8 mmol) was added dropwise. The mixture was allowed to slowly warm up to room temperature and was stirred for 15 hours. The reaction mixture was quenched upon addition of water, extracted three times with DCM and dried over magnesium sulfate. After filtration, the volatile was evaporated by rotavapor to afford precursor **33** as a white solid (12.6 g, quant.).

^{1}H NMR (400 MHz, Chloroform-*d*): δ 7.24 – 7.20 (m, 4H), 7.11 – 7.06 (m, 8H), 7.03 (d, *J* = 8.2 Hz, 4H), 2.31 (s, 6H), 1.29 (s, 18H).

^{13}C NMR (101 MHz, Chloroform-*d*): δ 148.24, 144.39, 144.05, 135.05, 131.05, 130.67, 127.94, 124.09, 63.45, 34.29, 31.38, 20.93.

EA: found: C 91.07 %, H 8.59 %; required: C 91.25 %, H 8.75 %.

GC-MS (EI, 70 eV): *m*/*z* (%) = 461.2 (10), 460.25 (30), 403.2 (17), 370.2 (33), 369.2 (87), 328.15 (25), 327.15 (100), 297.1 (10), 215.1 (23), 207.11 (10), 57.1 (44).

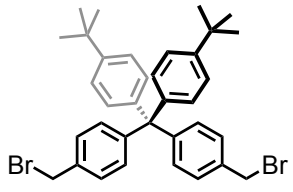

34

$C_{35}H_{38}Br_2$
618.50 g/mol

Bis(4-(bromomethyl)phenyl)bis(4-(*tert*-butyl)phenyl)methane (34): In a dry, degassed 500 ml two-necked flask equipped with a reflux condenser and a glass stopper, compound **33** (5.00 g, 10.9 mmol), *N*-bromosuccinimide (7.80 g, 43.4 mmol) and catalytic amounts of azobisisobutyronitrile (180 mg) were suspended in methyl formate (150 ml) under inert atmosphere. The reaction was activated by illumination with a 500 W halogen lamp and refluxed for 15 hours, then cooled to room temperature. The solvent was evaporated, and the residue dissolved in DCM. The mixture was washed four times with water and dried over magnesium sulfate. After filtration, the volatile was evaporated and the crude product subjected to column chromatography eluting with *c*-hexane/DCM (20:1) to afford bromine-precursor **34** as a white solid (4.00 g, 60 %).

^{1}H NMR (400 MHz, Chloroform-*d*): δ 7.27 (d, *J* = 1.8 Hz, 2H), 7.26 – 7.23 (m, 6H), 7.20 – 7.16 (m, 4H), 7.09 – 7.06 (m, 4H), 4.48 (s, 4H), 1.30 (s, 18H).

^{13}C NMR (101 MHz, Chloroform-*d*): δ 148.73, 147.35, 143.15, 135.16, 131.49, 130.60, 128.12, 124.40, 63.86, 34.35, 33.47, 31.38.

EA: found: C 67.82 %, H 6.51 %; required: C 67.97 %, H 6.19 %.

MS (MALDI-ToF, positive): *m*/*z* 618.15.

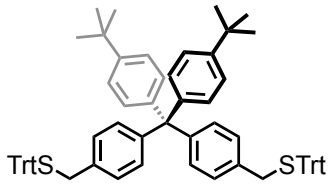

35

$C_{73}H_{68}S_2$
1009.47 g/mol

Bis(4-(*tert*-butyl)phenyl)bis(4-((tritylthio)methyl)phenyl)methane (35): Compound **34** (1.29 g, 2.09 mmol) and trityl thiol (1.49 g, 5.23 mmol) were dissolved in dry degassed THF (30 ml) under an atmosphere of argon. Sodium hydride (60 % in mineral oil, 836 mg, 20.9 mmol) was added and the mixture was stirred at room temperature for 15 hours. The reaction was quenched with water and extracted with MTBE. The combined organic fractions were washed with brine, dried over magnesium sulfate, filtered and evaporated to dryness. After purification by flash column chromatography eluting with *c*-hexane/DCM (3:2) compound **35** was obtained as colorless foam (2.02 g, 92 %).

^{1}H NMR (400 MHz, Chloroform-*d*): δ 7.48 – 7.43 (m, 5H), 7.30 (s, 4H), 7.26 (d, *J* = 1.7 Hz, 6H), 7.24 – 7.18 (m, 7H), 7.15 (d, *J* = 8.4 Hz, 2H), 7.08 - 7.04 (m, 5H), 7.00 (d, *J* = 8.3 Hz, 2H), 3.28 (s, 4H), 1.29 (s, 18H).

^{13}C NMR (101 MHz, Chloroform-*d*): δ 148.47, 146.07, 144.82, 143.74, 134.38, 131.28, 130.72, 129.79, 129.75, 128.19, 128.04, 126.79, 124.31, 67.51, 63.76, 36.74, 34.41, 31.50, 27.05.

MS (MALDI-ToF, positive): *m/z* 1010.21.

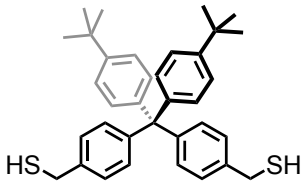

36

$C_{35}H_{40}S_2$
524.83 g/mol

((Bis(4-(*tert*-butyl)phenyl)methylene)bis(4,1-phenylene))dimethanethiol (36): The trityl-protected compound **35** (2.33 g, 2.31 mmol) was dissolved in DCM (15 ml) and triethylsilane (1.12 ml, 6.93 mmol) was added, followed by trifluoroacetic acid (1.20 ml, 4 % of the DCM volume). The reaction mixture immediately turned yellow and decolorized after approximately 2 minutes. After additional 10 minutes the reaction was quenched with saturated aqueous sodium hydrogen carbonate solution. The two phases were separated and the aqueous phase was washed with DCM. The combined organic fractions were dried over magnesium sulfate, filtered and evaporated to dryness. After purification by flash column chromatography eluting with *c*-hexane/DCM (2:1) compound **36** was obtained as a white solid (1.18 g, quant.).

or:

A solution of compound **34** (500 mg, 1.06 mmol) and thiourea (814 mg, 10.6 mmol) in 7 ml dry dimethyl sulfoxide under an atmosphere of argon was left stirring for 15 hours at 40 °C. DCM (20 ml) was added and the mixture was allowed to stir for 10 min until a white solid precipitated. The solid was filtrated, washed with additional DCM and dried *in vacuo*. The white solid was then redissolved in methanol (10 ml) and the solution was degassed with argon. An ice cold, degassed aqueous solution of sodium hydroxide (1 M, 20 ml) was added to the reaction mixture which was then acidified with an aqueous solution of hydrochloric acid (1 M, 30 ml). The mixture was extracted with DCM and the combined organic fractions were washed once with water. The organic phase was dried over magnesium sulfate, filtrated and evaporated to dryness. If needed, the product was purified by column chromatography (DCM 2:1 *c*-hexane) to obtain thiol-precursor **36** as a white solid (205-374 mg, 51-93 %).

^{1}H NMR (400 MHz, Chloroform-*d*): δ 7.25 – 7.21 (m, 4H), 7.21 – 7.11 (m, 8H), 7.11 - 7.04 (m, 4H), 3.72 (d, J = 7.5 Hz, 4H), 1.77 (t, J = 7.5 Hz, 2H), 1.30 (s, 18H).

^{13}C NMR (101 MHz, Chloroform-*d*): δ 148.53, 145.99, 143.56, 138.37, 131.42, 130.65, 126.97, 124.25, 63.66, 34.32, 31.38, 28.54.

HRMS (ESI-ToF, negative): *m/z* calculated for $C_{35}H_{40}S_2$: 523.2501 $[M-1H]^-$; found: 523.2501 $[M-1H]^-$.

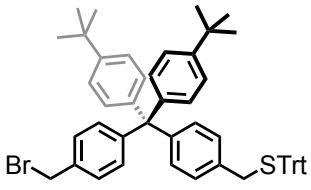

37

$C_{54}H_{53}BrS$
813.98 g/mol

(4-((4-(Bromomethyl)phenyl)bis(4-(*tert*-butyl)phenyl)methyl)benzyl)(trityl)sulfane (37): Compound **34** (100 mg, 16.2 mmol) was dissolved in dry THF (5 ml) in a 10 ml Schlenk-tube. Trityl thiol (27.6 mg, 97.0 µmol) was added to the solution, which was then degassed for 30 minutes with argon. Sodium hydride (60 % dispersion in mineral oil, 10.9 mg, 324 µmol) was added to the flask. The mixture was stirred at room temperature for 15 hours, and then quenched by addition of water, extracted with MTBE, washed twice with water, dried over magnesium sulfate, filtrated and the solvent was removed *in vacuo*. The crude product was subjected to column chromatography eluting with *c*-hexane/DCM (2:1) to afford compound **37** as a white solid (37.9 mg, 48 %).

^{1}H NMR (400 MHz, Chloroform-*d*): δ 7.48 – 7.43 (m, 5H), 7.30 (s, 4H), 7.26 (d, *J* = 1.7 Hz, 6H), 7.24 – 7.18 (m, 7H), 7.15 (d, *J* = 8.4 Hz, 2H), 7.08 – 7.04 (m, 5H), 7.00 (d, *J* = 8.3 Hz, 2H), 4.47 (s, 2H), 3.28 (s, 2H), 1.29 (s, 18H).

^{13}C NMR (101 MHz, Chloroform-*d*): δ 148.89, 147.94, 146.06, 145.03, 143.71, 135.32, 134.78, 131.83, 131.50, 130.94, 129.98, 128.50, 128.37, 128.27, 127.03, 124.62, 67.76, 64.09, 36.96, 34.66, 33.89, 31.71.

EA: found: C 79.91 %, H 6.83 %; required: C 79.68 %, H 6.56 %.

MS (MALDI-ToF, positive): *m/z* 837.4 $[M+Na]^+$.

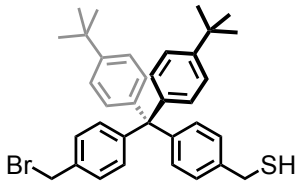

38

$C_{35}H_{39}BrS$
571.66 g/mol

(4-((4-(Bromomethyl)phenyl)bis(4-(*tert*-butyl)phenyl)methyl)phenyl)methanethiol (38):
The trityl-protected compound **37** (30.0 mg, 36.9 μmol) was dissolved in DCM (3 ml) and triethylsilane (8.93 μl, 55.4 μmol) was added, followed by trifluoroacetic acid (120 μl, 4 % of the DCM volume). The reaction mixture immediately turned yellow and decolorized after approximately 1 minutes. After additional 10 minutes the reaction was quenched with saturated aqueous sodium hydrogen carbonate solution. The two phases were separated and the aqueous phase was washed with DCM. The combined organic fractions were dried over magnesium sulfate, filtered and evaporated to dryness. After purification by flash column chromatography eluting with *c*-hexane/DCM (2:1) compound **38** was obtained as a white solid (20.9 mg, quant.).

^{1}H NMR (400 MHz, Chloroform-*d*): δ 7.27 – 7.22 (m, 6H), 7.20 – 7.12 (m, 6H), 7.10 – 7.06 (m, 4H), 4.48 (s, 2H), 3.72 (d, *J* = 7.5 Hz, 2H), 1.77 (t, *J* = 7.5 Hz, 1H), 1.30 (s, 18H).

MS (MALDI-ToF, negative): *m*/*z* 569.33 $[M-H]^-$.

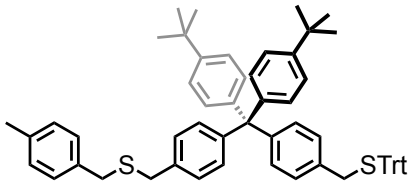

39

$C_{62}H_{62}S_2$
871.29 g/mol

(4-(Bis(4-(*tert*-butyl)phenyl)(4-(((4-methylbenzyl)thio)methyl)phenyl)methyl)benzyl)-(trityl)sulfane (39): To a dry, degassed 25 ml one-necked flask, compound **37** (35 mg, 43 µmol) was added and dissolved in dry THF (2 ml). *p*-Tolylmercaptane (8.8 µl, 65 µmol) was added to the solution which was then degassed for 15 minutes with argon. NaH (60 % dispersed in mineral oil, 8.60 mg, 215 µmol) was added to the reaction mixture. The mixture was stirred at room temperature for 2 hours, and then quenched by addition of water, extracted with MTBE, dried over $MgSO_4$ and the solvent was removed *in vacuo*. The crude product was subjected to column chromatography eluting with *c*-hexane/DCM (10:1) to afford compound **39** as a pale, yellowish solid (35.0 mg, 93 %).

^{1}H NMR (400 MHz, Chloroform-*d*): δ = 7.48 – 7.42 (m, 6H), 7.30 – 6.98 (m, 29H), 3.56 (d, *J* = 10.5 Hz, 4H), 3.28 (s, 2H), 2.31 (s, 3H), 1.29 (s, 18H).

^{13}C NMR (101 MHz, Chloroform-*d*): δ 148.45, 146.00, 145.85, 144.73, 143.66, 136.55, 135.52, 135.13, 134.33, 131.24, 130.67, 129.66, 129.16, 128.91, 128.10, 127.94, 126.70, 124.21, 67.42, 63.69, 36.66, 35.49, 35.23, 34.33, 31.40, 29.74, 21.14.

HRMS (ESI-ToF): *m/z* calculated for $C_{62}H_{62}S_2$: 888.4637 $[M+NH_4]^+$, 893.4191 $[M+Na]^+$, 909.3930 $[M+K]^+$; found: 888.4631 $[M+NH_4]^+$, 893.4185 $[M+Na]^+$, 909.3925 $[M+K]^+$.

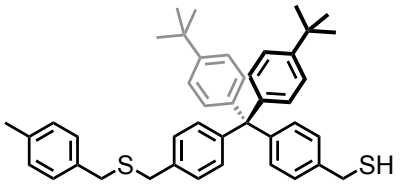

40

$C_{43}H_{48}S_2$
628.97 g/mol

(4-(Bis(4-(*tert*-butyl)phenyl)(4-(((4-methylbenzyl)thio)methyl)phenyl)methyl)phenyl)-methanethiol (40): In a 25 ml one-necked flask, compound **39** (91.0 mg, 104 µmol) was dissolved in DCM (5 ml). After addition of triethylsilane (151 µl, 936 µmol), the solution was degassed with argon for 20 minutes after which trifluoroacetic acid (200 µl, 4 % of DCM volume) was added to the mixture. An immediate color change to yellow, lasting for 30 seconds was observed. The mixture was stirred 1 hour at room temperature. The reaction was quenched by addition of saturated aqueous sodium bicarbonate solution. The aqueous phase was extracted three times with DCM, dried over Na_2SO_4 and the solvent was removed in vacuo. The crude product was subjected to column chromatography eluting with *c*-hexane/DCM (10:1) to afford compound **40** as a colorless oil (65.6 mg, quant.).

^{1}H NMR (400 MHz, Chloroform-*d*): δ 7.25 – 7.07 (m, 21H), 3.70 (d, *J* = 7.5 Hz, 2H), 3.57 (s, 2H), 3.55 (s, 2H), 2.31 (s, 3H), 1.75 (t, *J* = 7.5 Hz, 1H), 1.30 (s, 18H).

^{13}C NMR (101 MHz, Chloroform-*d*): δ 148.54, 146.06, 145.84, 143.65, 138.40, 136.57, 135.62, 135.14, 131.47, 131.28, 130.72, 129.18, 128.93, 127.98, 127.00, 124.27, 63.72, 35.54, 35.26, 34.36, 31.43, 28.58, 21.17.

HRMS (ESI-ToF): *m/z* calculated for $C_{43}H_{48}S_2$: 646.3541 $[M+NH_4]^+$, 651.3095 $[M+Na]^+$, found: 646.3536 $[M+NH_4]^+$, 651.3090 $[M+Na]^+$.

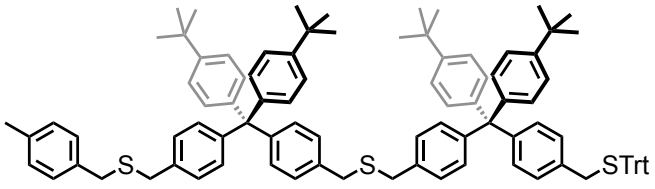

41

$C_{97}H_{100}S_3$
1362.04 g/mol

(4-(Bis(4-(*tert*-butyl)phenyl)(4-(((4-methylbenzyl)thio)methyl)phenyl)methyl)benzyl)(4-(bis(4-(*tert*-butyl)phenyl)(4-((tritylthio)methyl)phenyl)methyl)benzyl)sulfane (41): In a dry, degassed 25 ml one-necked flask, compound **39** (73.2 mg, 119 µmol) and **37** (107 mg, 131 µmol) were dissolved in dry THF (5 ml), and degassed with argon for 15 minutes. NaH (60 % dispersion in mineral oil, 23.8 mg, 595 µmol) was added to the mixture which was then stirred for 2 hours at room temperature, and then quenched by addition of water. The mixture was extracted with MTBE, dried over Na_2SO_4 and the solvent was removed *in vacuo*. The crude product was subjected to column chromatography eluting with *c*-hexane/DCM (10:1) to afford compound **41** as a pale solid (136 mg, 85 %).

^{1}H NMR (400 MHz, Chloroform-*d*): δ 7.48 – 7.43 (m, 6H), 7.30 – 7.17 (m, 16H), 7.16 – 7.04 (m, 27H), 7.02 – 6.98 (m, 2H), 3.61 – 3.55 (m, 8H), 3.27 (s, 2H), 2.31 (s, 3H), 1.29 (s, 18H), 1.28 (s, 18H).

^{13}C NMR (101 MHz, Chloroform-*d*): δ 148.49, 148.42, 145.96, 145.92, 145.90, 145.84, 144.70, 143.65, 143.62, 136.54, 135.55, 135.43, 135.36, 135.10, 134.30, 131.28, 131.25, 131.19, 130.68, 130.63, 129.68, 129.63, 129.14, 128.88, 128.40, 128.08, 127.92, 127.77, 127.72, 126.67, 124.21, 124.19, 67.39, 63.70, 63.66, 35.49, 35.37, 35.23, 34.32, 34.30, 34.28, 31.38, 31.37, 21.12.

HRMS (ESI-ToF): *m/z* calculated for $C_{97}H_{100}S_3$: 1384.6963 $[M+H/Na]^+$, 1400.6702 $[M+H/K]^+$; found: 1384.6912 $[M+H/Na]^+$, 1400.6652 $[M+H/K]^+$.

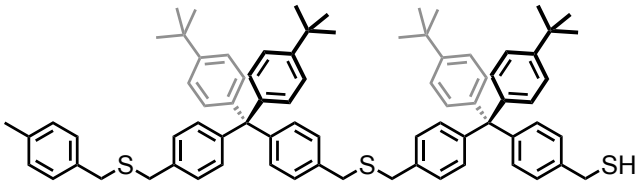

42

$C_{78}H_{86}S_3$
1119.72 g/mol

(4-((4-(((4-(Bis(4-(*tert*-butyl)phenyl)(4-(((4-methylbenzyl)thio)methyl)phenyl)methyl)-benzyl)thio)methyl)phenyl)bis(4-(*tert*-butyl)phenyl)methyl)phenyl)methanethiol (42): To a solution of compound **41** (117 mg, 86 μmol) in DCM (5 ml) in a 25 ml one-neck flask, triethylsilane (41.6 μl, 258 μmol) was added. After degassing the solution with argon for 15 minutes, trifluoroacetic acid (200 μl, 4 % of DCM volume) was added upon which a brief color to bright yellow was observed. The reaction mixture was allowed to stir at room temperature for 1 hour, and was thereafter quenched by addition of saturated aqueous sodium bicarbonate solution. The aqueous phase was extracted with DCM, dried over Na_2SO_4 and the solvent was removed *in vacuo*. The crude product was subjected to column chromatography eluting with *c*-hexane/DCM (10:1) to afford compound **42** as a pale solid (86 mg, 89 %).

^{1}H NMR (400 MHz, Chloroform-*d*): δ 7.25 – 7.07 (m, 21H), 3.70 (d, *J* = 7.5 Hz, 2H), 3.57 (d, *J* = 9.8 Hz, 4H), 2.31 (s, 3H), 1.75 (t, *J* = 7.5 Hz, 1H), 1.30 (s, 18H).

^{13}C NMR (101 MHz, Chloroform-*d*): δ 148.54, 146.06, 145.84, 143.65, 138.40, 136.57, 135.62, 135.14, 131.47, 131.28, 130.72, 129.18, 128.93, 127.98, 127.00, 124.27, 63.72, 35.54, 35.26, 34.36, 31.43, 28.58, 21.17.

HRMS (ESI-ToF): *m/z* calculated for $C_{78}H_{86}S_3$: 1119.5970 $[M+H]^+$, 1136.6235 $[M+NH_4]^+$, 1141.5789 $[M+Na]^+$, 1157.5529 $[M+K]^+$; found: 1119.5964 $[M+H]^+$, 1136.6230 $[M+NH_4]^+$, 1141.5784 $[M+Na]^+$, 1157.5523 $[M+K]^+$.

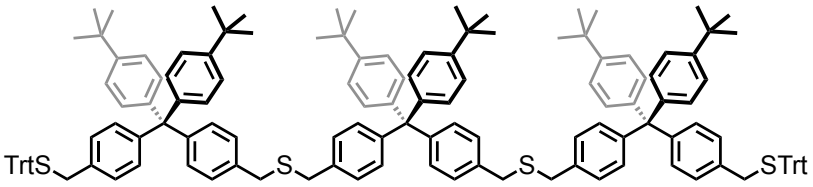

43

$C_{143}H_{144}S_4$
1990.97 g/mol

Trimer-STrt (43): Compound **37** (171 mg, 210 µmol) and thiol-precursor **36** (50 mg, 95.0 µmol) were dissolved in dry THF (10 ml) under an atmosphere of argon. Sodium hydride (60 % in mineral oil, 19.1 mg, 477 µmol) was added and the mixture was stirred for 5 hours at room temperature. The reaction was quenched with water and extracted with MTBE (3 x 30 ml). The combined organic fractions were washed with brine, dried over magnesium sulfate, filtrated and evaporated to dryness. Purification of the crude product was achieved by column chromatography eluting with *c*-hexane/DCM (3:2) to yield the trityl-protected trimer **43** as a colorless foam (166.4 mg, 88 %).

^{1}H NMR (400 MHz, Chloroform-*d*): δ 7.47 – 7.43 (m, 12H), 7.31 – 7.24 (m, 10H), 7.20 (m, *J* = 7.2, 19H), 7.14 – 7.10 (m, 16H), 7.09 – 7.03 (m, 17H), 6.99 (d, *J* = 8.5 Hz, 4H), 3.58 (d, *J* = 1.6 Hz, 8H), 3.27 (s, 4H), 1.27 (s, 54H).

^{13}C NMR (101 MHz, Chloroform-*d*): δ 148.43, 145.96, 145.91, 144.72, 143.65, 143.63, 135.44, 135.38, 134.32, 131.27, 131.24, 131.20, 130.67, 130.64, 129.64, 128.08, 127.91, 126.66, 124.20, 67.40, 63.72, 63.68, 36.63, 35.39, 34.30, 31.38.

HRMS (MALDI-ToF): *m/z* calculated for $C_{143}H_{144}S_4$: 2012.0043 $[M+Na]^+$; found: 2012.0049 $[M+Na]^+$.

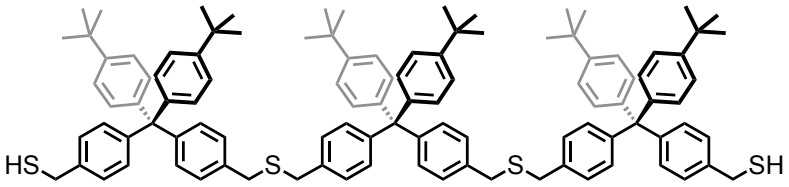

44

$C_{105}H_{116}S_4$
1506.32 g/mol

Trimer-SH (44): The trityl-protected trimer **43** (142 mg, 71.0 µmol) was dissolved in dry DCM (3 ml). Triethylsilane (34.6 µl, 215 µmol) was added, followed by trifluoroacetic acid (120 µl, 4 % of the dichloromethane volume). The mixture turned yellow and became colorless again after 30 seconds. Stirring was continued for further 10 minutes, then the reaction was quenched with a sat. sodium bicarbonate solution. The two phases were separated and the aqueous phase was extracted with DCM. The combined organic fractions were dried over magnesium sulfate, filtrated and evaporated to dryness. The crude was purified by column chromatography eluting with *c*-hexane/DCM (2:1) to give the dithiol trimer **44** as a colorless solid (107.7 mg, quant.).

^{1}H NMR (400 MHz, Chloroform-*d*): δ 7.22 (dd, *J* = 8.7, 1.5 Hz, 12H), 7.19 – 7.12 (m, 24H), 7.09 – 7.05 (m, 12H), 3.70 (d, *J* = 7.5 Hz, 4H), 3.59 (s, 8H), 1.75 (t, *J* = 7.5 Hz, 2H), 1.28 (d, *J* = 1.4 Hz, 54H).

^{13}C NMR (101 MHz, Chloroform-*d*): δ 148.59, 146.02, 143.76, 135.55, 131.53, 131.38, 131.38, 130.78, 128.05, 127.07, 124.33, 63.82, 35.52, 34.43, 31.51, 28.65.

HRMS (MALDI-ToF): *m*/*z* calculated for $C_{105}H_{116}S_4$: 1527.7858 $[M+Na]^+$; found: 1527.7852 $[M+Na]^+$.

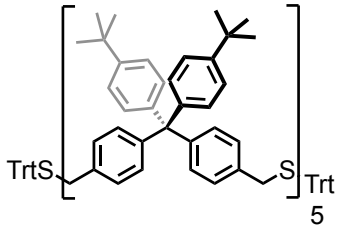

45

$C_{213}H_{220}S_6$
2972.46 g/mol

Pentamer-STrt (45): Compound **37** (118 mg, 145 µmol) and dithiol-trimer **44** (99.3 mg, 66.0 µmol) were dissolved in dry THF (3 ml) under an atmosphere of argon. Sodium hydride (60 % in mineral oil, 13.2 mg, 33.0 µmol) was added and the mixture was stirred for 5 hours at room temperature. The reaction was quenched with water and extracted with MTBE. The combined organic fractions were washed with brine, dried over magnesium sulfate, filtrated and evaporated to dryness. Purification of the crude product was achieved by flash column chromatography eluting with *c*-hexane/DCM (2:1) to yield the trityl-protected pentamer **45** as a colorless foam (163.0 mg, 83 %).

^{1}H NMR (400 MHz, Chloroform-*d*): δ 7.47 – 7.42 (m, 12H), 7.31 – 7.16 (m, 45H), 7.12 – 7.03 (m, 49H), 6.99 (d, *J* = 8.4 Hz, 4H), 3.58 (s, 16H), 3.26 (s, 4H), 1.27 (s, 90H).

^{13}C NMR (101 MHz, Chloroform-*d*): δ 148.48, 148.43, 145.91, 144.72, 143.65, 143.63, 135.45, 135.39, 134.32, 131.28, 131.25, 131.21, 130.68, 130.64, 129.64, 128.10, 127.94, 127.93, 126.68, 124.23, 124.20, 67.40, 63.72, 63.68, 36.64, 35.40, 34.31, 31.39, 26.94.

HRMS (MALDI-ToF): *m/z* calculated for $C_{213}H_{220}S_6$: 2992.5437 $[M+Na]^+$; found: 2992.5404 $[M+Na]^+$.

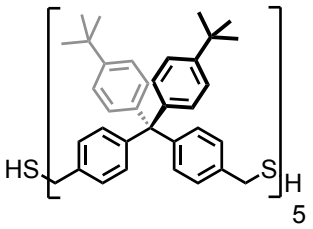

46

$C_{175}H_{192}S_6$
2487.82 g/mol

Pentamer-SH (46): The trityl-protected pentamer **45** (22.7 mg, 45.0 µmol) was dissolved in dry DCM (4 ml). Triethylsilane (22.7 µl, 141 µmol) was added, followed by trifluoroacetic acid (160 µl, 4 % of the dichloromethane volume). The mixture turned yellow and became colorless again after 30 seconds. Stirring was continued for further 60 minutes, then the reaction was quenched with a saturated aqueous solution of sodium bicarbonate. The two phases were separated and the aqueous phase was washed with DCM. The combined organic fractions were dried over magnesium sulfate, filtrated and evaporated to dryness. The crude was purified by column chromatography eluting with *c*-hexane/DCM (1:1) to give the dithiol-pentamer **46** as a colorless solid (107.7 mg, quant.).

^{1}H NMR (400 MHz, Chloroform-*d*): δ 7.45 – 7.38 (m, 21H), 7.37 – 7.33 (m, 25H), 7.28 (d, *J* = 5.8 Hz, 7H), 7.25 – 7.18 (m, 27H), 3.83 (d, *J* = 7.5 Hz, 4H), 3.72 (s, 16H), 1.88 (t, *J* = 7.5 Hz, 2H), 1.43 – 1.40 (m, 90H).

^{13}C NMR (101 MHz, Chloroform-*d*): δ 148.61, 148.59, 146.17, 146.10, 146.01, 143.78, 143.72, 138.48, 135.56, 131.31, 130.78, 128.07, 127.08, 124.26, 124.21, 63.54, 35.53, 35.47, 34.34, 30.92, 29.16.

HRMS (MALDI-ToF): *m/z* calculated for $C_{213}H_{220}S_6$: 2508.3246 $[M+Na]^+$; found: 2508.3149 $[M+Na]^+$.

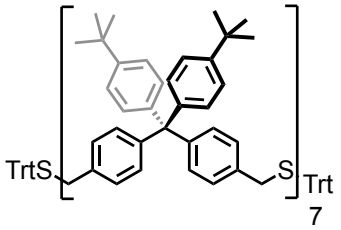

47

$C_{283}H_{296}S_8$
3953.96 g/mol

Heptamer-STrt (47): Compound **37** (71.2 mg, 175 µmol) and dithiol-pentamer **46** (87.1 mg, 35.0 µmol) were dissolved in dry THF (4 ml) under an atmosphere of argon. Sodium hydride (60 % in mineral oil, 7 mg, 175 µmol) was added and the mixture was stirred for 5 hours at room temperature. The reaction was quenched with water and extracted with MTBE. The combined organic fractions were washed with brine, dried over magnesium sulfate, filtrated and evaporated to dryness. Purification of the crude product was achieved by column chromatography eluting with *c*-hexane/DCM (1:1) to yield the trityl-protected heptamer **47** as a colorless foam (109.3 mg, 79 %).

^{1}H NMR (250 MHz, Chloroform-*d*): δ 7.48 – 7.42 (m, 12H), 7.31 – 7.26 (m, 8H), 7.24 – 7.21 (m, 17H), 7.19 (t, *J* = 1.6 Hz, 18H), 7.13 (s, 37H), 7.10 (d, *J* = 6.3 Hz, 23H), 7.07 – 7.02 (m, 23H), 6.98 (d, *J* = 8.4 Hz, 4H), 3.58 (s, 24H), 3.26 (s, 4H), 1.27 (s, 126H).

^{13}C NMR (101 MHz, Chloroform-*d*): δ 147.90, 148.65, 146.24, 145.24, 143.90, 143.54, 134.52, 135.51, 134.34, 130.90, 130.37, 130.33, 129.67, 129.37, 128.76, 127.22, 127.07, 127.05, 126.80, 124.35, 124.32, 67.52, 63.84, 63.80, 36.76, 35.52, 34.24, 31.52, 27.15.

HRMS (MALDI-ToF): *m/z* calculated for $C_{283}H_{296}S_8$: 3973.0825 $[M+Na]^+$; found: 3973.0830 $[M+Na]^+$.

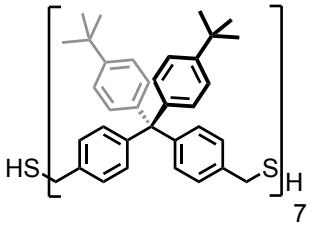

48

$C_{175}H_{192}S_6$
2487.82 g/mol

Heptamer-SH (48): The trityl-protected heptamer **47** (112 mg, 28.0 µmol,) was dissolved in dry DCM (4 ml). Triethylsilane (13.7 µl, 85.0 µmol) was added, followed by trifluoroacetic acid (160 µl, 4 % of the dichloromethane volume). The mixture turned yellow and became colorless again after 30 seconds. Stirring was continued for further 60 minutes, then the reaction was quenched with a saturated aqueous solution of sodium bicarbonate. The two phases were separated and the aqueous phase was extracted with dichloromethane. The combined organic fractions were dried over magnesium sulfate, filtrated and evaporated to dryness. The crude was purified by column chromatography eluting with *c*-hexane/DCM (1:1) to give the dithiol-heptamer **48** as a colorless solid (86.7 mg, quant.).

^{1}H NMR (250 MHz, Chloroform-*d*): δ 7.25 – 7.18 (m, 30H), 7.13 (s, 52H), 7.10 – 7.04 (m, 30H), 3.70 (d, *J* = 7.5 Hz, 4H), 3.58 (s, 24H), 1.74 (t, *J* = 7.5 Hz, 2H), 1.29 – 1.26 (m, 126H).

^{13}C NMR (101 MHz, Chloroform-*d*): δ 148.51, 148.49, 146.03, 145.92, 145.89, 143.66, 143.61, 138.37, 135.45, 131.28, 130.68, 127.95, 126.97, 124.25, 124.23, 63.72, 35.42, 35.38, 34.33, 31.41, 28.55.

HRMS (MALDI-ToF): *m/z* calculated for $C_{175}H_{192}S_6$: 3488.8634 $[M+Na]^+$; found: 3488.8624 $[M+Na]^+$.

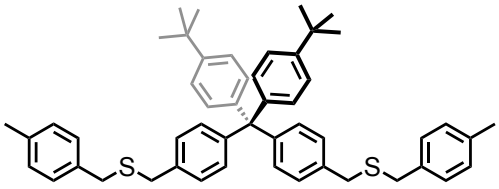

TPM1

$C_{51}H_{56}S_2$
733.13 g/mol

Monomer (TPM1): Thiol-precursor **36** (50.0 mg, 95.0 µmol) and 4-methylbenzyl bromide (38.8 mg, 0.21 mmol) were dissolved in dry THF (4 ml) under an atmosphere of argon. Sodium hydride (60 % in mineral oil, 38.0 mg, 10.0 µmol) was added at room temperature and the mixture was then stirred for 5 hours at room temperature. Water was added to quench the reaction and the mixture was extracted with MTBE. The combined organic fractions were washed with brine, dried over magnesium sulfate, filtrated and evaporated to dryness. After purification by column chromatography eluting with *c*-hexane/DCM 3:1 and automated recyclable GPC, monomer **TPM1** was obtained as a colorless oil (63.4 mg, 91 %).

^{1}H NMR (400 MHz, Chloroform-*d*): δ 7.31 – 7.27 (m, 4H), 7.21 (d, *J* = 8.1 Hz, 4H), 7.17 – 7.12 (m, 6H), 3.63 (d, *J* = 8.6 Hz, 8H), 2.37 (s, 6H), 1.35 (s, 18H).

^{13}C NMR (101 MHz, Chloroform-*d*): δ 148.96, 146.32, 144.12, 136.98, 136.02, 135.56, 131.71, 131.15, 129.59, 129.33, 128.36, 124.65, 64.16, 35.98, 35.71, 34.77, 31.83, 21.56.

HRMS (MALDI-ToF): *m/z* calculated for $C_{51}H_{56}S_2$: 755.3721 $[M+Na]^+$; found: 755.3716 $[M+Na]^+$.

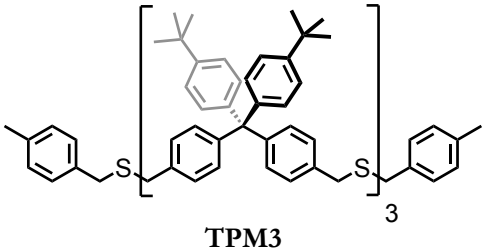

TPM3

$C_{121}H_{132}S_4$
1714.63 g/mol

Trimer (TPM3): Dithiol-trimer **44** (11.2 mg, 7.0 µmol) and 4-methylbenzyl bromide (4.13 mg, 22.0 µmol) were dissolved in dry THF (2 ml) under an atmosphere of argon. Sodium hydride (60 % in mineral oil, 1.50 mg, 37.0 µmol) was added and the mixture was stirred for 5 hours at room temperature. Water was added to quench the reaction and the mixture was extracted with MTBE. The combined organic fractions were washed with brine, dried over magnesium sulfate, filtrated and evaporated to dryness. After purification by column chromatography eluting with *c*-hexane/DCM (3:1) and automated recyclable GPC, trimer **TPM3** was obtained as a colorless oil (63.4 mg, 91 %).

^{1}H NMR (400 MHz, Chloroform-*d*): δ 7.22 (dd, *J* = 8.6, 4.0 Hz, 12H), 7.14 (dd, *J* = 4.2, 2.7 Hz, 28H), 7.11 – 7.05 (m, 16H), 3.61 – 3.54 (m, 16H), 2.31 (s, 6H), 1.28 (d, *J* = 3.5 Hz, 54H).

^{13}C NMR (101 MHz, Chloroform-*d*): δ 148.49, 145.92, 145.84, 143.64, 136.54, 135.55, 135.42, 135.10, 131.27, 131.24, 130.67, 130.65, 129.14, 128.88, 127.92, 124.20, 63.70, 34.31, 31.38, 29.71, 21.11.

HRMS (MALDI-ToF): *m/z* calculated for $C_{121}H_{132}S_4$: 1735.9110 $[M+Na]^+$; found: 1735.9089 $[M+Na]^+$.

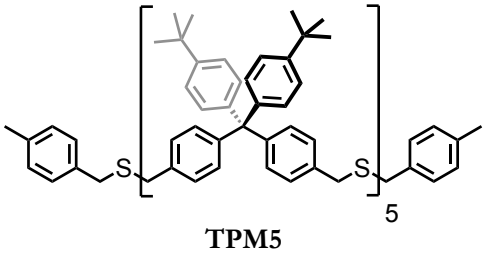

TPM5

$C_{191}H_{208}S_6$
2696.13 g/mol

Pentamer (TPM5): Dithiol-pentamer **46** (15.2 mg, 6.0 µmol) and 4-methylbenzyl bromide (2.83 mg, 15.0 µmol) were dissolved in dry THF (3 ml) under an atmosphere of argon. Sodium hydride (60 % in mineral oil, 1.22 mg, 31.0 µmol) was added at room temperature. The mixture was then stirred for 15 hours at room temperature. Water was added to quench the reaction and the mixture was extracted with MTBE. The combined organic fractions were washed with brine, dried over magnesium sulfate, filtrated and evaporated to dryness. After purification by column chromatography eluting with *c*-hexane/DCM (1:1) and automated recyclable GPC, pentamer **TPM5** was obtained as a colorless oil (12.4 mg, 77 %).

^{1}H NMR (250 MHz, Chloroform-*d*): δ 7.22 (dd, *J* = 8.6, 2.9 Hz, 21H), 7.16 – 7.10 (m, 42H), 7.07 (dd, *J* = 8.7, 1.8 Hz, 25H), 3.62 – 3.54 (m, 24H), 2.31 (s, 6H), 1.28 (d, *J* = 2.8 Hz, 90H).

^{13}C NMR (101 MHz, Chloroform-*d*): δ 148.47, 145.90, 143.64, 135.43, 131.27, 130.68, 130.66, 129.14, 128.88, 127.93, 124.21, 63.70, 35.40, 34.31, 31.38, 21.12.

HRMS (MALDI-ToF): *m*/*z* calculated for $C_{191}H_{208}S_6$: 2716.4498 $[M+Na]^+$; found: 2716.4491 $[M+Na]^+$.

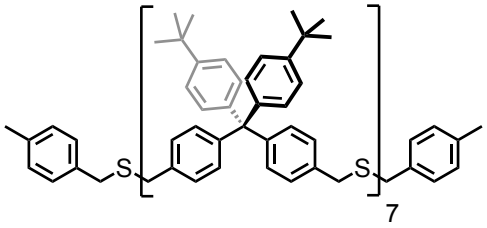

TPM7

$C_{261}H_{284}S_8$
3677.62 g/mol

Heptamer (TPM5): Dithiol-heptamer **48** (15.0 mg, 4.00 µmol,) and 4-methylbenzyl bromide (3.2 mg, 17.0 µmol) were dissolved in dry THF (3 ml) under an atmosphere of argon. Sodium hydride (60 % in mineral oil, 0.86 mg, 0.022 mmol) was added at room temperature. The mixture was then stirred for 15 hours at room temperature. Water was added to quench the reaction and the mixture was extracted with MTBE. The combined organic fractions were washed with brine, dried over magnesium sulfate, filtrated and evaporated to dryness. After purification by column chromatography eluting with *c*-hexane/DCM (1:1) and automated recyclable GPC, heptamer **TPM7** was obtained as a colorless oil (10.6 mg, 72 %).

^{1}H NMR (400 MHz, Chloroform-*d*): δ 7.24 – 7.18 (m, 28H), 7.12 (s, 56H), 7.11 – 7.04 (m, 36H), 3.62 – 3.52 (m, 32H), 2.31 (s, 6H), 1.38 – 1.20 (m, 112H).

^{13}C NMR (101 MHz, Chloroform-*d*): δ 148.69, 146.14, 143.78, 135.47, 132.41, 130.86, 130.70, 129.17, 129.02, 128.07, 124.25, 63.85, 35.51, 34.41, 31.51, 21.21.

HRMS (MALDI-ToF): *m*/*z* calculated for $C_{261}H_{284}S_8$: 3696.9886 $[M+Na]^+$; found: 3696.9924 $[M+Na]^+$.

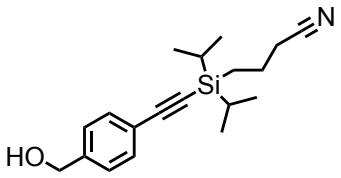

49

$C_{19}H_{27}NOSi$
313.52 g/mol

4-(((4-(Hydroxymethyl)phenyl)ethynyl)diisopropylsilyl)butanenitrile (49): To a degassed solution of 4-iodobenzyl alcohol (200 mg, 830 µmol), bis(triphenylphosphine)-palladium dichloride (23.5 mg, 30 µmol), and copper(I) iodide (6.3 mg, 30 µmol) in anhydrous degassed triethylamine (10 mL) and THF (5 ml) was added 4-(ethynyldiisopropylsilyl)butanenitrile (224 mg, 1.08 mmol) at room temperature. After, the reaction mixture was heated to 40 °C for 12 h, saturated aqueous ammonium chloride solution was added, and the mixture was extracted with ethyl acetate. The combined solution was washed with water, brine, and dried over magnesium sulfate. Flash column chromatography with *c*-hexane/EtOAc (10:1) as the eluent gave compound **49** as a colorless oil (251 mg, quant.).

^{1}H NMR (400 MHz, Chloroform-*d*): δ 7.44 (d, *J* = 7.8 Hz, 2H), 7.27 (d, *J* = 7.7 Hz, 2H), 4.62 (s, 2H), 2.69 (s, 1H), 2.42 (t, *J* = 6.8 Hz, 2H), 1.85 (p, *J* = 7.6 Hz, 2H), 1.15 – 1.03 (m, 14H), 0.82 (t, *J* = 8.6 Hz, 2H).

^{13}C NMR (101 MHz, Chloroform-*d*): δ 141.70, 132.14, 126.63, 121.95, 119.84, 107.82, 89.20, 64.50, 21.26, 20.71, 18.22, 17.98, 11.73, 9.60.

GC-MS (EI, 70 eV): *m*/*z* (%) = 270.95 (24), 269.95 (100), 242.9 (8), 241.9 (36), 224.9 (5), 223.9 (24), 214.9 (15), 213.9 (71), 200.9 (7), 199.9 (9), 188.9 (6), 174.9 (11), 158.95 (21), 129 (8), 128 (7), 115 (19), 106.55 (10).

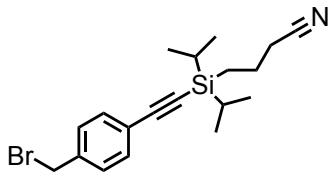

50

$C_{19}H_{26}BrNSi$
376.41 g/mol

4-(((4-(Bromomethyl)phenyl)ethynyl)diisopropylsilyl)butanenitrile (50): To a solution of compound **49** (270 mg, 860 µmol) in dry degassed THF (10 ml), phosphorus tribromide (82.6 µl, 860 µmol) was added dropwise at 0 °C. The reaction progress was monitored *via* GC-MS. After 3 hours, the reaction mixture was quenched by addition of a saturated aqueous solution of sodium bicarbonate and the aqueous phase was washed with ethyl acetate. The combined organic fractions were dried over magnesium sulfate, and the solvent was evaporated *in vacuo*. Flash column chromatography with *c*-hexane/EtOAc (10:1) as the eluent gave compound **50** as a yellow oil (320 mg, quant.).

^{1}H NMR (400 MHz, Benzene-d_6): δ 7.27 (d, J = 8.2 Hz, 2H), 6.78 (d, J = 8.2 Hz, 2H), 3.80 (s, 2H), 1.59 – 1.49 (m, 2H), 1.12 (s, 3H), 1.11 (s, 4H), 1.06 (s, 3H), 1.04 (s, 4H), 0.99 – 0.86 (m, 2H), 0.58 – 0.51 (m, 2H).

^{13}C NMR (101 MHz, Benzene-d_6): δ 141.20, 132.31, 125.93, 122.05, 119.84, 107.92, 89.29, 64.50, 25.16, 20.91, 18.22, 17.58, 11.73, 9.60.

GC-MS (EI, 70 eV): m/z (%) = 334.85 (24), 333.85 (100), 332.85 (26), 331.85 (99), 306.85 (8), 305.85 (29), 303.85 (31), 296 (16), 278.8 (12), 277.8 (56), 276.8 (11), 275.8 (55), 264.85 (13), 262.8 (12), 253.95 (12), 252.9 (10), 224.9 (13), 223.95 (21), 197.95 (13), 196.9 (33), 184.95 (12), 183.95 (12), 182.95 (12), 158 (12), 157 (11), 155 (9), 144 (9), 143 (31), 142 (42), 141 (17), 129 (8), 128 (17), 126.55 (16), 117.95 (9), 117 (11), 115 (20), 112.5 (16), 98.5 (34), 91.95 (8), 91.05 (12), 86 (13), 79 (10), 71 (11).

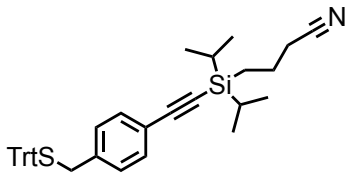

51

$C_{38}H_{41}NSSi$
571.90 g/mol

4-(Diisopropyl((4-((tritylthio)methyl)phenyl)ethynyl)silyl)butanenitrile (51): Compound **50** (215 mg, 570 µmol) was dissolved in dry THF (15 ml) in a 25 ml Schlenk-tube. Trityl thiol (253 mg, 910 µmol) was added to the solution, which was then degassed for 30 minutes with argon. Sodium hydride (60 % dispersion in mineral oil, 114 mg, 2.86 mmol) was added to the flask. The mixture was stirred at room temperature for 15 hours, and then quenched by addition of water, extracted with MTBE, washed twice with water, dried over magnesium sulfate, filtrated and the solvent was removed *in vacuo*. The crude product was subjected to column chromatography eluting with *c*-hexane/DCM (3:1) to afford compound **51** as a white solid (287 mg, 88 %).

^{1}H NMR (400 MHz, Chloroform-*d*): δ 7.25 – 7.15 (m, 15H), 7.09 (d, *J* = 8.2 Hz, 2H), 6.57 (d, *J* = 8.2 Hz, 2H), 3.92 (s, 2H), 2.40 (t, *J* = 7.0 Hz, 2H), 2.00 – 1.73 (m, 2H), 1.12 – 1.01 (m, 14H), 0.83 – 0.75 (m, 2H).

^{13}C NMR (101 MHz, Chloroform-*d*): δ 146.85, 144.58, 137.90, 132.13, 130.20, 129.59, 129.03, 127.27, 126.77, 121.60, 119.79, 107.79, 89.33, 67.57, 36.83, 21.29, 20.76, 18.20, 17.97, 11.74, 9.62.

GC-MS (EI, 70 eV): *m*/*z* (%) = 462 (11), 461 (29), 419 (33), 418 (100), 390 (23), 363 (25), 362 (66), 350 (14), 349 (19), 323 (13), 321 (13), 308 (11), 307 (19), 276 (11), 181 (40), 178 (11), 161 (11), 153 (15), 146 (14), 134 (14), 78 (26).

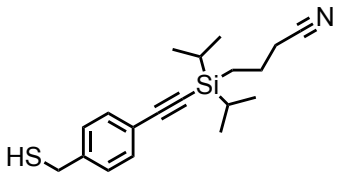

52

$C_{19}H_{27}NSSi$
329.58 g/mol

4-(Diisopropyl((4-(mercaptomethyl)phenyl)ethynyl)silyl)butanenitrile (52): Compound **51** (190 mg, 330 µmol,) was dissolved in dry DCM (8 ml). Triethylsilane (80.3 µl, 500 µmol) was added, followed by trifluoroacetic acid (320 µl, 4 % of the dichloromethane volume). The mixture turned yellow and became colorless again after 30 seconds. Stirring was continued for further 60 minutes, then the reaction was quenched with a saturated aqueous solution of sodium bicarbonate. The two phases were separated and the aqueous phase was washed with dichloromethane. The combined organic fractions were dried over magnesium sulfate, filtrated and evaporated to dryness. The crude was purified by column chromatography eluting with *c*-hexane/DCM (1:2) to give the compound **52** as a colorless solid (105 mg, quant.).

^{1}H NMR (400 MHz, Chloroform-*d*): δ 7.42 (d, *J* = 8.2 Hz, 2H), 7.27 (d, *J* = 7.9 Hz, 2H), 3.73 (d, *J* = 7.6 Hz, 2H), 2.43 (t, *J* = 7.0 Hz, 2H), 1.94 – 1.82 (m, 2H), 1.74 (t, *J* = 7.6 Hz, 1H), 1.14 – 1.06 (m, 14H), 0.89 – 0.77 (m, 2H).

^{13}C NMR (101 MHz, Chloroform-*d*): δ 141.96, 132.51, 128.15, 121.83, 119.92, 107.77, 89.59, 27.06, 21.44, 20.91, 18.35, 18.11, 11.88, 9.77.

GC-MS (EI, 70 eV): *m*/*z* (%) = 328 (100), 286 (71), 270 (30), 245 (70), 195 (28), 178 (34), 162 (37), 95 (28), 80 (28), 78 (27), 65 (32).

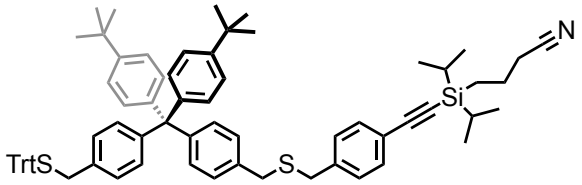

53

$C_{73}H_{79}NS_2Si$
1062.65 g/mol

Compound 53: Compound **52** (22.5 mg, 68.0 µmol) was dissolved in dry THF (6 ml) in a 10 ml Schlenk-tube. Compound **37** (69.5 mg, 85.0 µmol) was added to the solution, which was then degassed for 15 minutes with argon. Sodium hydride (60 % dispersion in mineral oil, 13.7 mg, 0.34 mmol) was added to the flask. The mixture was stirred at room temperature for 15 hours, and then quenched by addition of water, extracted with MTBE, washed twice with water, dried over magnesium sulfate, filtrated and the solvent was removed *in vacuo*. The crude product was subjected to column chromatography eluting with *c*-hexane/DCM (4:1) to afford compound **53** as a white solid (51.3 mg, 71 %).

^{1}H NMR (400 MHz, Chloroform-*d*): δ 7.50 – 7.42 (m, 6H), 7.41 (d, *J* = 8.2 Hz, 2H), 7.31 – 7.26 (m, 6H), 7.24 – 7.19 (m, 9H), 7.11 (s, 4H), 7.09 – 7.04 (m, 6H), 7.01 (d, *J* = 8.4 Hz, 2H), 3.59 (s, 2H), 3.54 (s, 2H), 3.29 (s, 2H), 2.41 (t, *J* = 6.9 Hz, 2H), 1.97 – 1.77 (m, 2H), 1.30 (s, 18H), 1.16 – 1.03 (m, 14H), 0.92 – 0.77 (m, 2H).

^{13}C NMR (101 MHz, Chloroform-*d*): δ 148.62, 146.08, 144.85, 143.74, 139.19, 135.20, 134.49, 132.30, 131.42, 131.34, 130.78, 129.78, 129.12, 128.23, 128.06, 128.04, 126.82, 124.34, 107.91, 67.55, 63.82, 36.77, 35.64, 35.26, 34.45, 31.51, 21.44, 20.91, 18.36, 18.13, 11.90, 9.78.

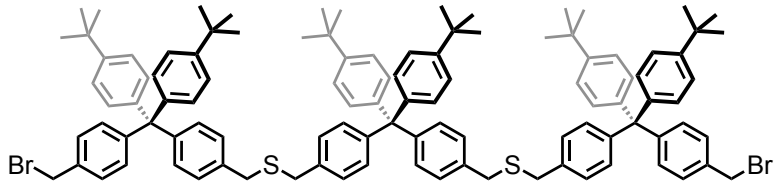

54

$C_{105}H_{114}Br_2S_2$
1600.00 g/mol

Bromine trimer (54): Bromine-precursor **34** (177 mg, 29.0 µmol) and sodium hydride (60 % in mineral oil, 22.9 mg, 57.0 µmol) were dispersed in dry degassed THF (5 ml) under an atmosphere of argon. Thiol-precursor **36** (50.0 mg, 95.0 µmol) dissolved in dry THF (3 ml) was then added *via* syringe pump during 1 hour to the reaction mixture and the reaction mixture was further stirred for 15 hours at room temperature. The reaction was quenched with water and extracted with MTBE. The combined organic fractions were washed with brine, dried over magnesium sulfate, filtrated and evaporated to dryness. Purification of the crude product was achieved by short column chromatography eluting with *c*-hexane/EtOAc (1:1) and automated recyclable GPC to yield the bromine trimer **54** as a colorless oil (35.5 mg, 39 %).

^{1}H NMR (400 MHz, Chloroform-*d*): δ 7.24 – 7.20 (m, 16H), 7.19 – 7.14 (m, 6H), 7.14 – 7.10 (m, 14H), 7.09 – 7.04 (m, 12H), 4.46 (s, 4H), 3.59 (s, 8H), 1.29 (s, 36H), 1.28 (s, 18H).

^{13}C NMR (101 MHz, Chloroform-*d*): δ 148.73, 148.63, 147.73, 146.05, 145.79, 143.75, 143.51, 135.52, 131.65, 131.40, 131.36, 130.77, 130.76, 128.17, 128.14, 128.07, 124.43, 63.90, 63.83, 35.49, 34.46, 33.65, 31.51, 29.86.

MS (MALDI-ToF, positive): broad peak at *m/z* 1620 $[M+Na]^+$.

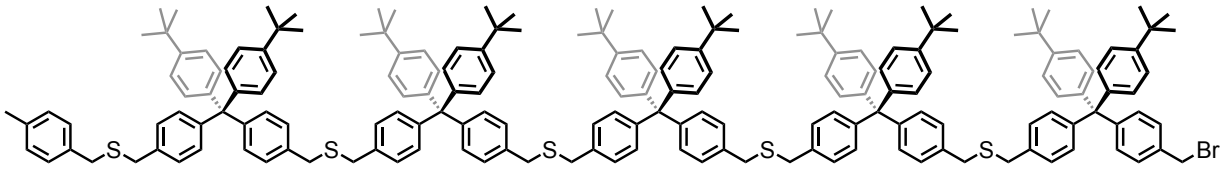

55

$C_{183}H_{199}BrS_5$
2638.81 g/mol

Mono-endcapped pentamer-Br (55): Compound **54** (27.2 mg, 170 µmol) was dissolved in dry THF (15 ml) in a 25 ml Schlenk-tube. Compound **42** (11.3 mg, 10.0 µmol) was added to the solution, which was then degassed for 30 minutes with argon. Sodium hydride (60 % dispersion in mineral oil, 3.40 mg, 85.0 µmol) was added to the flask. The mixture was stirred at room temperature for 15 hours, and then quenched by addition of water, extracted with MTBE, washed twice with water, dried over magnesium sulfate, filtrated and the solvent was removed *in vacuo*. Purification of the crude product was achieved by short column chromatography eluting with *c*-hexane/EtOAc (1:1) and automated recyclable GPC to yield the compound **55** as a colorless oil (6.40 mg, 24 %).

^{1}H NMR (400 MHz, Chloroform-*d*): δ 7.25 – 7.18 (m, 24H), 7.17 – 7.09 (m, 36H), 7.11 – 7.03 (m, 24H), 4.46 (s, 2H), 3.62 – 3.54 (m, 24H), 2.31 (s, 3H), 1.29 (s, 16H), 1.29 (s, 24H), 1.28 (s, 54H).

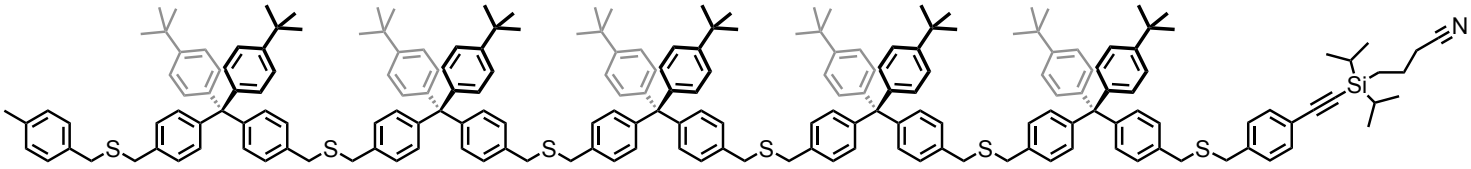

TPM5-Hog

$C_{202}H_{225}NS_6Si$
2887.47 g/mol

Monofunctionalized pentamer (TPM5-Hog): Compound **55** (6.40 mg, 2.43 µmol) was dissolved in dry degassed THF (2 ml) in a 5 ml Schlenk-tube. Compound **52** (2.40 mg, 7.29 µmol) was added to the solution, which was then degassed for 5 minutes with argon. Sodium hydride (60 % dispersion in mineral oil, 880 µg, 21.9 µmol) was added to the flask. The mixture was stirred at room temperature for 15 hours, and then quenched by addition of water, extracted with MTBE, washed twice with water, dried over magnesium sulfate, filtrated and the solvent was removed *in vacuo*. Purification of the crude product was achieved by short column chromatography eluting with *c*-hexane/EtOAc (1:1) and automated recyclable GPC to yield the monofunctionalized pentamer **TPM5-Hog** as a colorless oil (5.00 mg, 71 %).

^{1}H NMR (600 MHz, Chloroform-*d*): δ 7.40 (d, *J* = 8.2 Hz, 2H), 7.25 – 7.18 (m, 26H), 7.18 – 7.10 (m, 36H), 7.11 – 7.04 (m, 24H), 3.61 – 3.57 (m, 20H), 3.56 (s, 2H), 3.54 (s, 2H), 2.41 (t, *J* = 7.0 Hz, 2H), 2.31 (s, 3H), 1.91 – 1.81 (m, 2H), 1.29 (s, 36H), 1.28 (s, 54H), 1.13 – 1.05 (m, 21H), 0.84 – 0.80 (m, 2H).

^{13}C NMR (151 MHz, Chloroform-*d*): δ 148.66, 148.63, 148.61, 146.17, 146.06, 146.05, 146.04, 146.01, 145.98, 139.18, 136.67, 135.69, 135.60, 135.57, 135.56, 135.26, 135.24, 132.30, 131.44, 131.42, 131.41, 131.38, 130.82, 130.80, 130.80, 129.86, 129.59, 129.28, 129.11, 129.02, 128.44, 128.08, 128.07, 124.36, 124.35, 121.69, 119.92, 107.89, 89.49, 63.84, 35.66, 35.64, 35.54, 35.53, 35.36, 35.28, 34.45, 31.52, 29.85, 21.44, 21.26, 20.92, 18.37, 18.13, 14.28, 11.89, 9.77.

MS (MALDI-ToF, positive): broad peak at *m/z* 2910 $[M+Na]^+$, 2930 $[M+K]^+$.

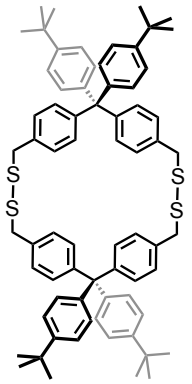

56

$C_{70}H_{76}S_4$
1045.62 g/mol

Compound 56: Dithiol-precursor **36** (7.30 mg, 0.014 mmol) was dissolved in THF (8 ml) in a 10 ml oven-dried Schlenk-tube. After addition of NaH (60 % in mineral oil, 1.33 mg, 33.0 µmol) the reaction mixture was stirred at ambient conditions for 15 hours and quenched with water. The aqueous phase was washed with MTBE and evaporated *in vacuo*. The crude product was subjected to flash column chromatography eluting with *c*-hexane/DCM (3:1) to afford cycle compound **56** as white solid (14.0 mg, quant.).

^{1}H NMR (400 MHz, Chloroform-*d*): δ 7.25 – 7.20 (m, 8H), 7.10 – 7.02 (m, 16H), 6.92 – 6.86 (m, 8H), 3.64 (s, 8H), 1.29 (s, 36H).

MS (MALDI-ToF, positive): *m*/*z* 1067.77 $[M+Na]^+$.

7.2.5 Tridentate **Tri**-Ligands

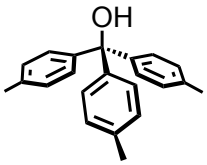

57

$C_{22}H_{22}O$
302.42 g/mol

Tri-*p*-tolylmethanol (57):[186] In a dry degassed 500 ml three-necked flask equipped with rubber septum, reflux condenser and addition funnel, Mg turnings (2.02 g, 83.2 mmol) were suspended in 20 ml dry degassed THF under argon atmosphere. 4-Bromotoluene (14.2 g, 83.2 mmol) dissolved in 20 ml dry, degassed THF were added dropwise. In order to activate the Grignard reagent, the mixture was heated with a heat gun until a reaction was observed, and subsequently stirred for three hours. Methyl *p*-toluate (5.00 g, 33.3 mmol) was dissolved in 20 ml dry degassed THF and added to the mixture, which was then refluxed for 24 hours. After cooling to room temperature, the reaction was quenched with a saturated aqueous solution of NH_4Cl. The aqueous phase was washed with MTBE. The combined organic phases were washed twice with water, dried over $MgSO_4$ and the solvent was evaporated. The crude product was subjected to column chromatography eluting with *n*-hexane/DCM (5:1) to obtain compound **57** as a white solid (9.87 g, 98 %).

^{1}H NMR (400 MHz, Chloroform-d): δ 7.17 – 7.12 (m, 6H), 7.09 (m, 6H), 2.70 (s, 1H), 2.32 (s, 9H).

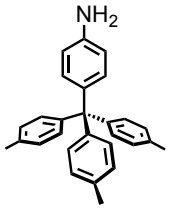

58

$C_{28}H_{27}N$
377.53 g/mol

4-(Tri-*p*-tolylmethyl)aniline (58):[161] To a 250 ml two-necked flask, freshly distilled aniline (11.1 ml, 121 mmol) was added and dissolved in concentrated hydrochloric acid (7.7 ml) and glacial acetic acid (45 ml). Compound **57** (9.17 g, 30.4 mmol) was added portionwise to the reaction mixture, which was then heated to 140 °C and refluxed during three hours. The volatile was evaporated under reduced pressure, the remaining solid was dissolved in DCM and neutralized with aqueous 1 M NaOH. The organic phase was washed three times with water and dried over Na_2SO_4. The product was allowed to precipitate by addition of cold MeOH to afford compound **58** as a white solid (7.60 g, 66 %).

^{1}H NMR (400 MHz, Chloroform-d): δ 7.08 (m, 6H), 7.02 (m, 6H), 6.98-6.93 (m, 2H), 6.57 – 6.52 (m, 2H), 3.55 (s, 2H), 2.30 (s, 9H).

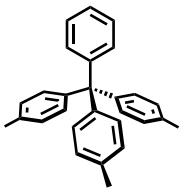

59

$C_{28}H_{26}$
362.52 g/mol

Tris(*p*-tolyl)methylbenzene (59):[187] To a dry, degassed 500 ml two-necked flask, BF_3OEt_2 (1.70 ml, 13.2 mmol) was added and cooled to -10 °C. Precursor **58** (2.50 g, 6.62 mmol) was dissolved in dry, degassed THF (30 ml) in a separate dry and degassed flask, and was then added dropwise. Additional dry degassed THF (5 ml) were used to rinse the flask that contained remaining starting material. The mixture was stirred at -10 °C for 45 minutes. The same procedure was repeated with $^tBuNO_2$ (1.40 ml, 11.6 mmol). Meanwhile, a 500 ml flask was prepared with $FeSO_4$ (1.11 mg, 7.32 mmol) dissolved in DMF (200 ml). The reaction mixture was slowly poured into the iron sulfate solution, leading to evolution of nitrogen. The mixture was stirred at room temperature for 2.5 hours, then poured into ice water. The mixture was extracted with DCM, washed twice with 1 M aqueous HCl, twice with water and dried over magnesium sulfate. After evaporation of the volatile in vacuo, the product was purified by column chromatography eluting with *c*-hexane/EtOAc (20:1) as a pale orange solid (1.92 g, 80 %).

^{1}H NMR (400 MHz, Chloroform-*d*): δ 7.24 – 7.19 (m, 4H), 7.18 – 7.13 (m, 1H), 7.12 – 7.00 (m, 12H), 2.30 (s, 9H).

^{13}C NMR (101 MHz, Chloroform-*d*): δ 147.34, 144.22, 135.23, 131.11, 131.01, 128.15, 127.38, 125.71, 64.00, 20.95.

GC-MS (EI, 70 eV): *m*/*z* (%) = 363.2 (10), 362.2 (32), 347.1 (13), 286.2 (18), 285.1 (67), 272.1 (22), 271.1 (100), 193.1 (20), 179.1 (27), 178.1 (25), 165.1 (10).

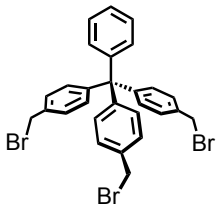

60

$C_{28}H_{23}Br_3$
599.20 g/mol

Tris((*p*-bromomethyl)phenyl)methylbenzene (60):[187] A dry, degassed 500 ml two-necked flask was equipped with a reflux condenser and a glass stopper. Compound **59** (1.87 g, 5.16 mmol), *N*-bromosuccinimide (5.51 g, 31.0 mmol) and AIBN (169 mg, 1.03 mmol) were suspended in 200 ml methyl formate under argon atmosphere. The suspension was degassed with argon for 30 minutes, then illuminated with a 500 W halogen lamp. The mixture was refluxed for 15 hours and then allowed to cool to room temperature. The crude precipitate was concentrated, and redissolved in DCM. The solution was washed four times with water, dried over $MgSO_4$, and the solvent was evaporated *in vacuo*. The crude product was subjected to automated column chromatography starting with *c*-hexane/DCM (20:1) and switched to *c*-hexane/DCM (10:1) after 4 column volumina, to give compound **60** as a white solid (1.56 g, 50 %).

^{1}H NMR (400 MHz, Chloroform-*d*): δ 7.30 – 7.27 (m, 6H), 7.26 – 7.20 (m, 3H), 7.20 – 7.16 (m, 8H), 4.47 (s, 6H).

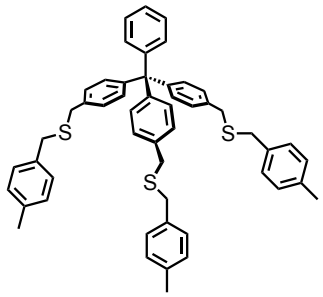

Tri-0

$C_{52}H_{50}S_3$
771.15 g/mol

Endcapped tridentate compound (Tri-0): In a dry, degassed 15 ml two-necked flask, compound **60** (52.4 mg, 870 µmol) and *p*-tolylmercaptane (71.1 µl, 530 µmol,) were dissolved in dry THF (5 ml). After degassing the mixture with argon for 15 minutes, sodium hydride (60 % dispersed in mineral oil, 35.0 mg, 870 µmol) was added. The mixture was allowed to stir at room temperature for 15 hours, after which time the reaction was quenched upon addition of water. The aqueous phase was extracted with MTBE. The combined organic phases were washed three times with water, dried over magnesium sulfate and evaporated to dryness. The product **Tri-0** was afforded by column chromatography eluting with *c*-hexane/DCM (5:1) as a yellowish oil (61.9 mg, 92 %).

^{1}H NMR (400 MHz, Chloroform-*d*): δ 7.25 – 7.06 (m, 29H), 3.58 (m, 12H), 2.31 (s, 9H).

^{13}C NMR (101 MHz, Chloroform-*d*): δ 146.72, 145.47, 136.61, 135.85, 135.07, 131.19, 131.08, 129.19, 128.91, 128.14, 127.53, 126.00, 64.32, 35.60, 35.22, 21.15.

HRMS (ESI-ToF): *m/z* calculated for $C_{52}H_{50}S_3$: 788.3418 $[M+NH_4]^+$, 793.2972 $[M+Na]^+$; found: 788.3413 $[M+NH_4]^+$, 793.2967 $[M+Na]^+$.

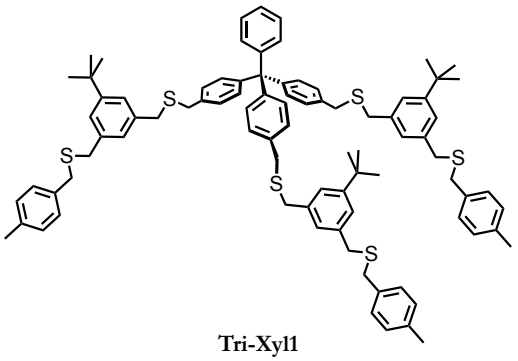

Tri-Xyl1

$C_{88}H_{98}S_6$
1348.11 g/mol

Tridentate monoxylene derivative (Tri-Xyl1): In a dry, degassed 25 ml one-necked flask, compound **60** (50.0 mg, 830 µmol) and thiol-derivative **9** (96.5, 292 µmol) were dissolved in dry THF (5 ml). After degassing the mixture with argon for 15 minutes, sodium hydride (60 % dispersed in mineral oil, 16.7 mg, 860 µmol) was added. The mixture was allowed to stir at room temperature for 2 hours, after which time the reaction was quenched upon addition of water. The aqueous phase was extracted three times with MTBE. The combined organic phases were dried over Na_2SO_4, and evaporated to dryness. The product **Tri-Xyl1** was afforded after column chromatography eluting with *c*-hexane/DCM (1:1) as a yellowish oil (86.0 mg, 77 %).

^{1}H NMR (400 MHz, Chloroform-*d*): δ 7.23 – 7.06 (m, 38H), 3.59 (2s, 12H), 3.55 (2s, 12H), 2.31 (s, 9H), 1.29 (s, 27H).

^{13}C NMR (101 MHz, Chloroform-*d*): δ 151.48, 146.72, 145.51, 138.07, 137.89, 136.56, 135.73, 135.10, 131.21, 131.07, 129.18, 128.95, 128.19, 127.57, 126.83, 126.02, 124.92, 124.81, 64.35, 36.17, 35.79, 35.43, 35.29, 34.68, 31.42, 21.17.

HRMS (ESI-ToF): *m/z* calculated for $C_{88}H_{98}S_6$: 1370.5969 $[M+H/Na]^+$; found: 1370.5918 $[M+H/Na]^+$.

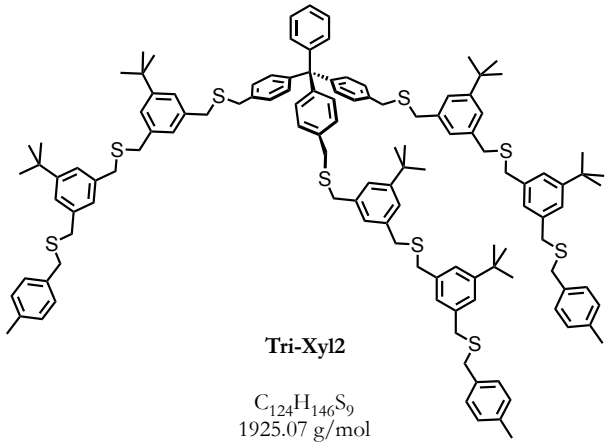

Tri-Xyl2

$C_{124}H_{146}S_9$
1925.07 g/mol

Tridentate dixylene derivative (Tri-Xyl2): To a dry, degassed 25 ml one-necked flask, compound **60** (17.4 mg, 290 µmol) and thiol-derivative **11** (53.1, 102 µmol) were added and dissolved in dry THF (5 ml). After degassing the mixture with argon for 15 minutes, sodium hydride (60 % dispersed in mineral oil, 11.6 mg, 290 µmol) was added. The mixture was allowed to stir at room temperature for 2 hours, after which time the reaction was quenched upon addition of water. The aqueous phase was extracted with MTBE. The combined organic phases were dried over Na_2SO_4, and evaporated to dryness. The crude product was filtrated and purified by automated recyclable GPC thereafter to yield tridentate compound **Tri-Xyl2** as a yellowish oil (22.0 mg, 39 %).

^{1}H NMR (400 MHz, Chloroform-*d*): δ 7.22 – 7.12 (m, 35H), 7.11 – 7.08 (m, 9H), 7.06 (s, 3H), 3.62 (s, 6H), 3.59 – 3.55 (m, 30H), 2.32 (s, 9H), 1.30 (s, 27H), 1.29 (s, 27H).

^{13}C NMR (101 MHz, Chloroform-*d*): δ 151.54, 151.51, 146.69, 145.47, 138.09, 137.98, 137.90, 136.54, 135.69, 135.09, 131.19, 131.04, 129.16, 128.93, 128.15, 127.54, 126.84, 126.79, 125.99, 124.90, 124.86, 124.76, 124.68, 64.32, 36.24, 35.92, 35.80, 35.44, 35.35, 34.66, 31.42, 31.41, 21.15.

HRMS (ESI-ToF): *m/z* calculated for $C_{124}H_{146}S_9$: 1945.8809 $[M+Na]^+$; found: 1945.8803 $[M+Na]^+$.

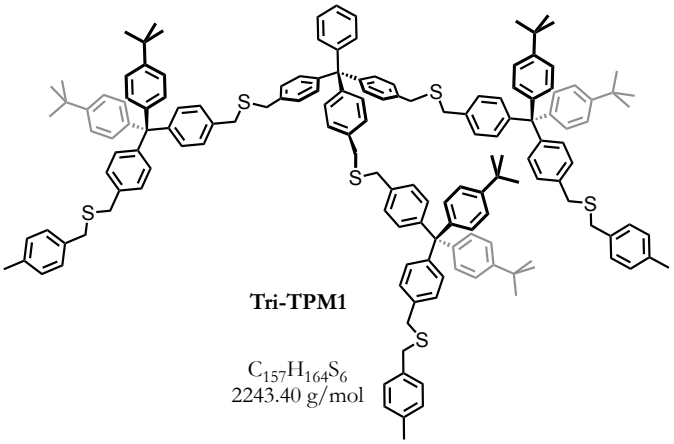

Tri-TPM1

$C_{157}H_{164}S_6$
2243.40 g/mol

Tridentate monotetraphenylmethane derivative (Tri-TPM1): In a dry, degassed 25 ml one-necked flask, compound **60** (20.0 mg, 33 µmol) and thiol-derivative **40** (71.9 mg, 117 µmol) were dissolved in dry THF (5 ml). After degassing the mixture with argon for 15 minutes, sodium hydride (60 % dispersed in mineral oil, 13.4 mg, 334 µmol) was added. The mixture was allowed to stir at room temperature for 2 hours, after which time the reaction was quenched upon addition of water. The aqueous phase was extracted with MTBE. The combined organic phases were dried over Na_2SO_4, and evaporated to dryness. The product **Tri-TPM1** was afforded by column chromatography eluting with *c*-hexane/DCM (2:1) and if necessary by additional automated recyclable GPC as a yellowish oil (44.0 mg, 61 %).

^{1}H NMR (400 MHz, Chloroform-*d*): δ 7.22 – 7.12 (m, 35H), 7.11 – 7.08 (m, 9H), 7.06 (s, 3H), 3.62 (s, 6H), 3.59 – 3.55 (m, 30H), 2.32 (s, 9H), 1.30 (s, 27H), 1.29 (s, 27H).

^{13}C NMR (101 MHz, Chloroform-*d*): δ 148.63, 146.78, 146.09, 145.97, 145.61, 143.78, 136.67, 135.84, 135.70, 135.54, 135.24, 131.43, 131.38, 131.29, 131.12, 130.82, 129.27, 129.02, 128.26, 128.05, 128.04, 127.65, 126.10, 124.34, 64.44, 63.84, 35.65, 35.63, 35.54, 35.38, 34.45, 31.52, 21.25.

HRMS (ESI-ToF): *m/z* calculated for $C_{157}H_{164}S_6$: 2264.1055 $[M+Na]^+$; found: 2264.1050 $[M+Na]^+$.

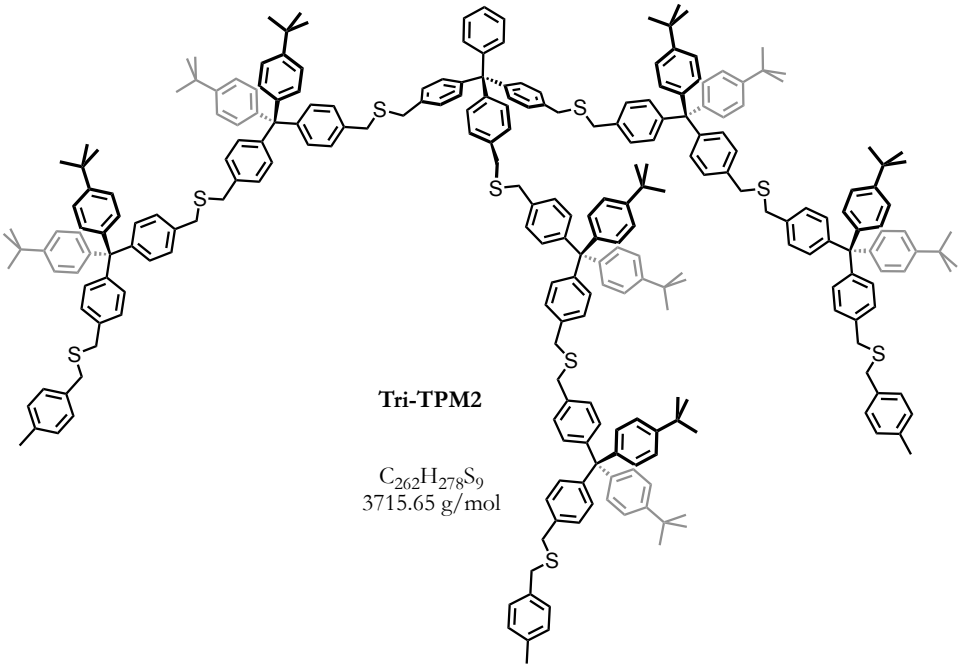

Tri-TPM2

$C_{262}H_{278}S_9$
3715.65 g/mol

Tridentate ditetraphenylmethane derivative (Tri-TPM2): In a dry, degassed 25 ml one-neck flask, compound **60** (13.1 mg, 220 µmol) and thiol-derivative **42** (85.8 mg, 77.0 µmol) were dissolved in dry THF (5 ml). After degassing the mixture with argon for 15 minutes, sodium hydride (60 % dispersed in mineral oil, 8.80 mg, 219 µmol) was added. The mixture was allowed to stir at room temperature for 15 hours, after which time it was quenched upon addition of water. The aqueous phase was extracted with MTBE. The combined organic phases were dried over Na_2SO_4, and evaporated to dryness. The crude product was purified by a short column chromatography eluting with *c*-hexane/EtOAC (1:1) followed by automated recyclable GPC thereafter to yield compound **Tri-TPM2** as a yellowish oil (72.0 mg, 89 %).

^{1}H NMR (400 MHz, Chloroform-*d*): δ 7.25 – 7.16 (m, 35H), 7.14 – 7.11 (m, 57H), 7.09 – 7.04 (m, 33H), 3.60 – 3.54 (m, 36H), 2.31 (s, 9H), 1.28 (s, 54H), 1.27 (s, 54H).

^{13}C NMR (101 MHz, Chloroform-*d*): δ 148.67, 148.66, 146.82, 146.11, 146.11, 146.09, 146.02, 145.65, 143.84, 143.82, 136.71, 135.90, 135.74, 135.62, 135.62, 135.59, 135.29, 131.48, 131.46, 131.43, 131.34, 131.17, 130.87 (x2), 130.85, 129.33, 129.07, 128.31, 128.13, 128.12, 128.11, 128.10, 127.70, 126.15, 124.40 (x2), 64.48, 63.89 (x2), 35.69 (x2), 35.60, 35.58, 35.58, 35.41, 34.51, 34.50, 31.58 (x2), 21.32.

HRMS (ESI-ToF): *m/z* calculated for $C_{262}H_{278}S_9$: 3734.9138 $[M+Na]^+$; found: 3734.9132 $[M+Na]^+$.

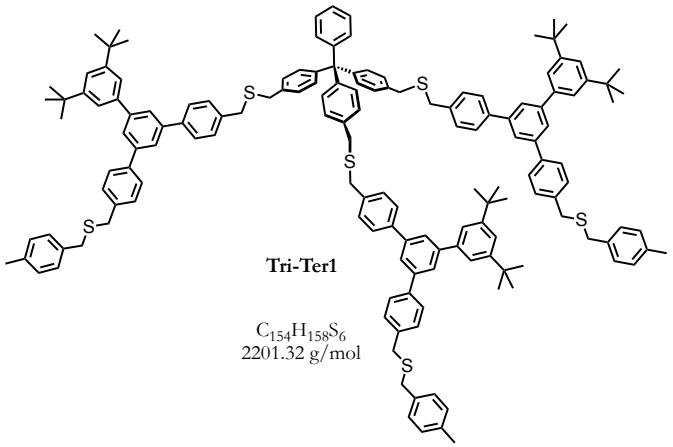

Tri-Ter1

$C_{154}H_{158}S_6$
2201.32 g/mol

Tridentate monoterphenyl derivative (Tri-Ter1): In a dry, degassed 25 ml one-necked flask, compound **60** (20 mg, 330 µmol) and thiol-derivative **26** (71.9 mg, 117 µmol) were dissolved in dry THF (5 ml). After degassing the mixture with argon for 15 minutes, sodium hydride (60 % dispersed in mineral oil, 13.4 mg, 334 µmol) was added. The mixture was allowed to stir at room temperature for 2 hours, after which time the reaction was quenched upon addition of water. The aqueous phase was extracted with MTBE. The combined organic phases were dried over Na_2SO_4, and evaporated to dryness. The product **Tri-Ter1** was afforded by a short column chromatography eluting with *c*-hexane/EtOAc (1:1) and subsequent automated recyclable GPC as a yellowish oil (44.0 mg, 61 %).

^{1}H NMR (400 MHz, Chloroform-*d*): δ 7.75 (dt, *J* = 2.3, 1.3 Hz, 9H), 7.68 – 7.62 (m, 11H), 7.49 (s, 9H), 7.42 – 7.37 (m, 12H), 7.25 – 7.11 (m, 30H), 3.71 – 3.61 (m, 24H), 2.35 (s, 9H), 1.40 (s, 54H).

MS (MALDI-ToF, positive): broad peak at *m/z* 2224 $[M+Na]^+$.

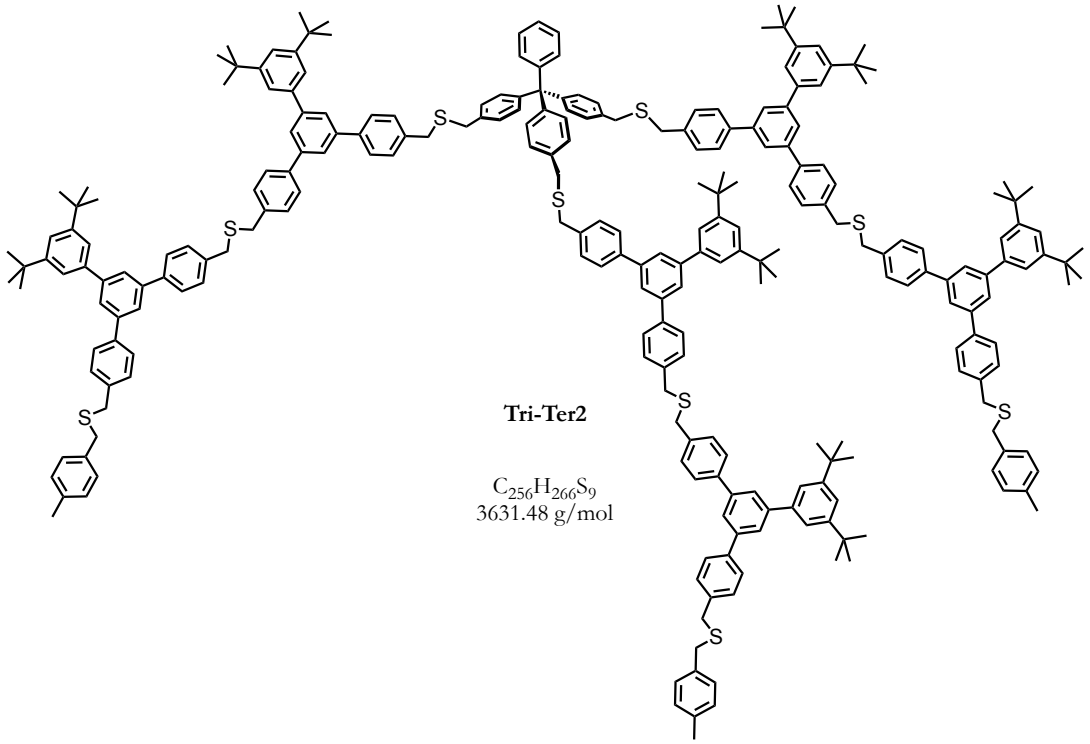

Tri-Ter2

$C_{256}H_{266}S_9$
3631.48 g/mol

Tridentate diterphenyl derivative (Tri-Ter2): In a dry, degassed 25 ml one-necked flask, compound **60** (20.0 mg, 330 µmol) and thiol-derivative **28** (71.9 mg, 0.117 mol) were dissolved in dry THF (5 ml). After degassing the mixture with argon for 15 minutes, sodium hydride (60 % dispersed in mineral oil, 13.4 mg, 334 µmol) was added. The mixture was allowed to stir at room temperature for 2 hours, after which time the reaction was quenched upon addition of water. The aqueous phase was extracted with MTBE (3 x 20 ml). The combined organic phases were dried over Na_2SO_4, and evaporated to dryness. The product **Tri-Ter2** was afforded by a short column chromatography eluting with *c*-hexane/EtOAc (1:1) and subsequent automated recyclable GPC as a yellowish oil (44.0 mg, 61 %).

^{1}H NMR (400 MHz, Chloroform-*d*): δ 7.78 (ddt, *J* = 7.2, 5.6, 1.7 Hz, 18H), 7.72 – 7.64 (m, 24H), 7.54 – 7.38 (m, 44H), 7.25 – 7.18 (m, 23H), 7.17 – 7.13 (m, 6H), 3.78 – 3.62 (m, 36H), 2.36 (s, 9H), 1.42 (s, 54H), 1.41 (s, 54H).

MS (MALDI-ToF, positive): broad peak at *m/z* 3652 $[M+Na]^+$.

7.2.6 **Cage**-Ligands

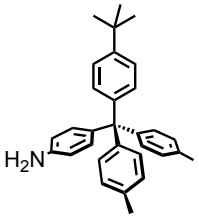

61

$C_{31}H_{33}N$
419.61 g/mol

(Bis(*p*-tolyl)-(4-(*tert*-butyl)phenyl)methyl)-*p*-aniline (61): To a 250 ml two-necked flask, distilled aniline (5.57 g, 59.9 mmol) was added and dissolved in concentrated hydrochloric acid (4 ml) and glacial acetic acid (50 ml). Precursor **29** (4.33 g, 12.6 mmol) was added portion-wise. The mixture was heated to 140 °C and refluxed for 15 hours under vigorous stirring, then allowed to cool to room temperature. The volatile was evaporated by reduced pressure and the remaining solid was dissolved in DCM and neutralized with aqueous 1 M NaOH. The organic phase was washed three times with water, dried over magnesium sulfate, and the solvent was evaporated. The crude product was subjected twice to column chromatography eluting first with *n*-hexane/EtOAc (1:1; with 1 % Et_3N) and then with *n*-hexane/DCM (1:1; with 1 % Et_3N) to afford compound **61** as a white solid (2.59 g, 49 %).

^{1}H NMR (400 MHz, Chloroform-*d*): δ 7.21 (m, 2H), 7.11 – 7.06 (m, 6H), 7.02 (m, 4H), 6.98 – 6.94 (m, 2H), 6.58 – 6.53 (m, 2H), 3.57 (s, 2H), 2.30 (s, 6H), 1.29 (s, 9H).

^{13}C NMR (101 MHz, Chloroform-*d*): δ 148.20, 144.69, 144.39, 143.93, 137.59, 135.00, 132.02, 131.02, 130.66, 127.99, 124.14, 114.11, 63.19, 34.32, 31.43, 20.96.

GC-MS (EI, 70 eV): *m*/*z* (%) = 420.2 (14), 419.2 (40), 329.1 (27), 328.1 (100), 287.1 (12), 286.1 (45).

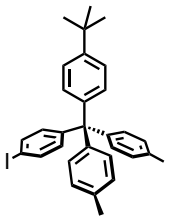

62

$C_{31}H_{31}I$
530.49 g/mol

(Di-(*p*-tolyl)-(4-(*tert*-butyl)phenyl)methyl)-*p*-iodobenzene (62): To a dry, degassed 250 ml two-necked flask, BF_3OEt_2 (573 µl, 9.54 mmol) was added and cooled to -10 °C. Precursor **61** (950 mg, 4.77 mmol) dissolved in DCM (50 ml) was added dropwise through a transfer needle. The mixture was stirred for 2 hours at -10 °C at which time the same procedure was repeated with $^tBuNO_2$ (474 µl, 8.35 mmol). After addition of potassium iodide (563 mg, 7.15 mmol) and iodine (4.93 mg, 6.20 mmol), the mixture was allowed to gradually heat up to room temperature and was then stirred for 20 hours. The reaction mixture was quenched with a saturated aqueous solution of sodium thiosulfate and the aqueous phase was extracted with MTBE. The combined organic phases were washed twice with water, dried over magnesium sulfate and the volatile evaporated by rotavapor. The crude product was subjected to column chromatography eluting with *c*-hexane/EtOAc (50:1) to yield compound **62** as a white solid (663 mg, 55 %).

^{1}H NMR (400 MHz, Chloroform-*d*): δ 7.56 – 7.51 (m, 2H), 7.25 – 7.20 (m, 2H), 7.09 – 7.02 (m, 10H), 6.99 – 6.94 (m, 2H), 2.31 (s, 6H), 1.29 (s, 9H).

^{13}C NMR (101 MHz, Chloroform-*d*): δ 148.64, 147.36, 143.71, 143.41, 136.45, 135.45, 133.24, 130.90, 130.57, 128.26, 124.42, 91.57, 63.70, 34.37, 31.42, 20.98.

GC-MS (EI, 70 eV): *m*/*z* (%) = 530.95 (17.4), 529.95 (43.3), 440 (25.2), 438.95 (100), 396.9 (42.33), 328.1 (30.05), 327.1 (89.5), 281 (29.95), 255 (19.58), 252.9 (18.03), 207.9 (17.73), 206.95 (69.92), 191 (15.79), 179 (16.49), 178 (15.7), 78 (25.11), 57.1 (29.26).

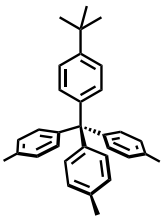

63

$C_{32}H_{34}$
418.62 g/mol

Tris(*p*-tolyl)-(4-(*tert*-butyl)phenyl)methane (63): To a dry, degassed 25 ml Schlenk tube, precursor **62** (672 mg, 1.27 mmol) was added, dissolved in 5 ml dry, degassed THF and cooled to -78 °C. After addition of methyl lithium (1.6 M in diethyl ether, 1.10 ml, 45.8 mmol), the mixture was allowed to slowly heat up to room temperature and was then stirred for 2 hours. The reaction mixture was quenched with water, and extracted three times with MTBE. The combined organic phases were washed twice with water, dried over magnesium sulfate, and the solvent was evaporated by reduced pressure to yield compound **63** as a pale yellowish solid (430 mg, 81 %).

^{1}H NMR (400 MHz, Chloroform-*d*): δ 7.24 – 7.20 (m, 2H), 7.12 – 7.07 (m, 8H), 7.05 – 7.01 (m, 6H), 2.30 (s, 9H), 1.29 (s, 9H).

^{13}C NMR (101 MHz, Chloroform-*d*): δ 148.27, 144.40, 144.08, 135.09, 131.00, 130.63, 128.03, 124.18, 63.55, 34.31, 31.39, 20.94.

GC-MS (EI, 70 eV): *m*/*z* (%) = 418.1 (22), 328.1 (26), 327.1 (100), 285.1 (36), 269.1 (11), 193.0 (11), 179.1 (11).

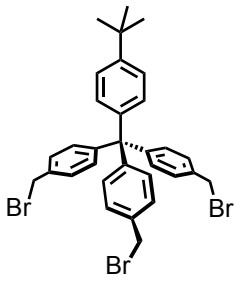

64

$C_{32}H_{31}Br_3$
655.31 g/mol

Tris(4-((bromomethyl)phenyl))-(4-(*tert*-butyl)phenyl)methane (64): A dry, degassed 500 ml two-neck flask was equipped with a reflux condenser and a glass stopper. Compound **63** (310 mg, 740 µmol), *N*-bromosuccinimide (791 mg, 4.45 mmol) and AIBN (6.20 mg, 370 µmol) were suspended in 50 ml methyl formate under argon atmosphere. The suspension was degassed with argon for 30 minutes, then illuminated with a 500 W halogen lamp. The mixture was refluxed for 15 hours and then allowed to cool to room temperature. The crude precipitate was concentrated, and redissolved in DCM. The solution was washed four times with water, dried over $MgSO_4$, and the solvent was evaporated *in vacuo*. The crude product was subjected to automated column chromatography starting with *c*-hexane/DCM (20:1) and switched to *c*-hexane/DCM (10:1) after 4 column volumina, to give compound **64** as a white solid (315 mg, 65 %).

^{1}H NMR (400 MHz, Chloroform-*d*): δ 7.31 – 7.22 (m, 8H), 7.21 – 7.15 (m, 6H), 7.10 – 7.04 (m, 2H), 4.48 (s, 6H), 1.30 (s, 9H).

^{13}C NMR (101 MHz, Chloroform-*d*): δ 149.11, 146.98, 142.80, 135.54, 131.49, 130.61, 128.43, 124.73, 64.24, 34.51, 33.42, 31.47.

MS (MALDI-ToF, positive): *m*/*z* 652.31.

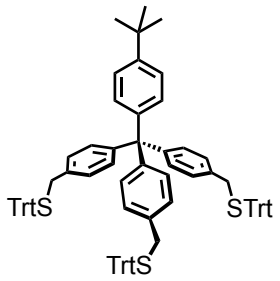

65

$C_{89}H_{76}S_3$
1241.77 g/mol

((((4-(*tert*-Butyl)phenyl)methanetriyl)tris(benzene-4,1-diyl))tris(methylene))tris(tritylsulfane) (65): Compound **64** (603 mg, 920 µmol) and trityl thiol (1.05 g, 3.68 mmol) were dissolved in dry degassed THF (30 ml) under an atmosphere of argon. Sodium hydride (60 % in mineral oil, 737 mg, 18.4 mmol) was added and the mixture was stirred at room temperature for 15 hours. The reaction was quenched with water and extracted with MTBE. The combined organic fractions were washed with brine, dried over magnesium sulfate, filtered and evaporated to dryness. After purification by flash column chromatography eluting with *c*-hexane/DCM (3:1) compound **65** was obtained as colorless foam (1.01 g, 88 %).

^{1}H NMR (400 MHz, Chloroform-*d*): δ 7.50 – 7.40 (m, 17H), 7.32 – 7.24 (m, 20H), 7.23 – 7.14 (m, 11H), 7.04 – 6.92 (m, 13H), 3.25 (s, 6H), 1.27 (s, 9H).

^{13}C NMR (101 MHz, Chloroform-*d*): δ 148.44, 145.67, 144.69, 143.36, 134.38, 131.05, 130.49, 129.64, 128.13, 127.91, 126.67, 124.27, 67.42, 36.57, 34.28, 31.34, 26.93.

MS (MALDI-ToF, positive): *m*/*z* 1241.11.

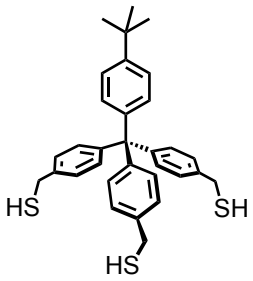

66

$C_{32}H_{34}S_3$
514.80 g/mol

(((4-(*tert*-Butyl)phenyl)methanetriyl)tris(benzene-4,1-diyl))trimethanethiol (66): The trityl-protected derivative **65** (500 mg, 403 µmol,) was dissolved in dry DCM (20 ml). Triethylsilane (390 µl, 2.42 mmol) was added, followed by trifluoroacetic acid (800 µl, 4 % of the dichloromethane volume). The mixture turned yellow and became colorless again after 1 minute. Stirring was continued for further 60 minutes, then the reaction was quenched with a saturated aqueous solution of sodium bicarbonate. The two phases were separated and the aqueous phase was extracted with dichloromethane. The combined organic fractions were dried over magnesium sulfate, filtrated and evaporated to dryness. The crude was purified by column chromatography eluting with *c*-hexane/DCM (1:2) to give the compound **66** as a white solid (189 mg, 91 %).

^{1}H NMR (400 MHz, Chloroform-*d*): δ 7.23 (d, *J* = 8.6 Hz, 2H), 7.19 (d, *J* = 8.5 Hz, 6H), 7.14 (d, *J* = 8.5 Hz, 6H), 7.08 (d, *J* = 8.6 Hz, 2H), 3.72 (d, *J* = 7.5 Hz, 6H), 1.77 (t, *J* = 7.5 Hz, 3H), 1.30 (s, 9H).

^{13}C NMR (101 MHz, Chloroform-*d*): δ 148.67, 145.70, 143.27, 138.50, 130.54, 127.10, 124.39, 63.82, 34.33, 31.35, 28.50.

MS (MALDI-ToF, negative): *m*/*z* 511.49.

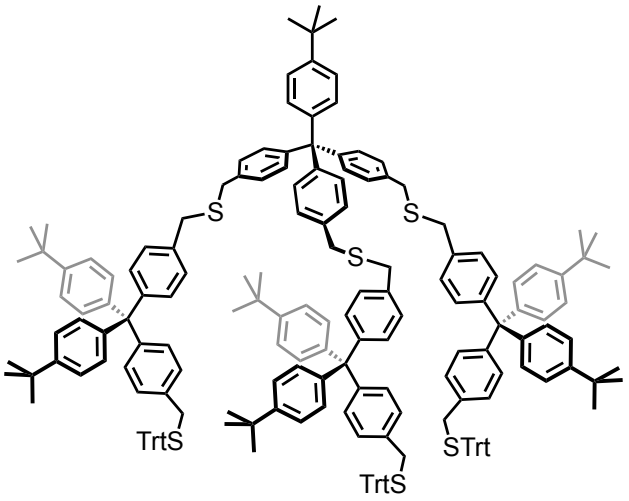

67

$C_{194}H_{190}S_6$
2714.01 g/mol

Compound 67: Compound **37** (164 mg, 200 µmol) and thiol-precursor **66** (25.9 mg, 50.0 µmol) were dissolved in dry THF (5 ml) under an atmosphere of argon. Sodium hydride (60 % in mineral oil, 60.4 mg, 1.51 mmol) was added and the mixture was stirred for 5 hours at room temperature. The reaction was quenched with water and extracted with MTBE. The combined organic fractions were washed with brine, dried over magnesium sulfate, filtrated and evaporated to dryness. Purification of the crude product was achieved by short column chromatography eluting with *c*-hexane/EtOAc (1:1) followed by automated recyclable GPC to yield the trityl-protected derivative **67** as a colorless foam (83.2 mg, 61 %).

^{1}H NMR (400 MHz, Chloroform-*d*): δ 7.48 – 7.41 (m, 17H), 7.30 – 7.23 (m, 22H), 7.22 – 7.16 (m, 22H), 7.12 (s, 11H), 7.10 (s, 11H), 7.08 – 7.03 (m, 20H), 7.01 – 6.96 (m, 6H), 3.57 (s, 12H), 3.26 (s, 6H), 1.27 (s, 63H).

^{13}C NMR (101 MHz, Chloroform-*d*): δ 148.54, 146.08, 146.03, 145.79, 144.83, 143.75, 135.71, 135.49, 134.43, 131.37, 131.32, 130.76, 129.76, 128.21, 128.17, 128.05, 128.02, 126.80, 124.46, 124.32, 77.36, 67.51, 63.80, 36.75, 35.55, 35.51, 34.42, 31.51.

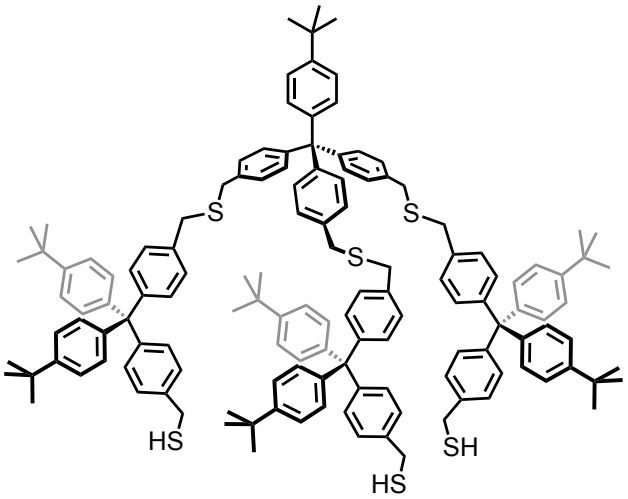

68

$C_{137}H_{148}S_6$
1987.05 g/mol

Compound 68: The trityl-protected derivative **67** (78.2 mg, 28.8 µmol,) was dissolved in dry DCM (2 ml). Triethylsilane (20.9 µl, 130 µmol) was added, followed by trifluoroacetic acid (80 µl, 4 % of the dichloromethane volume). The mixture turned yellow and became colorless again after 30 seconds. Stirring was continued for further 60 minutes, then the reaction was quenched with a saturated aqueous solution of sodium bicarbonate. The two phases were separated and the aqueous phase was extracted with dichloromethane. The combined organic fractions were dried over magnesium sulfate, filtrated and evaporated to dryness. The crude was purified by column chromatography eluting with *c*-hexane/DCM (1:3) to give the compound **68** as a colorless solid (48.6 mg, 85 %).

^{1}H NMR (400 MHz, Chloroform-*d*): δ 7.39 (s, 1H), 7.37 – 7.33 (m, 15H), 7.32 – 7.24 (m, 31H), 7.23 – 7.18 (m, 15H), 3.83 (d, *J* = 7.5 Hz, 6H), 3.72 (s, 6H), 3.72 (s, 6H), 1.88 (t, *J* = 7.5 Hz, 3H), 1.42 (s, 63H).

^{13}C NMR (101 MHz, Chloroform-*d*) δ 148.50, 146.00, 145.88, 145.67, 143.58, 138.35, 135.56, 135.42, 131.41, 131.26, 131.17, 130.65, 128.05, 127.93, 126.95, 124.23, 63.89, 63.67, 35.43, 34.31, 31.38, 29.72, 28.53.

MS (MALDI-ToF, negative): *m*/*z* 1984.21.

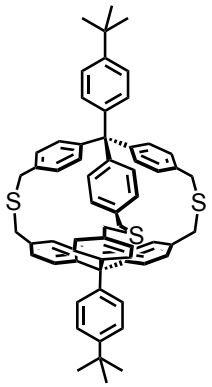

Cage-0

$C_{64}H_{62}S_3$
927.38 g/mol

Cage-derivative (Cage-0): Bromine-precursor **64** (38.2 mg, 58.3 µmol) and thiol-precursor **66** (30.0 mg, 58.3 µmol) were dissolved in dry degassed THF (60 ml) under an atmosphere of argon and the reaction mixture was degassed for 15 minutes. Sodium hydride (60 % in mineral oil, 21 mg, 0.86 mmol) was added and the mixture was stirred for 15 hours at room temperature. The reaction was quenched with water and extracted with MTBE. The combined organic fractions were washed with brine, dried over magnesium sulfate, filtrated and evaporated to dryness. Purification of the crude product was achieved by short column chromatography eluting with *c*-hexane/EtOAc (1:1) followed by automated recyclable GPC to yield **Cage-0** as a colorless solid (33.0 mg, 61 %).

^{1}H NMR (250 MHz, Chloroform-*d*): δ 7.21 (d, *J* = 8.6 Hz, 4H), 7.04 (d, *J* = 8.6 Hz, 4H), 6.83 (d, *J* = 8.4 Hz, 12H), 6.76 (d, *J* = 8.5 Hz, 12H), 3.81 (s, 12H), 1.28 (s, 18H).

^{13}C NMR (101 MHz, Chloroform-*d*): δ 148.69, 145.54, 142.79, 137.53, 131.10, 130.69, 127.72, 124.13, 63.60, 38.38, 31.33, 29.72.

MS (MALDI-ToF, positive): broad peak at *m*/*z* 950 $[M+Na]^+$, *m*/*z* 966 $[M+K]^+$.

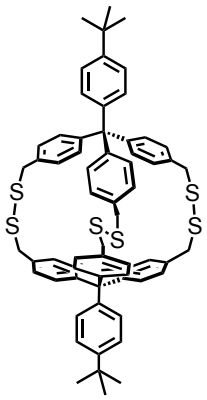

Cage-S

$C_{64}H_{62}S_6$
1023.56 g/mol

Cage-derivative (Cage-SS): Thiol-precursor **66** (60.0 mg, 117 μmol) was dissolved in dry THF (50 ml) under ambient conditions. Sodium hydride (60 % in mineral oil, 56.2 mg, 2.34 mmol) was added and the mixture was stirred vigorously for 15 hours at room temperature. The reaction was quenched with water and extracted with MTBE. The combined organic fractions were washed with brine, dried over magnesium sulfate, filtrated and evaporated to dryness. Purification of the crude product was achieved by a short column chromatography eluting with *c*-hexane/EtOAc (1:1) followed by automated recyclable GPC to yield **Cage-SS** as a white solid (15.5 mg, 52 %).

^{1}H NMR (400 MHz, Chloroform-*d*): δ 7.13 (dd, *J* = 8.2, 3.2 Hz, 6H), 7.01 – 6.88 (m, 26H), 3.68 (s, 12H), 1.30 (s, 18H).

^{13}C NMR (101 MHz, Chloroform-*d*): δ 148.29, 145.11, 142.43, 137.23, 131.99, 130.59, 127.12, 124.14, 63.61, 38.33, 31.38, 29.76.

MS (MALDI-ToF, positive): broad peak at *m*/*z* 1046 $[M+Na]^+$, *m*/*z* 1062 $[M+K]^+$.

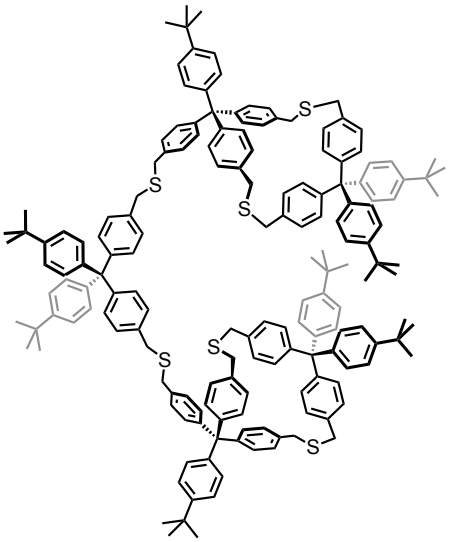

Cage-TPM-p

$C_{169}H_{176}S_6$
2399.63 g/mol

Pseudo cage-derivative (Cage-TPM-p): Bromine-precursor **64** (100 mg, 153 µmol) and thiol-precursor **36** (50.0 mg, 229 µmol) were dissolved in dry degassed THF (5 ml) under an atmosphere of argon and the reaction mixture was degassed for 15 minutes. Sodium hydride (60 % in mineral oil, 91.6 mg, 229 µmol) was added and the mixture was stirred for 15 hours at room temperature. The reaction was quenched with water and extracted with MTBE. The combined organic fractions were washed with brine, dried over magnesium sulfate, filtrated and evaporated to dryness. Purification of the crude product was achieved by short column chromatography eluting with *c*-hexane/EtOAc (1:1) followed by automated recyclable GPC to yield **Cage-TPM-p** as a colorless foam (44.0 mg, 24 %).

^{1}H NMR (400 MHz, Chloroform-*d*): δ 7.26 – 7.20 (m, 16H), 7.16 – 7.13 (m, 14H), 7.11 – 7.02 (m, 34H), 6.93 – 6.88 (m, 16H), 3.64 (s, 8H), 3.64 (s, 8H), 3.60 (s, 8H), 1.31 (s, 18H), 1.30 (s, 18H), 1.29 (s, 36H).

MS (MALDI-ToF, positive): broad peak at *m*/*z* 2422 $[M+Na]^+$, *m*/*z* 2438 $[M+K]^+$, *m*/*z* 2532 $[M+Cs]^+$.

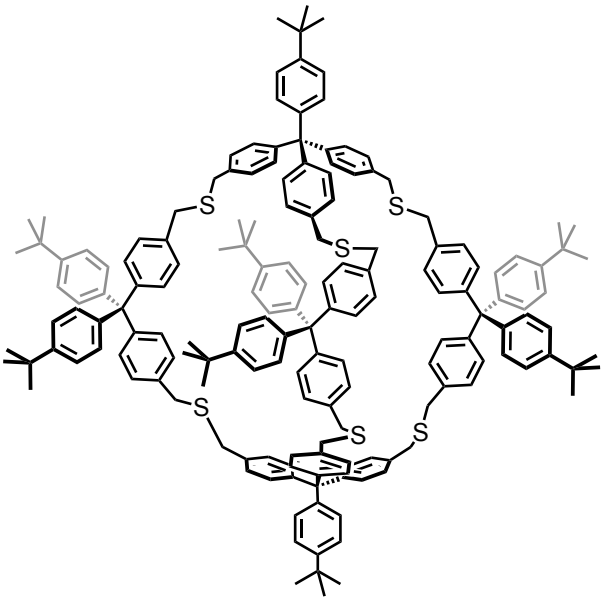

Cage-TPM

$C_{169}H_{176}S_6$
2399.63 g/mol

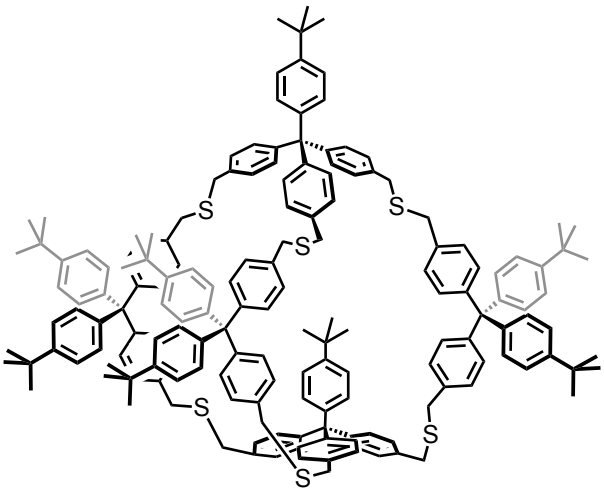

Cage-TPM-i

$C_{169}H_{176}S_6$
2399.63 g/mol

Mixture of Cage-TPM and Cage-TPM-i: Bromo-precursor **64** (6.62 mg, 10.1 µmol) and thiol-precursor **68** (20.1 mg, 10.1 µmol) were dissolved in dry degassed THF (50 ml) under an atmosphere of argon and the reaction mixture was degassed for 15 minutes. Sodium hydride (60 % in mineral oil, 24.2 mg, 606 µmol) was added and the mixture was stirred for 15 hours at room temperature. The reaction was quenched with water and extracted with MTBE. The combined organic fractions were washed with brine, dried over magnesium sulfate, filtrated and evaporated to dryness. Purification of the crude product was achieved by short column chromatography eluting with *c*-hexane/EtOAc (1:1) followed by automated recyclable GPC to yield a mixture of **Cage-TPM** and **Cage-TPM-i** as a colorless solid (10.4 mg, 43 %).

^{1}H NMR (600 MHz, Tetrachloroethane-d_2): δ 7.19 – 7.08 (m, 32H), 7.08 – 6.82 (m, 128H), 3.56 – 3.35 (m, 48H), 1.23 – 1.15 (m, 144H).

^{13}C NMR (151 MHz, Tetrachloroethane-d_2): δ 148.90, 148.80, 148.75, 146.21, 146.18, 145.92, 145.89, 143.66, 143.37, 135.74, 135.70, 135.68, 131.52, 131.45, 131.39, 131.29, 130.89, 130.87, 130.80, 128.30, 128.17, 124.62, 124.47, 120.59, 99.78, 80.09, 79.90, 79.72, 64.09, 64.06, 63.87, 63.85, 35.67, 35.53, 34.52, 34.50, 34.49, 31.68, 31.67, 31.63.

MS (MALDI-ToF, positive): broad peak at m/z 2422 $[M+Na]^+$, m/z 2438 $[M+K]^+$, m/z 2532 $[M+Cs]^+$.

8 Appendix

8.1 Linear Terphenyl-Based Ligand Coated Gold Nanoparticles

8.1.1 ^{1}H NMR of **Au-Ter7** and **Au-Ter9**

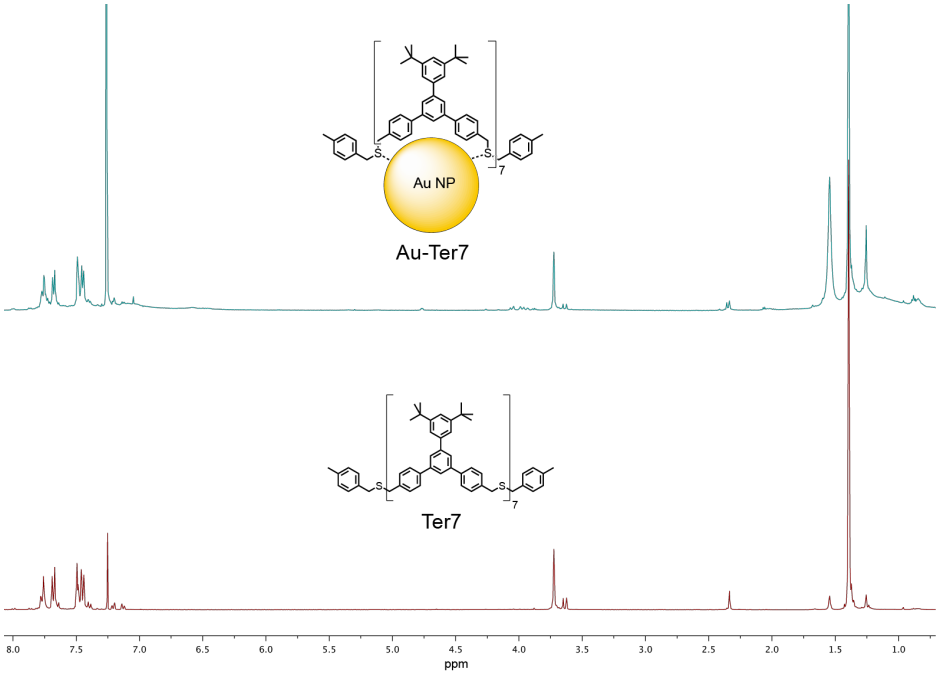

Figure 39: ^{1}H-NMR spectra of **Au-Ter7** (top) and the pure heptamer **Ter7** in chloroform-*d*.

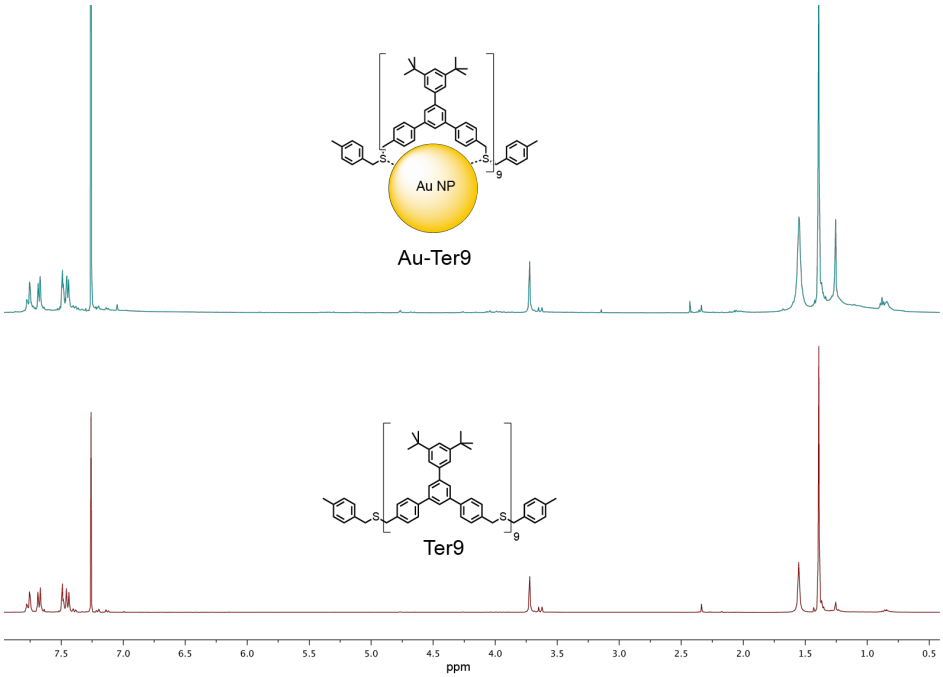

Figure 40: ^{1}H-NMR spectra of **Au-Ter9** (top) and the pure nonamer **Ter9** in chloroform-*d*.

8.1.2 Thermogravimetric Analysis of **Au-Ter7** and **Au-Ter9**

Thermogravimetric analyses (TGA) were performed by Annika Büttner or Cedric Wobill on a *Mettler Toledo TGA/SDTA851*^{e}. The samples were heated from 35 °C to 950 °C with a heating rate of 10 °C/minute. All samples show similar weight loss curves (Figure 41). Decomposition starts at around 200 °C and reaches a plateau at 600 °C. The weight loss is attributed to the decomposition and removal of the organic shell from the nanoparticle surface and the plateau is interpreted as the end of this process, when all the organic coating has been removed. The remaining substances are attributed to the residual gold. The numbers needed for the calculation of the amount of ligands enwrapping one AuNP is summarized in Table 1 for **Au-Ter7** and **Au-Ter9** can be calculated as follows (for **Au-Ter7**): from the TGA analysis the amount of organic ligand (160 µg) and the residual gold (450 µg) are obtained, and thus the resulting amount of substances (n_{Au} $2.28 \cdot 10^{-6}$ mol; n_{Lig} $4.47 \cdot 10^{-8}$ mol) can be calculated. The number of gold atoms present for one ligand is in this case calculated as 51.07, or in other words, 51.07 gold atoms are stabilized by one ligand. The diameter [nm] of **Au-Ter7** is 1.69 nm (obtained from TEM analysis) and therefore the amount of Au-atoms per NP is 149.28 (density of gold: 19.30 g/cm^3). Consequently, the amount of ligands (heptamer **Ter7**) stabilizing an entire AuNP is calculated as 2.92 in the case of **Au-Ter7**.

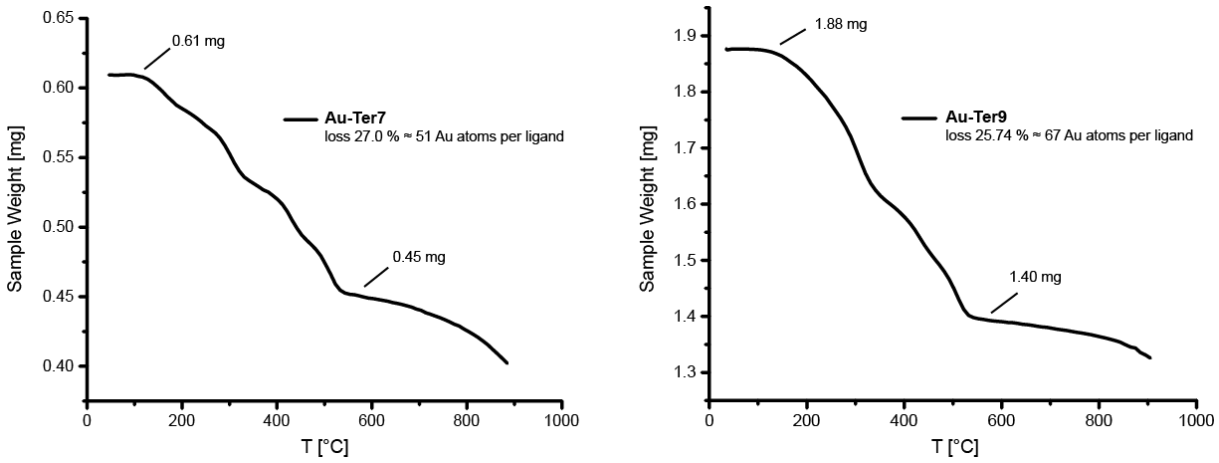

Figure 41: Thermogravimetric analyses of gold nanoparticles **Au-Ter7** (left) and **Au-Ter9** (right).

Table 1: Calculated amount of ligands enwrapping a single NP for **Au-Ter7** and **Au-Ter9**.

	m_{Lig} *[mg]*	M_{Lig} *[g/mol]*	n_{Lig} *[mol]*	m_{Au} *[mg]*	M_{Au} *[g/mol]*	n_{Au} *[mol]*	Au/Lig	AuNP Ø *[nm]*	Au/NP	**Lig/AuNP**
Au-Ter7	0.165	3579.43	4.47E-8	0.449	196.9665	2.283-6	51.07	1.71	149.28	**2.92**
Au-Ter9	1.879	4532.88	1.06E-7	1.399	196.9665	7.101E-6	67.06	1.73	154.64	**2.30**

8.2 Linear Tetraphenylmethane-Based Ligand Coated Gold Nanoparticles

8.2.1 ^{1}H NMR of **Au-TPM3**, **Au-TPM5** and **Au-TPM7**

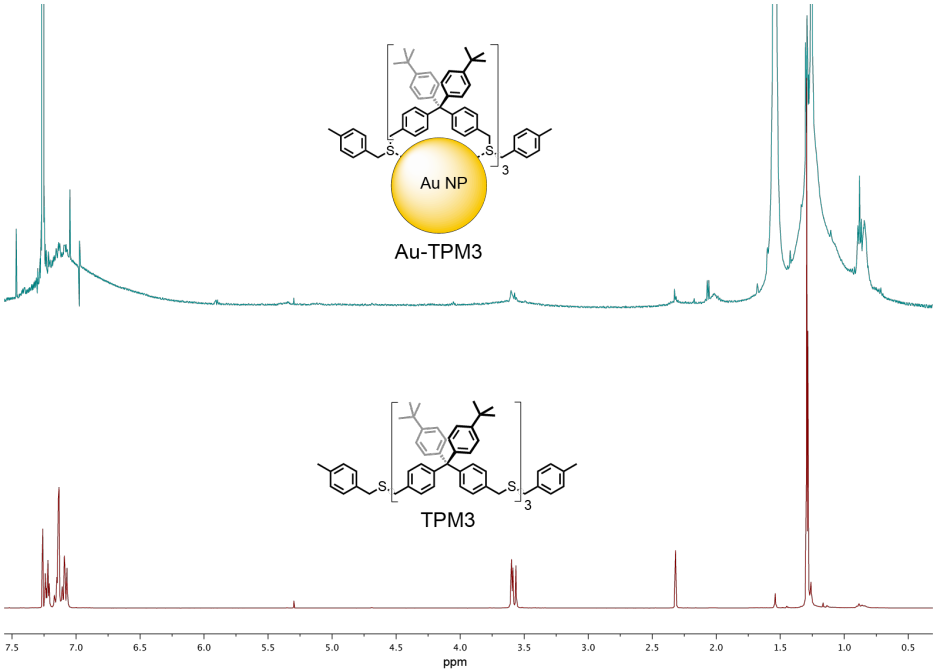

Figure 42: ^{1}H-NMR spectra of **Au-TPM3** (top) and the pure trimer **TPM3** in chloroform-*d*.

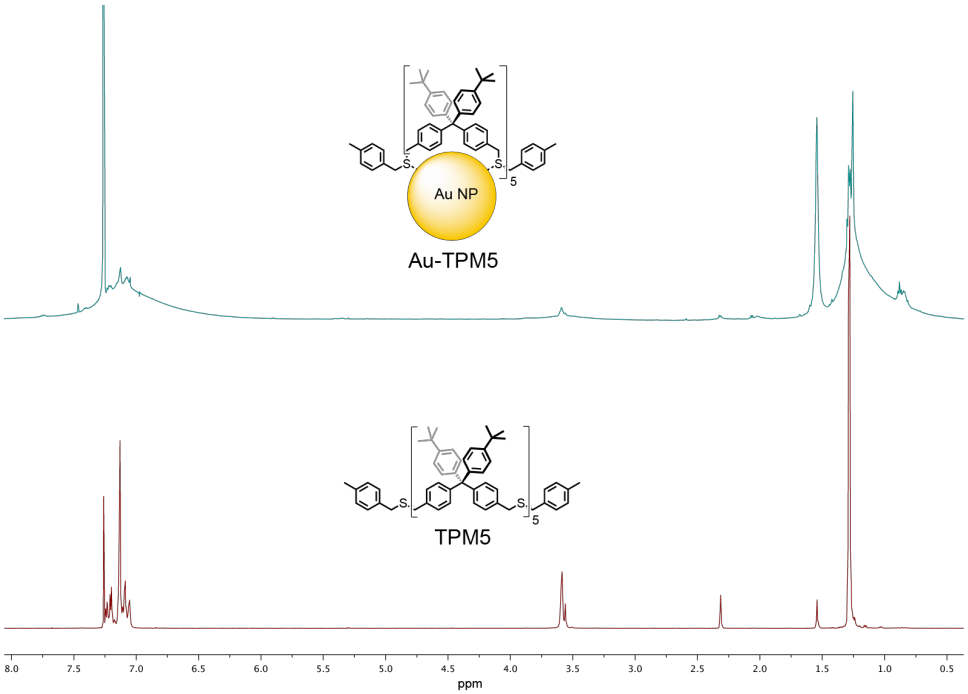

Figure 43: ^{1}H-NMR spectra of **Au-TPM5** (top) and the pure pentamer **TPM5** in chloroform-*d*.

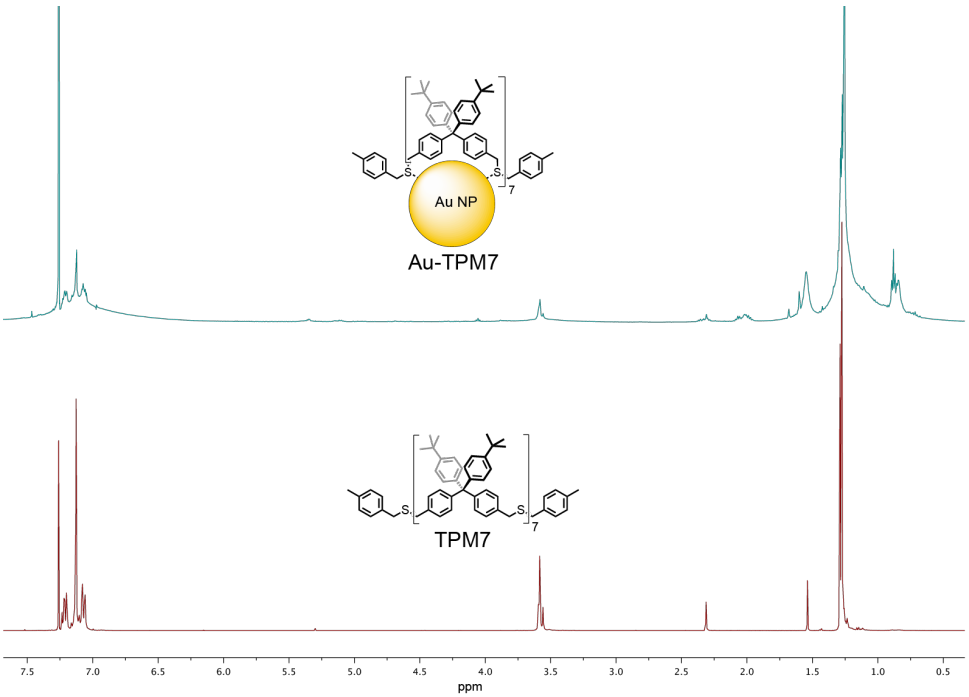

Figure 44: ^{1}H-NMR spectra of **Au-TPM7** (top) and the pure heptamer **TPM7** in chloroform-*d*.

8.2.2 Thermogravimetric Analysis of **Au-TPM3**, **Au-TPM5** and **Au-TPM7**

An explanation and interpretation of the calculation for the TGA-spectra is given under *subchapter 8.1.2* above.

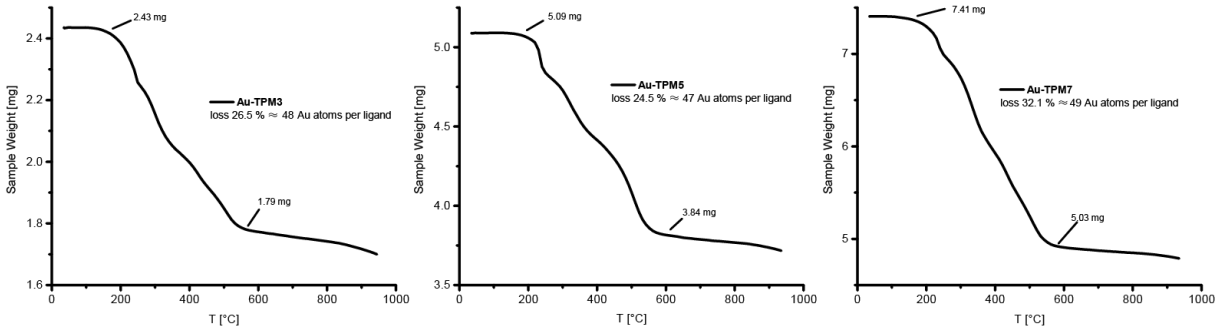

Figure 45: Thermogravimetric analyses of gold nanoparticles **Au-TPM3** (left), **Au-TPM5** (middle) and **Au-TPM7** (right).

Table 2: Calculated amount of ligands enwrapping a single NP for **Au-TPM3**, **Au-TPM5** and **Au-TPM7**.

	m_{Lig} *[mg]*	M_{Lig} *[g/mol]*	n_{Lig} *[mol]*	m_{Au} *[mg]*	M_{Au} *[g/mol]*	n_{Au} *[mol]*	Au/Lig	AuNP ⌀ *[nm]*	Au/NP	**Lig/AuNP**
Au-TPM3	0.646	1714.63	3.76E-7	1.792	196.9665	9.09E-6	24.16	1.16	48.27	**2.00**
Au-TPM5	1.253	2696.13	4.64E-7	3.841	196.9665	1.94E-5	41.96	1.15	47.04	**1.12**
Au-TPM7	2.384	3677.62	6.48E-7	5.030	196.9665	2.55E-5	39.39	1.17	49.53	**1.26**

8.3 Tripodal Dendritic-Based Ligand Coated Gold Nanoparticles

8.3.1 ^{1}H-NMR of **Au-Tri-Xyl2**, **Au-Tri-TPM1** and **Au-Tri-TPM2**

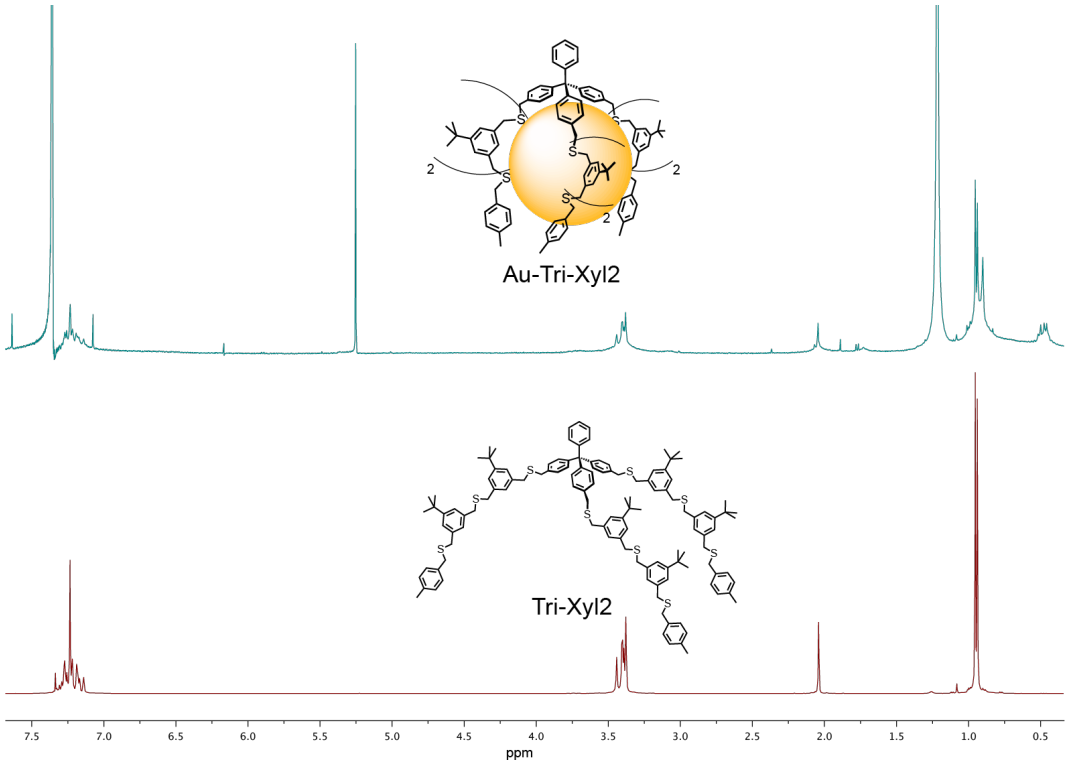

Figure 46: ^{1}H-NMR spectra of **Au-Tri-Xyl2** (top) and the pure ligand **Tri-Xyl2** in chloroform-*d*.

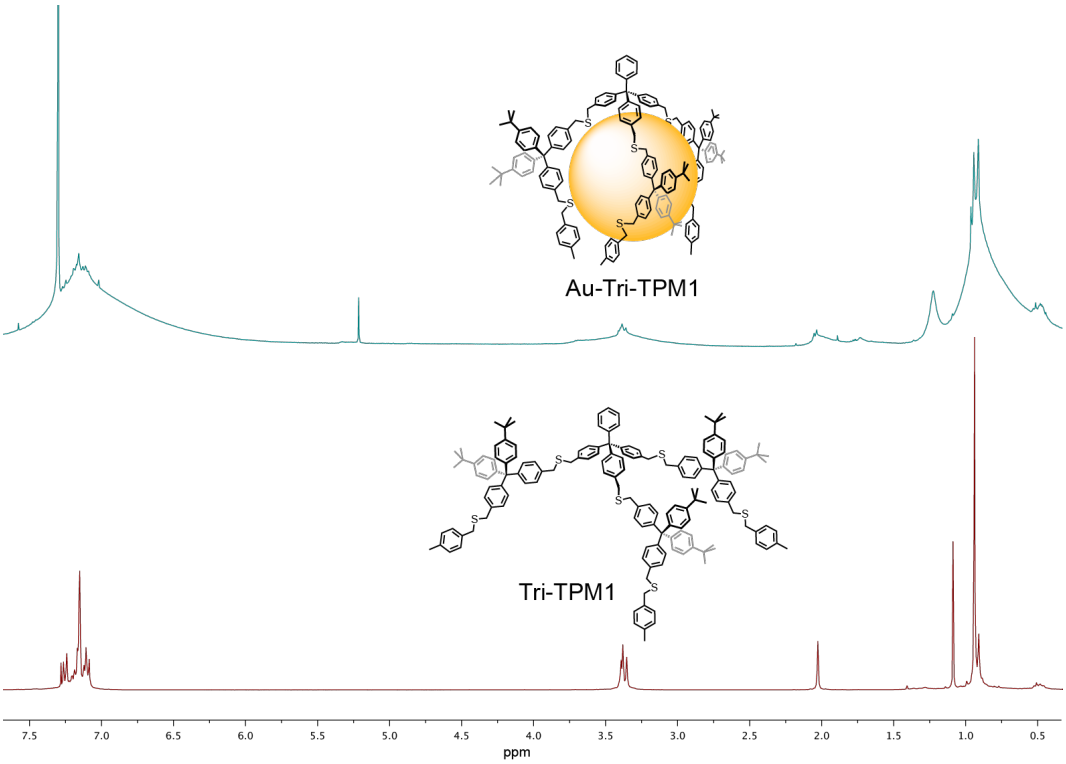

Figure 47: ^{1}H-NMR spectra of **Au-Tri-TPM1** (top) and the pure ligand **Tri-TPM1** in chloroform-*d*.

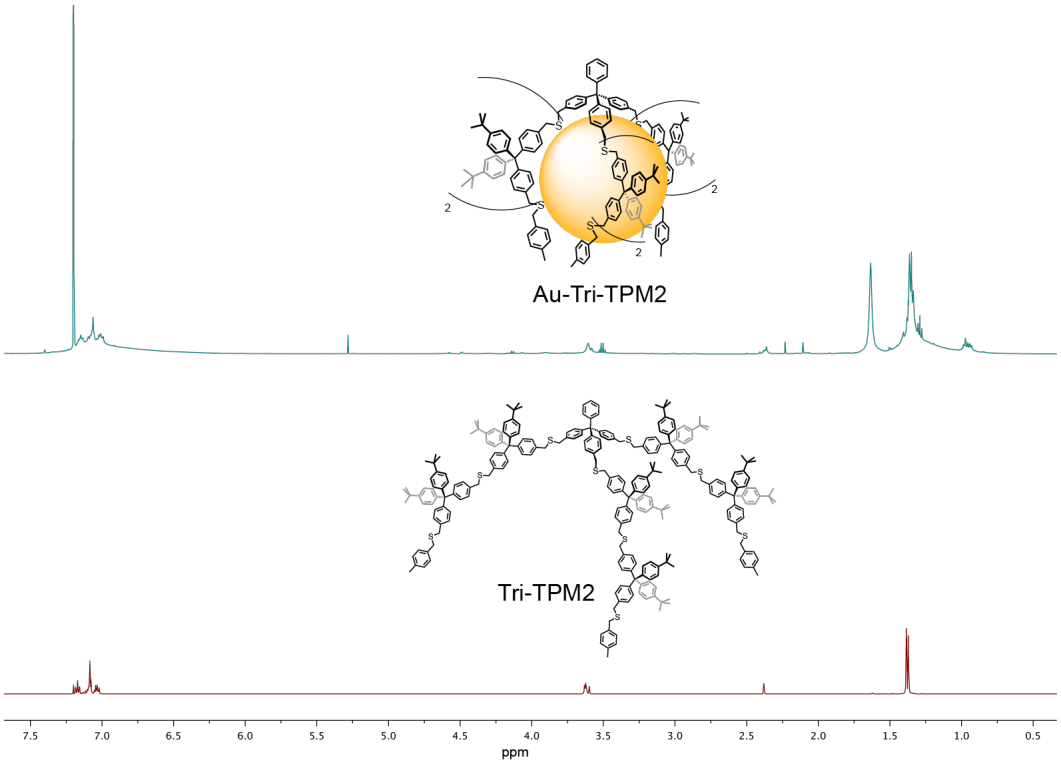

Figure 48: ^{1}H-NMR spectra of **Au-Tri-TPM2** (top) and the pure ligand **Tri-TPM2** in chloroform-*d*.

8.3.2 Thermogravimetric Analysis of **Au-Tri-Xyl2**, **Au-Tri-TPM1** and **Au-Tri-TPM2**

An explanation and interpretation of the calculation for the TGA-spectra is given under *subchapter 8.1.2* above.

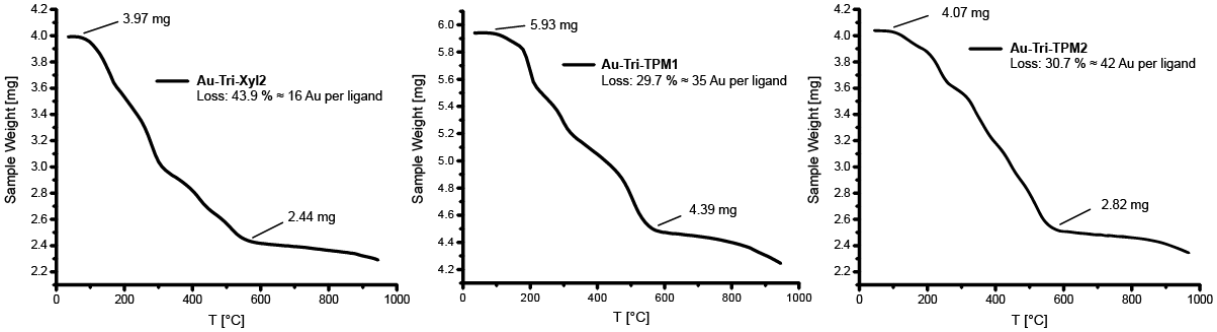

Figure 49: Thermogravimetric analyses of gold nanoparticles **Au-Tri-Xyl2** (left), **Au-Tri-TPM1** (middle) and **Au-Tri-TPM2** (right).

Table 3: Calculated amount of ligands enwrapping a single NP for **Au-Tri-Xyl1**, **Au-Tri-TPM1** and **Au-Tri-TPM2**.

	m_{Lig} *[mg]*	M_{Lig} *[g/mol]*	n_{Lig} *[mol]*	m_{Au} *[mg]*	M_{Au} *[g/mol]*	n_{Au} *[mol]*	Au/Lig	AuNP ⌀ *[nm]*	Au/NP	**Lig/AuNP**
Au-Tri-Xyl2	1.53	1925.07	7.94E-7	2.44	196.9665	1.23E-5	15.51	1.24	58.97	**3.97**
Au-Tri-TPM1	1.45	2243.40	6.46E-7	4.48	196.9665	2.26E-5	35.06	1.05	35.80	**1.02**
Au-Tri-TPM2	2.56	3715.65	6.90E-7	4.07	196.9665	2.05E-5	42.35	1.17	49.53	**1.17**

8.4 Tripodal Tetraphenylmethane-Based Cages

8.4.1 ^{1}H-NMR of the mixture **Au-Cage-TPM** and **Au-Cage-TPM-i**

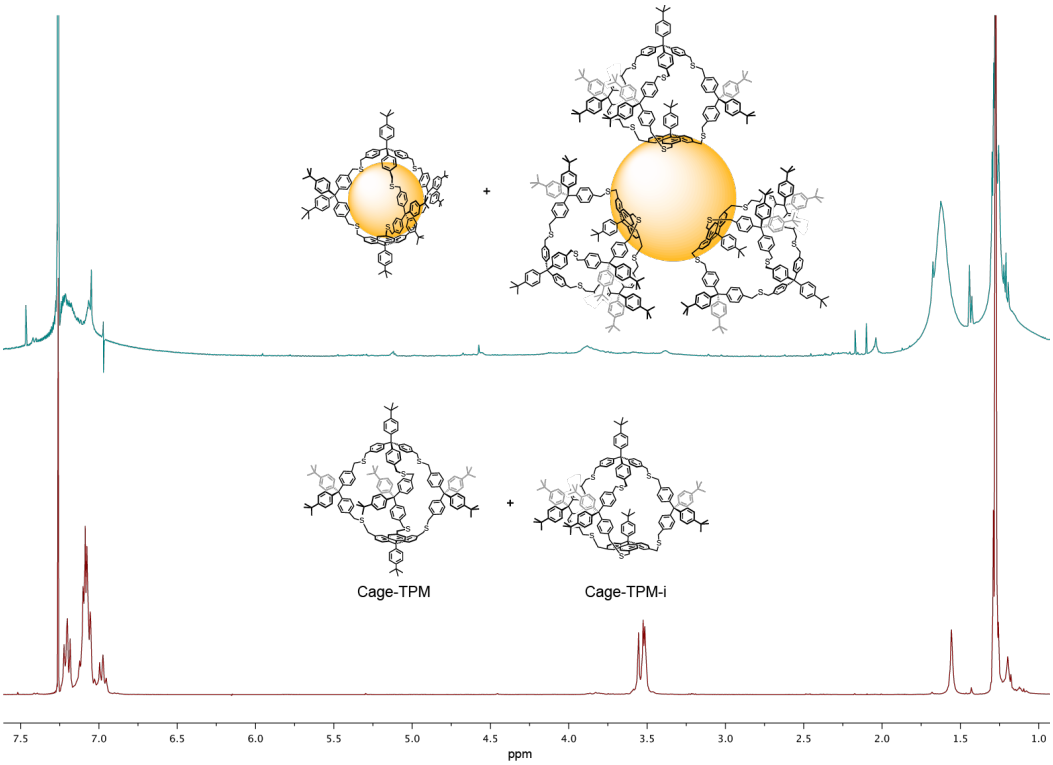

Figure 50: ^{1}H-NMR spectra of the mixture of **Au-Cage-TPM** and **Au-Cage-TPM-i** (top) and the ligands in chloroform-*d*.

8.4.2 Thermogravimetric analysis of the mixture **Au-Cage-TPM** and **Au-Cage-TPM-i**

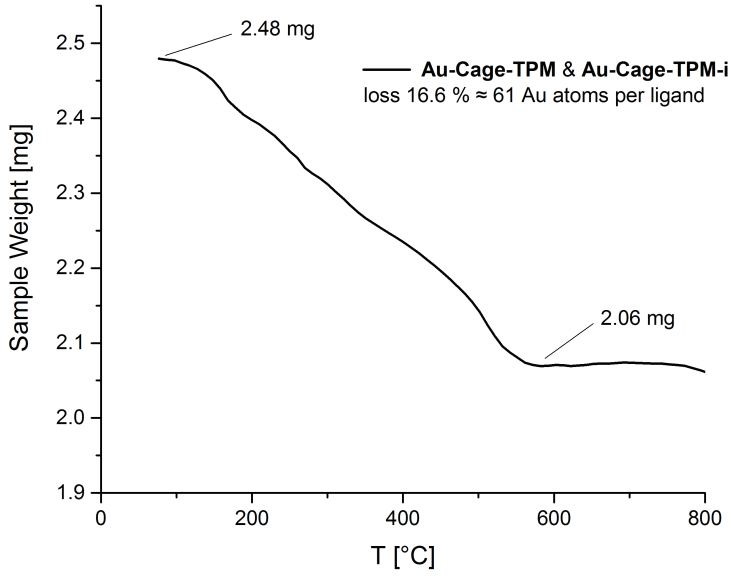

Figure 51: Thermogravimetric analyses of gold nanoparticles mixture of **Au-Cage-TPM** and **Au-Cage-TPM-i**.

Table 4: Calculated amount of ligands enwrapping a single NP for the mixture of **Au-Cage-TPM** and **Au-Cage-TPM-i**.

	m_{Lig} *[mg]*	M_{Lig} *[g/mol]*	n_{Lig} *[mol]*	m_{Au} *[mg]*	M_{Au} *[g/mol]*	n_{Au} *[mol]*	Au/Lig	AuNP ⌀ *[nm]*	Au/NP	**Lig/AuNP**
Mix	0.412	2399.63	1.71E-7	2.068	196.9665	1.05E-5	61.18	2.37	411.71	**6.72**

8.5 Size Control Study with 3 Ligands

8.5.1 ^{1}H-NMR of **Au-TPM7-16**, **Au-TPM7-32** and **Au-TPM7-64**

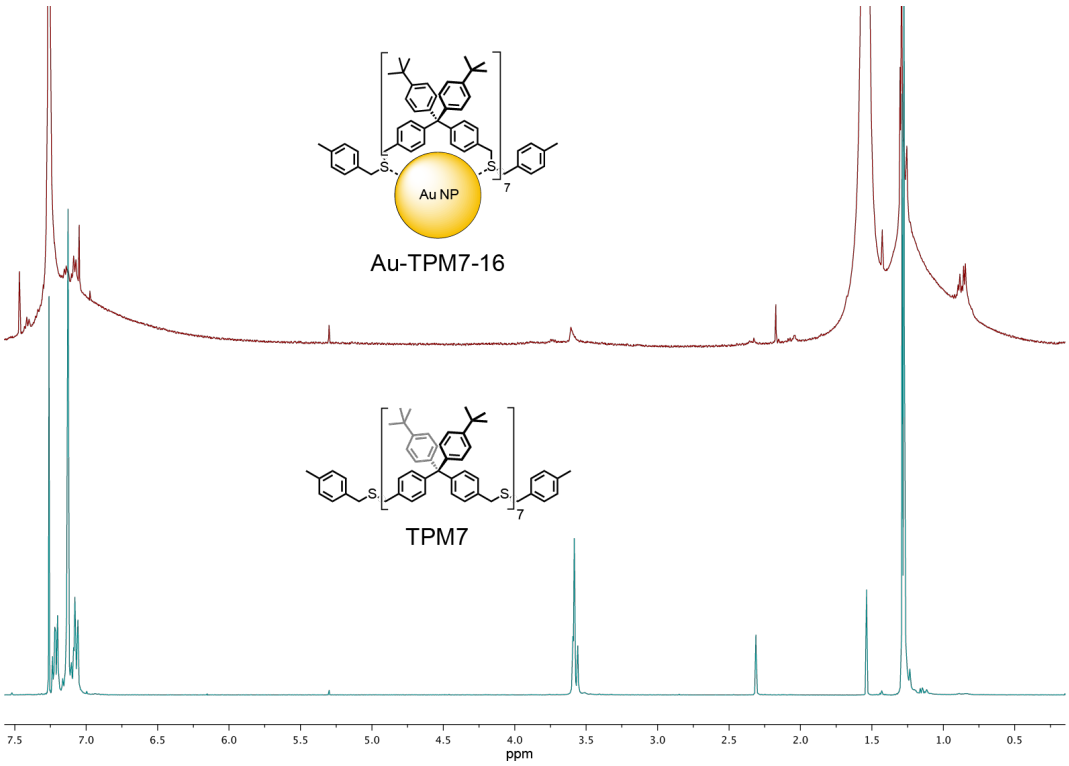

Figure 52: ^{1}H-NMR spectra of **Au-TPM7-16** (top) and the pure ligand **TPM7** in chloroform-*d*.

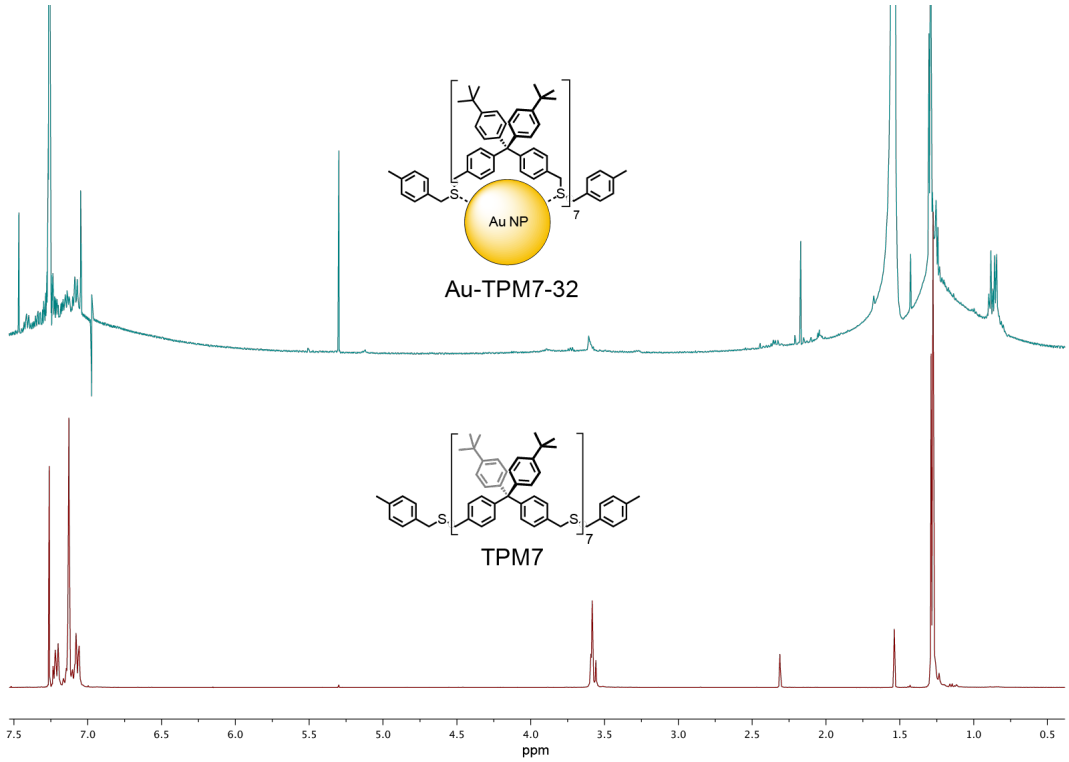

Figure 53: ^{1}H-NMR spectra of **Au-TPM7-32** (top) and the pure ligand **TPM7** in chloroform-*d*.

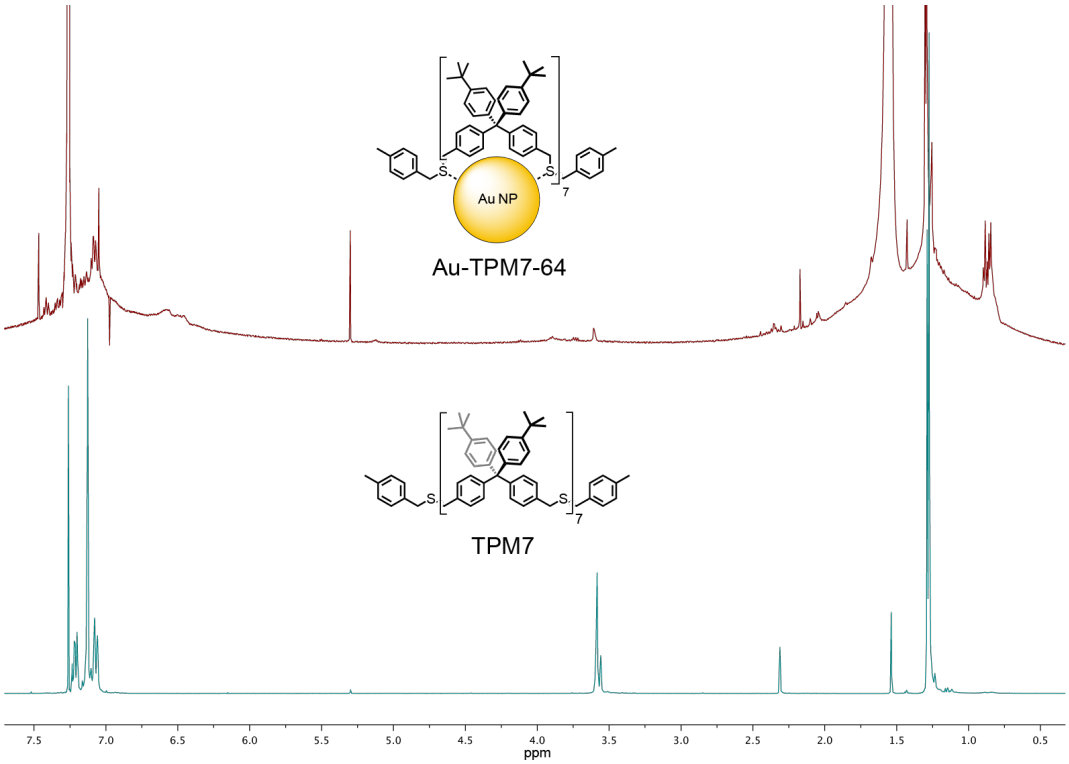

Figure 54: ^{1}H-NMR spectra of **Au-TPM7-64** (top) and the pure ligand **TPM7** in chloroform-*d*.

8.5.2 Thermogravimetric Analysis of **Au-TPM7-16**, **Au-TPM7-32** and **Au-TPM-64**

An explanation and interpretation of the calculation for the TGA-spectra is given under subchapter 8.1.2 above.

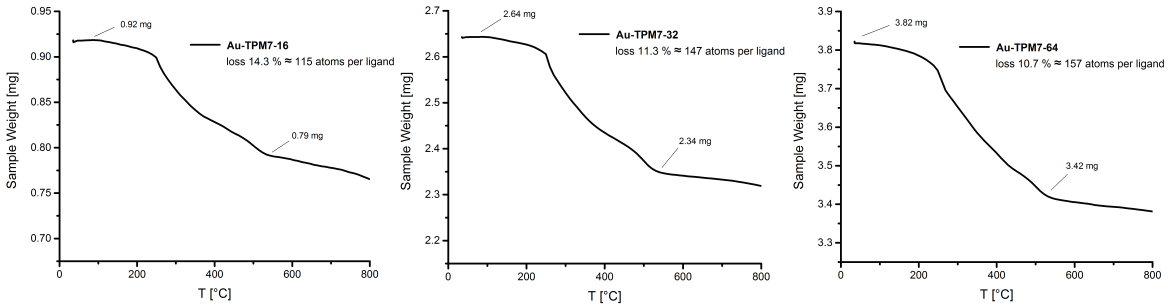

Figure 55: Thermogravimetric analyses of gold nanoparticles **Au-TPM7-16** (left), **Au-TPM7-32** (middle) and **Au-TPM7-64** (right).

Table 5: Calculated amount of ligands enwrapping a single NP for **Au-TPM7-16**, **Au-TPM7-32** and **Au-TPM7-64**.

	m_{Lig} *[mg]*	M_{Lig} *[g/mol]*	n_{Lig} *[mol]*	m_{Au} *[mg]*	M_{Au} *[g/mol]*	n_{Au} *[mol]*	Au/Lig	AuNP ⌀ *[nm]*	Au/NP	**Lig/AuNP**
Au-TPM7-16	0.130	3677.62	3.47E-8	0.790	196.9665	4.01E-6	115.32	1.94	225.81	**1.96**
Au- TPM7-32	0.297	3677.62	8.07E-8	2.346	196.9665	1.19E-5	147.46	2.23	342.97	**2.32**
Au- TPM7-64	0.406	3677.62	1.10E-7	3.417	196.9665	1.73E-5	157.20	2.47	466.06	**2.96**

8.5.3 Thermal Stability Measurements of Au-TPM7-16, -32 and -64

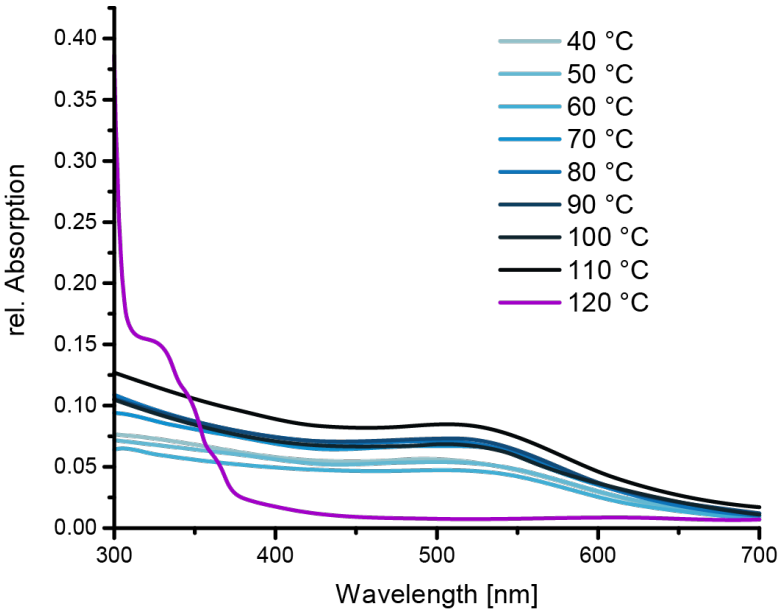

Figure 56: UV-Vis spectra showing the thermal stability of **Au-TPM7-16** recorded in toluene (p-xylene added for 120 °C). AuNPs were gradually heated up 10 °C for 1 hour.

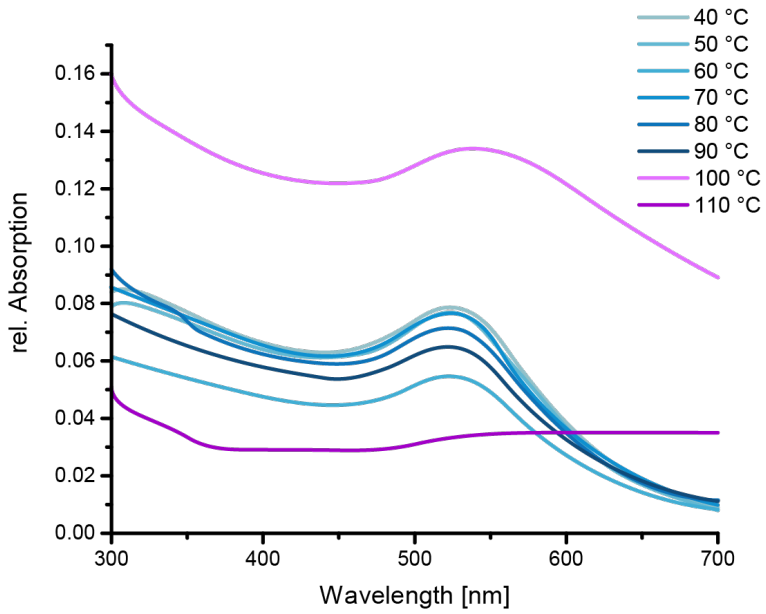

Figure 57: UV-Vis spectra showing the thermal stability of **Au-TPM7-32** recorded in toluene. AuNPs were gradually heated up 10 °C for 1 hour.

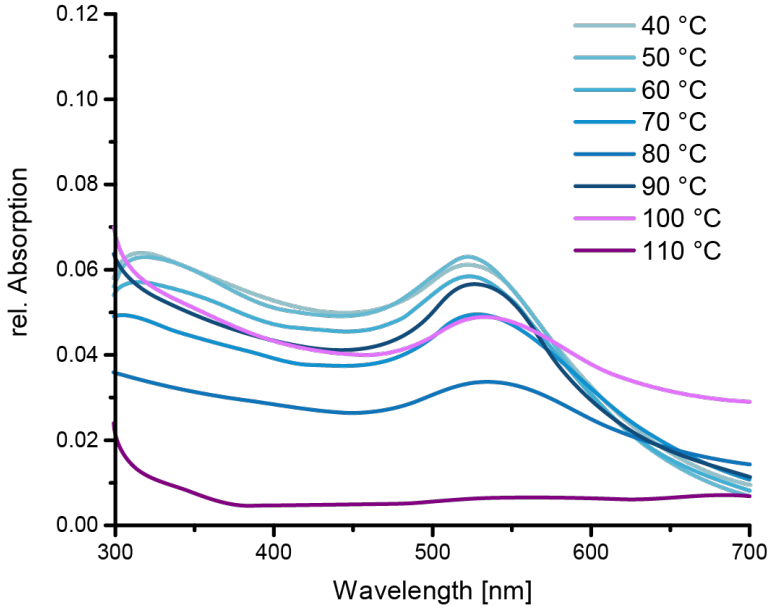

Figure 58: UV-Vis spectra showing the thermal stability of **Au-TPM7-64** recorded in toluene. AuNPs were gradually heated up 10 °C for 1 hour.

9 Abbreviations

Ac	acetyl
AIBN	azobisisobutyronitrile
aq.	aqueous
AuNCs	gold nanoclusters
AuNPs	gold nanoparticles
Bn	benzyl
br	broad
Bu	butyl
CPDIPS	(3-cyanopropyl)diisopropylsilyl
d	duplet
DIBAL-H	diisobutylaluminium hydride
DIPEA	*N,N*-diisopropylethylamin
DOESY	diffusion-ordered spectroscopy
DMF	dimethylsulfoxide
DMSO	dimethylsulfoxide
DNA	2'-deoxyribonucleic acid
EA	elemental analysis
EI	electron impact
eq.	equivalent
ESI	electron spray ionization
Et	ethyl
Et_3N	triethyl amine
Et_2NH	diethyl amine
EtOAc	ethyl acetate
FG	functional group
GC	gas chromatography
GPC	gel permeation chromatography
HPLC	high pressure liquid chromatography
h	hour
hν	light
m	multiplet
m/z	mass per charge
MALDI	matrix-assisted laser desorption/ionization

Me	methyl
min	minutes
MS	mass spectrometry
MTBE	*tert*-butyl methyl ether
MW	microwave
NC	nanocluster
NBS	*N*-bromosuccinimide
NMR	nuclear magnetic resonance
NP	nanoparticle
OPE	oligo(phenylene-ethynyl)
PAMAM	poly(amidoamine)
PG	protecting group
Ph	phenyl
ppm	parts per million
q	quartet
quant.	quantitative
RT	room temperature
s	singlet
SAM	self-assembled monolayer
SEM	scanning electron microscopy
t	triplet
TBAF	tetra-*n*-butylammonium fluoride
TEA	triethylamine
TEM	transmission electron microscopy
TFA	trifluoroacetic acid
TGA	thermogravimetric analysis
THF	tetrahydrofuran
TIPS	triisopropylsilyl
TLC	thin layer chromatography
TMS	trimethylsilyl
TOAB	tetra-*n*-octylammonium bromide
ToF	time of flight
Trt	trityl
UV-Vis	ultraviolet and visible

10 Literature

[1] M.-C. Daniel, D. Astruc, *Chem. Rev.* **2004**, *104*, 293–346.

[2] Milton Kerker, *J. Colloids Interface Sci.* **1985**, *105*, 297–314.

[3] http://www.britishmuseum.org/research/collection

[4] P. Mulvaney, *MRS Bull.* **2001**, *26*, 1009–1014.

[5] F. Antonii., *Panacea Aurea-Auro Potabile*, **1618**.

[6] M. Faraday, *Philos. Trans. R. Soc. Lond.* **1857**, *147*, 145–181.

[7] P. P. Edwards, J. M. Thomas, *Angew. Chem. Int. Ed.* **2007**, *46*, 5480–5486.

[8] T. Graham, *Philos. Trans. R. Soc. Lond.* **1861**, *151*, 183–224.

[9] G. Schmid, B. Corain, *Eur. J. Inorg. Chem.* **2003**, *2003*, 3081–3098.

[10] G. Schmid, *Angew. Chem. Int. Ed.* **2008**, *47*, 3496–3498.

[11] G. Mie, *Ann. Phys.* **1908**, *330*, 377–445.

[12] R. Zsigmondy, *The Chemistry of Colloids*, BiblioBazaar, **2008**.

[13] P. Zhao, N. Li, D. Astruc, *Coord. Chem. Rev.* **2013**, *257*, 638–665.

[14] R. Zsigmondy, J. Alexander, *Colloids and the Ultramicroscope: A Manual of Colloid Chemistry and Ultramicroscopy*, J. Wiley & Sons, **1909**.

[15] R. Zsigmondy, C. Sönnichsen, *One Hundred Years of Nanoscience with the Ultramicroscope*, Shaker Verlag, **2007**.

[16] T. Svedberg, *The Formation of Colloids*, London, J. & A. Churchill, **1921**.

[17] T. Svedberg, R. Fåhraeus, *J. Am. Chem. Soc.* **1926**, *48*, 430–438.

[18] M. Das, K. H. Shim, S. S. A. An, D. K. Yi, *Toxicol. Environ. Health Sci.* **2011**, *3*, 193–205.

[19] J. Turkevich, P. C. Stevenson, J. Hillier, *Discuss. Faraday Soc.* **1951**, *11*, 55–75.

[20] G. Frens, *Nature* **1973**, *241*, 20–22.

[21] J. Liao, L. Bernard, M. Langer, C. Schönenberger, M. Calame, *Adv. Mater.* **2006**, *18*, 2444–2447.

[22] G. Schmid, *Chem. Rev.* **1992**, *92*, 1709–1727.

[23] G. Schmid, L. F. Chi, *Adv. Mater.* **1998**, *10*, 515–526.

[24] M. Haruta, N. Yamada, T. Kobayashi, S. Iijima, *J. Catal.* **1989**, *115*, 301–309.

[25] N. Li, M. Echeverría, S. Moya, J. Ruiz, D. Astruc, *Inorg. Chem.* **2014**, *53*, 6954–6961.

[26] X. Wu, C. Lu, Z. Zhou, G. Yuan, R. Xiong, X. Zhang, *Environ. Sci. Nano* **2014**, *1*, 71–79.

[27] M. Stratakis, H. Garcia, *Chem. Rev.* **2012**, *112*, 4469–4506.

[28] B. S. Takale, M. Bao, Y. Yamamoto, *Org. Biomol. Chem.* **2014**, *12*, 2005–2027.

[29] M. Giersig, P. Mulvaney, *Langmuir* **1993**, *9*, 3408–3413.

[30] M. Brust, M. Walker, D. Bethell, D. J. Schiffrin, R. Whyman, *J. Chem. Soc. Chem. Commun.* **1994**, *7*, 801–802.

[31] D. Bethell, M. Brust, D. J. Schiffrin, C. Kiely, *J. Electroanal. Chem.* **1996**, *409*, 137–143.

[32] M. Brust, C. J. Kiely, *Colloids Surf. Physicochem. Eng. Asp.* **2002**, *202*, 175–186.

[33] C. Burda, X. Chen, R. Narayanan, M. A. El-Sayed, *Chem. Rev.* **2005**, *105*, 1025–1102.

[34] S. Eustis, M. A. El-Sayed, *Chem. Soc. Rev.* **2006**, *35*, 209–217.

[35] T. K. Sau, C. J. Murphy, *J. Am. Chem. Soc.* **2004**, *126*, 8648–8649.

[36] J. Pérez-Juste, I. Pastoriza-Santos, L. M. Liz-Marzán, P. Mulvaney, *Coord. Chem. Rev.* **2005**, *249*, 1870–1901.

[37] X. Huang, S. Neretina, M. A. El-Sayed, *Adv. Mater.* **2009**, *21*, 4880–4910.

[38] M. Hu, F. S. Ou, W. Wu, I. Naumov, X. Li, A. M. Bratkovsky, R. S. Williams, Z. Li, *J. Am. Chem. Soc.* **2010**, *132*, 12820–12822.

[39] W. Huang, W. Qian, M. A. El-Sayed, *J. Am. Chem. Soc.* **2006**, *128*, 13330–13331.

[40] J. Neddersen, G. Chumanov, T. M. Cotton, *Appl. Spectrosc.* **1993**, *47*, 1959–1964.

[41] S. Besner, A. V. Kabashin, F. M. Winnik, M. Meunier, *J. Phys. Chem. C* **2009**, *113*, 9526–9531.

[42] T. K. Sau, A. L. Rogach, F. Jäckel, T. A. Klar, J. Feldmann, *Adv. Mater.* **2010**, *22*, 1805–1825.

[43] M. Hu, J. Chen, Z.-Y. Li, L. Au, G. V. Hartland, X. Li, M. Marquez, Y. Xia, *Chem. Soc. Rev.* **2006**, *35*, 1084–1094.

[44] N. Khlebtsov, L. Dykman, *Chem. Soc. Rev.* **2011**, *40*, 1647–1671.

[45] C. J. Murphy, A. M. Gole, J. W. Stone, P. N. Sisco, A. M. Alkilany, E. C. Goldsmith, S. C. Baxter, *Acc. Chem. Res.* **2008**, *41*, 1721–1730.

[46] P. K. Jain, K. S. Lee, I. H. El-Sayed, M. A. El-Sayed, *J. Phys. Chem. B* **2006**, *110*, 7238–7248.

[47] S. Link, M. A. El-Sayed, *J. Phys. Chem. B* **1999**, *103*, 4212–4217.

[48] Y.-C. Yeh, B. Creran, V. M. Rotello, *Nanoscale* **2012**, *4*, 1871–1880.

[49] http://www.physicscentral.com/explore/action/gold.cfm

[50] S. Srivastava, B. L. Frankamp, V. M. Rotello, *Chem. Mater.* **2005**, *17*, 487–490.

[51] K. L. Kelly, E. Coronado, L. L. Zhao, G. C. Schatz, *J. Phys. Chem. B* **2003**, *107*, 668–677.

[52] S. Link, M. A. El-Sayed, *Int. Rev. Phys. Chem.* **2000**, *19*, 409–453.

[53] K.-H. Su, Q.-H. Wei, X. Zhang, J. J. Mock, D. R. Smith, S. Schultz, *Nano Lett.* **2003**, *3*, 1087–1090.

[54] L. M. Liz-Marzán, *Langmuir* **2006**, *22*, 32–41.

[55] G. Schmid, *Adv. Eng. Mater.* **2001**, *3*, 737–743.

[56] G. Schmid, *Nanoparticles: From Theory to Application*, John Wiley & Sons, **2011**.

[57] M. Homberger, U. Simon, *R. Soc. Lond. Philos. Trans. Ser. A* **2010**, *368*, 1405–1453.

[58] R. Liffmann, M. Homberger, M. Mennicken, S. Karthäuser, U. Simon, *RSC Adv.* **2015**, *5*, 102981–102992.

[59] A. Leifert, Y. Pan-Bartnek, U. Simon, W. Jahnen-Dechent, *Nanoscale* **2013**, *5*, 6224–6242.

[60] G. Schmid, U. Simon, *Chem. Commun.* **2005**, 697–710.

[61] M. Zhu, C. M. Aikens, F. J. Hollander, G. C. Schatz, R. Jin, *J. Am. Chem. Soc.* **2008**, *130*, 5883–5885.

[62] R. Jin, *Nanoscale* **2010**, *2*, 343–362.

[63] H. Qian, M. Zhu, Z. Wu, R. Jin, *ResearchGate* **2012**, *45*, 1470–9.

[64] X. Huang, B. Li, H. Zhang, I. Hussain, L. Liang, B. Tan, *Nanoscale* **2011**, *3*, 1600–1607.

[65] M. K. Harbola, *Proc. Natl. Acad. Sci. U. S. A.* **1992**, *89*, 1036–1039.

[66] H. Li, L. Li, A. Pedersen, Y. Gao, N. Khetrapal, H. Jónsson, X. C. Zeng, *Nano Lett.* **2015**, *15*, 682–688.

[67] M. Walter, J. Akola, O. Lopez-Acevedo, P. D. Jadzinsky, G. Calero, C. J. Ackerson, R. L. Whetten, H. Grönbeck, H. Häkkinen, *Proc. Natl. Acad. Sci.* **2008**, *105*, 9157–9162.

[68] M. Zhu, E. Lanni, N. Garg, M. E. Bier, R. Jin, *J. Am. Chem. Soc.* **2008**, *130*, 1138–1139.

[69] R. Guo, R. W. Murray, *J. Am. Chem. Soc.* **2005**, *127*, 12140–12143.

[70] D. Lee, R. L. Donkers, G. Wang, A. S. Harper, R. W. Murray, *J. Am. Chem. Soc.* **2004**, *126*, 6193–6199.

[71] R. L. Donkers, D. Lee, R. W. Murray, *Langmuir* **2004**, *20*, 1945–1952.

[72] M. Cui, Y. Zhao, Q. Song, *TrAC Trends Anal. Chem.* **2014**, *57*, 73–82.

[73] V. L. Jimenez, D. G. Georganopoulou, R. J. White, A. S. Harper, A. J. Mills, D. Lee, R. W. Murray, *Langmuir* **2004**, *20*, 6864–6870.

[74] J. B. Tracy, M. C. Crowe, J. F. Parker, O. Hampe, C. A. Fields-Zinna, A. Dass, R. W. Murray, *J. Am. Chem. Soc.* **2007**, *129*, 16209–16215.

[75] Y. Negishi, K. Nobusada, T. Tsukuda, *J. Am. Chem. Soc.* **2005**, *127*, 5261–5270.

[76] W. W. Weare, S. M. Reed, M. G. Warner, J. E. Hutchison, *J. Am. Chem. Soc.* **2000**, *122*, 12890–12891.

[77] S. Knoppe, Q.-F. Zhang, X.-K. Wan, Q.-M. Wang, L.-S. Wang, T. Verbiest, *Ind. Eng. Chem. Res.* **2016**, *55*, 10500–10506.

[78] H. D. Jin, A. Garrison, T. Tseng, B. K. Paul, C.-H. Chang, *Nanotechnology* **2010**, *21*, 445604.

[79] T. Peterle, P. Ringler, M. Mayor, *Adv. Funct. Mater.* **2009**, *19*, 3497–3506.

[80] T. Peterle, A. Leifert, J. Timper, A. Sologubenko, U. Simon, M. Mayor, *Chem. Commun.* **2008**, *29*, 3438–3440.

[81] J. P. Hermes, F. Sander, T. Peterle, R. Urbani, T. Pfohl, D. Thompson, M. Mayor, *Chem. – Eur. J.* **2011**, *17*, 13473–13481.

[82] J. P. Hermes, F. Sander, U. Fluch, T. Peterle, D. Thompson, R. Urbani, T. Pfohl, M. Mayor, *J. Am. Chem. Soc.* **2012**, *134*, 14674–14677.

[83] J. P. Hermes, F. Sander, T. Peterle, C. Cioffi, P. Ringler, T. Pfohl, M. Mayor, *Small* **2011**, *7*, 920–929.

[84] F. Sander, U. Fluch, J. P. Hermes, M. Mayor, *Small* **2014**, *10*, 349–359.

[85] C. J. Murphy, A. M. Gole, S. E. Hunyadi, C. J. Orendorff, *Inorg. Chem.* **2006**, *45*, 7544–7554.

[86] D. A. Giljohann, D. S. Seferos, W. L. Daniel, M. D. Massich, P. C. Patel, C. A. Mirkin, *Angew. Chem. Int. Ed.* **2010**, *49*, 3280–3294.

[87] S. Zeng, K.-T. Yong, I. Roy, X.-Q. Dinh, X. Yu, F. Luan, *Plasmonics* **2011**, *6*, 491–506.

[88] B. D. Chithrani, A. A. Ghazani, W. C. W. Chan, *Nano Lett.* **2006**, *6*, 662–668.

[89] B. D. Chithrani, W. C. W. Chan, *Nano Lett.* **2007**, *7*, 1542–1550.

[90] E. Vivès, J. Schmidt, A. Pèlegrin, *Biochim. Biophys. Acta* **2008**, *1786*, 126–138.

[91] M.-C. Bowman, T. E. Ballard, C. J. Ackerson, D. L. Feldheim, D. M. Margolis, C. Melander, *J. Am. Chem. Soc.* **2008**, *130*, 6896–6897.

[92] D. S. Seferos, D. A. Giljohann, H. D. Hill, A. E. Prigodich, C. A. Mirkin, *J. Am. Chem. Soc.* **2007**, *129*, 15477–15479.

[93] C. D. Medley, J. E. Smith, Z. Tang, Y. Wu, S. Bamrungsap, W. Tan, *Anal. Chem.* **2008**, *80*, 1067–1072.

[94] I. H. El-Sayed, X. Huang, M. A. El-Sayed, *Nano Lett.* **2005**, *5*, 829–834.

[95] I. H. El-Sayed, X. Huang, M. A. El-Sayed, *Cancer Lett.* **2006**, *239*, 129–135.

[96] R. D. Powell, C. M. R. Halsey, J. F. Hainfeld, *Microsc. Res. Tech.* **1998**, *42*, 2–12.

[97] W. P. Faulk, G. M. Taylor, *Immunochemistry* **1971**, *8*, 1081–1083.

[98] D. A. Schultz, *Curr. Opin. Biotechnol.* **2003**, *14*, 13–22.

[99] R. A. Sperling, P. R. Gil, F. Zhang, M. Zanella, W. J. Parak, *Chem. Soc. Rev.* **2008**, *37*, 1896–1908.

[100] J. H. W. Leuvering, P. J. H. M. Thal, M. van der Waart, A. H. W. M. Schuurs, *Fresenius J Anal Chem* **1980**, *301*, 132.

[101] R. Wilson, *Chem. Soc. Rev.* **2008**, *37*, 2028–2045.

[102] M. Haruta, *Catal. Today* **1997**, *36*, 153–166.

[103] I. N. Remediakis, N. Lopez, J. K. Nørskov, *Angew. Chem. Int. Ed Engl.* **2005**, *44*, 1824–1826.

[104] M. Comotti, W.-C. Li, B. Spliethoff, F. Schüth, *J. Am. Chem. Soc.* **2006**, *128*, 917–924.

[105] B. K. Min, C. M. Friend, *Chem. Rev.* **2007**, *107*, 2709–2724.

[106] R. Coquet, K. L. Howard, D. J. Willock, *Chem. Soc. Rev.* **2008**, *37*, 2046–2076.

[107] O. Lopez-Acevedo, K. A. Kacprzak, J. Akola, H. Häkkinen, *Nat. Chem.* **2010**, *2*, 329–334.

[108] H. Yoshida, Y. Kuwauchi, J. R. Jinschek, K. Sun, S. Tanaka, M. Kohyama, S. Shimada, M. Haruta, S. Takeda, *Science* **2012**, *335*, 317–319.

[109] C. D. Pina, E. Falletta, L. Prati, M. Rossi, *Chem. Soc. Rev.* **2008**, *37*, 2077–2095.

[110] T. Ishida, M. Haruta, *Angew. Chem. Int. Ed.* **2007**, *46*, 7154–7156.

[111] R. Klajn, J. F. Stoddart, B. A. Grzybowski, *Chem. Soc. Rev.* **2010**, *39*, 2203–2237.

[112] R. Klajn, P. J. Wesson, K. J. M. Bishop, B. A. Grzybowski, *Angew. Chem. Int. Ed.* **2009**, *48*, 7035–7039.

[113] P. Calero, E. Aznar, J. M. Lloris, M. D. Marcos, R. Martínez-Máñez, J. V. Ros-Lis, J. Soto, F. Sancenón, *Chem. Commun.* **2008**, *14*, 1668–1670.

[114] T. Toyama, K. Higashiguchi, T. Nakamura, H. Yamaguchi, E. Kusaka, K. Matsuda, *J. Phys. Chem. Lett.* **2016**, *7*, 2113–2118.

[115] B. Long, K. Nikitin, D. Fitzmaurice, *J. Am. Chem. Soc.* **2003**, *125*, 15490–15498.

[116] R. Klajn, L. Fang, A. Coskun, M. A. Olson, P. J. Wesson, J. F. Stoddart, B. A. Grzybowski, *J. Am. Chem. Soc.* **2009**, *131*, 4233–4235.

[117] R. Klajn, M. A. Olson, P. J. Wesson, L. Fang, A. Coskun, A. Trabolsi, S. Soh, J. F. Stoddart, B. A. Grzybowski, *Nat. Chem.* **2009**, *1*, 733–738.

[118] J. F. Hainfeld, *Science* **1987**, *236*, 450–453.

[119] M. Karg, N. Schelero, C. Oppel, M. Gradzielski, T. Hellweg, R. von Klitzing, *Chem. – Eur. J.* **2011**, *17*, 4648–4654.

[120] F. Sander, T. Peterle, N. Ballav, F. von Wrochem, M. Zharnikov, M. Mayor, *J. Phys. Chem. C* **2010**, *114*, 4118–4125.

[121] D. Thompson, J. P. Hermes, A. J. Quinn, M. Mayor, *ACS Nano* **2012**, *6*, 3007–3017.

[122] X.-M. Li, M. R. de Jong, K. Inoue, S. Shinkai, J. Huskens, D. N. Reinhoudt, *J. Mater. Chem.* **2001**, *11*, 1919–1923.

[123] A. Taubert, U.-M. Wiesler, K. Müllen, *J. Mater. Chem.* **2003**, *13*, 1090–1093.

[124] Y. Hosokawa, S. Maki, T. Nagata, *Bull. Chem. Soc. Jpn.* **2005**, *78*, 1773–1782.

[125] A. D'Aléo, R. M. Williams, F. Osswald, P. Edamana, U. Hahn, J. van Heyst, F. D. Tichelaar, F. Vögtle, L. De Cola, *Adv. Funct. Mater.* **2004**, *14*, 1167–1177.

[126] E. Boisselier, A. K. Diallo, L. Salmon, C. Ornelas, J. Ruiz, D. Astruc, *J. Am. Chem. Soc.* **2010**, *132*, 2729–2742.

[127] R. M. Crooks, M. Zhao, L. Sun, V. Chechik, L. K. Yeung, *Acc. Chem. Res.* **2001**, *34*, 181–190.

[128] K. Esumi, A. Kameo, A. Suzuki, K. Torigoe, *Colloids Surf. Physicochem. Eng. Asp.* **2001**, *189*, 155–161.

[129] H.-M. Huang, C.-Y. Chang, I.-C. Liu, H.-C. Tsai, M.-K. Lai, R. C.-C. Tsiang, *J. Polym. Sci. Part Polym. Chem.* **2005**, *43*, 4710–4720.

[130] I. Hussain, S. Graham, Z. Wang, B. Tan, D. C. Sherrington, S. P. Rannard, A. I. Cooper, M. Brust, *J. Am. Chem. Soc.* **2005**, *127*, 16398–16399.

[131] D. Wan, Q. Fu, J. Huang, *J. Appl. Polym. Sci.* **2006**, *101*, 509–514.

[132] G. A. DeVries, M. Brunnbauer, Y. Hu, A. M. Jackson, B. Long, B. T. Neltner, O. Uzun, B. H. Wunsch, F. Stellacci, *Science* **2007**, *315*, 358–361.

[133] M. Sakamoto, D. Tanaka, T. Teranishi, *Chem. Sci.* **2013**, *4*, 824–828.

[134] P. G. M. Wuts, T. W. Greene, *Greene's Protective Groups in Organic Synthesis*, John Wiley & Sons, **2006**.

[135] D. A. Pearson, M. Blanchette, M. L. Baker, C. A. Guindon, *Tetrahedron Lett.* **1989**, *30*, 2739–2742.

[136] C. E. Hoyle, C. N. Bowman, *Angew. Chem. Int. Ed.* **2010**, *49*, 1540–1573.

[137] P. Lustenberger, F. Diederich, *Helv. Chim. Acta* **2000**, *83*, 2865–2883.

[138] K. G. Thomas, J. Zajicek, P. V. Kamat, *Langmuir* **2002**, *18*, 3722–3727.

[139] R. Costi, A. E. Saunders, U. Banin, *Angew. Chem. Int. Ed.* **2010**, *49*, 4878–4897.

[140] Y. Negishi, T. Nakazaki, S. Malola, S. Takano, Y. Niihori, W. Kurashige, S. Yamazoe, T. Tsukuda, H. Häkkinen, *J. Am. Chem. Soc.* **2015**, *137*, 1206–1212.

[141] O. Plietzsch, A. Schade, A. Hafner, J. Huuskonen, K. Rissanen, M. Nieger, T. Muller, S. Bräse, *Eur. J. Org. Chem.* **2013**, *2013*, 283–299.

[142] M. M. Alvarez, J. T. Khoury, T. G. Schaaff, M. N. Shafigullin, I. Vezmar, R. L. Whetten, *J. Phys. Chem. B* **1997**, *101*, 3706–3712.

[143] R. McCaffrey, H. Long, Y. Jin, A. Sanders, W. Park, W. Zhang, *J. Am. Chem. Soc.* **2014**, *136*, 1782–1785.

[144] K. Naka, H. Itoh, Y. Chujo, *Langmuir* **2003**, *19*, 5496–5501.

[145] C. R. van den Brom, P. Rudolf, T. T. M. Palstra, B. Hessen, *Chem. Commun.* **2007**, *46*, 4922–4924.

[146] H. Ozawa, M. Kawao, H. Tanaka, T. Ogawa, *Langmuir* **2007**, *23*, 6365–6371.

[147] C.-P. Chak, S. Xuan, P. M. Mendes, J. C. Yu, C. H. K. Cheng, K. C.-F. Leung, *ACS Nano* **2009**, *3*, 2129–2138.

[148] B. D. Myers, Q.-Y. Lin, H. Wu, E. Luijten, C. A. Mirkin, V. P. Dravid, *ACS Nano* **2016**, *10*, 5679–5686.

[149] Q. Liu, M. Guo, Z. Nie, J. Yuan, J. Tan, S. Yao, *Langmuir* **2008**, *24*, 1595–1599.

[150] G. Gaefke, S. Höger, *Synthesis* **2008**, *2008*, 2155–2157.

[151] N. M. Jenny, M. Mayor, T. R. Eaton, *Eur. J. Org. Chem.* **2011**, *2011*, 4965–4983.

[152] A. S. Hay, *J. Org. Chem.* **1962**, *27*, 3320–3321.

[153] K. Nikitin, E. Lestini, M. Lazzari, S. Altobello, D. Fitzmaurice, *Langmuir* **2007**, *23*, 12147–12153.

[154] T. Weidner, N. Ballav, U. Siemeling, D. Troegel, T. Walter, R. Tacke, D. G. Castner, M. Zharnikov, *J. Phys. Chem. C* **2009**, *113*, 19609–19617.

[155] T. Sakata, S. Maruyama, A. Ueda, H. Otsuka, Y. Miyahara, *Langmuir* **2007**, *23*, 2269–2272.

[156] M. Lukas, K. Dössel, A. Schramm, O. Fuhr, C. Stroh, M. Mayor, K. Fink, H. v. Löhneysen, *ACS Nano* **2013**, *7*, 6170–6180.

[157] M. Lindner, M. Valášek, J. Homberg, K. Edelmann, L. Gerhard, W. Wulfhekel, O. Fuhr, T. Wächter, M. Zharnikov, V. Kolivoška, *et al.*, *Chem. - Eur. J.* **2016**, *22*, 13218–13235.

[158] M. Valášek, M. Lindner, M. Mayor, *Beilstein J. Nanotechnol.* **2016**, *7*, 374–405.

[159] A. Schramm, C. Stroh, K. Dössel, M. Lukas, M. Fischer, F. Schramm, O. Fuhr, H. v. Löhneysen, M. Mayor, *Eur. J. Inorg. Chem.* **2013**, *2013*, 70–79.

[160] M. Valášek, K. Edelmann, L. Gerhard, O. Fuhr, M. Lukas, M. Mayor, *J. Org. Chem.* **2014**, *79*, 7342–7357.

[161] T. Sakata, S. Maruyama, A. Ueda, H. Otsuka, Y. Miyahara, *Langmuir* **2007**, *23*, 2269–2272.

[162] M. Valášek, M. Lindner, M. Mayor, *Beilstein J. Nanotechnol.* **2016**, *7*, 374–405.

[163] M. Lindner, M. Valášek, J. Homberg, K. Edelmann, L. Gerhard, W. Wulfhekel, O. Fuhr, T. Wächter, M. Zharnikov, V. Kolivoška, *et al.*, *Chem. – Eur. J.* **2016**, *22*, 13218–13235.

[164] F. Sander, J. P. Hermes, M. Mayor, H. Hamoudi, M. Zharnikov, *Phys. Chem. Chem. Phys.* **2013**, *15*, 2836–2846.

[165] M. Brust, M. Walker, D. Bethell, D. J. Schiffrin, R. Whyman, *J Chem Soc Chem Commun* **1994**, 801–802.

[166] G. Schmid, M. Bäumle, M. Geerkens, I. Heim, C. Osemann, T. Sawitowski, *Chem Soc Rev* **1999**, *28*, 179–185.

[167] C. Zhang, X. Li, C. Tian, G. Yu, Y. Li, W. Jiang, C. Mao, *ACS Nano* **2014**, *8*, 1130–1135.

[168] B. Mondal, K. Acharyya, P. Howlader, P. S. Mukherjee, *J. Am. Chem. Soc.* **2016**, *138*, 1709–1716.

[169] M. Frisch, G. Trucks, H. Schlegel, G. Scuseria, M. Robb, J. Cheeseman, G. Scalmani, V. Barone, B. Mennucci, G. Petersson, *et al.*, *Gaussian 09 Revis. B01 Gaussian Inc Wallingford CT* **2009**.

[170] R. Ditchfield, W. J. Hehre, J. A. Pople, *J. Chem. Phys.* **1971**, *54*, 724–728.

[171] D. A. Tomalia, S. N. Khanna, *Chem. Rev.* **2016**, *116*, 2705–2774.

[172] N. Bodappa, U. Fluch, Y. Fu, M. Mayor, P. Moreno-García, H. Siegenthaler, T. Wandlowski, *Nanoscale* **2014**, *6*, 15117–15126.

[173] F. Kretschmer, S. Mühlig, S. Hoeppener, A. Winter, M. D. Hager, C. Rockstuhl, T. Pertsch, U. S. Schubert, *Part. Part. Syst. Charact.* **2014**, *31*, 721–744.

[174] K. Saha, S. S. Agasti, C. Kim, X. Li, V. M. Rotello, *Chem. Rev.* **2012**, *112*, 2739–2779.

[175] L.-Y. Chen, C.-W. Wang, Z. Yuan, H.-T. Chang, *Anal. Chem.* **2015**, *87*, 216–229.

[176] M. J. Hostetler, J. E. Wingate, C.-J. Zhong, J. E. Harris, R. W. Vachet, M. R. Clark, J. D. Londono, S. J. Green, J. J. Stokes, G. D. Wignall, *et al.*, *Langmuir* **1998**, *14*, 17–30.

[177] T. Chen, Z. Luo, Q. Yao, A. X. H. Yeo, J. Xie, *Chem. Commun.* **2016**, *52*, 9522–9525.

[178] S. M. Ansar, F. S. Mohammed, G. von White, M. Budi, K. C. Powell, O. T. Mefford, C. L. Kitchens, *J. Phys. Chem. C* **2016**, *120*, 6842–6850.

[179] S. R. K. Perala, S. Kumar, *Langmuir* **2013**, *29*, 9863–9873.

[180] Z. Wang, B. Tan, I. Hussain, N. Schaeffer, M. F. Wyatt, M. Brust, A. I. Cooper, *Langmuir* **2007**, *23*, 885–895.

[181] M. Azubel, R. D. Kornberg, *Nano Lett.* **2016**, *16*, 3348–3351.

[182] E. W. Elliott, P. M. Haben, J. E. Hutchison, *Langmuir* **2015**, *31*, 11886–11894.

[183] A. Uehara, S. G. Booth, S. Y. Chang, S. L. M. Schroeder, T. Imai, T. Hashimoto, J. F. W. Mosselmans, R. A. W. Dryfe, *J. Am. Chem. Soc.* **2015**, *137*, 15135–15144.

[184] J. P. Hermes, F. Sander, T. Peterle, C. Cioffi, P. Ringler, T. Pfohl, M. Mayor, *Small Weinh. Bergstr. Ger.* **2011**, *7*, 920–929.

[185] P. R. Ashton, M. Bělohradský, D. Philp, J. F. Stoddart, *J. Chem. Soc. Chem. Commun.* **1993**, 1269–1274.

[186] M. Horn, H. Mayr, *Chem. – Eur. J.* **2010**, *16*, 7469–7477.

[187] J. Tian, Y.-D. Ding, T.-Y. Zhou, K.-D. Zhang, X. Zhao, H. Wang, D.-W. Zhang, Y. Liu, Z.-T. Li, *Chem. – Eur. J.* **2014**, *20*, 575–584.

Curriculum Vitae

Name	**Mario Lehmann**
Adresse	Rosenweg 28 3007 Bern
Tel.	079 303 99 70
E-Mail	mario.lehmann@unibas.ch
Geburtsdatum	19.11.1986
Nationalität	Schweiz
Familienstand	ledig

Ausbildung

09/2012 - heute	PhD (Verteidigung bevorstehend) in organischer Chemie, Universität Basel PhD Thesis: Multidentate Thioether-Based Ligands Controlling the Stability and Size of Gold Nanoparticles. Gruppe von Prof. Dr. Marcel Mayor, Universität Basel.
09/2009 - 09/2011	MSc in Chemie, Universität Bern Master Thesis: Synthetic Explorations of Zwitterionic Stable Semi-Quinone Radicals; Study of π-Extended BDF-Based MOF Systems; Ru(II) and Os(II)-Terpy Compounds for Molecular Electronics. Gruppe von Prof. Dr. Silvio Decurtins, Universität Bern.
09/2005 - 09/2009	BSc in Chemie, Universität Bern Bachelor Thesis: Synthetic Explorations of Enlarged π-Systems. Gruppe von Prof. Dr. Silvio Decurtins, Universität Bern

Lehrtätigkeit während PhD

03/2014 - 03/2016	Organisation, Betreuung und Lehre „Blockkurs in Nanochemie“ in organischer Chemie für Bachelor-Studenten in Nano-Wissenschaften, Departement für Chemie, Universität Basel.
03/2014 - 03/2015	Aufsicht und Betreuung von Master-Thesen in organischer Chemie sowie verschiedener Semesterpraktika für Chemiestudenten, Departement für Chemie, Universität Basel.
03/2013 - 03/2015	Lehr-Assistent für Labor-Praktika in organischer Chemie für Chemie-, Biologie und Pharmazie-Studenten, Departement für Chemie, Universität Basel.

Publikationen

M. Lehmann, E. H. Peters, M. Mayor, '*Size Matters: Influence of Gold-to-Ligand Ratio and Sulfur-Sulfur Distance of Linear Thioether Heptamers on the Size of Gold Nanoparticles*', *Helv. Chim.* Acta. **2017**, DOI: 10.1002/hcla.201600395.

M. Lehmann, E. H. Peters, M. Mayor, '*Linear Tetraphenylmethane-Based Thioether Oligomers Stabilising an Entire Gold Nanoparticle by Enwrapping*', *Chem. Eur. J.* **2016**, 22, 2261-2265.

C. Yi, C. Blum, M. Lehmann, S. Keller, S.-X. Liu, D. Fre, A. Neels, J. Hauser, S. Schürch, S. Decurtins, 'Versatile Strategy to Access Fully Functionalized Benzodifurans: Redox-Active Chromophores for the Construction of Extended π-Conjugated Materials', *J. Org. Chem.* **2010**, *75*, 3350-3357.